Self-organized surface relief gratings in azo-polymer thin-films

Sohrab Ahmadi-Kandjani

Université d'Angers
UFR Sciences
Laboratoire POMA

Année 2007
N° d'ordre : 804

Réseaux de surface auto-organisés dans les films minces d'azo-polymères

THESE DE DOCTORAT

Spécialité : Physique

ECOLE DOCTORALE D'ANGERS

Présentée et soutenue publiquement

Le : 12 October 2007

à : l'Université d'Angers

par : Sohrab AHMADI KANDJANI

Devant le jury ci-dessous:

Rapporteur, Jacques DELAIRE, Professeur, Ecole Normale Supérieure de Cachan

Rapporteur, Stanislaw H. KUCHARSKI, Professeur, Wroclaw University of Technology, Pologne

Examinateur, Pascal ROYER, Enseignant-chercheur, Université de Technologie Troyes

Examinateur, Habib TAJALLI, Professeur, University of Tabriz, Iran

Examinateur, Régis BARILLE, Professeur, Université d'Angers

Examinateur, Sylvie DABOS-SEIGNON, Chargée de Recherches, Université d'Angers

Examinateur, Christophe HUBERT, Maître de Conférences, Université Jean Monnet

Directeur de thèse, Jean-Michel NUNZI, Professeur, Université d'Angers
Co-encadrant: Régis BARILLE, Professeur, Université d'Angers

Laboratoire des Propriétés Optiques des Matériaux et Applications, UMR CNRS 6136, Université d'Angers, 2 Bd Lavoisier, 49045 ANGERS

ED363

To the memory of my father, Khalil AHMADI KANDJANI

Abstract

Nature is a beautiful combination of patterns. Natural patterns are self-organized. Well defined self-organized patterns also can appear in laboratory conditions for different systems. In this thesis we present pattern formation via self-organization of azo molecules under light illumination. Illuminated azo molecules undergo a trans-cis-trans photoisomerization and diffuse in the polymer film far from brightness. We show that it is possible to form spontaneous patterns on the surface of azo-polymer films under coherent light exposure. The pattern orientation depends on light polarization and polarization multiplexing for more than two states is possible. The experimental results for different incidence angle are fitted by a simple theoretical model based on stimulated Wood's anomalies. Various patterns were inscribed by varying input beam polarization and incidence angle. Under incoherent beam illumination, diffusion of azo-molecules is random (no correlation between them) and it is impossible to create a well defined pattern. Presence of an additional low power coherent beam causes pattern formation. Information about formed pattern in the coherent region, propagate in a self-organized manner and cover whole region of incoherent beam. Only a few percent of informed molecules is enough for self-organization. In addition, we also studied light induced birefringence and surface relief grating formation in a series of azo-polymers. Some possible applications of these patterns are presented.

Résumé

Dans cette thèse, je présente la formation de structures utilisant l'auto-organisation de molécules azo. Lorsqu'elles sont éclairées par la lumière, ces molécules subissent une photoisomérisation *trans-cis-trans* et bougent dans le film mince polymère loin des zones éclairées. Je montre qu'il est possible de former des structures spontanées sur la surface des films azopolymères (réseaux de surface) sous éclairement d'une lumière cohérente. L'orientation de la structure dépend de la polarisation de la lumière. Différentes structures peuvent être inscrites en faisant varier la polarisation du faisceau d'entrée et l'angle d'incidence. Les résultats expérimentaux pour différents angles d'incidence sont expliqués en utilisant le formalisme théorique des anomalies de Wood. D'autre part, sous illumination d'une lumière incohérente, la diffusion des molécules azo est aléatoire et il n'y a pas de corrélation spatiale entre elles. En revanche, la présence d'un faible faisceau de lumière cohérente additionnel permet de former un réseau de surface. L'information alors, inscrite sur la région éclairée par le faisceau cohérent se propage de manière auto-organisée et couvre la totalité de la région éclairée par le faisceau incohérent. Seules quelques pourcents de molécules ayant reçu de l'information suffisent à générer l'auto-organisation. Une dernière partie concerne la biréfringence photo-induite et la formation d'un réseau de surface dans une série d'azopolymères. Quelques applications possibles de ces structures sont présentées.

Acknowledgments

I will always recall with fondness my four-year stay in Angers. It has truly been a privilege and rewarding experience to work in the creative atmosphere of the group of Prof. Dr. Jean-Michel NUNZI. First and foremost I would like to thank him for his continuous guidance, support and encouragement and for being an inexhaustible source of ideas and inspiration. Without him this work would have been impossible to accomplish. He also taught me several other things aside from physics. His compassion and kindness makes me realize how lucky I am to have him as my advisor.

I am grateful to Prof. Régis BARILLE, who gave me expert guidance, generous professional support and invaluable ideas. Apart from being my co-advisor he became my best firend. Meny thanks to him for the translation of the abstract and for carfully reading of manuscript. I am deeply indebted to Dr. Sylvie DABOS-SEIGNON. She was very kind to me and always concerned about my and my family well-being. Also she introduced me to AFM mesearment technique. I am also grateful to Prof. Stanislaw KUCHARSKI and Dr. E. ORTYL for synthesizing and characterizing the compounds used in this thesis.

I would like to thank the members of my thesis jury. My special thanks go to Prof. Jacques DELAIRE, Prof. Stanislaw KUCHARSKI and Dr. Sylvie DABOS-SEIGNON for carefully reading the manuscript and for their insightful comments. I would also like to thank Prof. Pascal ROYER, Prof. Jean-Michel NUNZI, Prof. Habib TAJALLI, Prof. Régis BARILLE, and Dr. Christophe HUBERT for accepting to be in the jury.

I thank prof. André MONTEIL, director of POMA, for providing an opportunity to work in his laboratory.

I would also like to express my gratitude towards Zacaria and Hassina. They have been very kind and always ready to hear and help me.

Sincere thanks to all the POMAers for making stay in Angers such an enjoyable one: Unni-our dada , Gabi, Amel, Ali, Serge-le roi, Sudhir, Wallace, Ajay, Katherine and Fei-my officemates, Abdel, Adil and Karim. I would also like to thank all members of POMA: Marie-France, René, Alain, Nicolas, Christian, Dominique, Christophe, Marie-Thérèse for being kind to me at all the times.

I would like to thank R. FILMON and R. MALLET; Service Commun d'Imageries et d'Analyses Microscopiques (SCIAM), Angers, for some AFM images presented in this thesis.

Last, but certainly not least, I would like to give my special thanks and all my love to my wife, Sara and my dauther, Celine. Without their love, support, understanding, and caring, I would not have survived.

Finally, I would like to thank the members of my family and the family of my wife, though so far away, has always been close to us, making us feel safe.

This thesis was funded by the Ministry of Science, Research & Technology of IRAN, University of Tabriz and the FP6-EC Project IST- 511437 MicroHolas.

Table of Contents

List of Figures

Chapter I

Chapter II

Chapter III

Chapter IV

List of Tables

List of Symbols

A	Conserved birefringence
B, C	Constants
d	Thickness of film
I	Light intensity
K	Wave number
M_w	Mean molecular weight
m	Diffraction order
N	Concentration of molecules
P	Pressure
r	Ratio of molecules which move under coherent beam
Tg	Glass transition temperature
α	Polarization angle
χ	Susceptibility
δ	Divergence angle
Δn	Birefringence
ε	Extinction coefficient
ϕ	Photoisomerization quantum yield
Φ	Angle between light polarization and azo dipole axis
φ	Detection angle of luminescence
λ	Wavelength of light
Λ	Pitch of grating
μ	Viscosity
π	Phase difference
θ	Incidence angle
θ'	Diffraction angle
ρ	In plane rotation angle
σ_μ	Spatial coherence length
$\sigma_{T,C}$	Absorption cross section of the trans and cis isomers
τ	Relaxation time

List of Abbreviations

AFM	Atomic Force Microscope
Alq3	Aluminium tris (8-hydroxyquinoline)
CCD	Charge-Coupled Device
DC-EFM	Dynamic Contact-Electrostatic Force Microscopy
GB	Gigabyte
GPC	Gel Permeation Chromatography
ITO	Indium Tin Oxide
LB	Langmuir-Blodgett
LC	Liquid Crystal
LCP	Left-hand Circular Polarization
LIPSS	Laser-Induced Periodic Surface Structures
NF	Neutral Filter
NLO	NonLinear Optics
p	Transverse Magnetic(TM) polarization
RCP	Right-hand Circular Polarization
s	Transverse Electric (TE) polarization
SBN	Strontium Barium Niobate
SEM	Scanning Electron Microscope
SHG	Second Harmonic Generation
SRG	Surface Relief Grating
TB	Terabyte
THF	TetraHydroFuran
UV	UltraViolet
2D, 3D	Two, three Dimensional

"How far mathematics will suffice to describe, and physics to explain, the fabric of the body, no man can foresee."

d'Arcy Thompson (1860-1948). *On Growth and Form*. University Press, Cambridge, 2nd edition 1952.

"I find the great thing in this world
is not so much where we are,
but in what direction we are moving."
Oliver Wendell Holmes (1809-1894)

General Introduction

Our environment is a composite of numerous self-organized patterns. An interesting feature of self-organization is the appearance of patterns such as stripes, hexagons, spirals and other complex forms in very different natural or laboratory systems. Patterns on the skin of animals, the nest of social insects, bacterial colonies and so on are examples of self-organized patterns in living objects. However, a look at inorganic nature reveals that formation of pattern is not peculiar to living objects. Pattern formation is the rule also in the non-living world. Formation of galaxies, stars, clouds, rain drops, lightning, river systems, mountains, crystals, all forms of erosion - all testify the generation of ordered structures.

In optics self-organized regular patterns emerge from uniform or randomly structured input optical fields. These patterns can be used in image formation and manipulation techniques to increase the sensitivity or resolution of optical systems, the manufacturing of optical neural networks and associative memories and the use of fractal and wavelet algorithms for image compression.

It is instructive to look for common principles in the generation of all these structures to find a universal explication or model.

Surface relief grating (SRG) formation in azo-polymeric materials is a new form of grating formation in optical materials. SRG is a young branch of research and lot of questions remain unanswered. Migration (diffusion) of azo-molecules from bright region of two coherent beams interference to its dark region result grating formation on the surface of polymer film. This is a density grating and it is stable below glass transition temperature of the polymer. SRG formation is very sensitive to the parameters of optical setup. Several models have been developed to explain SRG formation, but their disadvantages make them inadequate to explain all of experimental results.

Spontaneous hexagonal pattern formation has been reported on the surface of azo-polymer thin films when exposed with a single coherent laser beam. The subject of our study concerns the self-organization of azo-molecules to form a regular pattern in a homogeneous azo-polymer film.

In this thesis we present a simple experimental method based on diffusion of azo-molecules irradiated with a uniform single laser beam. Patterns are sensitive to the polarization of laser beam and polarization multiplexing of more than two states could be achieved. As it will be

explained in this dissertation in a later chapter, it is possible to self-organize azo-molecules by illuminating them with a large incoherent laser beam accompanied with a small low power coherent laser beam. Self-organization starts from coherent beam region and propagates step by step and finally covers the whole incoherent beam region because of cooperative self-organization of azo-molecules. The last part of the study deals with the applications of this new method of self-organization. We proposed cooperative self-organization of individual azo-molecules as optical processors and logic gate for neural networks. In this study, self-organized SRG patterns are used for controlling neuron growth direction, waveguide coupler, optical diffuser and 2D chiral structure.

Overview of the thesis

The first chapter is devoted to the presentation of self-organization and a general review of azo-polymer film deformation. A brief summary of self-organization in nature and optics will be given. The idea of surface relief grating formation, proposed models and its possible applications will be developed in this chapter. We will discuss single laser beam deformation of azo-polymer films in greater details because our study is based on self-organization of azo-polymers. In this chapter we will also present our polymeric materials and experimental results about light induced birefringence and two beam SRG formation.

In the second chapter we present our experimental results of spontaneous ripple pattern formation in the azo-polymers in question. We study the effects of material structure, optical setup (power, polarization and incident angle of laser beam), reversibility and relaxation of pattern. We also present polarization multiplexing of more than two polarization states for digital optical data storage using spontaneous ripple patterns.

The third chapter will be devoted to describe incoherent light induce self-organization in azo-polymers. We will give more details on the mechanism of cooperative self-organization of azo-molecules.

In the last chapter we present some applications of self-organized patterns. We will present our experimental results of nonlocal communication of azo-molecules. We also discuss the possibility of creation of neural networks with these systems. The experimental results of other applications such as waveguide coupler, light diffuser and 2D chirality are discussed.

In the appendixes, the relation between coherency of light and visibility of interference pattern, and a simple model of azo-molecule photo-isomerization are discussed in great details.

Chapter I

Self-organization and surface relief gratings

I-1- Introduction

The scientific study of self-organizing systems is relatively new, although questions about how organization arises have of course been raised since ancient times. Many natural systems show organization (e.g. galaxies, planets, chemical compounds, cells, organisms and societies). There has been a tremendous increase in the study of self-organization in optical systems. This chapter is devoted to review of some natural self-organized systems, optical patterns and surface relief grating (SRG) formation as a basic for self-organized SRG formation in azo-polymers. We first will give introduction on the self organization in nature as well as in optics. We will present a discussion on SRG formation in azo-polymers including proposed mechanisms and some applications. We will also discuss one beam deformation of azo-materials. A new series of azo-polymers will be introduced. The results of light induced birefringence and SRG formation will be presented.

I-2- Self organization in nature

Pattern formation is a truly interdisciplinary science. The similarity in fundamental mechanisms and the accompanying mathematics brings together scientists from many disciplines, such as biology, chemistry, fluid dynamics, material science, mathematics, medicine, geophysics, ecology, physics and surface science. Natural patterns turn up all over. They show up as ripples in the sand washed by the tide or the undulating ripples of a desert dune. One sees them on the tips of one's fingers as fingerprints, as well as in the stripes of a tiger or zebra and the spots of a leopard. Honeycomb is another example of self-organization in nature (Figure I-1).

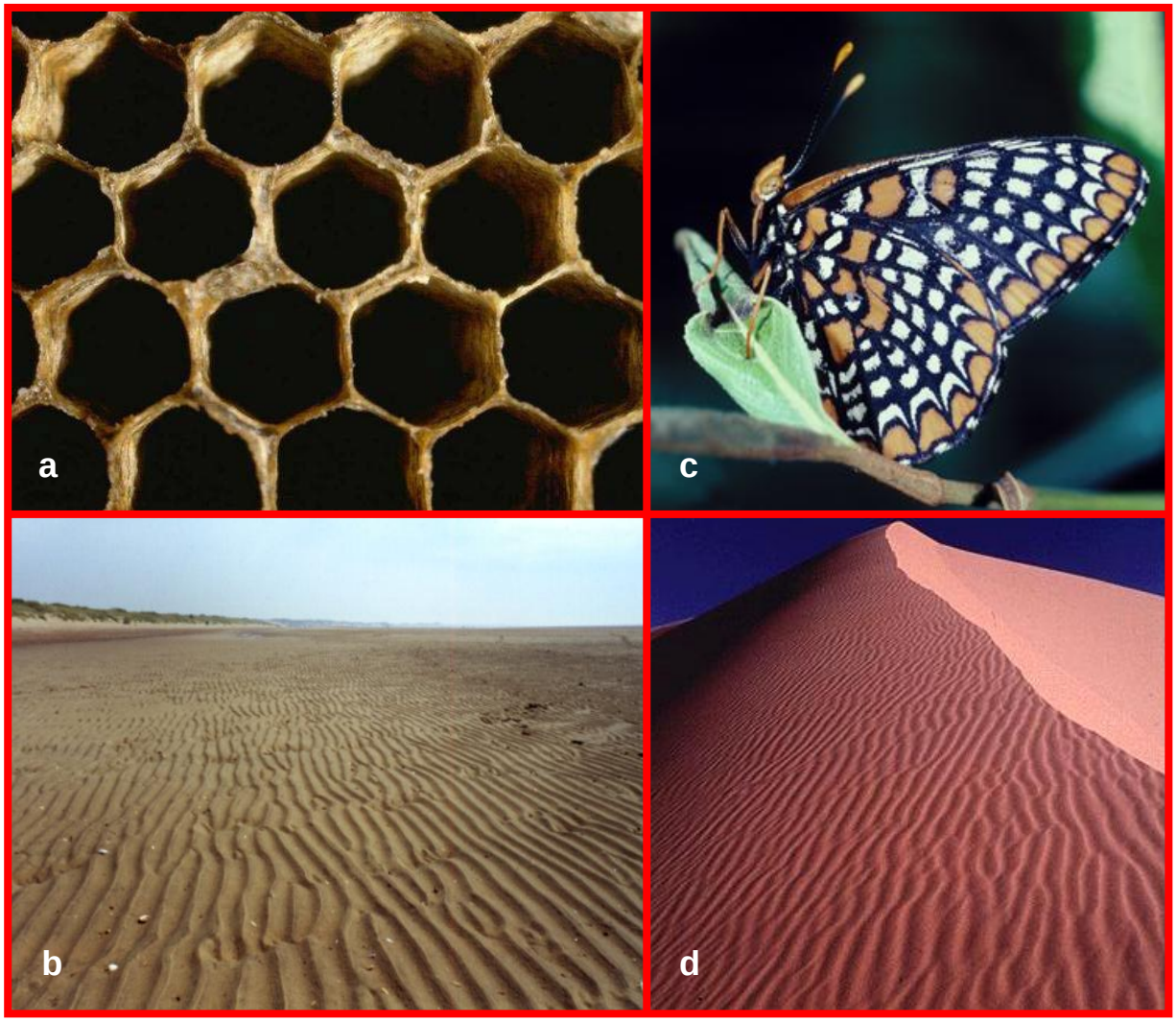

Figure I-1: Some self-organized patterns in nature. a) Hexagonal structure of honeycomb, b) Ripple pattern on the sand-flats left at low-tide c) Pattern on a butterfly's wing c) Ripples pattern of a desert dune

The honeycomb cells repeat their hexagonal symmetry to cover whole surface of a honeycomb. The honeybee is naturally able to measure dimension of honeycomb cells. Thousands of individual honeybees work cooperatively to build a regular honeycomb structure. But a beehive is not only a simple array of hexagonal cells, each comb has three separate regions: a central part for brood, a ring of cells around central part that filled with pollen and finally a large marginal region of cells for storing of honey [1, 2].

Another natural architect is the nautilus. The shell of nautilus has a logarithmic spiral shape. This precise curve develops naturally as the shell increases in size but does not change its shape. The process of self-similar growth yields a logarithmic spiral. We can find the same spiral in the horns of mountain sheep and in the path traced by a moth drawn towards a light.

The nests of social insects like ants and termites are another example of self-organization in nature. Different kind of delicate and highly regular structures have been built by numerous groups of ants and termites. For example, the nest of Apicotermes termites comprise a lot of heaped horizontal chambers connected by helix-shaped vertical passages that are used as spiral staircases [3]. From outside the nest includes a series of regularly spaced pores that open towards corridors circulating inside the internal wall of the nest.

Traditional scientific fields attempt to explain these features by referencing the micro properties or laws applicable to their component parts; for example they assumed that seashells (decorated with bold patterns of stripes and dots) were precisely specified in the genetic blueprint contained in the mollusk’s DNA. But some years ago, scientists, skilled in both biology and computer science, began to look at pattern formation in an exciting new way. One of the first things they realized was that two individuals of the same species were similar, but not identical. Like the fingerprints on one's hand, they are alike yet not alike. This simple observation led them to hypothesize that the patterns on shells, the stripes on a zebra, and the ridges on our fingertips are not rigidly predetermined by the genetic information inside the cell's nucleus. Organisms are not built as a house is built, by meticulously following an architect's plans. Instead, genes appear to take a more generalized approach, specifying sets of basic rules whose implementation results in organized form and pattern.

In the day life we can see several type of self-organization like cubic structure of salt crystals and six-sided stars or hexagonal needles shape of snowflakes.

All of natural patterns are not regular; we can find some irregular patterns like billowy clouds, flickering flames, lightning bolts, the pattern of veins on a leaf and the architecture of the lung's passageways. Such objects have been called fractals and they are not simply random system. They often display an underlying structure, a kind of regular irregularity.

One of the greatest biological mysteries yet to be solved is how a single egg, apparently without structure, becomes a child. The human cell does not contain enough information to specify the location and connections of every neuron in the brain. Therefore, much of the body's organization must arise by means of more simple developmental rules. In nature many systems display extreme complexity, although their fundamental components may be rather simple. The brain is an organ of high complexity, but an isolated neuron cannot think. Complexity results from interactions between large numbers of simpler components. Simple interactions between a large numbers of subunits or components of a system could yield intricate and beautiful patterns.

The study of complexity provides new insights into how patterns develop in nature. One exciting finding is that order often arises spontaneously from disorder; patterns can emerge through a process of self-organization.

Self-organized systems are structure formations without any clear association from outside of the system. Any system that takes a form that is not imposed from outside (by walls, machines or forces) can be said to self-organize. In other words, a self-organization results from the interactions among the components of the system and is an internal phenomenon. The organization can develop in either time or space, maintain a stable form or show transient phenomena. The size of self-organized patterns typically is much larger than the size of individual components and in some natural patterns their ratio can reach 10^4-10^5. General resource flows within self-organized systems are expected (dissipation), although not critical to the concept itself. For example in spite of conflicting actions between insects, collective structures which fulfil numerous functional and adaptive requirements are produced [4]. Noise (fluctuations) can allow metastable systems to escape one basin and to enter another, thus over time the system can approach an optimum organization or may swap between the various patterns, depending upon the size and nature of the perturbations. For instance, individual insects are not able to process a large quantity of information but simply their response to stimulus from other individuals or environment (these stimulus don’t carry any

signs, simply they are attractive or repulsive, activating or inhibiting) lead to pattern formation. The individual units just have access to local information [5, 6].

The field of self-organization seeks general rules about the growth and evolution of systemic structure, the forms it might take, and finally methods that predict the future organization that will result from changes made to the underlying components (past construction sets the stage for new building actions)[7].

With simple computer programs that simulate a natural process we can visualize most of simple self-organized patterns in nature. Cellular automata are one of the well known categories of computer programs in this field. They are simulations played on the equivalent of a computer checkerboard. In the simplest version, one starts with a single row of cells. Concerning seashells, each square of the checkerboard represents a hypothetical cell along the edge of the snail's mantle. The cell could either produce a colour pigment or none at all. By developing the system, the state of cell (whether it produces pigment or not) is determined by the initial state of cell and the state of its nearest neighbour cells on either side. We can assume a rule for pigment production; if the cell and one of its nearest neighbours currently produce pigment, then the cell will continue to produce pigment in the future. The state of the cells changes over time and each row of the checkerboard displays the next step in the process, just as the growing shell displays its developmental history. It is interesting to know that even if one starts out with a completely random array of cells at the beginning, a remarkably organized pattern emerges (order arises from disorder). More complicated cellular automata models have been developed to explain the stripes on zebras, the mottled patterns on fish, the growth of snowflakes, and even clustering of neurons in the brain.

Nevertheless, studying nature requires timescales appropriate for the natural system, and this restricts our studies to identifiable qualities that are easily reproduced, precluding investigations involving the full range of possibilities that may be encountered. However, mathematics deals easily with generalised and abstract systems and produces theorems applicable to all possible members of a class of systems. By creating mathematical models, and running computer simulations, we are able to quickly explore large numbers of possible starting positions and to analyse the common features that result. Even small systems have almost infinite initial options, so even with the fastest computer currently available, we usually can only sample the possibility space. Yet this is often enough for us to discover

interesting properties that can then be tested against real systems, thus generating new theories applicable to complex systems and their spontaneous organization.

I-3- Pattern formation in optics

Several researches have been developed on the study of the structure formation in optical systems because optics has several advantages such as flexibility and the simplicity of handling. The interaction of an intense laser beam with a nonlinear medium (a medium in which the optical properties depend on the intensity of the incident light) can lead to spontaneous patterning. The interplay of spatial coupling by diffraction and nonlinearity is responsible for the pattern formation. There are various configurations in which optical pattern formation is studied. Arecchi et al. reviewed pattern formation in NLO (Nonlinear Optics) materials in reference 8.

Single mirror feedback is one of the common optical setup to demonstrate optical pattern formation (Figure I-2). The system is a thin nonlinear medium irradiated from one side by a spatially smooth collimated beam with a feedback mirror a distance *d* away to generate a counterpropagating beam in nonlinear medium. Usually diffusion length of materials is much larger than light wavelength and we can neglect gratings with small pitch arising from interference of forward and backward beams. These counterpropagating beams interact in media to create spatial instabilities that lead to regular pattern formation.

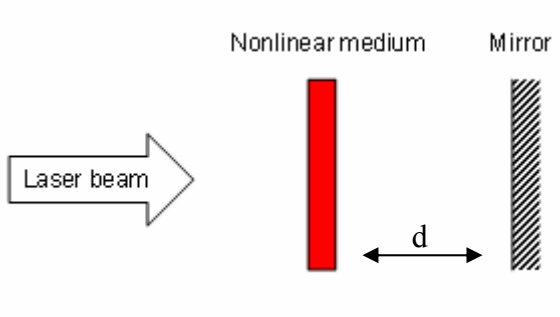

Figure I-2: Single-mirror feedback experiment

Several types of patterns like; stripes, squares, triangles, hexagons and more exotic quasiperiodic or superlattice planforms in different types of NLO materials including atomic vapours, liquid crystals, and photorefractive crystals have been produced [9-18]. Recently Aumann et al. report the possibility of selection between hexagons and stripes or squares in a

pattern forming optical system. A heated cell (length L = 15mm) containing sodium vapour in a buffer gas atmosphere has been irradiated by a laser beam. The cell temperature was about 340°C (sodium particle density was approximately 10^{14} cm^{-3}) [19]. By increasing the ellipticity of the laser beam polarization from zero they obtained a transition from squares (Figure I-3-a) to positive hexagons (Figure I-3-b) followed by stripes (Figure I-3-c) and finally by negative hexagons in sodium vapour (Figure I-3-d).

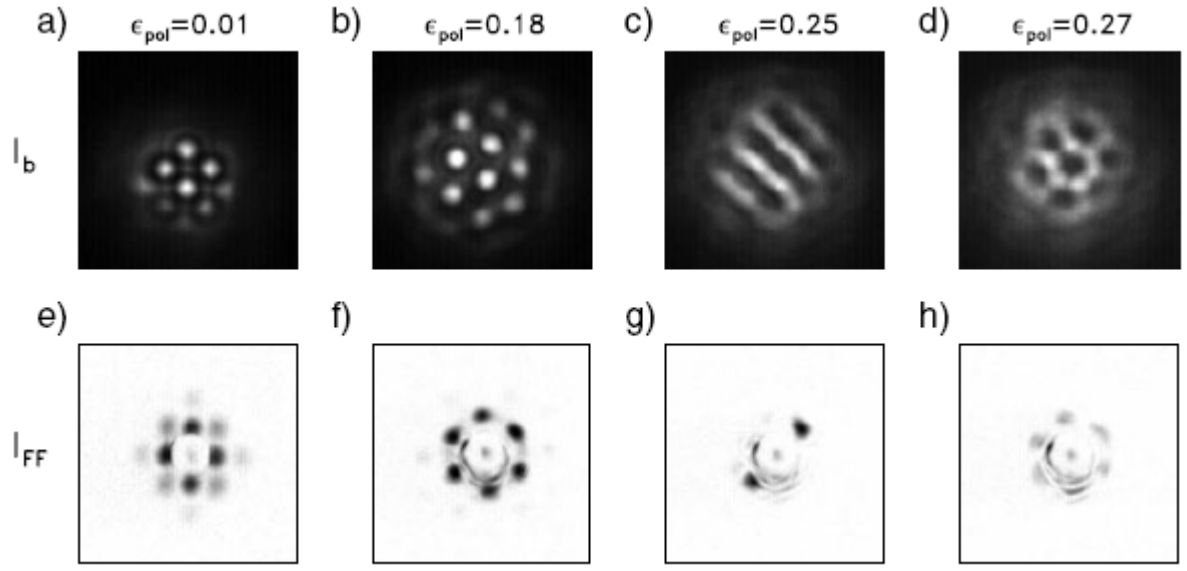

Figure I-3: Transition sequence from squares to positive hexagons, to stripes and finally to negative hexagons for increasing positive ellipticity. a)–d) Total near field intensity distribution of the backward laser beam. e)–h) Optical Fourier transform of the transmitted laser beam [19].

Bennink et al. reported feedback free hexagonal pattern formation by simple passage of a single laser beam through sodium vapour cell [20]. Because of nonlinear optical self-action effects, when a laser beam propagates through sodium vapour, it breaks up into three components. Honeycomb pattern formation in far-field is the result of coherent superposition of the diffraction pattern from each of the three beams (figure I-4).

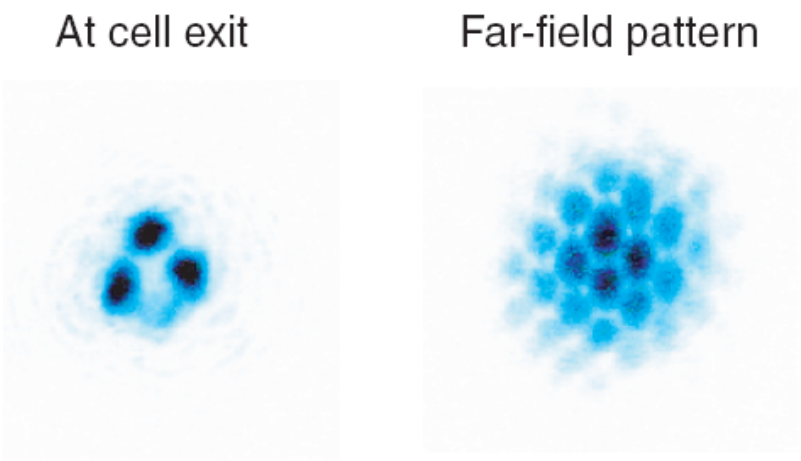

Figure I-4: Example of pattern formation as observed in the near field (left) and far field (right). Typical conditions were input power, 150 mW; input beam diameter, 160 mm; laser frequency, 2 GHz blue-detuned from the sodium D2 line; cell length, 7 cm; and number density, 8 x10^{12} cm^{-3} [27].

They have presented deviation of patterns by varying laser power and laser frequency. In the particular case of a 47 mW laser power, they observed strip patterns in far-field. The laser powers for this pattern formation are above the self-trapping power of system.

The coherence of optical beams is necessary for interference effects and consequently is an important parameter in optical pattern formation. But several studies of pattern formation with partially spatially incoherent light, created from a coherent laser beam, have shown that coherent light is not mandatory for pattern formation, only there is an instability threshold for such systems in comparison with coherent light [21-27].This threshold can be related to the balance point between constructive (nonlinear self-focusing) and destructive (linear diffusion) effects and depends on the correlation statistics [28]. The pattern formation with incoherent light is possible when the response time of the nonlinearity of system is much longer than the characteristic time of light random phase fluctuations so speckle structure doesn't perturbed pattern formation.

Schwartz et al. presented spontaneous pattern formation in (Strontium Barium Niobate) SBN: 60 photorefractive crystal with an incoherent white light originating from an ordinary incandescent light bulb [29]. Figure I-5 shows experimental setup and the light intensity distribution at the crystal output. Spatial correlation distance and temporal coherence length of light source were ~8 mm and 0.5 mm respectively. Nonlinearity was controlled by an externally applied bias field parallel to C axis of crystal. The extraordinarily polarized portion

of unpolarized input light (parallel to the *c* axis) propagates in a nonlinear fashion and serves as a signal beam .The ordinary polarized beam serves as background beam. A CCD camera is used to monitor the intensity distribution of extraordinary beam. Below threshold they did not observe pattern. Above threshold a stripe pattern with period of 40 μm is formed and by future increasing applied electric field, pattern becomes dipper.

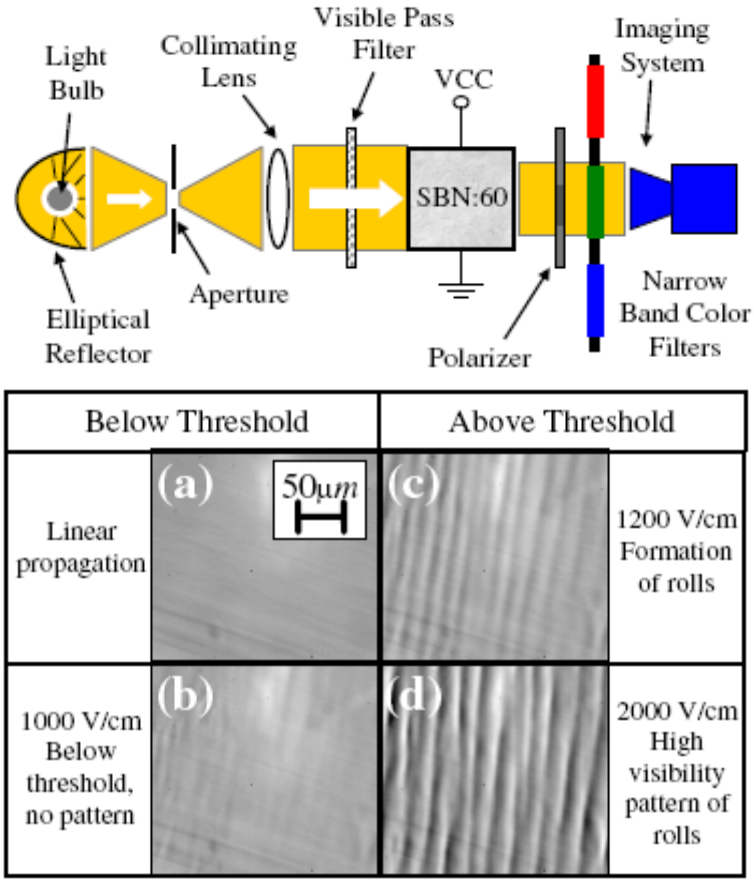

Figure I-5: up) Experimental setup; down) Total intensity distribution at the output face of the crystal: homogeneous intensity at linear propagation (a) and stable nonlinear propagation below the modulational instability threshold (b); pattern formation above threshold (c), (d) [29].

The experimental results showed that for all temporal frequencies, threshold value and periodicity of pattern are the same which confirm that pattern formation in this system is a collective phenomenon.

For the first time Hubert et al. showed that, under certain experimental conditions, it is possible to observe a two dimensional hexagonal structures on the surface of an azo-polymer

with a single continuous wave laser beam [30, 31]. It is important to note that this process of structuring is different from that leading to the formation of SRGs: here only one beam is necessary against two for the formation of SRGs. Moreover, in the case of SRG formation, the azo molecules suffer a bright and dark zones corresponding to interferences pattern of two writing coherent beams and they follow this pattern with a phase difference of π to create SRG. In the case of spontaneous patterning, on the scale of the molecule, there are no intensity or polarization gradient. In whole of irradiated surface, it does not have a priori dark zones where the molecules are not excited and all the molecules are continuously subjected to the laser light. Figure I-6 shows the setup used for this experiment.

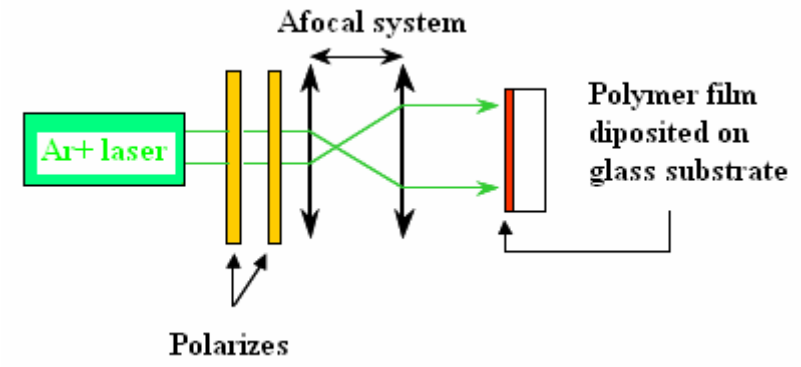

Figure I-6: Experimental setup for spontaneous patterning on azo polymer surface. Scheme taken from Ph D thesis of Christophe Hubert (CEA-R-6038, September 2003).

A typical atomic force microscope (AFM) image of the self-organized structure on the surface of an azo-polymer is presented in the figure I-7. The laser irradiation induced regularly spaced structures with the form of circles. If six circles are considered, it is possible to define a hexagon whose principal axis is directed according to the direction of polarization of the light. In the image, this hexagon is schematized in white. The obtained structures are not perfectly regular.

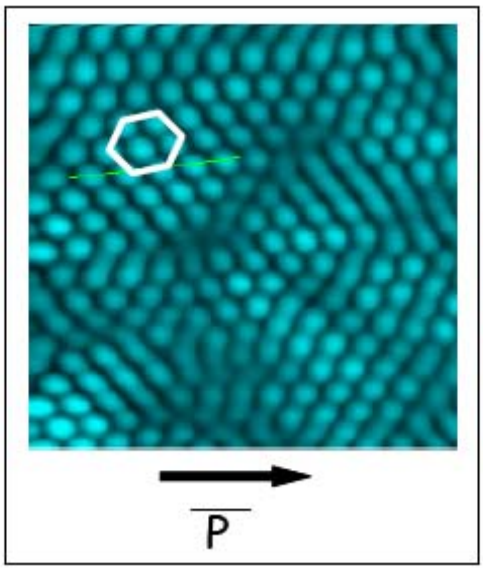

Figure I-7: Typical AFM image of self-organized structure on the surface of an azo-polymer film. The thickness of film is 220 nm. The structure inscribed by a p polarized Ar+ laser (514 nm, 300 mW/cm^2) for 100 minutes [Ph D thesis of Christophe Hubert (CEA-R-6038, September 2003)].

The period of these structures were in the order of laser light wavelength and the amplitudes were several hundreds of nanometre. The direction of orientation of the structures follows the direction of laser beam polarization. And for circular polarization there is no defined direction for the orientation of induced structure. For the same experimental conditions, the polarization direction doesn't affect the modulation amplitude of the structure. The modulation amplitude was sensitive to the incidence angle and strongly decreases as the incidence angle exceeds 5° for both *s* and *p* polarization [32]. The growth rates of induced structures were increased linearly by the intensity of irradiation. Also the results showed that these structures are not totally reversible not only optically but also by increasing the temperature of samples over Tg of polymer film.

As a direct application of such structures, Hubert et al. have studied the effect of two dimensional (2D) microstructuring on the photoluminescence properties of an Organic Light-Emitting Diode [33]. Figure I-8 shows the fabricated device structure. The results showed that the amount of photo-luminescent light extracted from the patterned part of the device was 3.4 times larger than extracted from the nonpatterned part. Extracted light intensity significantly depends on the observation angle.

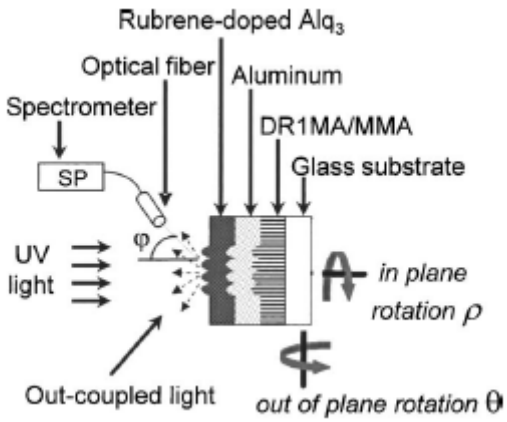

Figure I-8- The structure of the light-emitting device: a rubrene-doped Alq_3 light-emitting layer is evaporated onto the aluminum-coated DR1MA/MMA structured polymer film. The out-coupled light from the device resulting from photo-excitation of the luminescent layer with ultraviolet UV light (λ^{exc}=350 nm) is collected by an optical fiber set at an angle φ from normal incidence and analyzed by a spectrometer. Only one part of the polymer surface is patterned for comparison with a nonpatterned structure. The sample can be rotated around different axes: out of plane (angle θ) or in plane (angle ρ). Thicknesses of the DR1MA/MMA, aluminum and Alq_3 layers were, respectively, equal to 500, 100, and 100 nm [33].

I-4- Photochemistry of azobenzene

Azobenzene is a chemical compound composed of two phenyl rings linked by an N=N double bond. The term *azobenzene* or simply *azo* is often used to refer to a wide class of molecules that share the core azobenzene structure, with different chemical functional groups extending from the phenyl rings (technically, these compounds should be referred to as *diazenes*). The azobenzene compounds strongly absorb light, and were historically used as dyes in a variety of industries. One of the most intriguing properties of azos is photo-isomerization behavior between two isomers, the trans and cis configurations [34]. The two isomers can be switched with particular wavelengths of light: ultraviolet or blue light, which corresponds to the energy gap of the π-π* (S_2 state) transition, for trans-to-cis conversion, and blue light, which is equivalent to that of the n-π* (S_1 state) transition, for cis-to-trans isomerization. For a variety of reasons, the cis- isomer is less stable than the trans (for instance, it has a distorted configuration and breaks the aromaticity of the trans configuration). Thus, cis-azobenzene

will thermally relax back to the trans via cis-to-trans isomerization. The trans isomer is more stable by approximately 50 kJ/mol, and the barrier to photo-isomerization is on the order of 200 kJ/mol [35-37].

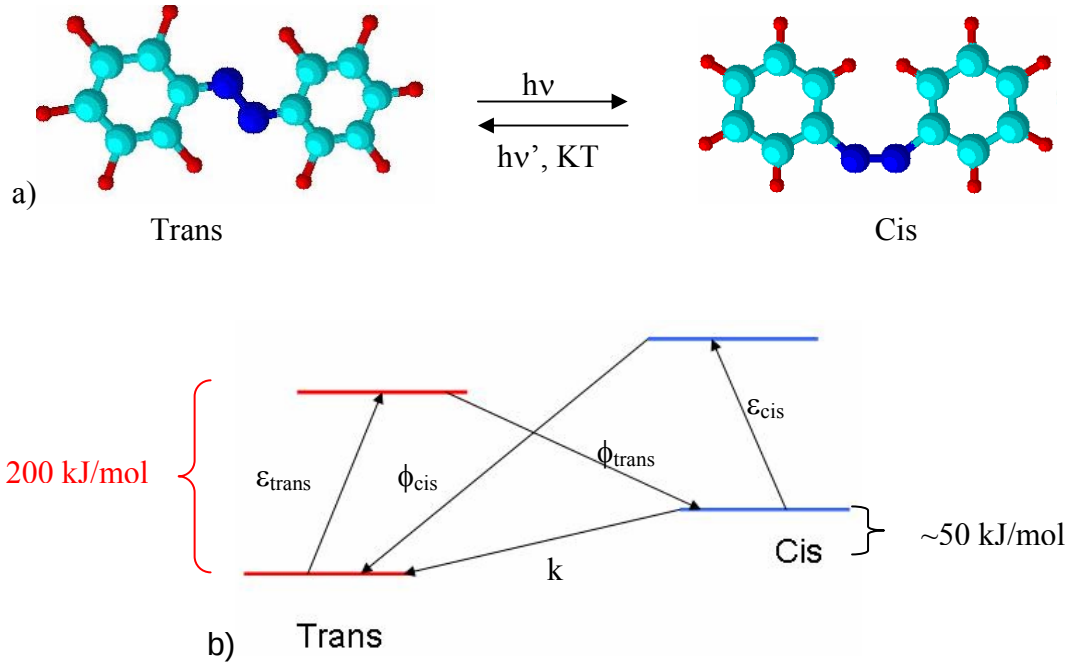

Figure I-9: Azobenzene can be converted from the *trans* to the *cis* state photochemically, and will revert back to the stable *trans* state thermally. Alternately, the *cis* to trans conversion can be effectuated with a distinct wavelength of light. (b) Simplified state model for azobenzene chromophores. The exinction coefficients are denoted ε, whereas the quantum yields for the photoisomerizations are labelled ϕ. The rate of thermal relaxation is denoted by k.

The exact wavelength at which azobenzene isomerization occurs depends on the particular structure of each azo molecule, but they are typically grouped into three classes [34]: the azobenzene-type molecules, the amino-azobenzenes, and the pseudo-stilbenes (Figure I-10).

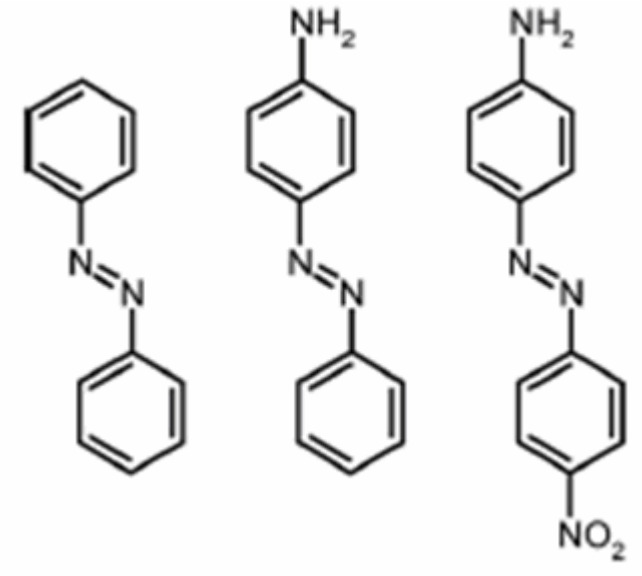

a b c

Figure I-10: Examples of azobenzene molecules that fall into the three spectroscopic classes: (a) azobenzenes (b) aminoazobenzenes, and (c) pseudo-stilbenes.

These azos are yellow, orange, and red, respectively, owing to the subtle differences in their electronic absorption spectra. The compounds similar to the unsubstituted azobenzene exhibit a low-intensity n-π* absorption in the visible region, and a much higher intensity π-π* absorption in the ultraviolet. Ortho- or para-substituted azo dyes with electron-donating groups (such as aminos), are classified as amino-azobenzenes, and tend to closely spaced n-π* and π-π* bands in the visible. The pseudo-stilbene class is characterized by substituting the 4 and 4' positions of the two azo rings with electron-donating and electron-withdrawing groups (that is, the two opposite ends of the aromatic system are functionalized). This push-pull configuration results in a strongly asymmetric electron distribution, which modifies a host of optical properties. In particular, it shifts the absorption spectra of the trans- and the cis-isomers, so that they effectively overlap. Thus, for these compounds a single wavelength of light in the visible region will induce both the forward and reverse isomerization. Under illumination, these molecules will be constantly cycling between the two isomeric states. This, in part, explains why the pseudo-stilbenes give rise to the most efficient photo-response, especially in cases where motion of the azo chromophore is required. In cases where the azo isomerization is being used as a switch, or where a two-state system is desired, this overlap of the spectra is obviously undesirable. The photo-isomerization of azobenzene is extremely rapid, occurring on picosecond timescales [38, 39]. The thermal back-relaxation varies greatly depending on the compound: usually hours for azobenzene-type molecules, minutes for

aminoazobenzenes, and seconds for the pseudo-stilbenes. The energy barrier for this thermal isomerization is on the order of 90 kJ/mol [40, 41]. Even in the case of the parent azobenzene, the *cis* lifetime is not long enough for the molecule to be treated as a stable two state system. Considerable research has gone into elongating the *cis* lifetime, which would then allow the two states to be selected without unwanted interconversion (useful in applications that require two stable states, such as data storage). Typically, bulky substituents have been used to hinder the thermal back reaction. For instance, a polyurethane with the azo chromophore in the main-chain exhibited a lifetime of 4 days (thermal rate-constant of $k = 2.8\times10^{-6}$ s^{-1}, at 3°C) [42], and an azo substituted with bulky pendants had a lifetime of 60days ($k < 2\times10^{-7}$ s^{-1}, at room temperature) [43]. The inherent conformational strain of macrocyclic azobenzene compounds has been used to create a much more stable *cis* populations, with lifetimes of 20 days ($k = 5.9\times10^{-7}$ s^{-1}) [44], 1 year (half-life 400 days, $k =2\times10^{-8}$ s^{-1}) [45, 46], or even a lifetime of 6 years ($k = 4.9\times10^{-9}$ s^{-1}) [47]. Similarly, using the hydrogen-bonding of peptide segments, a *cis* lifetime of <40 days ($k = 2.9\times10^{-7}$ s^{-1}) was achieved [48]. In extreme cases, the *cis* species can be stabilized by completely preventing isomerization: by attachment to a surface [49], synthesis of ring-like molecules [50], or even, in the case of the parent azobenzene, crystallization of the *cis* form [51,52]. These experiments again emphasize that the azo isomerization requires a large geometric change in molecular configuration. The thermal back-relaxation is generally first-order, although the distribution of highly constrained configurations that arise in a glassy polymer matrix can lead to anomalously fast decay components [53-56]. Accordingly, higher matrix crystallinity increases the decay rate [57].

The mechanism of isomerization has been the subject of some debate, with two pathways identified as viable: a rotation about the N=N bond, with disruption of the double bond, or via an inversion, with a semi-linear and hybridized transition state (Figure I-11). It has been suggested that the trans-to-cis conversion occurs via rotation into the S_2 state, whereas inversion gives rise to the cis-to-trans conversion. It is still under discussion which excited state plays a direct role in the series of the photoisomerization behavior. However, the latest research on femtosecond transition spectroscopy has suggested that the S_2 state undergoes internal conversion to the S_1 state, and then the trans-to-cis isomerization proceeds. The conversion from *trans* to *cis* reduces the distance between the ends of the moiety (between the 4 and 4' positions): from 0.99 nm in the *trans* state to 0.55 nm in the *cis* state [58-60]. This change in geometry results in a change in the molecular dipole, increasing it from essentially zero in the *trans* state to 3.1 D in the *cis* form (for the parent azobenzene) [51] . The free

volume requirement of the *cis* is larger than the *trans* [61], with estimates of approximately 0.12 nm^3 required for isomerization to proceed via an inversion of the azo bond [55, 62], and 0.28 nm^3 for a rotation about the azo bond [42]. This large molecular change generates a nanoscale force, which has been successfully measured in single-molecular force spectroscopy experiments [63, 64].

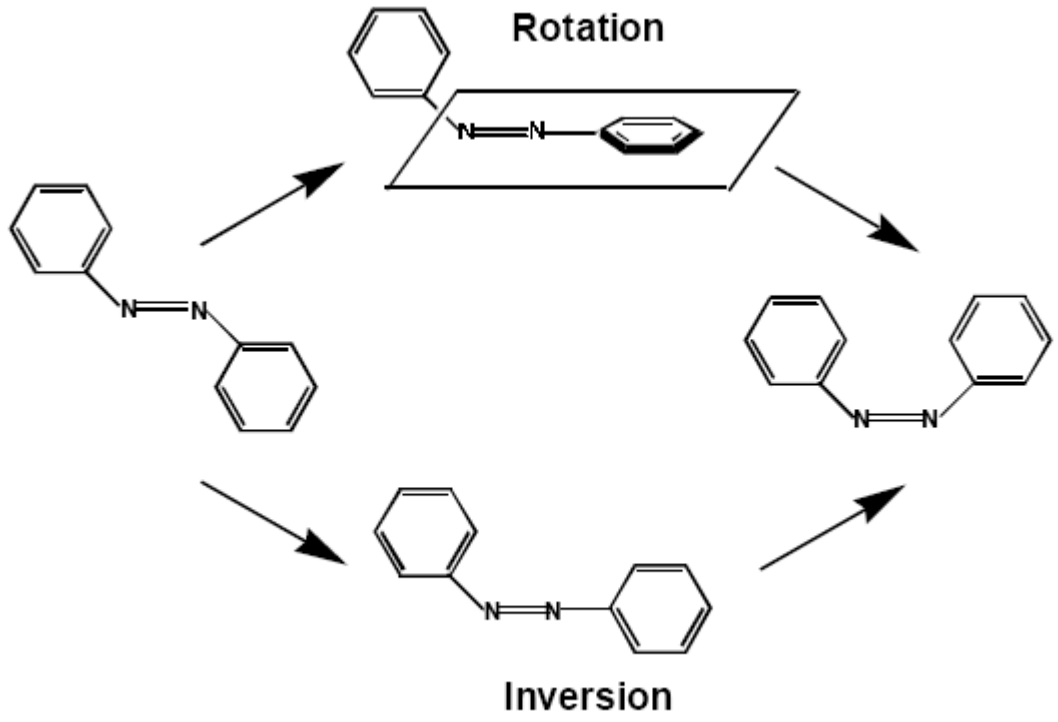

Figure I-11: Rotation and inversion mechanisms pathways for azobenzene isomerization process.

Azobenzene units are extremely sensitive to packing and aggregation, with π–π stacking causing shifts in the absorption spectra, and changes in photophysical properties. When the azos are aligned in a parallel fashion (head-to-head), they are called J-aggregates, and give rise to a red-shift compared to the well-isolated chromophore spectrum. If the dipoles are instead antiparallel (head-to-tail), they are called H-aggregates, and one observes a blue-shift. The local packing can be influenced, of course, by solvent conditions and molecular architecture. For instance, local water concentration in tetrahydrofuran (THF) solutions can markedly change the azo isomerization behaviour [65]. In fact, even a small water fraction (a few percent) was found to be sufficient to give rise to measurable differences [66]. In these cases, as water content increases, the azo units are driven to aggregate. This aggregated population necessarily exhibits a hindered isomerization.

I-5- Photo-induced orientation

The photo-isomerization of azobenzene is a unique form of light-induced molecular motion. This motion can also lead to motion on larger length scales. For instance, polarized light will cause the molecules to isomerize and relax in random positions. However, those relaxed (trans) molecules that fall perpendicular to the incoming light polarization will no longer be able to absorb, and will remain fixed (the probability of photon absorption varies as $\cos^2\Phi$, where Φ is the angle between the light polarization and the azo dipole axis.). Thus, there is a statistical enrichment of chromophores perpendicular to polarized light (orientational hole burning) (Figure I-12). The photo-orientation is reversible: isotropy can be restored using circularly polarized light, or a new orientation direction can be selected by irradiation with a new polarization.

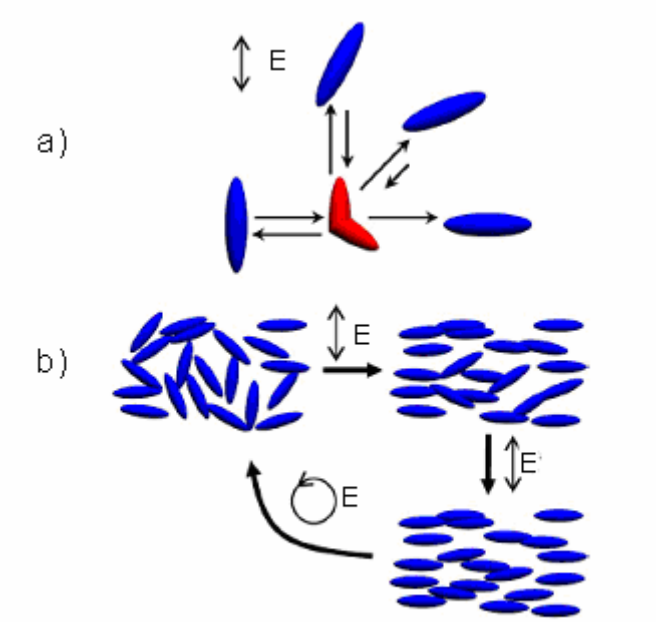

Figure I-12: The mechanism of statistical photo-orientation of azo molecules. (a) The molecules aligned along the polarization direction of the incident light will isomerize, and take on a new random orientation. The molecules that lie perpendicular to the polarization of light cannot absorb a photon and remain fixed. (b) An initially isotropic distribution of chromophores will become progressively aligned with polarized irradiation. Irradiation with circularly polarized light can restore isotropy [K. G. Yager, C. J. Barrett, Journal of Photochemistry and Photobiology A: Chemistry, 2006, **182**, 250–261].

Polarized irradiation will make an azo-material anisotropic and therefore optically birefringent and dicroic [67, 68]. In these systems, the physical and optical properties such as

the absorption spectrum, dipole moment, refractive index, and molecular conformation can be reversibly changed through the trans-cis isomerization of azobenzene. This photo-orientation can also be used to orient other materials (especially in liquid crystal systems). For instance, it has been used to selectively orient liquid crystal domains, and to create NLO materials and high density data storage [69-74]. Azo isomerization can also be used as switching elements for microelectronics and to photo-switch the liquid crystal phase of a material [75-79]
The azobenzene moiety is robust and adaptable, having been incorporated into a wide variety of different system types, including: small molecules, doped into polymeric systems, supramolecular assemblies, liquid crystals, and covalently bonded to crystalline or amorphous polymers. Although doping is an easy and convenient way to include azobenzene in a matrix of choice, it is usually found that mobility leads to aggregation and crystallization of the azo molecules, making the resultant films heterogeneous and optically cloudy. Thus, by far the most often-employed incorporation strategy is to covalently bind the azo chromophore to a polymer backbone [80].

In 1995, it was discovered that exposing a thin film of azo-polymer to a light intensity (or polarization) gradient leads to spontaneous surface patterns [81, 82]. In essence, the polymer material will reversibly deform so as to minimize the amount of material exposed to the light. This phenomenon is not laser ablation, since it readily occurs at low power and the transformation is reversible. The exact mechanism of this surface holography is still unresolved, although it is clearly related to the azobenzene isomerization.

I-6- A new series of azo-polymers

In this work we present a series of new azo copolymers for light induced phenomena. The chromophoric monomers were derivatives of azobenzene containing heterocyclic sulfonamide moieties. The monomers of the methylacrylate type contained aliphatic spacers of different length between chromophoric and methylacrylic groups. These monomers were polymerized in order to obtain homopolymers and copolymerized with butyl 2-methylacrylate (MB) and 2-ethylhexyl acrylate (AI) to get copolymers containing various percentages of chromophoric units [83].
The structures of copolymers that used in this work are presented in figure I-13.

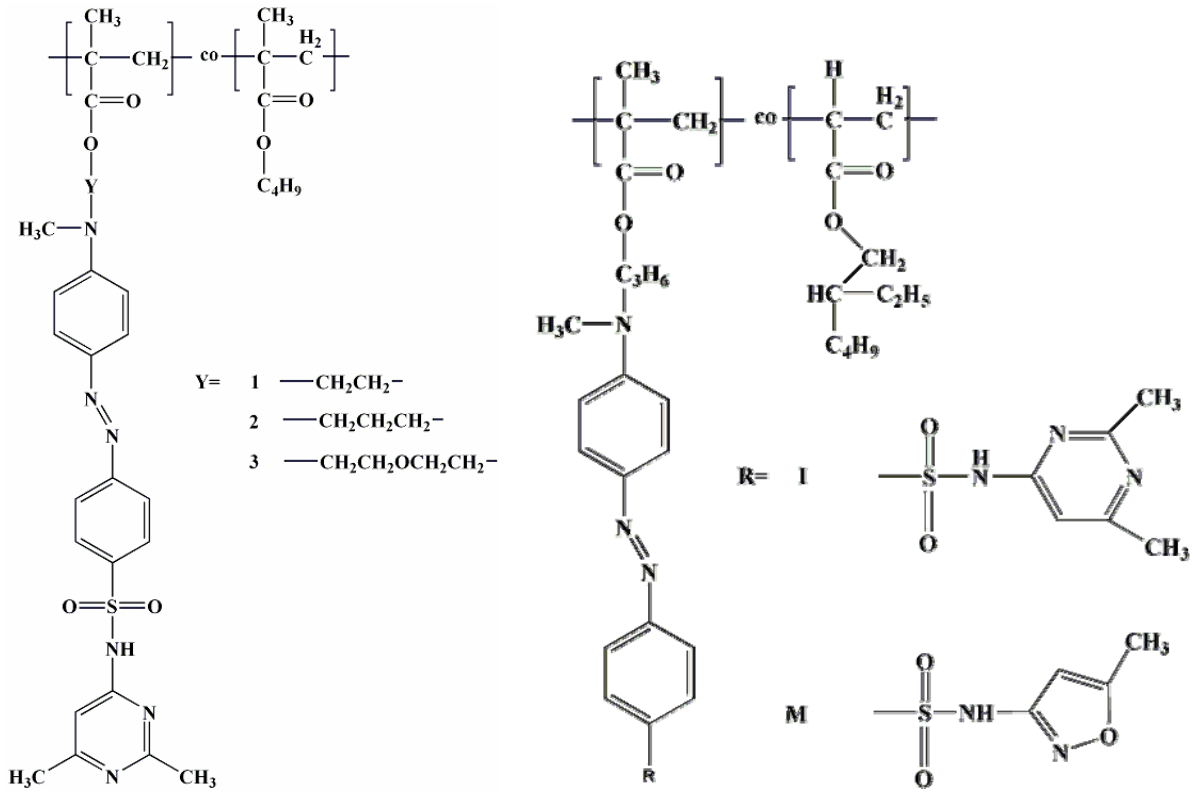

Figure I-13: Chemical structures of copolymers: a) MBYI and b) AI2I&M copolymer series.

I-6-1-Characteristics of the monomers and polymers [83]

The purity of monomers and polymers was determined by thin layer chromatography using Merk Silicagel aluminium foils.

Melting temperatures (M.p.), maximum absorbance wavelength (λ_{max}) and dipole moments (μ) of side chain units are presented in table I-1. Symbols follow SMILES notation. Melting temperatures of the monomers containing sulfisomidine heterocyclic ring (2, 6-dimethylpyrimidin-4-yl) of the YI(IZO-n) series are higher than sulfamethoxazole monomer 2M(MET-2). Dipole moments have been calculated by Gaussian RHF/3-21g for isolated molecule. The dipole moment of trans isomer of 2I is grater than 3I and 1I and that of 2M is smaller than all of others.

Table I-1- Characteristics of monomers

Monomer	M.p (K)	λ_{max} (nm)	$\mu / 10^{-30}$ (C m)	
			trans	cis
1I(IZO-1)	457.5-461	440	34.10	27.84
2I(IZO-2)	448-451	446	35.29	17.53
3I(IZO-3)	401-403	450	34.65	13.28
2M(MET-2)	395-397	454	29.31	14.14

IZO-1:2-[{4-[(E)-(4-{[(2,6-dimethylpyrimidin-4-yl)amino]sulfonyl}phenyl)diazenyl]phenyl} -(methyl)amino] ethyl 2-methylacrylate. **IZO-2** : 3-[{4-[(E)-(4-{[(2,6-dimethylpyrimidin-4-yl)amino]sulfonyl}phenyl) diazenyl] phenyl}-(methyl)amino] propyl 2-methylacrylate. **IZO-3** : 2-{2-[{4-[(E)-(4-{[(2,6-dimethylpyrimidin-4-yl) amino]sulfonyl}phenyl)diazenyl] phenyl}-(methyl)amino] ethoxy } ethyl 2-methylacrylate. **MET-2** : 3-(methyl{4-[(E)-(4-{[(5-isoxazol-3-yl)amino]sulfonyl}phenyl)diazenyl]phenyl}-amino) propyl 2-methylacrylate.

Mean molecular weight, $\overline{M}_W$, of polymers has been determined by GPC using Waters 917 columns, RIDK-102 detector and APEX ver. 3.1 recorder. A mobile phase was γ-butyrolactone and molecular weight referes to polystyrene standards.

A Mettler Toledo DSC has been used for glass transition temperature (Tg) determination of polymers with scanning of 20K/min.

Table I-2 shows glass transition temperature, wavelength of maximum absorbance and absorbance at the working wavelength of the polymers. MB1I has highest and AI2M the lowest Tg. The maximum absorption wavelengths are around 435 nm and MB3I has highest absorption for the concentration of 50 mg/ml of polymers in the solution.

Table I-2- Characteristics of the polymers

Polymer	$\overline{M}_n$	$\overline{M}_W$	Tg (°C)	λ_{max} (nm)	A_{488}
MB1I(IZO-1/20 MB)	12600	15900	86.2	433	1.3
MB2I(IZO-2/20 MB)	10750	15800	71.1	438	1.33
MB3I(IZO-3/20 MB)	11750	16500	71.5	435	1.55
AI2I(IZO-2/20 MB)	11450	16250	57.5	435	1.13
AI2M(MET-2/20 AI)			53	445	1.42

MB- butyl 2-methylacrylate, AI- 2-ethylhexyl acrylate

I-6-2-Absorption spectrum

The thin films were made by spin coating of THF solutions of the polymers on the glass substrate. The concentration of polymer in the solution was 50-70 mg/ml. After spin coating, we put the film at temperature over Tg of polymers for a night in an oven to remove the

remained solvents. The thicknesses of the polymeric thin films were measured by Dektak-6M Stylus Profiler and were in the range of 0.5-1 μm for different concentrations and speed of coating. The UV-visible spectra were made using lamda19 spectrophotometer. Figure I-14 shows the spectrum of the polymer films.

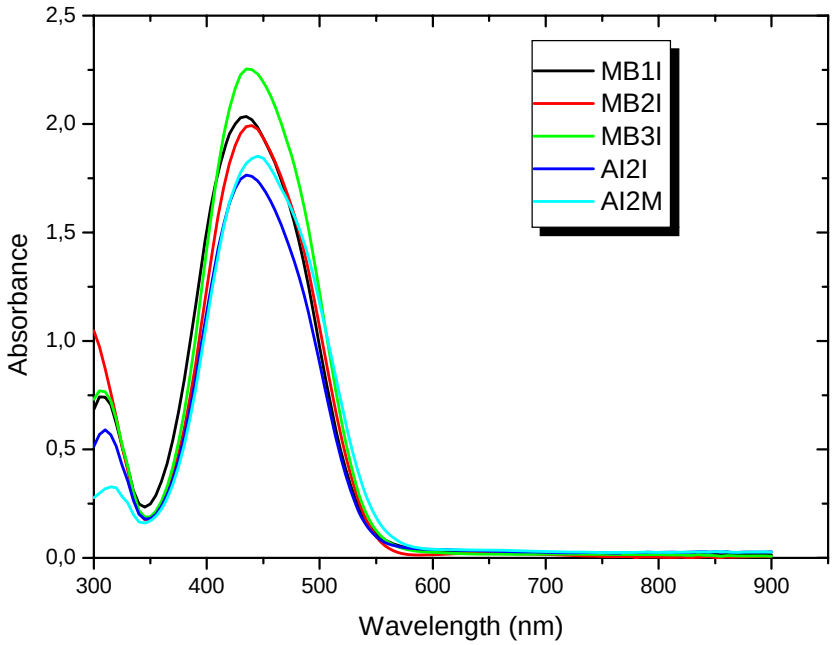

Figure I-14: Absorption spectrum of azo-polymer films

It is obvious from figure I-14 and the data of table I-2 that absorption spectra (bonds) lies in the blue-green region of spectrum and for wavelengths bigger than 600 nm the films are transparent. For this reason we can use blue-green lasers, such as Ar^{+} or diode lasers, as writing beam to create light-induced birefringence, two beams surface relief gratings and self-organized structures and red He-Ne laser as probe.

I-7- Light induced birefringence

The first report on photoinduced anisotropy in azo polymer was about the change of its physical property, dichroism, under illumination with polarized light [84]. Photoinduced dichroism was explained by the reorientations of the photon-absorbing molecules to a preferred direction [85, 86]. Later, it was known that this photoinduced rotation of molecules was associated with the photoinduced isomerization of azobenzene [87, 88]. Since the photoinduced dichroism and birefringence of azobenzene were applied to optical holography [89-92], azobenzene containing polymers have been widely studied in the past decade because of their capability of application for reversible optical data storage.

The mechanisms of inducing the birefringence by linearly polarized light can be simply understood. First of all, azo dye molecules in the coated layer in the film are initially in the more stable trans state, and the direction of the long axis of each molecule is random. When a linearly polarized light is illuminating the film, the trans molecule absorbs the light and transfers to an excited state. After the lifetime of the excited state, the excited molecule returns to the initial trans-state or cis-state. The molecule in one of the two states can absorb the light again. The absorption of the cis-state molecule does not depend on the polarization state of light, but absorption of the trans molecule is proportional to $\cos^2\Phi$, where Φ is the angle between the polarization and the long axis of the molecule. This is called angular selective absorption, and it leads to angular hole burning. As the azobenzene molecules undergo this cycle more and more, trans molecules are gradually oriented perpendicular to the polarization direction of incident light. Because of anisotropy of trans molecules, birefringence is induced Figure I-15.

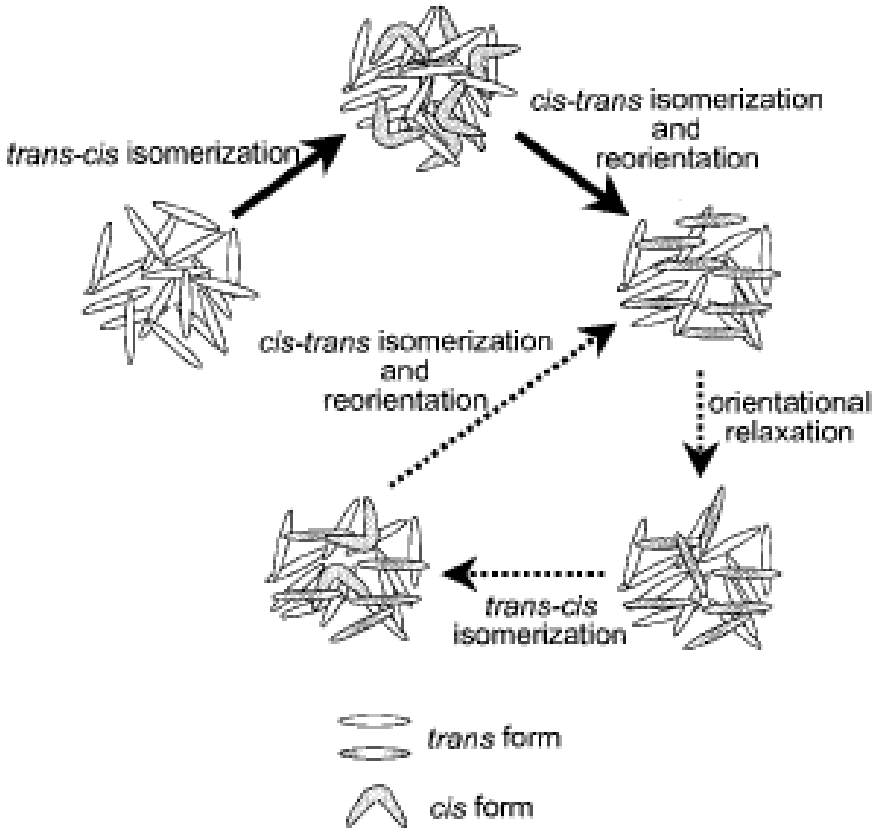

Figure I-15- Schematic illustration for the mechanism of photo-chemically induced birefringence in an amorphous azo-polymer [M. Hasegawa, T. Ikawa, M. Tsuchimori, O. Watanabe, Journal of Applied Polymer Science, 2002, **86**, 17–22].

The experimental setup for measuring light-induced birefringence is shown in figure I-16. An Ar^+ laser (488 nm) is used as pump beam inside the absorption band of polymers, and a He-Ne laser (633 nm) is used as a probe beam. A laser beam at 632.8 nm did not affect the film, because its wavelength is far enough from the absorption band of materials not to be absorbed by the polymer.

The transmission of the He-Ne laser through the film placed between crossed polarizers is recorded by a photodiode as a function of time after irradiation with the pump beam polarization set at 45° angle with respect to the probe beam polarization. The intensity of the incident probing beam was reduced to a few percent of the pumping beam intensity. This intensity was enough to ensure that the probe beam did not affect the molecular orientation.

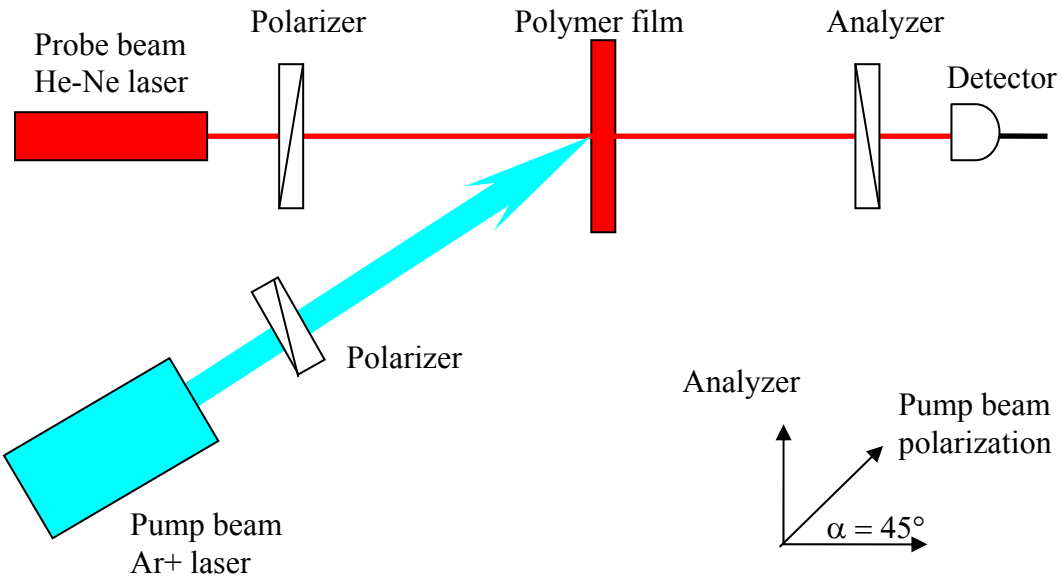

Figure I-16: Experimental setup for measurements of the light-induced birefringence. The polarization direction of pump beam set to 45° with respect to polarizer and analyzer direction of probe beam.

The pump induces optical anisotropy in the film via trans-cis-trans photoisomerization and reorientation of azo dyes. Birefringence modulus Δn is given by equation (1):

$$\Delta n = \frac{\lambda_o}{\pi d} \arcsin\left(\sqrt{\frac{I(t)}{I_o}}\right), \qquad (1)$$

where λ_0, d, I (t) and I_0 are wavelength of the probe beam, thickness of the film, intensity of transmitted and incident probe beam, respectively.

Figure I-17 shows a typical birefringence excitation - relaxation sequence. The pump beam is turned on at point A, the stable trans isomer of azo unit absorb the pump light and undergo a trans-cis photo-isomerization and then cis isomer relax thermally or by absorbing the pump light to trans isomer that finally is perpendicular to pump beam polarization, create an anisotropy in the film and the birefringence signal increases rapidly and reaches saturation. The writing beam is then turned off at point B; because of thermal relaxation, the orientation distribution of trans isomers changes and the birefringence decreases and approaches to a

constant value that will be kept constant for a long time in the dark. This birefringence can be erased by illuminating the sample by a circularly polarized pump beam or by increasing the temperature over Tg of polymer.

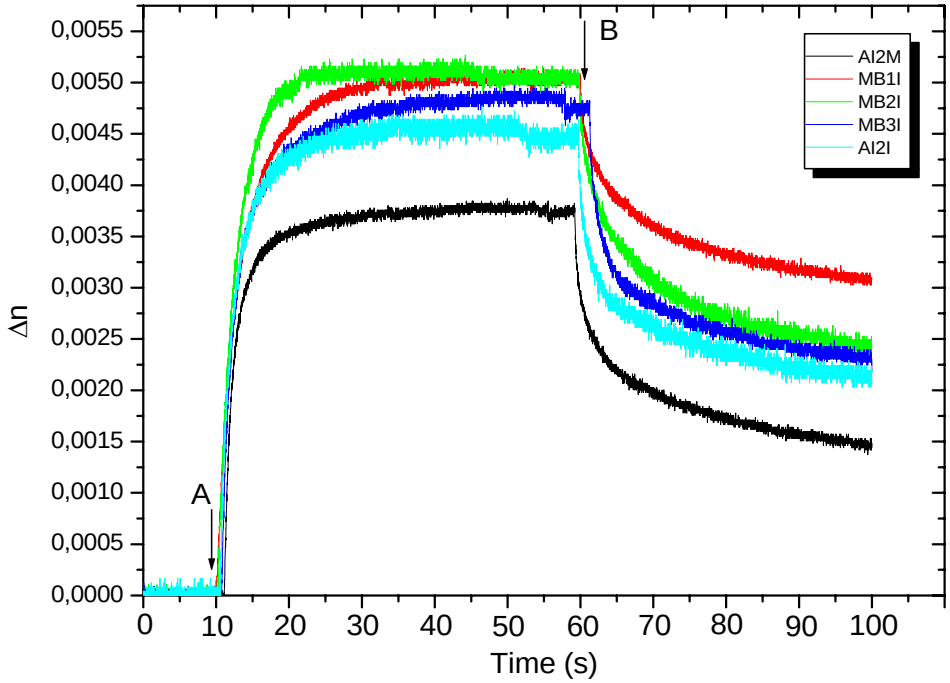

Figure I-17: Birefringence Δn in polymer films as a function of time: (A) The pump (writing) beam is turned on. (B) The writing beam is turned off. Pump beam intensity is 100 mW/cm^2. The birefringence is measured by a He-Ne laser at 632.8 nm.

The dynamics of birefringence decay, in the absence of pump beam, have been studied by biexponential function for the assumption of fast and slow decays [93].
The biexponential function is

$$\Delta n(t) = A + B\exp(-\alpha_1 t) + C\exp(-\alpha_2 t) \qquad (2)$$

where A is the birefringence conserved for a long times, α_1, α_2 are the decay constants with amplitudes of B and C respectively. The fast process (α_1) is mainly attributed to the isomerization response of the azo groups, while the slow process (α_2) is associated with the

movement of local polymer segments [94]. The normalized parameters obtained by fitting equation 2 to the experimental results summarized in table I-3. K is cis-trans thermal relaxation rate [95].The results show that for low-Tg azo-polymers, saturated value of Δn_s and stable values of the photoinduced birefringence A decrease with the decrease of Tg. The relaxation rates, α_1 and α_2, of the photoinduced birefringence increase with the decrease of Tg. As the Tg decreases, the mobility of azo chromophores is higher and thermal back relaxation of photo-oriented chromophores is more favourable [96].

Table I-3- Data for the photoinduced birefringence and kinetic of the relaxation.

Polymer	A	B	C	α_1 (1/s)	α_2 (1/s)	K(1/s)	Δn_s
MB1I	0.66	0.279	0.275	0.446	0.053	-	0.0051
MB2I	0.67	0.307	0.3099	0.476	0.068	0.0944	0.0052
MB3I	0.63	0.374	0.268	0.431	0.032	-	0.0048
AI2I	0.68	0.354	0.276	0.63	0.045	-	0.0045
AI2M	0.6	0.33	0.319	0.9	0.058	0.1617	0.0038

The process is interpreted as trans-cis-trans isomerization and reorientation of the azobenzene derivatives. Many write-erase cycles can be achieved without significant degradation. These results show that the polymer films in question can be used for reversible optical data storage purposes.

I-8- SRG formation in a series of azo-polymers

I-8-1- Introduction

In 1995, a remarkable, unusual and unexpected effect was discovered simultaneously by two independent research groups in the azo-polymer materials well below their glass transition temperature [81, 82]. Since these first two articles, more than 800 articles have been published to characterize the phenomena, to suggest the possible mechanisms and to propose some future applications. When the material was irradiated with two coherent laser beams (which generate a sinusoidally varying light intensity or polarization pattern at the sample surface), the materials spontaneously deformed in order to generate a sinusoidal surface relief grating (SRG) in this case the first order diffraction efficiency of a low power He-Ne laser (in the wavelength that polymer is transparent) will increase excessively. This is a one-step fabrication technique. Usually SRG topological formation is monitored by AFM to distinguish between bulk (birefringence) and surface gratings. This surface deformation is reversible and the original film thickness could be recovered upon heating the material past its glass-to-rubber transition temperature (*T*g) and/or in many cases even at room temperature by impinging a single beam of laser light with the appropriate polarization. SRG has been studied on azo dye doped polymers (guest-host systems) [97, 98], amorphous side-chain and main-chain azopolymers [99-104], and on liquid crystalline azo-polymers [105-108], mostly in the form of spin-coated films. Sol/gel materials [109], Langmuir-Blodgett (LB) films [110], and films assembled by ionic layer-by-layer interactions [111-113], single crystals [114] and more recently monomeric glasses [115,116] have also been used. Monomeric glasses have fast response to writing process and smaller birefringence in comparison to grafted polymers [116]. In azo dye doped systems, the chromophores are not attached to the polymer chains and their photoisomeric movements are not followed by the polymer chains and consequently the surface modulation is very weak. This surface modulation is difficult to observe with AFM. Liu et al. were synthesized azo derivative with fluorescent group which allowed them to use fluorescence confocal microscopy for observation of molecular migration [117]. Polymer chain migration, which is thought to be responsible for the large surface relief features, however, does not appear to occur. As expected, the formation of the surface grating in the main chain polymers was much slower than the side chain polymers. This is because the polymer has a rigid backbone and the azobenzene groups are bound to the backbone at both ends, which restrict the mobility of the chromophores. However, when it is considered that these main chain polymers have very high *T*gs, and relatively low absorption at the

writing wavelength compared to the side chain polymers, the observation of the surface modulation is quite remarkable. The results of several research groups show that side-chain azo-polymers are the best materials for inscription of SRG.

In addition, multiple gratings, up to 10, could be recorded on the same spot, provided that the polarization of the writing beams was properly selected, which allowed a variety of complex patterns to be produced. It is well-established that the surface-patterning phenomenon is strongly polarization dependent [118]. Both the efficiency of the process (as measured by topography height) and the exact shape of structures are affected by the incident polarization state. The two s polarized writing beams produce the largest light intensity variation (the intensity recording condition). However, there is no polarization gradient of the resultant electric field and no component of resultant electric field along the grating vector direction. This configuration only produces a very low diffraction efficiency and small surface modulation for the SRG (<10 nm). Under the polarization recording conditions, the two writing beams have orthogonal polarization (s-p). The resultant electric field on the film surface has the largest variation but the light intensity is uniform over the entire irradiated area. Very small surface modulation and diffraction efficiency are obtained under this purely polarization recording condition.

Under other recording conditions (p:-p, +45°: −45° and RCP: LCP), variations of both light intensity and the resultant electric field polarization on the film exist simultaneously. The SRGs formed have much larger values for the surface modulation and diffraction efficiency.

It has been observed by several authors that illuminated regions of the grating correspond to pits and dark regions to peaks of the surface, except in the case of side-chain liquid crystalline polyester of low *T*g where the opposite result was obtained. In essence, the topography encodes both the incident light intensity pattern and the polarization pattern [119].

I-8-2- Two beams experiment

Figure I-18 shows the typical experimental setup used for inscribing SRGs. The 488 nm line of an argon ion laser is expanded to a diameter of 8 mm and partly split by a mirror and reflected onto the polymer film surface.These two beams of equal intensity with appropriate polarizations made to impinge on the surface of sample. The interference of these beams can make intensity and/or polarization gradient on the sample surface depending on their

polarization. We used orthogonally polarized beam configuration (right and left circular) for interfering beams. The probe beam was a p-polarized 5 mW He-Ne laser at 633 nm. Efficiencies were measured as the percentage of first-order diffracted beam to the transmitted light intensities. The pitch of SRGs can be controlled by changing the angle between the writing beams. The periodicity can be calculated using the relationship $\Lambda=2\pi/k=\lambda/2\sin(\theta)$. The angle ($\theta$) is maintained at ~ 10° to obtain a grating periodicity of Λ ~ 1.4 µm.

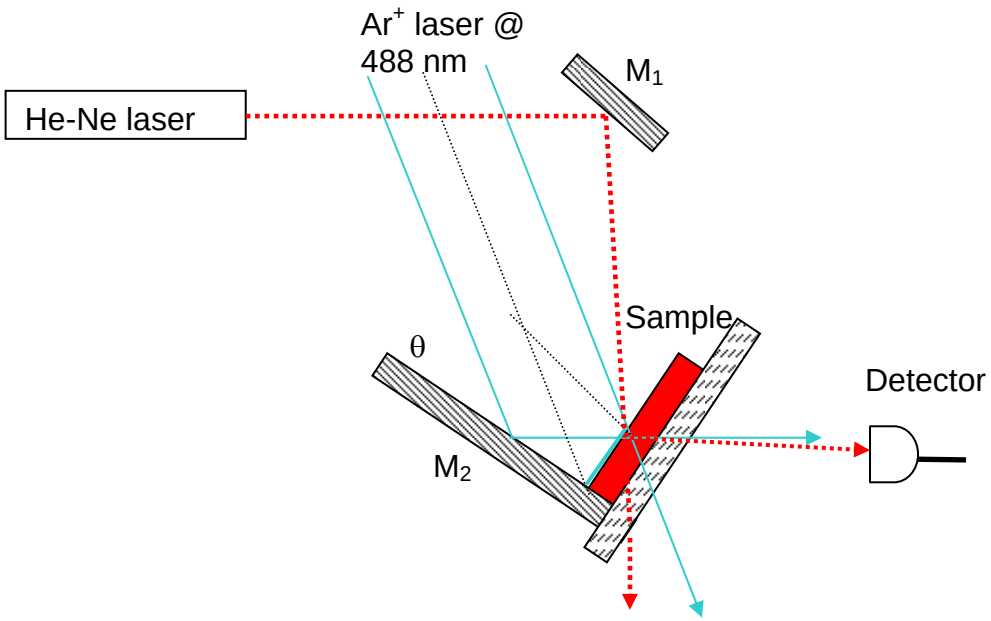

Figure I-18: Experimental setup for the SRG formation. M_1 and M_2 are the mirrors. The diffracted beam intensity of probe beam was recorded by a photodiode.

The surface morphology of the samples was imaged with a Pico SPM from Molecular Imaging .Atomic force microscopy was used in contact mode with a maximum scanning area of 6.5 x 6.5 µm (figure I-19).

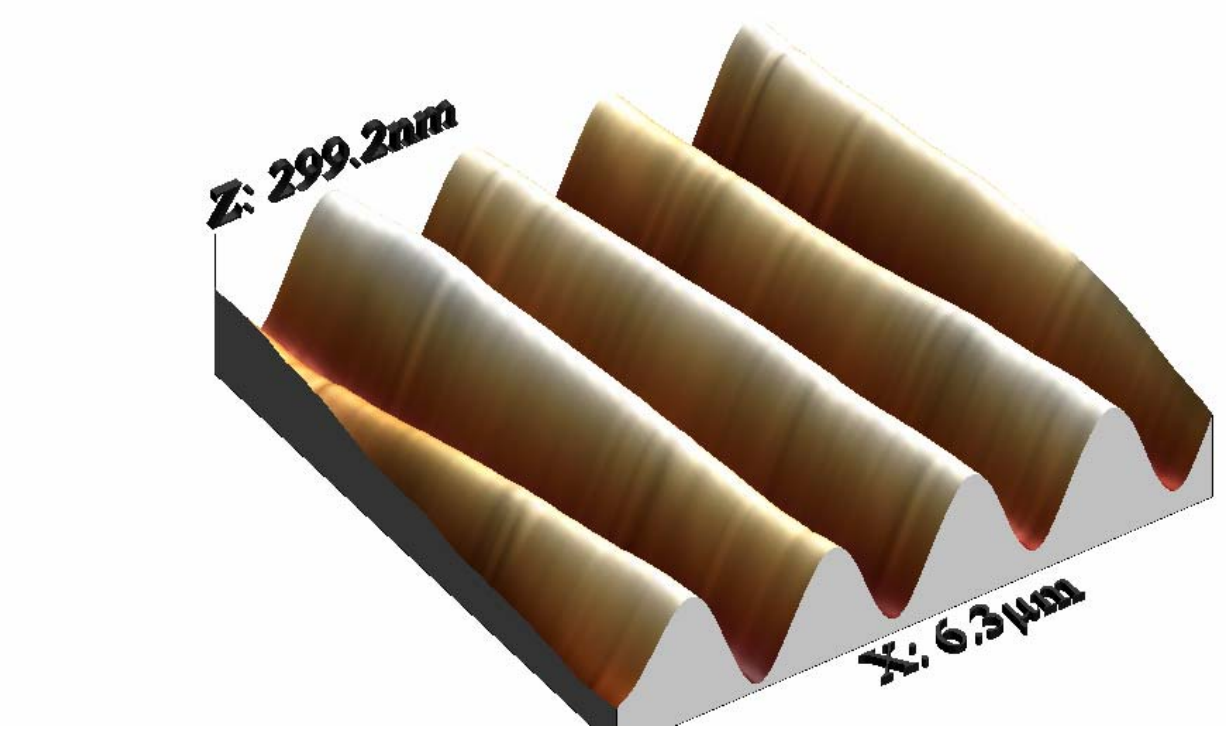

Figure I-19: Typical AFM image of formed SRG on the surface of Azo-polymer film with thickness of 500 nm. The depth of groves is ~235 nm.

The diffraction efficiencies for polymers with different spacers (MB1I, MB2I, and MB3I) were presented in figure I-20. By increasing the length of the spacer, the diffraction efficiency was found to decrease. It can be because of highest Tg of MB1I in comparison with others [120]. The Tgs of MB2I and MB3I are very close but the dipole moment of 2I is bigger than 3I and it can have higher efficiency. The weight-averaged molecular weight also affects the deformation efficiency. As the viscosity is dependent on the size of the chains, in polymers of higher molecular weight the rate and extent of grating formation should also be decreased [121].

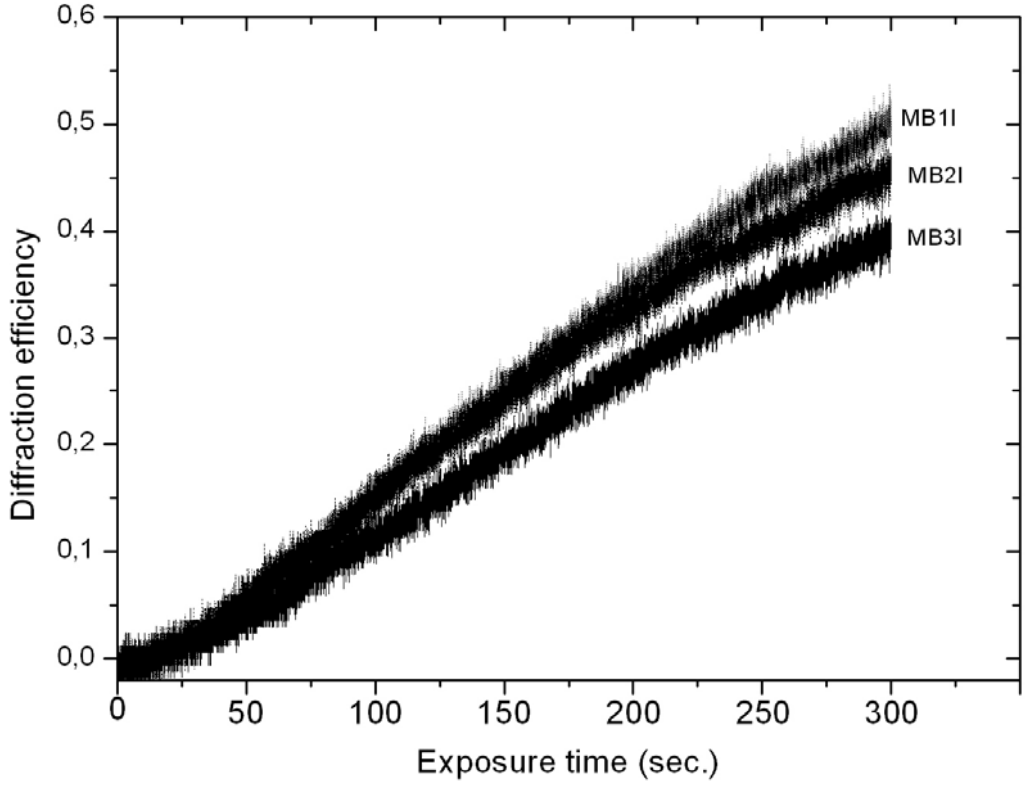

Figure I-20- Diffraction efficiencies of SRG formed on the surface of azo polymer films with different chromospheres length as a function of time.

Figure I-21 shows the diffraction efficiency for polymers with different azo side chain (AI2I and AI2M). The diffraction efficiency of AI2I is higher than AI2M. It can attributed to high Tg and low average molecular weight of AI2I and high dipole moment of its azo-dye in comparision with AI2M [120, 121].

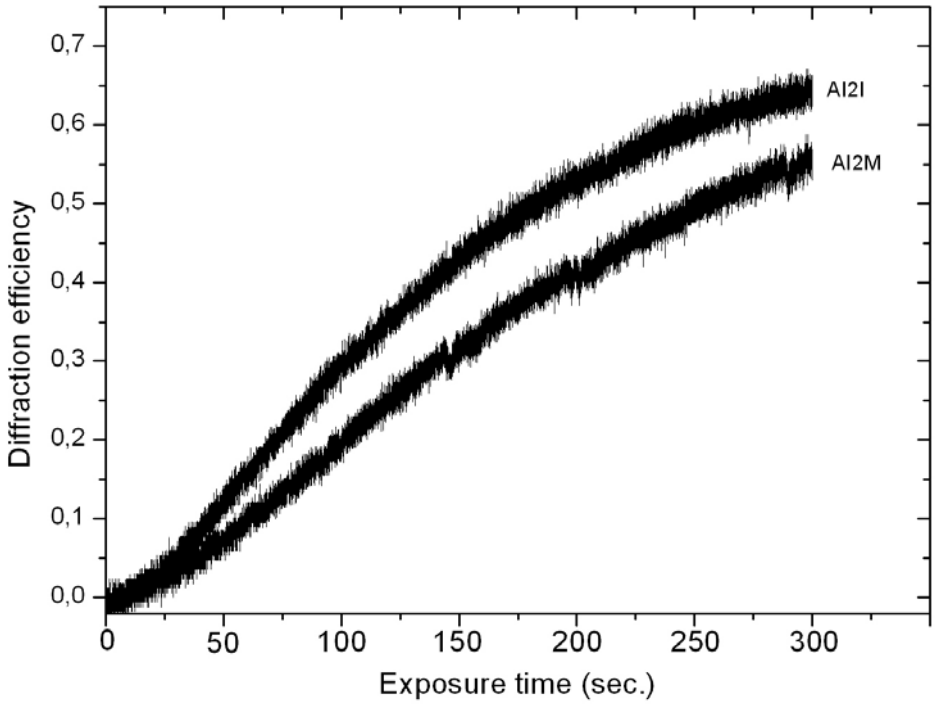

Figure I-21: Diffraction efficiencies of SRG formed on the surface of azo polymer films with different chromophores as a function of time.

I-8-3- Crossed gratings formation

We checked the possibility of inscribing two sets of gratings on the same area of the polymer film (figure I-22). On a set of SRGs of an azopolymer thin film, interfering two laser beams were irradiated to append another set of gratings. As a result, appended gratings were superposed on initial gratings and the direction of the mass transfer in the SRG formation was turned to be restricted along its wave-vector [82].

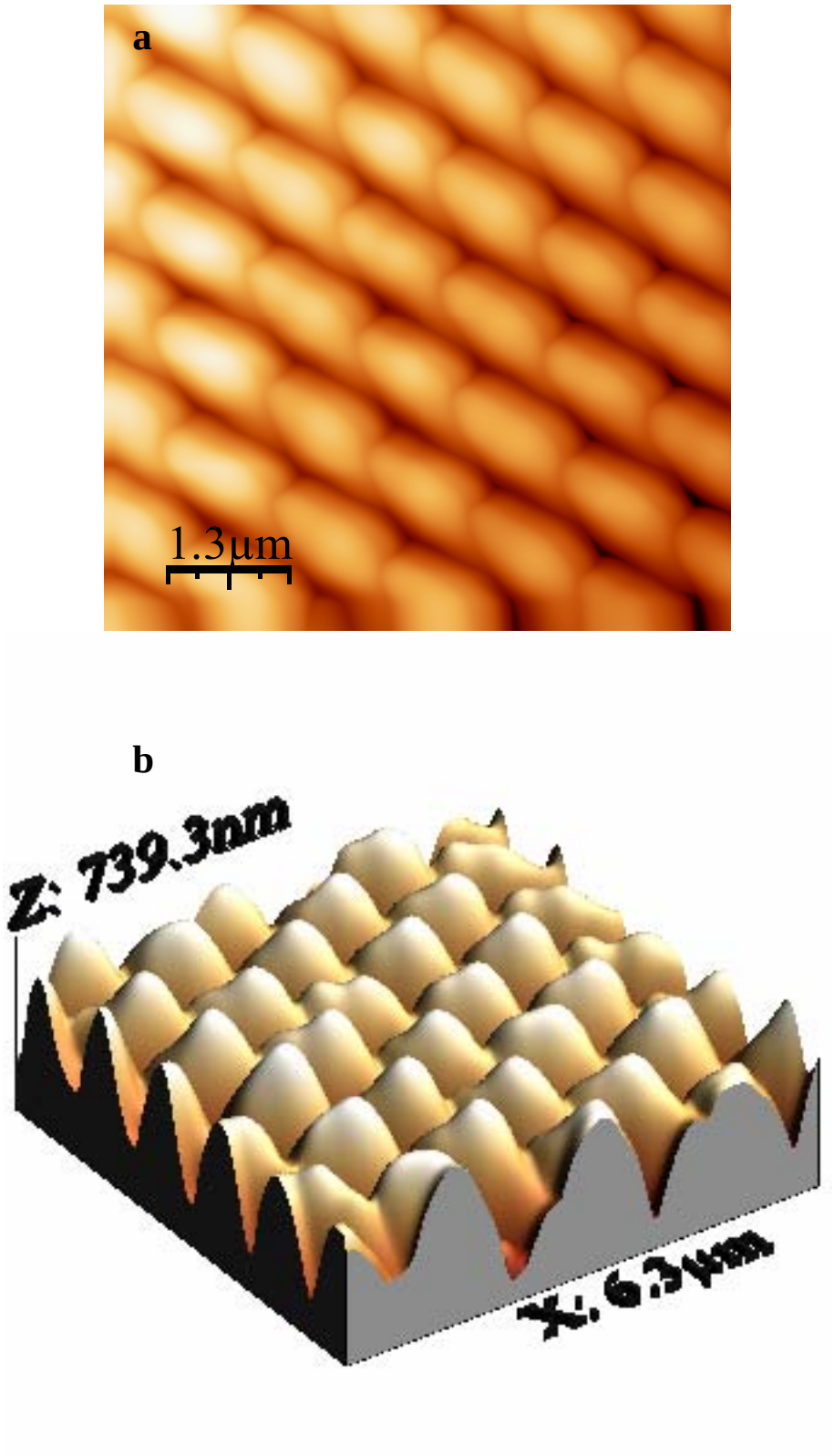

Figure I-22: a) 2D and b) 3D view of AFM image of two grating recorded on the same area of MB2I polymer film.The pitch and depth of SRGs are 1 µm and 550 nm ; 1.2 µm and 200 nm, respectively.

I-8-4- Mechanisms of SRG formation

There remains, however, much controversy surrounding the fundamental origins of all-optical surface patterning of azo thin films, and no proposed mechanism appears to provide a suitable explanation for all observations. Here we will review almost all the proposed mechanisms:

I-8-4-a- Isomerization pressure model

This model is based on pressure gradient induced transport deformation and the resulting viscoelastic flow to form surface gratings on the azo polymer films [122,123]. The pressure gradients arise from the increased *cis* population in the bright regions, together with the *cis* isomer's large free volume requirement and the viscoelastic flow of the polymer is related to the velocity components by Navier–Stokes equations (Figure I-23). The thickness h of polymeric film, its molecular mass M, its viscosity μ (proportional to M) as well as the pressure P are taken into account and lead to an expression of the temporal evolution of polymeric film thickness:

$$\frac{\partial h}{\partial t} \propto \frac{d^3}{\mu} \cdot \frac{\partial^2 P}{\partial X^2} \propto \frac{d^3}{M} \cdot \frac{\partial^2 P}{\partial X^2} \qquad (3)$$

where X represents the direction according to which the distribution of intensity or polarization takes place. The theoretical dependence of the rate of inscription ($\partial d / \partial t$) to the thickness of polymeric film (d^3) is checked in experiments [93] for low thicknesses of polymeric films.

Based on this, a relationship between the grating formation rate and intensity of the writing beams, molecular weight of the polymer and thickness of the film is derived and experimentally verified.

For thinner films, there is excellent agreement of the experimentally observed and predicted writing efficiency and film thickness. Inscription rate is found to increase linearly as a

function of light intensity and is accurately accounted for by this model. The gradient of isomerization pressure model however, does not adequately account for the strong polarization dependent grating formation process. The theory predicts the highest pressure gradients for two *s*-polarized beams. This is in contradiction with experimental data, which demonstrate negligible diffraction efficiency for this geometry.

Sumaru et al. have developed this approach to successfully describe the evolution of the surface relief gratings over longer time periods for any initial thickness of polymer film [124,125]. However, this model does not take into account the influence of the polarization of writing beams.

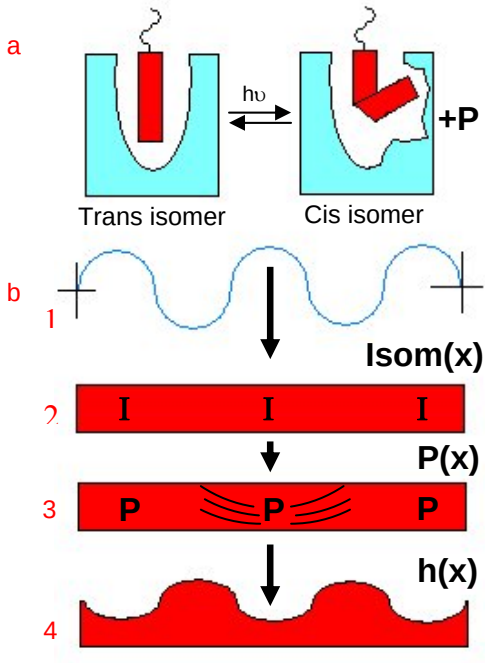

Figure I-23: Schematic representation of isomerization pressure model. a) Trans-cis photoisomerization and difference in the free volume requirement for trans and cis isomers. b) Intensity modulation rise from two coherent beams interference (1) that causes more isomerization (2), more pressure (3) and finally deformation of polymer surface (4).

I-8-4-b- Gradient electric force mechanisms

This model has been proposed by Kumar et al. [126,127] and is based on the interaction of the azo chromophore functionalized macromolecules with the optical field induces polarization in the material in the direction of the field. Efficient *trans-cis-trans* photoisomerization cycling leads to a photostationary state when there is a net chromophore orientation perpendicular to the field direction. The associated decrease in the refractive index and hence the susceptibility of the material defines the direction of flow of the polymer chains. The unique aspect of the azo polymer system is that these processes occur simultaneously and the time averaged effect results in transport of the polymer chains in the field gradient direction. The process is initiated at the film surface and continues through the bulk of the material as the polymer layers are moved, leading to high amplitude gratings [128]. The force responsible for the movement of the polymer involves a spatial variation of the susceptibility of the material and an electric field gradient (figure I-24).

In this case the time-averaged force would take the form:

$$\vec{f} = \left\langle \left(\vec{P}.\nabla \right) \vec{E} \right\rangle \tag{4}$$

where $P = \varepsilon_0 \chi E$ and E are the optical field induced polarization in the material and electric field amplitude of optical field, respectively. Thus, the grating inscription would be related to the spatially-varying materials susceptibility χ, the magnitude of the electric field E, and the gradient of the electric field. This naturally includes the polarization dependence observed in experiments.

In this model a photo-induced plasticization is assumed, allowing material mobility well below Tg. The force density estimated for conventional lasers is 100 N/m^3 which is two orders of magnitude smaller than that of the gravitational force (10^4 N/m^3), and thus is too small to be of influential importance.

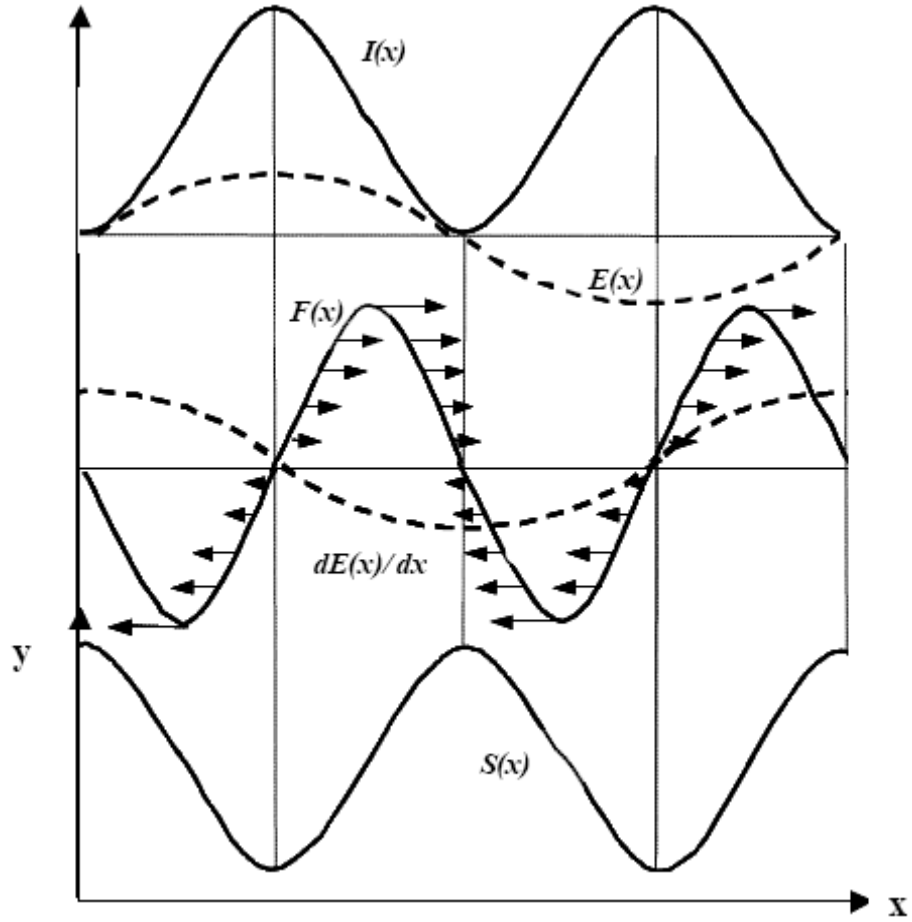

Figure I-24: Schematic representation of model. The intensity and surface modulations have phase difference of π [129].

More recently Yang et al. have developed this model by adding magnetic force to have an electromagnetic force [129].This electromagnetic force is driving force for SRG formation process. They assumed that the medium is not a magnetic medium. They considered polymeric material as an incompressible viscous fluid and used Navier-stokes equation to describe the motion of material. The obtained theoretical results of the inscription rates and the expected z-component surface velocity directions are in good agreement with experimental result. Again the heart of this model is photoplasticization of polymeric material.

I-8-4-c- Thermal mechanisms

Models involving thermal effects appear to be the most readily proposed. Thermal gradients would be created due to the inhomogeneous illumination (light interference pattern) of the sample surface, but their magnitude and persistence time would be expected to depend strongly on material parameters, geometry, and size scale. Such mechanisms would be sensitive to the intensity of the light interference pattern, but not its polarization, counter to observations. For example, SRGs have been written using a pure polarization pattern, where the intensity of the light at the film surface is constant. Attempts to produce SRGs with absorbing chromophores other than azobenzene have not been successful, and it appears that the isomerization is necessary for the process. Experiments at high laser intensity [130] (and experiments with pulsed systems [131], which are equivalently high intensity) on the other hand show neither polarization dependence nor a strict on azobenzene chromophores.

Recently Yager et al. have created a simulation, to clarify the role of thermal gradients in the SRG inscription process [132]. They showed that thermal gradients are negligible for typical modest irradiations (for the intensities of 50mW/cm^2 the temperature of sample raise about 5K) [133], and the temperature gradient achieved within the sample is on the order of 10^{-4} K, and does not appear to vary with inscription or geometric conditions. This gradient cannot lead to an appreciable spatial variation of material properties, and certainly does not explain the dependence of SRG inscription on many variables.

The pulsed irradiations are likely causing destructive sample ablation, and not mass transport.

I-8-4-d- Permittivity gradient model

Baldus and Zilker have proposed a mechanism for SRGs formation based on spatial variation of the permittivity of material due to the periodic alignment of the polymer side-chains caused by intensity or polarization modulation of interfering writing beams. This gradient of permittivity under an optical electric field results in a force [134].
This force is proportional to the square of the optical electric field in the grating vector direction, and to the gradient of permittivity at any point:

$$\vec{f}(x) = -\frac{\varepsilon_0}{2}\vec{E}^2(x)\nabla\varepsilon \qquad (5)$$

Material is moved out of areas with high gradients of permittivity, and in general is moved out of areas of illumination and causes the modulations of the surface (figure I-25).

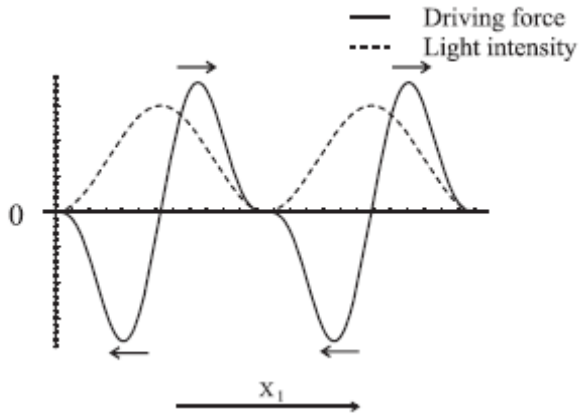

Figure I-25: X_1 component of force under a periodical modulation of the incident light. The material is pulled out of areas with high gradients of the permittivity (arrows denote the force direction) [134].

In this model they assumed that the softening of the material can achieve thermally, and trans-cis cycles of the side chains, and therefore chromophore reorientation, play a negligible role.

I-8-4-e- Asymmetric diffusion (migration) model

Nunzi et al. have developed a model based on the anisotropic translation diffusion of azo dyes in a direction that is parallel to the polarization direction of the writing beam [135-137]. This translation is due to the photo-excitation and thermal re-conversion (photoinduced trans-cis-trans isomerization cycles) of chromophores (figure I-26).

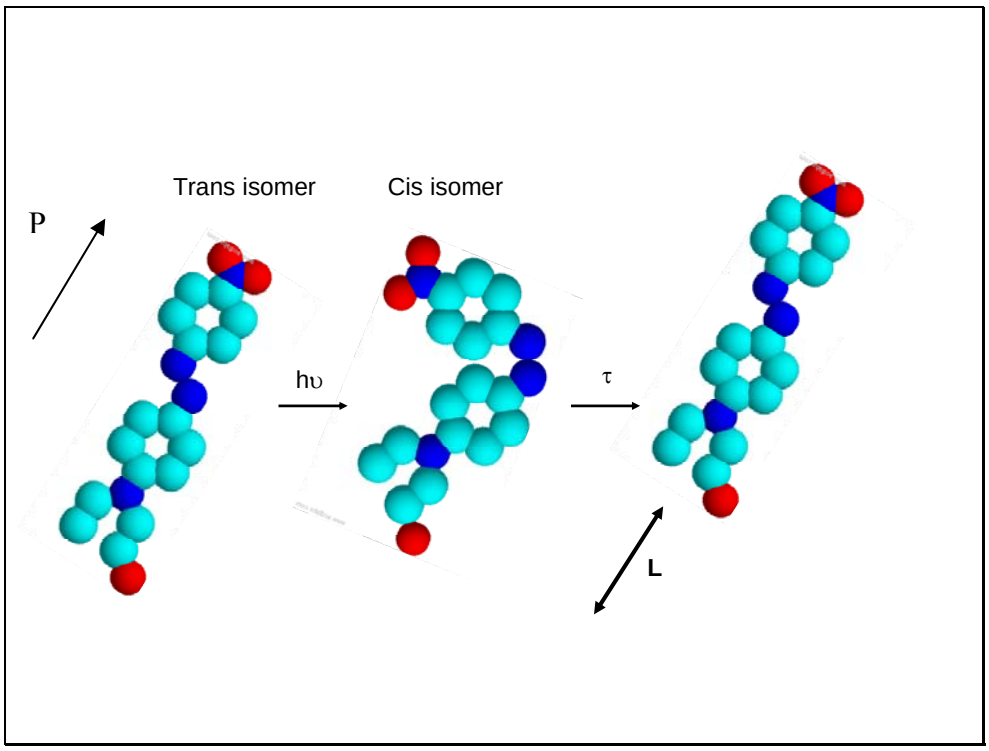

Figure I-26: Photoinduced worm-like motion of disperse red 1 azo molecule.

The probability of undergoing a statistical random-walk is related to the probability of excitation, which in turn is related to the intensity of light and the angle between the electric field vector of the light and the chromophore dipole moment. There is thus a net flux of molecules out of areas of light and into the dark, aided by pointing the dipoles towards the dark regions through a polarization-dependent photo-alignment. Once a molecule has diffused into a dark region, there is a zero probability of it being excited back into a light region, and hence the azo molecules would be expected to congregate coincident with the interference pattern, and produce a surface relief grating. Attached azo molecules to backbone polymer chains can act as tractors that pull the polymer material. This model explains very well the polarization dependence observed in the azo polymer films.

I-8-4-f- Mean-field model

Mechanisms based on electromagnetic forces seem promising, since these naturally include both the intensity and polarization state of the incident radiation. In the mean- field model, each chromophore is subject to a potential resulting from the dipoles of all other chromophores [138,139].

Under irradiation, chromophores at any given point will be oriented perpendicular to the light polarization at that point. The mean-field that they generate will tend to align other chromophores in the same direction, and also causes an attractive force between side-by-side chromophores oriented in the same direction. Overall, this results in a net force on chromophores in illuminated areas, causing them to order and aggregate.

This mechanism predicts a collection of mass in the areas of high light intensity, at the expense of areas of lower intensity.

Theoretical predictions of the polarization dependence of the periodicity and shape of the surface relief profiles have been found to agree well with the experimental results. However, the model presumes a spatially constant intensity when two orthogonally polarized beams interfere at an angle ($\theta>0$).

This treatment, based on the intrinsic mobility of the LC materials, does not account for the dip (instead of peak) inscribed in the material where the intensity is maximum, observed in the amorphous azo polymers.

I-8-4-g- A remark on models

More recently, Yager et al. have measured the elastic modulus of azo materials by AFM in force-distance mode to describe the effect of photosoftening on the SRG formation [140].The obtained average modulus of film were 219 ± 70 kPa and 336 ± 62 kPa before and during irradiation, respectively. The results showed that there is no significant difference between these two cases. Thus in azo materials the photosoftening effects are negligibly small and any model that relies upon significant photosoftening to explain mass transport should be eliminated.

I-9- Single beam deformation of azo-polymers

Following the discovery of SRG and the ability of deformation of the azo-polymer surface by the interference of two coherent beams, several research groups started to study the possibility of deformation of azo-polymer systems under illumination of a single laser beam. In this section we will review some of these effects.

I-9-1- Focused beam

A single laser beam surface deformation experiment was performed by Bian et al. to study the phase relation between writing beams interference pattern and SRG. The results help to a deeper understanding of the grating formation mechanism [141,142].
The experimental setup is shown in figure I-27. A linearly polarized He-Ne laser beam at 544 nm, with a well-defined Gaussian light intensity profile, is focused by a spherical (or cylindrical) lens. The polymer sample film is placed at the focal plane of the lens. The intensity of the laser beam is adjusted by inserting different neutral density filters (NF). The different polarization states of the laser beam are achieved by inserting a properly oriented half- or quarter-wave plate. At the sample surface the radius (or the half width of the cylindrical Gaussian beam) of the laser beam is 3.0 μm.

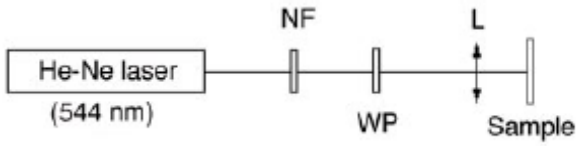

Figure I-27: Experimental setup used for single beam surface deformation.

Figure I-28 shows AFM image of the polymer film surface after illumination. The figures display two important characteristics. First, the photoinduced surface deformation depends strongly to the input laser beam polarization direction. The maximum deformation happens along the direction of laser beam polarization (x direction in Fig I-28-a). Second, the surface deformation profile along the polarization is not proportional (positively or negatively) to the

laser intensity. Instead, it approximates to the second derivative of the laser intensity along the polarization direction (x-axis).

According to the migration (diffusion) model, the azo molecules have tendency to move from higher intensity region of beam (more trans-cis-trans photoisomerization) to the lower one and finally to the dark region in the direction of laser beam polarization and deform the surface of polymer film.

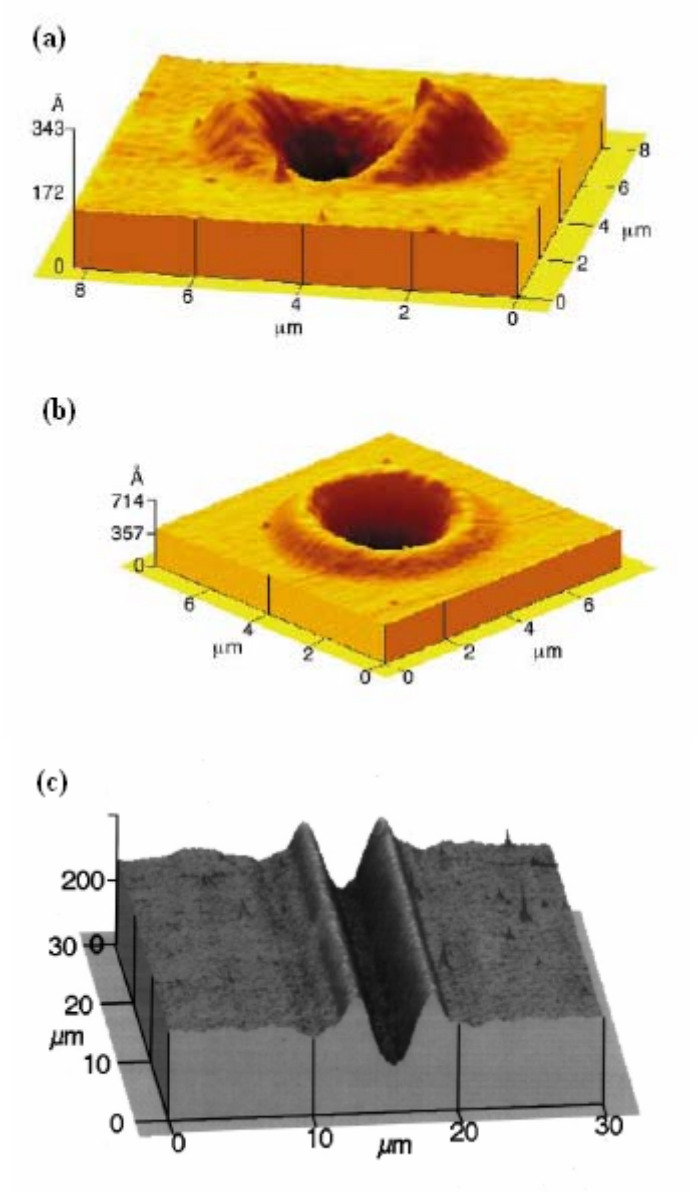

Figure I-28: AFM image of the surface deformation of an epoxy-based azo polymer (PDO3) film induced with a) linear and b) circular polarization. Intensity in the center of the laser beam is 328 mW/cm^2. The sample film is exposed for 70min.c) one-dimensional Gaussian beam with linear polarization along the direction of light intensity gradient [141, 142].

At higher intensities of writing laser beam, in addition to the surface deformation induced the migration of polymer chain, a central peak in the surface profile appears (figure I-29). One can related this effect to the high-intensity photo-thermal effects and photochemical reaction such as degradation and bleaching of the chromophores. Photocrosslinking or photothermally induced crosslinking may also occur.

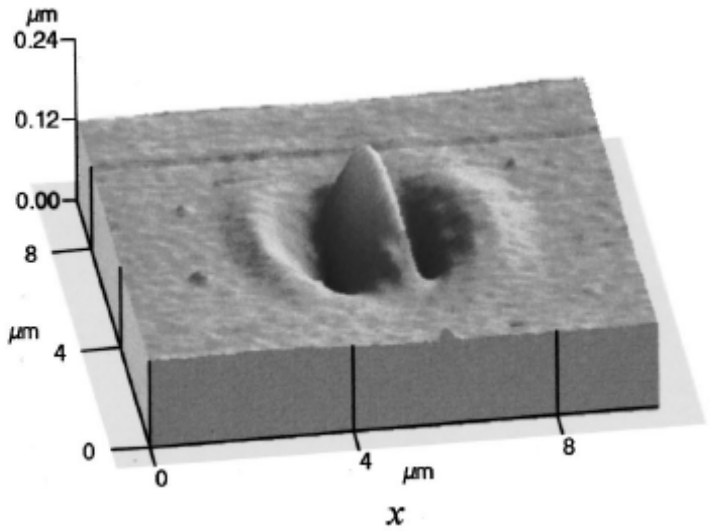

Figure I-29: AFM image of surface deformation induced by linearly polarized (along the *x* axis) Gaussian beam with high intensity 865 W/cm^2 for 3 s [142].

The single-beam experiment is particularly relevant to reveal the photoinduced lateral migration of polymer chains and to deduce the phase shift of the SRG with respect to the interference pattern since no such unambiguous assignment could be given in the grating writing experiment.

I-9-2- Photomechanical effects

Bulk expansion and contraction of azobenzene materials have also been observed [143,144]. In one report, an azo LC (liquid-crystal) polymer thin film was made to bend and unbend by exposing it to polarized light. The direction of the macroscopic motion could be controlled by the polarization direction of incident light. The bending occurred because the free surface of the material contracted more than the inside of the thin film (due to absorption of laser light as it passes through the material). Furthermore, the photomechanical effect can be heavily optimized and may turn out to be a highly efficient photo-actuator [145].

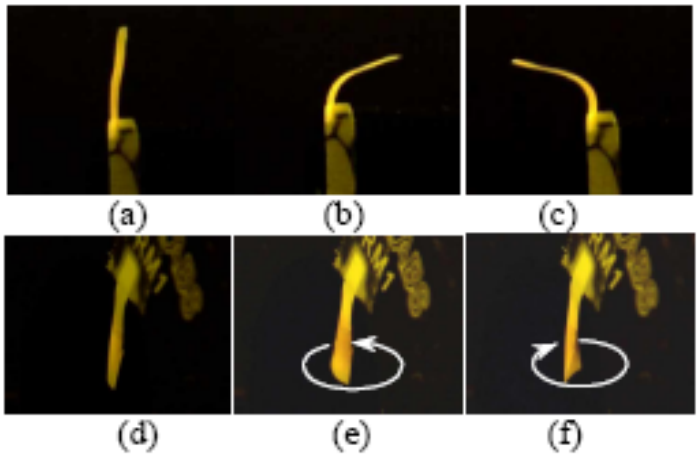

Figure I-30: Photos of optically induced polymer deformation. (a) The fresh azo LC polymer film (1 mm x 7 mm x 20 μm), (b) the polymer is bent away from the laser for the beam polarized perpendicular to the film orientation; (c) and it is bent towards the laser if the polarization is along the film orientation;(d) the polymer film (2 mm x 12 mm x 20 μm) used for inducing twist deformations with a laser beam of tilted polarization; (e) counter-clockwise folding of the polymer film for -45° polarization; (f) clockwise folding of the film for 45° polarization The power density of the laser beam is 0.25 W/cm^2 [145].

I-9-3- Manipulation of azo polymer colloidal spheres

The availability of spherical colloids that are uniform in size, composition, and surface charge has played an important role in explanation of the optical, rheological, and electro-kinetic properties characteristic of colloidal materials [146]. Spherical colloids have also been exploited as building blocks to generate three-dimensionally periodic lattices (e.g., colloidal crystals, opals, and inverse opals) through self-assembly. To this end, these structures have been explored as a unique system to generate photonic band gaps that are useful in controlling the propagation of electromagnetic waves in three dimensions of space [147]. Despite their predominant role in colloid science, spherical colloids are not necessarily the best candidate for all studies on colloids. For example, computational studies have indicated that they are not well-suited for use as building blocks in generating photonic crystals with complete band gaps due to the degeneracy caused by the spherical symmetry of lattice points [148]. Nonspherical particles may offer some immediate advantages over the spherical counterparts in applications that require colloidal systems with higher complexities and crystalline lattices of lower symmetries. There are several techniques to produce monodispersed nonspherical colloids.

For example, by mechanically stretching spherical colloids embedded in polymeric matrices, it was possible to obtain ellipsoidal beads as monodispersed samples.

Li et al. observed photoinduced shape deformation of colloidal spheres based on azo polymers [149,140]. This approach of nonspherical colloides formation can have several advantages such as controllability, uniformity, handiness and so on. The samples were prepared by solution casting of colloidal spheres under gravity on clean silicon wafers. The colloidal spheres were irradiated by a collimated linearly polarize Ar^+ laser (488 nm, 150 mW/cm^2) at normal incidence. Figure I-31 shows Scanning Electron Microscope (SEM) of irradiated colloids.

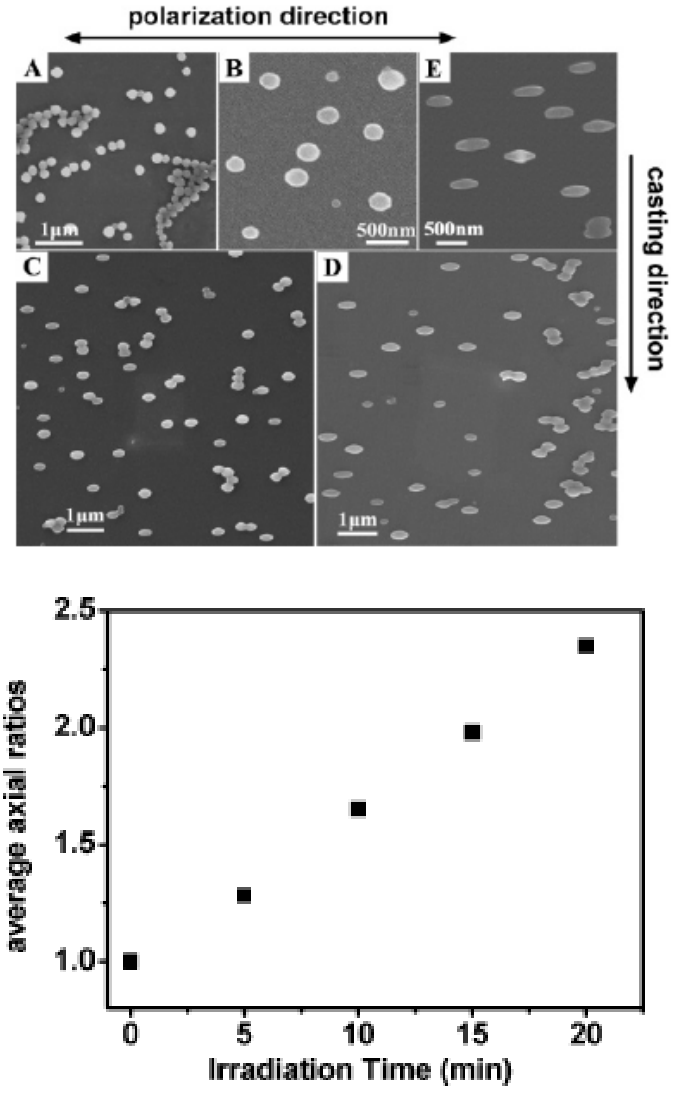

Figure I-31: Up) SEM images of colloidal spheres before irradiation (A); and after irradiation for different periods of time; (B) 5 min, *l*/*d*) 1.28; (C) 10 min, *l*/*d*) 1.65; (D) 15 min, *l*/*d*) 1.98; and (E), 20 min, *l*/*d*) 2.35.Down) Relationship between the average axial ratios (*l*/*d*) of the colloidal particles and the irradiation time [149].

As one can see from figure, the irradiated colloidal spheres are elongated in the direction of light polarization and perpendicular to the casting direction. The average axial ratios of colloids (l/d) increase linearly with the exposure time. By applying two laser beams with orthogonal polarization one can stretch the colloidal spheres in two dimensions and 2D arrays of colloidal spheres can stretch uniformly by a single laser beam in the direction of polarization.

I-9-4-Laser Induced Periodic Surface Structure (LIPSS)

There are several possibilities to create periodic structures on the surface of materials by a laser beam. Pulsed laser radiations of power density above the material damage threshold cause the ablation of material and can be used to write a periodic structure on the materials surfaces through a mask (the periodicity is related to the resolution of optical system and the response of material). However, periodic structures can also be developed on a surface at intensities below this threshold. The properties of Laser-Induced Periodic Surface Structures (LIPSS) have been frequently studied since the first report about them [151]. LIPSS formation is general on condensed media, i.e., the production of these structures is possible also on the surface of metals [152], semiconductors [153,154], dielectrics [155], quartz [156], and polymers [157-164]. In the literatures about polymers, the LIPSS were generated with a series of low fluence, polarized, short wavelength laser pulses. These structures are important because the period of the LIPSS is in the order of magnitude of the wavelength of the writing beam (sub-micrometer), and their appearance causes adhesion enhancement of the surface. The experimental results showed that the period of the LIPSS depends on the material, the wavelength and the angle of incidence of the radiation; the line-shaped structures are parallel to the direction of polarization. The peculiarity of the LIPSS is that these structures develop on original material surface having a small roughness, as a result of treatment with one laser beam having a uniform intensity distribution. The dependence of the LIPSS period on the angle of incidence of s and p polarized beams shows that the interference between the incoming and the surface scattered waves plays an important role in the structure formation, but the whole mechanism is very complex, and there is no sufficient explanation of the structure formation process in case of polymers in the literature. Csete et al. have studied the role of surface roughness in LIPSS formation process [165]. They found that the scattering from the surface object is the origin of LIPSS formation and that the intensity maximums of scattered beams interference are correspond to minimums of the surface topology.

Lu et al. recently reported the effect of pre-rubbing treatment [166] of the polymide film on the LIPSS formation. They found that the rubbing of surface with clothes can create microgrooves on the surface of polymer that can act as waveguide for LIPSS formation. When the rubbing direction was parallel to the polarization direction of the incidence laser, the amplitude and periodicity of LIPSS were greater than those on unrubbed and perpendicularly rubbed films, but these microgrooves can affect the regularity of the formed LIPSS. To overcome this disadvantage of pre-rubbing, more recently these authors investigated the effect of pre-irradiation treatments [167] of the polymer film on the development of LIPSS. The pre-irradiation was done by exposing the polymer surface to a pulsed UV laser at a level of laser fluence lower than the threshold of LIPSS formation. The LIPSS amplitude was greater in the case where the polarizations of laser beams for the first and second irradiations were parallel than in the case where they were perpendicular and with the fresh polymer films (figure I-32). This pre-irradiation decreased the LIPSS formation threshold.

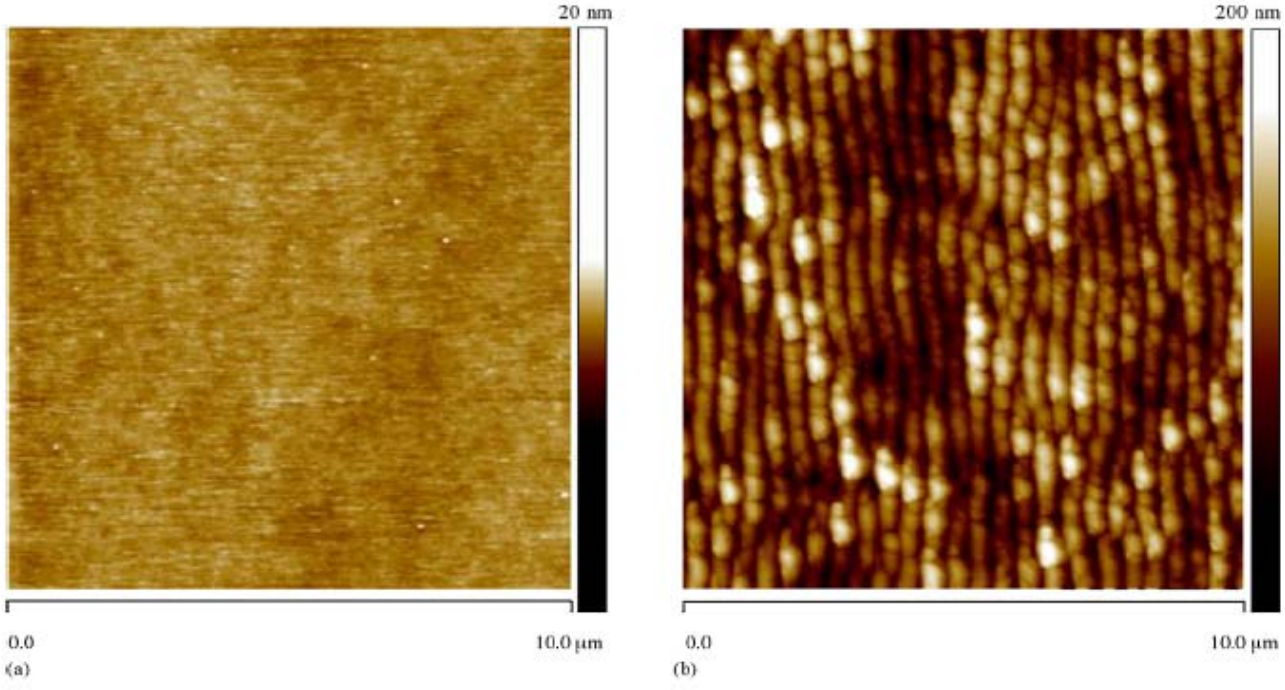

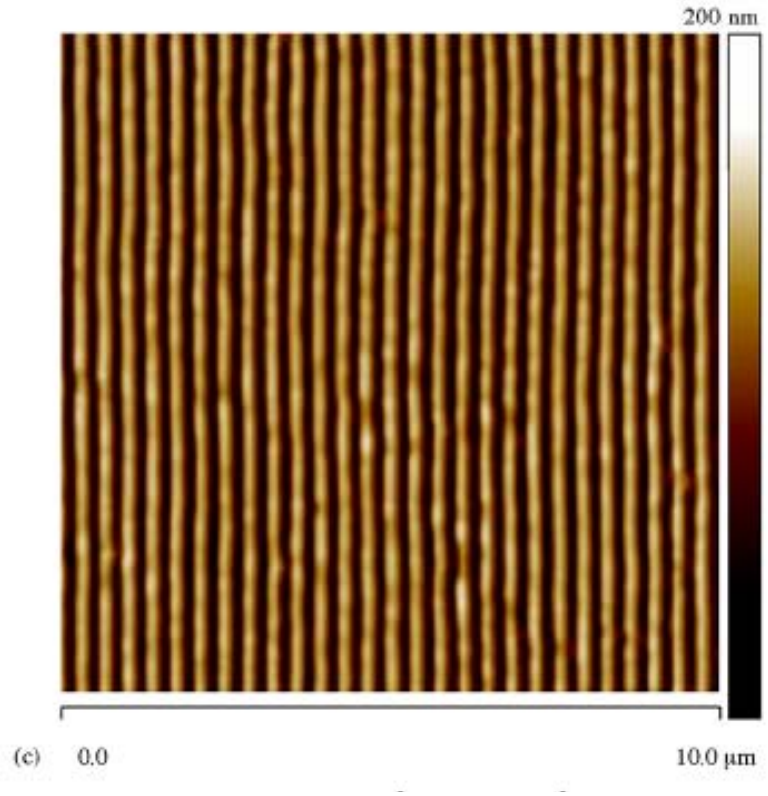

Figure I-32: AFM images of PI surfaces irradiated at the laser fluence of: (a) 8.4 mJ/cm^2, (b) 14.8 mJ/cm^2 and (c) pre-irradiated at a fluence of 8.4 mJ/cm^2 and then exposed to a laser fluence of 11.6 mJ/cm^2 [167].

Recently, it was found that the single beam of fundamental (1.06 μm) and second harmonic (532 nm) waves of neodymium doped yttrium–aluminum–garnet (Nd:YAG) nanosecond pulsed laser induced the periodic structures on a surface of azobenzene polymer depending on the polarization of laser beam. The periodic structure induced by the single pulsed laser beam was classified to the similar type of LIPSS. Figure I-33 shows the AFM image of such kind of structures on the surface of an azo polymer inscribed by 200 shots of a linearly polarized frequency doubled Nd:YAG laser beam with energy of 500 mW/pulse. The grating vector of formed LIPSS is perpendicular to the laser beam polarization direction. The pitch of grating is 400 nm and the amplitude of peaks is 120 nm [168]. The pitch and amplitude of LIPSS depend to the laser shots numbers and film thicknesses and increase by increasing them and saturate.

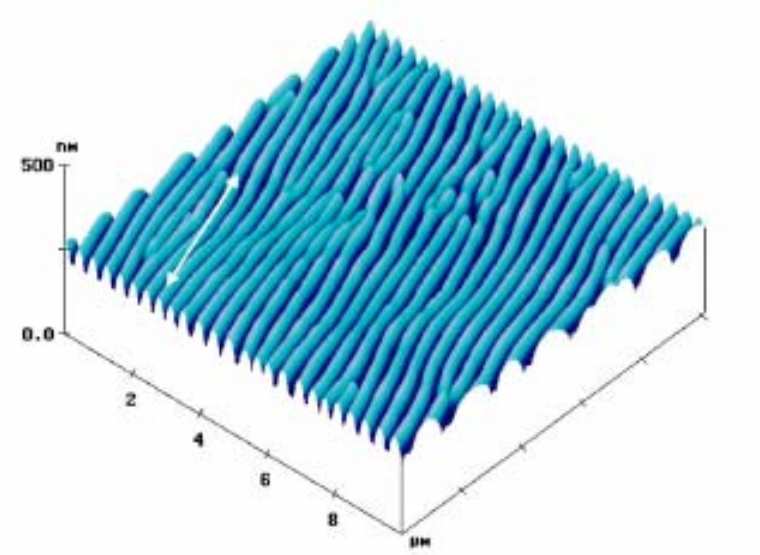

Figure I-33: AFM pictures of LIPSS on an azo-polymer film. Double ended arrow in the picture indicates the direction of laser beam polarization [168].

Rochon and Ivanov reported that over a power threshold, periodic ripples (LIPPS like) grow on the surface of azo-polymer film under an infrared-laser beam illumination [169].The pitch and amplitude of LIPSS are 700 nm and 100 nm, respectively. The ripples are parallel to infrared laser polarization.

I-10- Possible applications of SRG

The ability to deform surfaces of polymers well below Tg with light is certainly a novel and unexpected phenomenon with many potential technological applications. Moreover, as far as fundamental science is concerned, the study of SRGs allows one to probe surface and material-flow properties of polymers at a micron or submicron scale. The potential for technological applications was realized as soon as the first SRGs were observed. However, most efforts have been concentrated on the exploration of new materials and fabrication of SRGs under different experimental conditions. In particular, the aim has been to further the understanding of the complex processes involved. A number of real applications have nevertheless been demonstrated that indicates the multitude of devices that can be fabricated by exploiting the capability of inscribing SRGs on azo-polymer films. In the following sections we shall comment upon several of these initiatives.

I-10-1- Couplers

Introduction of light into the waveguides is one of the important challenges of photonics. Usually, for this task, prisms have to be glued at the entrance point. Based on the fact that the diffraction efficiency of such a grating is extremely high (up to 50% in one direction).The SRGs can be used as a coupler to coupling light into and out of waveguides (Figure I-34). They can be inscribed either on a whole azo polymer film, or at the end of classical waveguide, by dropping a small amount of azo polymer solution, evaporating the solvent and subjecting the film to interfering light [170]. Output coupling of both 633 and 830 nm light could be performed in the waveguides [171].

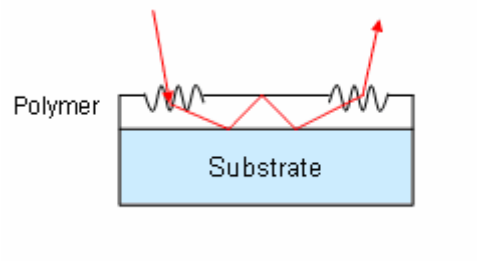

Figure I-34: Schematic representation of input and output coupling by use of SRG on top of a waveguide.

I-10-2- Filters

SRGs can use to produce a narrow band waveguide filter with a bandwidth less than 1 nm [172]. The device consists of a glass substrate, a classical waveguide deposited on it and an azo-polymer film on top of waveguide. Optically inscribed SRGs can act as coupler of incident light to the waveguide and simply by rotating, this device will allow the beam with a certain wavelength to couple into a waveguide mode at a particular angle. In this angle the transmission of the beam decreases by more than 50% (figure I-35).

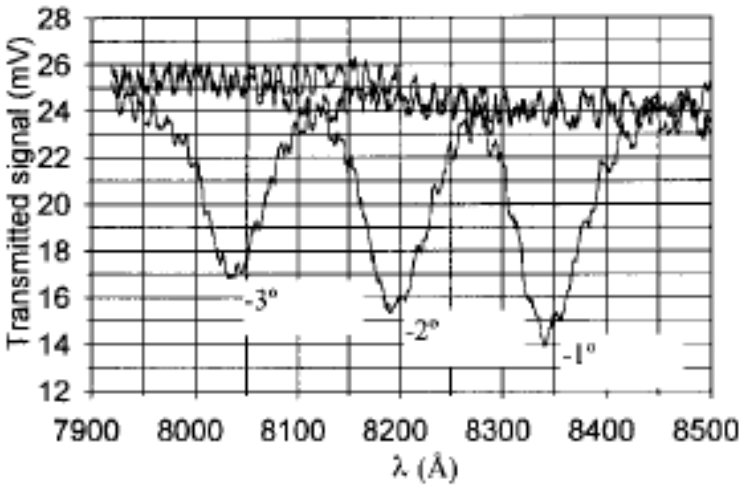

Figure I-35: Three fixed angles of incidence on the SRG, produce three wavelength filters [172].

I-10-3- Polarization separator

SRGs can also be used as polarization separator (discriminator). Since the orientation of the azobenzene groups can be controlled with polarized light, the material can be used not only to record intensity holograms but also to simultaneously record a polarization hologram. The case of the pattern formed by two interfering contra-circularly polarized beams is a mixed one. In this case there is only a small intensity modulation and the pattern is characterized by a spatial modulation of the local polarization. This produces a spatial modulation of the orientation of the azo groups within the recording film. When unpolarized light is transmitted through this grating, right circularly polarized light is diffracted in one direction and left circularly polarized light is diffracted in the other. This is illustrated in Figure I-36. The film thus acts as a polarization separator [173].

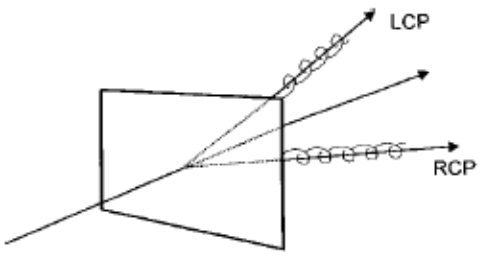

Figure I-36: Schematic view of a polarization separator. The incoming light is separated according to the handedness of its polarization by the polarization holographic volume grating. LCP = left circularly polarized. RCP = right circularly polarized [173].

Kumar et al. found that, with the same experimental setup and for grating with 1μm pitch and amplitude of 150 nm, the +1 order diffracted beam of an unpolarized He-Ne probe beam (633 nm) was horizontally polarized [80]. Figure I-37 shows schematic of this polarization discriminator.

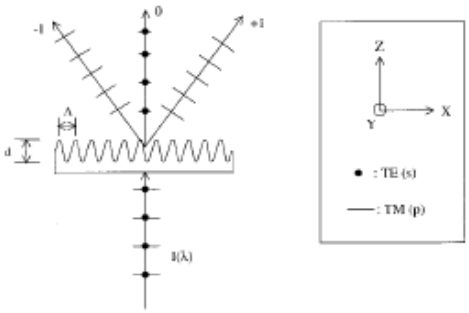

Figure I-37: Schematic of polarization discriminator [80]

I-10-4- Liquid Crystal Orientation

Traditionally alignment in LC cells has been done by physical rubbing. The LC molecules could be aligned on the surfaces with azobenzene molecules, which undergo cis–trans isomerization changes on irradiating with UV light. Also, the SRG could align the LC molecules along the grating direction by topologically induced regular structure [174-176].
This technique gives a zero pretilt angle alignment and the ease of variation of the grating size can be used in the preparation of in-plane switching liquid crystal optical devices. Furthermore, the possibility of photo-inducing an optically erasable twisted nematic state within the liquid crystal cell opens the avenue for optically driven liquid crystal displays. Figure I-38 represents the LC orientation by use of SRG.

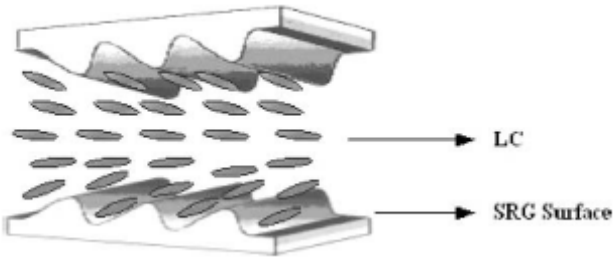

Figure I-38: Schematic of LC orientation [176]

I-10-5- Holography Applications

The ease of inscription of SRGs and their stability makes them suitable in one-step holographic image storage applications. One object mask can place in the path of one of the interfering beams. The beam carrying the object mask information interfere with another collimated beam at the recording medium plane and it can form a surface relief hologram. An expanded He-Ne laser can use to reconstruct the holographic image [80].

Munakata et al. demonstrated a Fourier transform hologram recording using SRG formation technique [177]. A circularly polarized Ar+ laser (488 nm) used as writing beam (figure I-39).

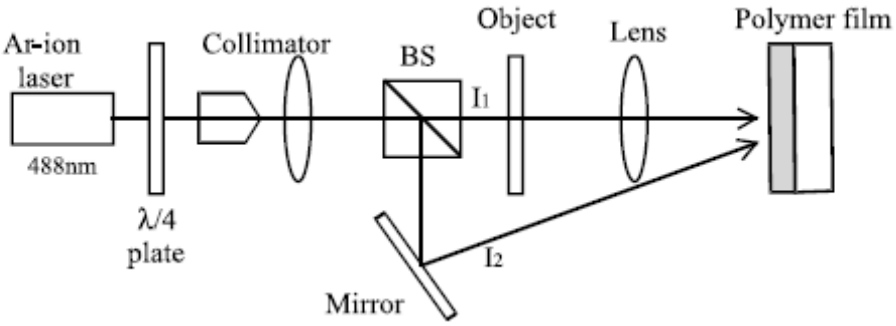

Figure I-39: Experimental setup for the Fourier transform hologram recording [177]

The letters A and E were used as object and Fourier transformed on the film by a lens (figure I-40).

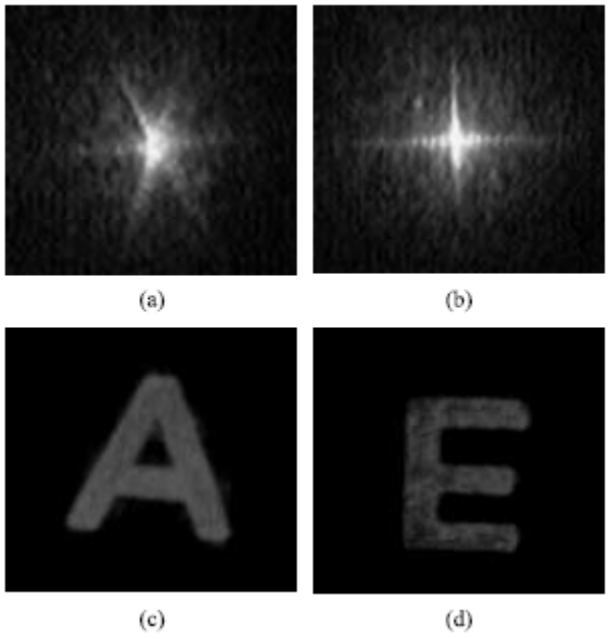

Figure I-40: The Fourier transform holograms of a) letter A and b) Letter E recorded on the azo-polymer film and the reconstructed images c)letter A and d)letter E [177].

I-10-6- Electro-optical device and Second Harmonic Generation

SRG can be used as an active diffraction device when it is subjected to poling because the azo polymer film exhibits an electro-optic effect. The modulation of a surface-relief electro-optic grating with this SRG has also been reported [178]. This group also showed that by applying corona discharge the diffraction efficiency increase from 2% to 40%. Using this increase one can fabricate a surface-relief electro-optic grating with high diffraction efficiency at a relatively low writing power [179].

Another application was second harmonic generation (SHG), in which an SRG-inscribed urethane-urea copolymer film was poled with a corona discharge at 150°C, above the Tg of the copolymer [180]. An efficiency of 2.12% for SHG conversion at a guided fundamental power of 264 W was demonstrated. The film could be poled at a temperature greater than Tg, with no erasure of the SRG. The detailed microscopic structure of the poled SRG has been studied with confocal polarized Raman microspectroscopy and SHG near-field scanning optical microscopy [181-183].

More recently Chang et al. fabricated a χ^2 periodic structure by electric field poling of the SRG of an azobenzene containing polymer film [184]. The measurement of the diffraction efficiency (DE) and SHG signal, allowed them to monitor the SRG variations. The molecular alignment inside the poled SRG is probed by the image obtained with a dynamic-contact electrostatic force microscope (DC-EFM). The DC-EFM maps electric properties such as the surface potential and the charge distribution of a sample surface by measuring the electrostatic force between the surface and a biased AFM cantilever and simultaneously it can give topological image of surface. After electric field poling, the DE and SRG depth increase and reach double of the initial values. The DC-EFM image of poled SRG has shown a sinusoidal distribution of polar ordering along one axis with a period which is the same as of the topological AFM image, whereas it was constant along other one. Based on these results, the microstructure of the poled SRG was found to belong to the C_{2v} point-group symmetry (Figure I-41). The polarization dependence of the electro-optics effects further confirmed the optically biaxial structure of the poled SRG, which is in agreement with the results reported by Lagugné-Labarthet et al. [182].

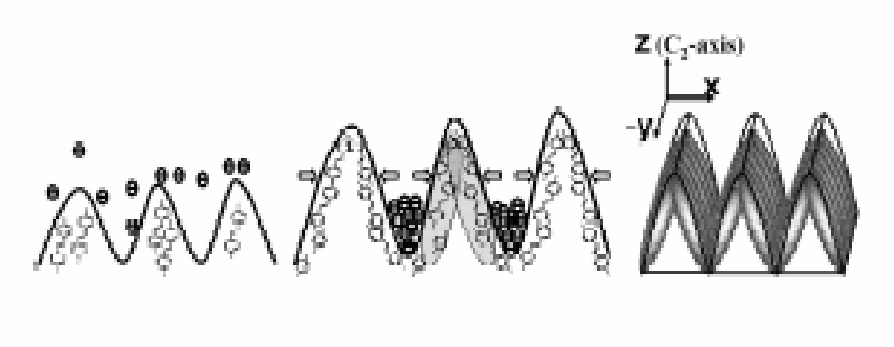

Figure I-41: The development of C_{2v} symmetry in the poled SRG by a lateral force during the corona poling process [184].

I-10-7- Cell growth

Cell-surface interactions and cell patterning are very important from scientific and engineering points of view. The controlling of the cell growth on the patterned surfaces lead to some important applications such as neural network organization, the biocompatibility test of biomedical or prosthetic implants in an organized manner, and the creation of high-resolution cell-based biosensors. There are several techniques based on photolithography or micro-contact printing to pattern the surfaces for this application

Baac et al. have cultured Primary human astrocytes (HAs) on the surface of a holographically made SRG (the pitch and depth were 1μm and 250 nm) [185]. The cells were preferentially attached onto the SRG pattern forming a monolayer were aligned along the direction of the submicron-sized SRG (normal to the grating wave vector).The cultured cells on the flat and SRG regions are shown in figure I-42.

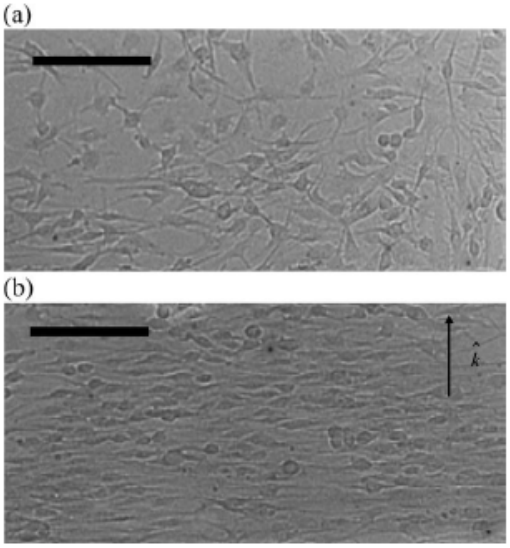

Figure I-42: The controlled cell orientation 7 days after inoculation (scale bar = 100 Am). The cells are proliferated with random orientation in the flat region (a), but still toward the groove direction (b) [185].

The cells were densely populated with random orientation forming multiple layers over the whole flat region of substrate 7 days after inoculation. In the SRG regions, in contrast, the cell proliferation was still toward the groove direction. The pitch and depth of SRGs can be control easily and depending on the nature of cell one can select suitable material for SRG formation. Consequently SRGs are one of the effective candidates for the cell orientation and patterning to organize cell networks.

I-10-8- Substrate patterning for photonic applications

Usually in device fabrication such as thin film transistors, liquid crystal displays, organic light emitting diodes and plasma display panels patterned transparent layers (for example ITO) are mandatory. Yang et al. proposed a patterning process based on SRG formation on azo-polymer film [186]. To obtain a patterned substrate, a ITO deposited glass substrate was coated with an azo-polymer film, SRG was inscribed on the surface of azo-polymer film using interference of two coherent laser beams, then a plasma-etcher was used to etch polymer film in order that the valleys of grating get in touch with ITO layer. Finally the ITO was etched in dilute hydrochloric acid and the sample was washed with an appropriate solvent to remove residual azo-polymer. The process is shown in figure I-43 schematically.

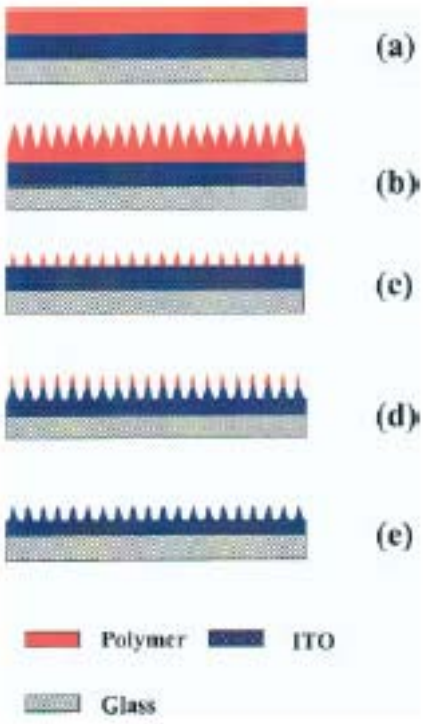

Figure I-43: Substrate patterning process. a) Sample before SRG formation. b) SRG inscribed on the surface of azo-polymer film. c) The polymer has etched with plasma-etcher. d) ITO layer etched with hydrochloric acid. e) Residual polymer washed with an appropriate organic solvent [186].

I-11- Conclusion

In summary, we introduced some natural and optical self-organized pattern formation. Also we reviewed SRG formation mechanisms in azo-polymers and their applications. Interference of two coherent laser beams has been used to writing surface relief grating on azo-polymer films. Formation and development of SRG depend on the material characteristics and experimental details. Several mechanisms were proposed to explain the origin of this phenomenon. The basic of these mechanisms as well as their advantages and disadvantages were explained. The idea of one beam manipulation of azo-materials was developed. Single laser beam is deformed surface of azo-polymer materials with the material diffusion in the direction of input beam polarization. Photo-mechanical deformation of azo-polymer film (expansion and contraction) was discussed. Azo-colloids spheres have been deformed by a single laser beam. Laser induced periodic surface structure formation were discussed in details. Surface relief gratings can give rise to some interesting applications. Couplers, filters, polarization separator, liquid crystal orientation, holography applications, electro-optical device and Second Harmonic Generation, cell growth and substrate patterning for photonic applications were some of them discussed in this chapter. Light induced birefringence and surface relief grating formation of a new series of azo-polymers were presented.

In the next chapter we will present a simple experimental setup for spontaneous SRG formation on azo-polymer films. We will discuss influence of input laser beam parameters and material structures on the self-organized SRG formation. Reversibility and relaxation of formed gratings will be studied. Polarization multiplexing will be described in this system.

I-12- References

1- S. Camazine, J. Sneyd, M. J. Jenkins, J. D. Murray, A mathematical model of self-organizing pattern formation on the combs of honey-bee colonies, J. Theor. Bio. , 1990, **147**, 553-571.

2- S. Camazine, Self-organizing pattern formation on the combs of honeybee colonies, Behav. Ecol. Sociobiol., 1991, **28**, 61-76.

3- J. Desneux, Structures 'atypiques' dans les nidifications souterraines d'*Apicotermes lamani* Sj. (Isoptera, Termitidae) mises en évidence par la radiographie, Insectes Soc., 1956, **3**, 277-281.

4- A. Bouillon, Les termites du Katanga, Natur. Belges, 1958, **39**, 198-207.

5- J. –L. Deneubourg, S. Goss, Collective patterns and decision making, Ethol. Ecol. Evol., 1989, **1**, 295-311.

6- S. Camazine, J. –L. Deneubourg, N. Franks, J. Sneyd, G. Theraulaz, E. Bonabeau, Self organization in biological systems, Princeton, NJ: Princeton University Press, 2001.

7- N. R. Franks, A. B. Sendova-Franks, Brood sorting by ants: distributing the workload over the work-surface, Behav. Ecol Sociobiol., 1992, **30**, 109-123.

8- F. T. Arecchi, S. Boccaletti, P. L. Ramazza, Pattern formation and competition in nonlinear optics, Phys. Rep., 1999, **318**, 1-83.

9- G. Grynberg, Mirrorless four-wave mixing oscillation in atomic vapors, Opt. Commun., 1988, **66,** 321-324.

10- J. Pender, L. Hesselink, Degenerate conical emission in atomic-sodium vapour, J. Opt. Soc. Am. B, 1990, **7,** 1361-1373.

11- R. Macdonald, H. J. Eichler, Spontaneous optical pattern formation in a nematic liquid crystal with feedback mirror, Opt. Commun., 1992, **89,** 289-295.

12- M. Tamburrini, M. Bonavita, S. Wabnitz, E. Santamato, Hexagonally patterned beam filamentation in a thin liquid-crystal film with a single feedback mirror, Opt. Lett., 1993, **18,** 855-857.

13- V. I. Bespalov, V. I. Talanov, Filamentary structure of light beams in nonlinear liquids, JETP Lett., 1966, **3**, 307-310.

14- M. D. Iturbe-Castillo, M. Torres-Cisneros, J. J. Sanchez-Mondragon, S. Chavez-Cerda, S. I. Stepanov, V. A. Vysloukh, G. E. Torres-Cisneros, Experimental evidence of modulation instability in a photorefractive Bi12TiO20 crystal, Opt. Lett., 1995, **20**, 1853-1855.

15- R. Malendevich, L. Jankovic, G. Stegeman, J. S. Aitchison, Spatial modulation instability in a Kerr slab waveguide, Opt. Lett., **26**, 2001, 1879-1881.

16- L. A. Lugiato, Transverse nonlinear optics: Introduction and review, Chaos Solitons Fractals, 1994, **4**, 1251-1258.

17- P. M. Lushnikov, A. V. Mamaev, Spontaneous hexagon formation in photorefractive crystal with a single pump wave, Opt. Lett., 1999, **24**, 1511-1513.

18- G. D'Alessandro, W. J. Firth, Spontaneous hexagon formation in a nonlinear optical medium with feedback mirror, Phys. Rev. Lett., 1991, **66**, 2597-2600.

19- Aumann A., Ackemann T., Lange W., Selection between hexagonal, square and stripe patterns in a polarization instability: an experimental investigation, Ann. Phys. (Leipzig), 2004, **13**, 379 – 390.

20- R. S. Bennink, V. Wong, A. M. Marino, D. L. Aronstein, R. W. Boyd, C. R. Stroud, Jr., S. Lukishova, D. J. Gauthier, Honeycomb pattern formation by laser-beam filamentation in atomic sodium vapor, Phys. Rev. Lett., 2002, **88**, 113901.

21- M. Soljacic, M. Segev, T. Coskun, D. N. Christodoulides, A. Vishwanath, Modulation instability of incoherent beams in noninstantaneous nonlinear media, Phys. Rev. Lett., 2000, **84**, 467-470.

22- S.M. Sears, M. Soljacic, D. N. Christodoulides, M. Segev, Pattern formation via symmetry breaking in nonlinear weakly correlated systems, Phys. Rev. E, 2002, **65**, 036620 .

23- D. Kip, M. Soljacic, M. Segev, E. Eugenieva, D. N. Christodoulides, Modulation instability and pattern formation in spatially incoherent light beams, Science, 2000, **290**, 495-498.

24- D. Kip, M. Soljacic, M. Segev, S. M. Sears, D. N. Christodoulides, (1-1)- Dimensional modulation instability of spatially incoherent light, J. Opt. Soc. Am. B, 2002, **19**, 502-512.

25- J. Klinger, H. Martin, Z. Chen, Experiments on induced modulational instability of an incoherent optical beam, Opt. Lett., 2001, **26**, 271-273.

26- H. Buljan, M. Soljacic, T. Carmon, M. Segev, Cavity pattern formation with incoherent light, Phys. Rev. E, 2003, **68**, 016616.

27- T. Carmon, H. Buljan, M. Segev, Spontaneous pattern formation in a cavity with incoherent light, Opt. Express, 2004, **12**, 3481-3487.

28- D. Anderson, L. Helezynski-Wolf, M. Lisak, V. Semenov, Features of modulational instability of partially coherent light: Importance of the incoherence spectrum, Phys. Rev. E, 2004, **69**, 025601.

29- T. Schwartz, T. Carmon, H. Buljan, M. Segev, Spontaneous pattern formation with incoherent white light, Phys. Rev. Lett., 2004, **93**, 223901.

30- C. Hubert, E. Malcor, I. Maurin, J. -M. Nunzi, P. Raimond, C. Fiorini, Microstructuring of polymers using a light-controlled molecular migration processes, Appl. Surf. Sci., 2002, **186**, 29-33.

31- C. Hubert, C. Fiorini-Debuisschert, I. Maurin, J.-M. Nunzi, P. Raimond, Spontaneous patterning of hexagonal structures in an azo-polymer using light-controlled mass transport, Adv. Mater., 2002, **14**, 729-732.

32- C. Hubert, C. Fiorini-Debuisschert, P. Raimond, J.-M. Nunzi, J. –J. Simon, L. Escoubas, Spontaneous photo-induced structuration of the surface of Azo-benzene polymer by the molecular migration effect, Nonl. Opt., Quant. Opt., 2004, **31**, 221-230.

33- C. Hubert, C. Fiorini-Debuisschert, R. L. Hassiaoui, P. Raimond, J.-M. Nunzi, Emission properties of an organic light-emitting diode patterned by a photo-induced autostructuration process, Appl. Phys. Lett., 2005, **87**, 191105.

34- H. Rau, in *Photochemistry and Photophysics*; Vol. **2**, edited by J. Rebek (CRC Press, Boca Raton, FL, 1990), 119-141.

35- F.W.Schulze, H.J. Petrick, H.K.Cammenga, H.Klinge, Thermodynamic properties of the structural analogs benzo[c]cinnoline, trans-azobenzene, and cis-azobenzene, Z. Phys. Chem. (Muenchen, Ger.), 1977, **107,** 1-19.

36- I.Mita, K.Horie, K.Hirao, Photochemistry in polymer solids. 9. Photoisomerization of azobenzene in a polycarbonate film, Macromolecules, 1989, **22**, 558-563.

37- S. Monti, G. Orlandi, P. Palmieri, Features of the photochemically active state surfaces of azobenzene, Chem. Phys., 1982, **71**, 87-99.

38- T. Kobayashi, E.O. Degenkolb, P.M. Rentzepis, Picosecond spectroscopy of 1-phenylazo-2-hydroxynaphthalene, J. Phys. Chem., 1979, **83**, 2431-2434.

39- I.K. Lednev, T.-Q. Ye, R.E. Hester, J.N. Moore, Femtosecond Time-Resolved UV-Visible Absorption Spectroscopy of *trans*-Azobenzene in Solution, J. Phys. Chem., 1996,**100**, 13338-13341.

40- E.V. Brown, G.R. Granneman, Cis-trans isomerism in the pyridyl analogs of azobenzene. Kinetic and molecular orbital analysis, J. Am. Chem. Soc., 1975, **97**, 621-627.

41- P. Haberfield, P.M. Block, M.S. Lux, Enthalpies of solvent transfer of the transition states in the cis-trans isomerization of azo compounds. Rotation vs. the nitrogen inversion mechanism, J. Am. Chem. Soc., 1975, **97**, 5804-5806.

42- L. Lamarre, C.S.P. Sung, Studies of physical aging and molecular motion by azochromophoric labels attached to the main chains of amorphous polymers, Macromolecules, 1983, **16,** 1729-1736.

43- Y. Shirota, K. Moriwaki, S. Yoshikawa, T. Ujike, H. Nakano, 4-[Di(biphenyl-4-yl)amino]azobenzene and 4,4'-bis[bis(4'-*tert*-butylbiphenyl-4-yl)amino] azobenzene as a novel family of photochromic amorphous molecular materials, J. Mater.Chem., 1998, **8**, 2579-2581.

44- Y. Norikane, K. Kitamoto, N. Tamaoki, Novel Crystal Structure, Cis-Trans Isomerization, and Host Property of Meta-Substituted Macrocyclic Azobenzenes with the Shortest Linkers, J. Org. Chem., 2003, **68**, 8291-8304.

45- H. Rau, D. Roettger, Photochromic azobenzenes which are stable in the trans and cis forms, Mol. Cryst. Liq. Cryst. Sci. Techol. A, 1994, **246**,143-146.

46- D. Rottger, H. Rau, J. Photochem. Photobiol. A, Photochemistry of azobenzenophanes with three-membered bridges, 1996, **101**, 205-214.

47- S.A. Nagamani, Y. Norikane, N. Tamaoki, Photoinduced hinge-like molecular motion: studies on Xanthene-based cyclic azobenzene dimers, J. Org. Chem., 2005, **70**, 9304-9313.

48- M.S. Vollmer, T.D. Clark, C. Steinem, M.R. Ghadiri, Photoswitchable hydrogen-bonding in self-organized cylindrical peptide systems, Angew. Chem., Int. Ed., 1999, **38**, 1598-1601.

49- B.K. Kerzhner, V.I. Kofanov, T.L. Vrubel, Photoisomerization of aromatic azo compounds adsorbed on a hydroxylated surface, Zhurnal Obshchei Khimii, 1983, **53**, 2303-2306.

50- U. Funke, H.F. Gruetzmacher, Dithia-diaza[n. 2] paracyclophane-enes, Tetrahedron, 1987,**43**, 3787-3795.

51- G.S. Hartley, Cis form of azobenzene, Nature (London U.K.), 1937, **140**, 281.

52- G.S. Hartley, The *cis*-form of azobenzene and the velocity of the thermal *cis*⟶*trans*-conversion of azobenzene and some derivatives, J. Chem. Soc., 1938, 633-642.

53- W.J. Priest, M.M. Sifain, Photochemical and thermal isomerization in polymer matrices: Azo compounds in polystyrene, J. Polym. Sci. Part A-1: Polym. Chem., 1971, **9**, 3161-3168.

54- C.S. Paik, H. Morawetz, Photochemical and thermal isomerization of azoaromatic residues in the side chains and the backbone of polymers in bulk, Macromolecules, 1972, **5**, 171-177.

55- C. Barrett, A. Natansohn, P. Rochon, Cis-Trans thermal isomerization rates of bound and doped azobenzenes in a series of polymers, Chem. Mater., 1995, **7**, 899-903.

56- C. Barrett, A. Natansohn, P. Rochon, Thermal Cis-Trans Isomerization rates of azobenzenes bound in the side chain of some copolymers and blends, Macromolecules, 1994, **27**,4781-4786.

57- N. Sarkar, A. Sarkar, S. Sivaram, Isomerization behavior of aromatic azo chromophores bound to semicrystalline polymer films, J. Appl. Polym. Sci., 2001, **81**, 2923-2928.

58- J.J. de Lange, J.M. Robertson, I. Woodward, X-ray crystal analysis of trans-azobenzene, Proc. Roy. Soc. (London), 1939, **A171,** 398-410.

59- G.C. Hampson, J.M. Robertson, Bond lengths and resonance in the *cis*-azobenzene molecule, J. Chem. Soc., 1941, 409-413.

60- C.J. Brown, A refinement of the crystal structure of azobenzene, Acta Crystallogr., 1966, **21,** 146-152.

61- T. Naito, K. Horie, I. Mita, Photochemistry in polymer solids: 12. Effects of main-chain structures and formation of hydrogen bonds on photoisomerization of azobenzene in various polymer films, Polymer, 1993, **34**, 4140-4145.

62- T. Naito, K. Horie, I. Mita, Photochemistry in polymer solids. 11. The effects of the size of reaction groups and the mode of photoisomerization on photochromic reactions in polycarbonate film, Macromolecules, 1991, **24**, 2907-2911.

63- T. Hugel, N.B. Holland, A. Cattani, L. Moroder, M. Seitz, H.E. Gaub, Single-molecule optomechanical cycle, Science (Washington, DC, U.S.), 2002, **296**, 1103-1106.

64- N.B. Holland, T. Hugel, G. Neuert, A. Cattani-Scholz, C. Renner, D. Oesterhelt, L. Moroder, M. Seitz, H.E. Gaub, Single molecule force spectroscopy of azobenzene polymers: switching elasticity of single photochromic macromolecules**,** Macromolecules, 2003, 36, 2015-2023.

65- Y. Li, Y. Deng, X. Tong, X. Wang, Formation of photoresponsive uniform colloidal spheres from an amphiphilic azobenzene-containing random copolymer, Macromolecules, 2006, **39**, 1108-1115.

66- K. Tanaka, Y. Tateishi, T. Nagamura, Photoisomerization of azobenzene probes tagged to polystyrene in thin films, Macromolecules, 2004, **37**, 8188-8190.

67- A. Natansohn, P. Rochon, M. Pezolet, P. Audet, D. Brown, S. To, Azo polymers for reversible optical storage. 4. cooperative motion of rigid groups in semicrystalline polymers, Macromolecules, 1994, **27**, 2580-2585.

68- R. Hagen, T. Bieringer, Photoaddressable polymers for optical data storage, Adv. Mater. (Weinheim, Ger.), 2001, **13**, 1805-1810.

69- P.M. Blanchard, G.R. Mitchell, A comparison of photoinduced poling and thermal poling of azo-dye-doped polymer films for second order nonlinear optical applications, Appl. Phys. Lett., 1993, **63**, 2038-2040.

70- P.M. Blanchard, G.R. Mitchell, Localized room temperature photo-induced poling of azo-dye-doped polymer films for second-order nonlinear optical phenomena, J. Phys. D: Appl. Phys., 1993, **26**, 500-503.

71- Z. Sekkat, C.-S. Kang, E.F. Aust, G. Wegner, W. Knoll, Room-temperature photoinduced poling and thermal poling of a rigid main-chain polymer with polar Azo dyes in the side chain, Chem. Mater., 1995, **7**, 142-147.

72- X.L. Jiang, L. Li, J. Kumar, S.K. Tripathy, Photoassisted poling induced second harmonic generation with in-plane anisotropy in azobenzene containing polymer films, Appl. Phys. Lett., 1996, **69**, 3629-3631.

73- J.-M. Nunzi, C. Fiorini, A.-C. Etil´e, F. Kajzar, All-optical poling in polymers: dynamical aspects and perspectives, Pure Appl. Opt.: J. Eur. Opt. Soc. A, 1998, **7**, 141-150.

74- X. Zhong, X. Yu, Q. Li, S. Luo, Y. Chen, Y. Sui, J. Yin, Identification of the alignment of azobenzene molecules induced by all-optical poling in polymer film, Opt. Commun., 2001,**190**, 333-337.

75- K. Ichimura, Photoalignment of liquid-crystal systems, Chem. Rev., 2000, **100**, 1847-1874.

76- V. Shibaev, A. Bobrovsky, N. Boiko, Photoactive liquid crystalline polymer systems with light-controllable structure and optical properties, Prog. Polym. Sci., 2003, **28**, 729-836.

77- Y.L. Yu, T. Ikeda, Alignment modulation of azobenzene-containing liquid crystal systems by photochemical reactions, J. Photochem. Photobiol. C, 2004, **5**, 247-265.

78- S.T. Sun, W.M. Gibbons, P.J. Shannon, Alignment of guest-host liquid crystals with polarized laser light, Liq. Cryst., 1992, **12**, 869-874.

79- K. Anderle, R. Birenheide, M.J.A. Werner, J.H. Wendorff, Molecular addressing? Studies on light-induced reorientation in liquid-crystalline side chain polymers, Liq. Cryst., 1991, **9**, 691-699.

80- N.K. Viswanathan, D.Y. Kim, S. Bian, J. Williams, W. Liu, L. Li, L. Samuelson, J. Kumar, S.K. Tripathy, Surface relief structures on azo polymer films, J. Mater. Chem., 1999, **9**, 1941-1955.

81- P. Rochon, E. Batalla, A. Natansohn, Optically induced surface gratings on azoaromatic polymer-films, Appl. Phys. Lett., 1995, **66,**136-138.

82- D. Kim, S. Tripathy, L. Lian, J. Kumar, Laser-induced holographic surface-relief gratings on non-linear-optical polymer-films, Appl. Phys. Lett., 1995, **66,**1166-1168.

83- E. Ortyl, R. Janik, S. Kucharski, Methylacrylate polymers with photochromic side chains containing heterocyclic sulfonamide substitued azobenzene, Eur. Poly. J., 2002, **38**, 1871–1879.

84- A.Teitel, Über eine besondere mechanische wirkung des polarisierten lichts, Naturwissenschaften, 1957, **44**, 370-371.

85- B. S. Neporent, O. V.Stolvova, Orientational photodichroism of viscous solutions, Optika i Spektroskopiya, 1961, **10**, 287-288.

86- B. S. Neporent, O. V. Stolvova, Reversible orientational photodichroism in viscous solutions of complex organic substances, Optika i Spektroskopiya , 1963, **14**, 624-633.

87- A. M. Makushenko, B. S. Neporent, O. V. Stolvova, Reversible orientational photodichroism and photoisomerization of aromatic azo compounds. I. System model, Optika i Spektroskopiya, 1971, **31**,557-564.

88- A. M. Makushenko, B. S. Neporent, O. V. Stolvova, Reversible orientational photodichroism and photoisomerization of complex organic compounds in viscous solutions. II. Azobenzene and substituted derivatives of azobenzene, Optika i Spektroskopiya, 1971, **31**,741-748.

89- P. Rochon, J. Gosselin, A. Natansohn, S. Xie, Optically induced and erased birefringence and dichroism in azoaromatic polymers, Appl. Phys. Lett., 1992, **60**, 4-5.

90- A. Natansohn, P. Rochon, J. Gosselin, S. Xie , Azo polymers for reversible optical storage. 1.Poly[4'- [[2- (acr yloyloxy)ethyll ethylaminol-4-ni troazo benzene], Macromolecules, 1992,**25**, 2268-2273.

91- A. Natansohn, P. Rochon, Azo Polymers for reversible optical storage. 2. Poly[4‘4 [24 acryloyloxy)ethyl]ethylamino]-2-c hloro-4-nitroazobenzene], Macromolecules 1992,**25**, 5531-5532.

92- A. Natansohn, P. Rochon, M. S. Ho and C. Battett, Azo polymers for reversible optical storage. 6. Poly[4-[2-(methacryloyloxy)ethyl]azobenzene], Macromolecules, 1995, **28**, 4179-4183.

93- M. S. Ho, A. Natansohn, P. Rochon, Azo polymers for reversible optical storage. 7. The effect of the size of the photochromic groups, Macromolecules, 1995, **28,** 6124-6127.

94- L. Zhang, Z. Cai, V. Ninulescu, K. Jin, Z. Liang, Photoinduced birefringence and numerical solution of a new dynamic model in an amorphous copolymer containing azobenzene groups, Chinese J. Polym. Sci., 2001, **19**, 255-263.

95- E. Ortyl, S. Kucharski, Refractive index modulation in polymeric photochromic films, Cent. Eur. J. Chem., 2003, **2**, 137-159.

96- C. Barrett, B. Choudhury, A. Natansohn, P. Rochon., Azocarbazole polymethacrylates as single-component electrooptic materials, Macromolecules, 1998, **31**, 4845-4851.

97- F. L.Labarthet, T. Buffeteau, C. Sourisseau, Analyses of the diffraction efficiencies, birefringence, and surface relief gratings on azobenzene-containing polymer films, J. Phys. Chem. B, 1998, **102***,* 2654-2662.

98- N. Sertova, I. Petkov, C. Fiorini, P. Raimond, J.-M. Nunzi, Photoinduced surface relief grating formation in polymers doped with bis-azodyes , Molecular Crystals and Liquid Crystals Science and Technology Section A: Molecular Crystals and Liquid Crystals, 2002, **374**, 77-84.

99- J. A. Delaire, K. Nakatani, Linear and nonlinear optical properties of photochromic molecules and materials, Chem. Rev., 2000, **100**, 1817-1845.

100- A. Natansohn; P. Rochon, Photoinduced motions in azo-containing polymers, Chem. Rev., 2002, **102**, 4139-4175.

101- O. N. Oliveira, L. Li, J. Kumar, S. K. Tripathy, In Photoreactive Organic Thin Films; Sekkat, Z., Knoll, K., Eds.; Academic Press: San Diego, CA, 2002; 429-486.

102- Y. He, H. Wang, X. Tuo, X. Wang, Synthesis, self-assembly and photoinduced surface-relief gratings of a polyacrylate-based Azo polyelectrolyte, Opt. Mater., 2004, **26**, 89-93.

103- V. Borger, O. Kuliskovska, K. G. Hubmann, J. Stumpe, M. Huber, H. Menzel, Novel polymers to study the influence of the azobenzene content on the photo-induced surface relief grating formation, Macromol. Chem. Phys., 2005, **206**, 1488-1496.

104- B. Loppinet, E. Somma, N. Vainos, G. Fytas, Reversible holographic grating formation in polymer solutions, J. Am. Chem. Soc., 2005, **127**, 9678-9679.

105- A. Stracke, J. H. Wendorff, D. Goldmann, D. Janietz, B. Stiller, Gain effects in optical storage: thermal induction of a surface relief grating in a smectic liquid crystal, Adv. Mater., 2000, **12**, 282-285.

106- T. Ubukata, T. Seki, K. Ichimura, Surface relief gratings in host-guest supramolecular materials, Adv. Mater. 2000, **12**, 1675-1678.

107- T. Yamamoto, M. Hasegawa, A. Kanazawa, T. Shiono, T. Ikeda, Holographic gratings and holographic image storage via photochemical phase transitions of polymer azobenzene liquid-crystal films, J. Mater. Chem., 2000**, 10**, 337-342.

108- P. S. Ramanujam, N. C. Holme, S.Hvilsted, Atomic force and optical near-field microscopic investigations of polarization holographic gratings in a liquid crystalline azobenzene side-chain polyester, Appl. Phys. Lett., 1996, **68**, 1329-1331.

109- J. Wang, P. Xu, X. Li, J. Shen, G. Wu, B. Zhou, Optical properties of sol-gel coatings on plastic foils embossed with surface-relief gratings, J. Sol-Gel Sci. Tech., 2002, **23**, 73–77.

110- C. R. Mendoca, R. Dhanabalan, D. T. Balogh, L. Misoguti, D. S. dos Santos, M. A. Pereira-da-Silva, J. A. Giacometti, S. C. Zilio, O. N. Oliveira, Optically induced birefringence and surface relief gratings in composite Langmuir-Blodgett (LB) films of Poly[4'-[[2-(methacryloyloxy)ethyl]ethylamino]-2-chloro-4-nitroazobenzene] (HPDR13) and cadmium stearate, Macromolecules, 1999, **32**, 1493-1499.

111- J.-A. He, S. Bian, L. Li, J. Kumar, S. K. Tripathy, L. A. Samuelson, Photochemical behavior and formation of surface relief grating on self-assembled Polyion/Dye composite film, J. Phys. Chem. B, 2000, **104**, 10513-10521.

112- L. M. Goldenberg, O. Kulikovska, J. Stumpe, Thermally stable holographic surface relief gratings and switchable optical anisotropy in films of an azobenzene-containing polyelectrolyte, Langmuir, 2005, **21**, 4794-4796.

113- Y. He, H. Wang, X. Tuo, W. Deng, X. Wang, Synthesis, self-assembly and photoinduced surface-relief gratings of a polyacrylate-based Azo polyelectrolyte, Opt. Mater., 2004, **26**, 89-93.

114- H. Nakano, T. Tanino, Y. Shirota, Surface relief grating formation on a single crystal of 4-(dimethylamino)azobenzene, Appl. Phys. Lett., 2005, **87**, 061910-061912.

115- Y. Shirota, Photo- and electroactive amorphous molecular materials- molecular design, syntheses, reactions, properties, and applications, J. Mater. Chem., 2005, **15**, 75-93.

116- E. Ishow, B. Lebon, Y. He, X. Wang, L. Bouteiller, L. Galmiche, K. Nakatani, Structural and photoisomerization cross studies of polar photochromic monomeric glasses forming surface relief gratings, Chem. Mater., 2006, **18**, 1261-1267.

117- L.-H. Liu, K. Nakatani, R. Pansu, J. -J. Vachon, P. Tauc, E. Ishow, Fluorescence patterning through photoinduced migration of squaraine-functionalized azo derivatives, Adv. Mater., 2007, **19**, 433-436.

118- X. L. Jiang, J.Kumar, D. Y. Kim, V. Shivshankar, S. K. Tripathy, Polarization dependent recordings of surface relief gratings on azobenzene containing polymer films, Appl. Phys. Lett., 1996, **68**, 2618-2620.

119- S. K. Tripathy, D. Y. Kim, X. L. Jiang, L. Li, T. Lee, X. Wang, J. Kumar, Photofabrication of surface relief gratings using photodynamic polymers, Mol. Cryst. Liq. Cryst., 1998, **314**,245-255.

120- N. C. R. Holme, L. Nikolova, P. S. Ramanujam, S. Hvilsted, An analysis of the anisotropic and topographic gratings in a side-chaine liquid crystalline azobenzene polyester, Appl. Phys. Lett., 1997, **70**, 1518-1520.

121- O. Watanabe, M. Narita, T. Ikawa, M. Tsuchimori, Photo-induced deformation behavior depending on the glass transition temperature on the surface of urethane copolymers containing a push–pull type azobenzene moiety, Polymer, 2006, **47**, 4742–4749.

122- C. J. Barrett, A. Natansohn, P. Rochon, Mechanism of optically inscribed high-efficiency diffraction gratings in azo polymer films, J. Phys. Chem., 1996, **100***,* 8836-8842.

123- C. J. Barrett, P.Rochon, A.Natansohn, Model of laser-driven mass transport in thin films of dye-functionalized polymers, J. Chem.Phys., 1998, **105***,* 1505-1516.

124- K. Sumaru, T. Yamanaka, T. Fukuda, H. Matsuda, Photoinduced surface relief gratings on azo-polymer films: analysis by a fluid mechanics model, Appl. Phys. Lett., 1999**, 75**, 1878-1880.

125- K. Sumaru, T. Fukuda, T. Kimura, H. Matsuda, T. Yamanaka, Photoinduced surface relief formation on azopolmymer films: a driving force and formed relief profile, J. Appl. Phys., 2002, **91**, 3421-3430.

126- J. Kumar, L. Li, X. L. Jiang, D. Y. Kim, T. S. Lee, S. Tripathy, Gradient force: the mechanism for surface relief grating formation in azobenzene functionalised polymers, Appl. Phys. Lett., 1998**, 72**, 2096-2098.

127- T. Fukuda, H. Matsude, T. Shiraga, T. Kimura, M. Kato, N. K. Viswanathan, J. Kumar, S.K. Tripathy, Photofabrication of surface relief grating on films of azobenzene polymer with different dye functionalization, Macromelecules, 2000, **33**, 4220-4225.

128- N. K. Viswanathan, S. Balasubramanian, L. Li, J. Kumar, S. K. Tripathy, Surface initiated mechanism for the formation of relief gratings on azo-polymer films, J. Phys. Chem., 1998, **102**, 6064-6070.

129- K. Yang, S. Yang, J. Kumar, Formation mechanism of surface relief structures on amorphous azopolymer films, Phys. Rev. B, 2006, **73**, 165204.

130- S. Bian, J. Williams, D. Kim, L. Li, S. Balasubramanian, J. Kumar, S. K Tripathy, Photoinduced surface deformations on azobenzene polymer films, J. Appl. Phys., 1999, **86**, 4498-4508.

131- O. Baldus, A. Leopold, R. Hagen, T. Bieringer, S. Zilker, Surface relief gratings generated by pulsed holography: a simple way to polymer nanostructures without isomerizing side-chains, J. Chem. Phys., 2001, **114**,1344-1349.

132- K. G. Yager, C. J. Barret, Temperature modeling of laser-irradiated azo-polymer thin films, J. Chem. Phys. 2004, **120**, 1089-1096.

133- S. Bauer-Gogonea, S. Bauer, W. Wirges, R. Gerhard-Multhaupt, Pyroelectrical investigation of the dipole orientation in nonlinear optical polymers during and after photoinduced poling, J.Appl. Phys., 1994, **76**, 2627-2635.

134- O. Baldus, S. Zilker, Surface relief gratings in photoaddressable polymers generated by CW holography, Appl. Phys. B, 2001;**72**, 425-427.

135- P. Lefin, C. Fiorini, J. -M. Nunzi, Anisotropy of the photo-induced translation diffusion of azobenzene dyes in polymer matrices , Pure and applied optics, 1998, **7**, 71-82.

136- P. Lefin, C. Fiorini, J. -M. Nunzi, Anisotropy of the photoinduced translation diffusion of azo-dyes, Opt. Mat., 1998, **9**, 323-328.

137- C. Fiorini, N. Prudhomme, G. De Veyrac, I. Maurin, P. Raimond, J.-M. Nunzi, Molecular migration mechanism for laser induced surface relief grating formation, Synthetic Metals, 2000, **115**, 121-125.

138- I. Naydenova, L. Nikolova, T. Todorov, N. Holme, P. Ramanujam, S. Hvilsted, Diffraction from polarization holographic gratings with surface relief in side-chain azobenzene polyesters, J. Opt. Soc. Am. B ,1998; **15**,1257-1265.

139- T. Pedersen, P. Johansen, N. Holme, P. Ramanujam, S. Hvilsted, Mean-field theory of photoinduced formation of surface reliefs in side-chain azobenzene polymers, Phys. Rev. Lett., 1998, **80,** 89-92.

140- K. G. Yager, C. J. Barrett, Photomechanical surface patterning in azo-polymer materials, Macromolecules; 2006; **39**, 9320-9326.

141- S. Bian, L. Li, J. Kumar, D. Y. Kim, J. Williams, S. K. Tripathy, Single laser beam-induced surface deformation on azobenzene polymer films, Appl. Phys. Lett., 1998, **73**, 1817-1819.

142- S. Bian, J. Williams, D. Y. Kim, L. Li, S. Balasubramanian, J. Kumar, S. K. Tripathy, Photoinduced surface deformation on azobenzene polymer films, Appl. Phys. Lett., 1999, **86**, 4498-4508.

143- Y. Yu, M. Nakano, and T. Ikeda, Directed bending of a polymeric film by light, Nature, 2003, **425**, 145.

144- T. Ikeda, M. Nakano, Y. Yu, O. Tsutsumi, A. Kanazawa, Anisotropic bending and unbending behavior of azobenzene liquid-crystalline gels by light exposure, Adv. Mater., 2003, **15**, 201-205.

145- N. Tabiryan, S. Serak, X.M. Dai, T. Bunning, Polymer film with optically controlled formand actuation, Opt. Express, 2005, **13,** 7442-7448.

146- Y. Xia, B. Gates, Y. Yin, Y. Lu, Monodispersed colloidal spheres: old materials with new applications**,** Adv. Mater., 2000, **12**, 693-713.

147- Y. Xia, Photonic crystals, a special issue in Adv. Mater. 2001, **13**, 369.

148- Z. Y. Li, J. Wang, B. Y. Gu., Full band gap in Fcc and Bcc photonic band gaps structure: non-spherical atom, J. Phys. Soc. Jpn. 1998, **67**, 3288-3291.

149- Y. Li, Y. He, X. Tong, X. Wang, Stretching effect of linearly polarized Ar^+ laser single-beam on azo polymer colloidal spheres, Langmuir, 2006**, 22**, 2288-2291.

150- Y. Li, Y. He, X. Tong, X. Wang, Photoinduced deformation of amphiphilic azo polymer colloideal spheres, J. Am. Chem. Soc., 2005, **127**, 2402-2403.

151- M. Birnbaum, Semiconductor surface damage produced by ruby lasers, J. Appl. Phys., 1965, **36**, 3688-3689.

152- P. Simon, J. Ihlemann, Ablation of submicron structures on metals and semiconductors by femtosecond UV-laser pulses, Appl. Surf. Sci., 1997, **109-110**, 25-29.

153- Y.F. Lu, W.K. Choi, Y. Aoyagi, A. Kinomura, K. Fujii, Controllable laser-induced periodic structures at silicon–dioxide/silicon interface by excimer laser irradiation, J. Appl. Phys., 1996, **80**,7052-7056.

154- A.E. Siegman, P.M. Fauchet, Stimulated Wood's anomalies on laser-illuminated surfaces, IEEE J. Quantum Electron., 1986, **22**,1384-1403.

155- P.A. Temple, M.J. Soileau, Polarization charge model for laser-induced ripple patterns in dielectric materials, IEEE J. Quantum Electron., 1981, **17**, 2067-2072.

156- F. Keilmann, Y.H. Bai, Periodic surface structures frozen into carbon dioxide laser-melted quartz, Appl. Phys.A, 1982, **29**, 9-18.

157- M. Bolle, S. Lazare, Submicron periodic structures produced on polymer surfaces with polarized excimer laser ultraviolet radiation**,** Appl. Surf. Sci., 1993, **65-66**,349-54.

158- M. Bolle, S. Lazare, Large scale excimer laser production of submicron periodic structures on polymer surfaces, Appl. Surf. Sci., 1993, **69**, 31-37.

159- M. Bolle, S. Lazare, Characterization of submicrometer periodic structures produced on polymer surfaces with low-fluence ultraviolet laser radiation, J. Appl. Phys., 1993, **73**, 3516-3524.

160- S. Lazare, P. Benet, Surface amorphization of Mylar$^{(R)}$ films with the excimer laser radiation above and below ablation threshold: Ellipsometric measurements, J. Appl. Phys., 1993, **74**, 4953-4957.

161- M. Sendova, H. Hiraoka, Sub-half-micron periodic structures on polymer surfaces with polarized laser irradiation, Jpn. J. Appl. Phys., 1993, **32**, 6182-6184.

162- M. Sendova, H. Hiraoka, Laser induced periodic structures on polymer surfaces; Surface Modification Technologies VII, Proceedings of the International Conference, 7th, Sanjo, Japan, (1994), 641-648.

163- S. Lazare, W. Guan, D. Drihole, M. Bolle, J. Lopez, Ablation and surface modification of polymers with ultraviolet laser radiation J. Photopolym. Sci. Tech., 1995, **8**,495-503.

164- M. Csete, O. Marti, Zs. Bor, Laser-induced periodic surface structures on different poly-carbonate films, Appl. Phys. A, 2001, **73**, 521–526.

165- M. Csete, S.Hild, A. Plettl, P. Ziemann, Zs. Bor, O. Marti, The role of original surface roughness in laser-induced periodic surface structure formation process on poly-carbonate films, Thin Solid Films, 2004, **453 –454**, 114–120.

166- X. M. Lu, Q. H. Lu, J. Yin, Z. K. Zhu, Z. G. Wang, Laser-induced periodic surface structure on a polymer surface: the effect of a pre-rubbing treatment on the surface structure, J. Poly. Sci. B: Poly. Phys., 2003, **41**, 1273–1280.

167- X. Li, X. Lu, Q. Lu, Effect of irradiation history on the preparation of laser induced periodic microstructure on polyimide surface, Appl. Surf. Sci., 2007, **253,** 3690–3695.

168- N. Tsutsumi, A. Fujihara, Pulsed laser induced spontaneous gratings on a surface of azobenzene polymer, Appl. Phys. Lett., 2004, **85**, 4582-4584.

169- P. Rochon, M. Ivanov, Inrared-laser induced periodic structures in azobenzene polymer film, Mol. Cryst. Liq. Cryst, 2006, **446**, 89-98.

170- J. Paterson, A. Natansohn, P. Rochon, C. L. Callender, L. Robitaille, Optically inscribed surface relief diffraction gratings on azobenzene-containing polymers for coupling light into slab waveguides Appl. Phy. Lett., 1996, **69**, 3318-3320.

171- C. Barrett, A. Natansohn, P. Rochon, Photoinscription of channel waveguides and grating couplers in azobenzene polymer thin films in Proc. SPIE- Int. Soc. Opt. Eng. 1997, **3006**, 441-449.

172- R. J. Stockermans, P. L. Rochon, Narrow-band resonant grating waveguide filters constructed with azobenzene polymers. Appl. Opt. 1999, **38**, 3714–3719.

173- A. Natansohn, P. Rochon, Photoinduced motions in azobenzene-based amorphous polymers: possible photonic devices, Adv. Mater, 1999, **11**, 1387-1391.

174- X. T. Li, A. Natansohn, P. Rochon, Photoinduced liquid crystal alignment based on a surface relief grating in an assembled cell, Appl. Phys. Lett., 1999, **74**, 3791-3793.

175- D. Dantsker, J. Kumar, S. K. Tripathy, Optical alignment of liquid crystals, J. Appl. Phys., 2000, **87**, 4318-4325.

176- J. Y. Young Kim, T. H. Kim, T. Kimura, T. Fukuda, H. Matsuda, Surface relief grating and liquid crystal alignment on azobenzene functionalized polymers, Opt. Mater.,2002, **21,** 627–631.

177- K. Munakata, K. Harada, M. Itoh, S. Umegaki, T. Yatagai, A new holographic recording material and its diffraction efficiency increase effect: the use of photoinduced surface deformation in azo-polymer film, Opt. Commun., 2001, **191**, 15-19.

178- K. Munakata, K. Harada, N. Yosikawa, M. Itoh, S. Umegaki, T. Yatagai, Direct fabrication methods of surface relief electro-optic gratings in azo-polymer films, Opt. Rev.,1999, **6,** 518-521.

179- K. Munakata, K. Harada, H. Anji, M. Itoh, T. Yatagai, S. Umegaki, Diffraction efficiency increase by corona discharge in photoinduced surface-relief gratings on an azo polymer film, Opt. Lett., 2001, **26**, 4-6.

180- Y. L. Che, O. Sugihara, C. Egami, H. Fujimura, Y. Kawata, N. Okamoto, M. Tsuchimori, O. Watanabe, Fabrication of surface relief grating with second-order nonlinearity using urethane-urea copolymer films, Japanese J. Appl. Phys. Part 1—Regular Papers Short Notes & Review Papers, 1999, **38**, 6316–6320.

181- F. L. Labarthet, J. L. Bruneel, T. Buffeteau, C. Sourisseau, Chromophore orientations upon irradiation in gratings inscribed on Azo-dye polymer films: a combined AFM and confocal raman microscopic study, J. Phys. Chem. B, 2004**, 108**, 6949-6960.

182- F. L. Labarthet, C. Sourisseau, R. D. Schaller, R. J. Saykally, P. Rochon, Chromophore orientations in a nonlinear optical azopolymer diffraction grating: even and odd order parameters from far-field raman and near-field second harmonic generation microscopies, J. Phys. Chem. B, 2004**, 108**, 17059-17068.

183- F. L. Labarthet, C. Sourisseau, J. L. Bruneel, Spectroscopic linear and nonlinear optical characterization of azopolymer gratings inscribed on p(DR1M) thin films, Mol. Cryst. Liq. Cryst., 2006, **446**, 81-88.

184- H. J. Chang, B. Kang, H. Choi, J. W. Wu, Microstructure of a poled surface-relief grating and its electro-optic response, Opt. Lett., 2005, **30**, 183-185.

185- H. Baac, J.-H. Lee, J.-M. Seo, T. H. Park, H. Chung, S.-D. Lee, S. J. Kim, Submicron-scale topographical control of cell growth using holographic surface relief grating, Mater. Sci. Eng. C, 2004, **24**, 209–212.

186- S. Yang, K. Yang, L. Niu, R. Nagarajan, S. Bian, A. K. Jain, J. Kumar, Patterning of substrate using surface relief structures on an azobenzene-functionalized polymer film, Adv. Mater., 2004,**16**, 693-696.

Chapter II

Self-organized SRG on the methylacrylate azo polymer films

II-1- Introduction

In this chapter we will present our results of self-organized SRG formation on the methylacrylate azo polymer films. First, we describe a simple experimental method to induce self-organized SRG formation. We give the evolution of the pitch as well as amplitude of such structures with time. In the previous chapter we have described one beam experiment and the process of spontaneous hexagonal pattern formation on azo-polymer films. Here we will show how it is possible to create and control a periodic structure on the surface of an azo-polymer film by a single CW laser beam irradiation. The polarization multiplexing is presented. We will present effects of different parameters on the structure formation. We will give our experimental results for some new azo-polymers.

S. Ahmadi Kandjani, R. Barille, S. Dabos-Seignon, J. –M. Nunzi, E. Ortyl, S. Kucharski, Multistate polarization addressing using a single beam in an azo polymer film, Opt. Lett., 2005, **30**, 1986-1988.

II-2- Introduction to self-organized SRG

The properties of polymers containing photochromic azo dyes have received tremendous attention owing to the possibility that they can be used to obtain optically addressed birefringence and dichroism. This has led to investigation of the holographic optical storage properties of azo polymers. It is now well established that, following light excitation whose wavelength lies in the absorption band, trans-cis isomerization takes place, leading to further thermal orientation diffusion that facilitates a molecular rotation within the polymer matrix. This finally leads to a full reorientation of the azo dye molecules. More recent results showed that SRGs were also further induced into the photo-excitation of azo polymer films. Photo-induced SRGs were interpreted as a consequence of molecular translation controlled by the optical field. An interference pattern of coherent light beams was used for irradiation of the materials, and modification of the film surface was controlled by the light interference pattern. Two beams are usually necessary for SRG formation but it was also recently demonstrated that single beam interaction can induce well ordered structures (section I-3) [1].

II-3- Spontaneous surface grating formation

II-3-1- Wood anomalies

In 1902 R. W. Wood observed anomalies on diffraction efficiency of gratings [2, 3]. These anomalies are locations on an efficiency curve (efficiency plotted vs. wavelength) at which the efficiency changes abruptly. These sharp peaks and troughs in an efficiency curve are sometimes referred to as Wood's anomalies. Anomalies are rarely observed in P polarization (polarization of light parallel to the grating grooves) efficiency curves, but they are often seen in S (polarization of light perpendicular to the grating grooves) polarization curves (see Figure II-1).

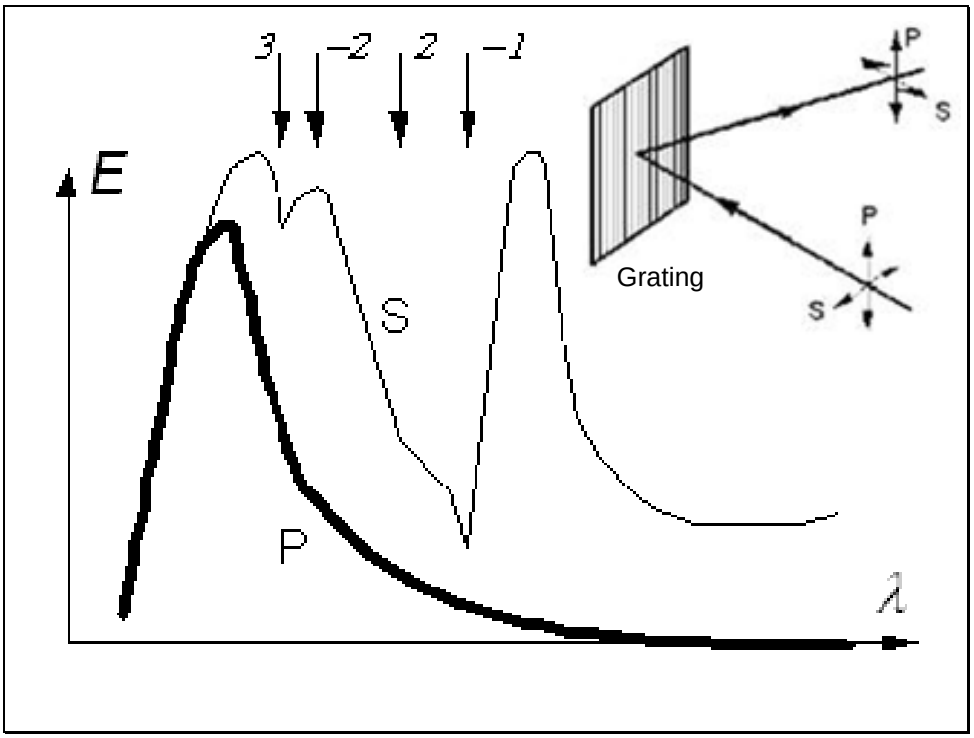

Figure II-1: Anomalies in the first order for a typical grating with triangular grooves. The P efficiency curve (thick line) is smooth, but anomalies are evident in the S curve (thin line). The passing-off locations are identified by their spectral order at the top of the figure. Inset, S and P polarizations, the p polarization components of the incident and diffracted beams are polarized parallel to the grating grooves; the S components are polarized perpendicular to the p components. Both the s and p components are perpendicular to the propagation directions.

Lord Rayleigh predicted the locations (in the spectrum) where such anomalies would be found: he suggested that anomalies occur when light of a given wavelength λ' and spectral order m' is diffracted at |θ' |= 90° from the grating normal (i.e., it passes over the grating horizon at grazing angle) [4, 5]. In this order (m'), the diffracted light lies in the plane of the grating. It is not possible for light bryond this point to be diffracted behind grating. In another word a propagating order changes into evanescent order, as the wavelength of the incident beam is changed. Thus there is a discontinuity in the diffracted power vs. λ in order m' at wavelength λ', and the power that would diffract into this order is redistributed back into the other propagating spectral orders. The power appears as an addition to the spectral response, with a sharp cut on at the wavelength λ' and a steep decline to the red. This additional efficiency is almost entirely polarized perpendicular to the grating rulings.

We can find the locations of these anomalies from Rayleigh diffraction condition for gratings:

$$k_0\left(\sin\theta - \sin\theta'\right) = \pm m k_g \qquad (1)$$

Where θ, θ' and m are incidence angle, diffraction angle and diffraction order, respectively. $k_0 = 2\pi n_0/\lambda$; λ is wavelength of incident beam and n_0 is refractive index of the grating medium. $k_g = 2\pi/\Lambda$; Λ is the pitch of grating.

In the case of $\theta' = \pm 90^o$ (diffraction of mth order along the surface of grating, "grazing angle") we can rewrite equation 1 as:

$$m\lambda_m = n_0\Lambda\left(1 \pm \sin\theta\right) \qquad (2).$$

The wavelength λ_m gives us the locations of Wood's anomalies.

II-3-2- Stimulated Wood's anomalies [6]

Normal incidence of a laser beam on the surface of a material can create a spontaneously generated surface ripples. The pitch of such gratings is close to the input laser beam wavelength, i.e. incident laser beam suffer a strong self-induced diffraction at grazing angle. In this case wavelength of input laser, incidence angle and the pitch of resulting spontaneous grating will satisfy the relation 2.

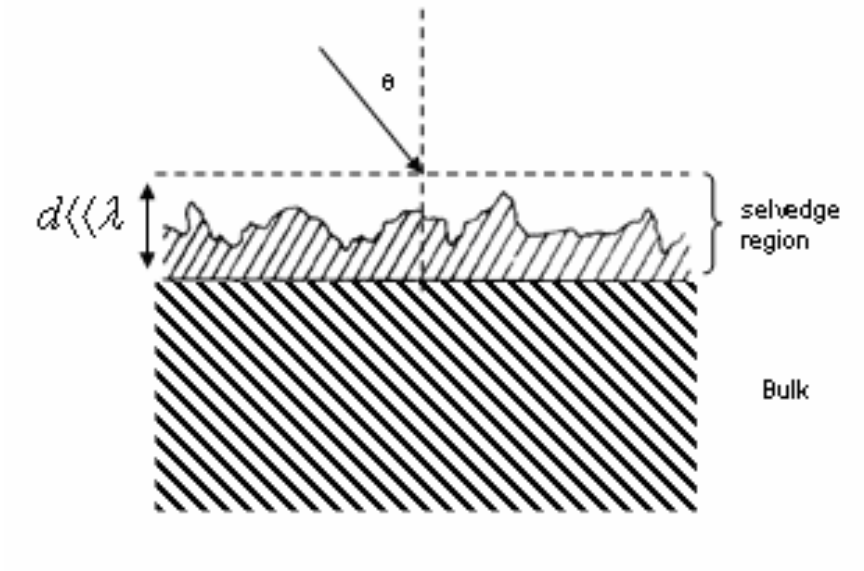

Figure II-2: The geometry of light incident on a rough surface.

Usually the surface of materials has random irregularities. These irregularities can be assumed as the superposition of many different surface gratings with different spatial frequencies. Any one of these surface grating components can diffract incident laser beam into a number of diffracted orders (figure II-2). The beam scattered into these orders will interfere with input beam to produce an intensity pattern on the surface which has the same spatial frequency as original grating component. Therefore any component can produce interference pattern on the surface. This sinusoidal intensity variation may cause the corresponding spatial frequency component of the surface irregularity to increase in amplitude. Thus it will diffract additional input beam intensity to the same component that will increase the amplitude of beam modulation on the surface; consequently the amplitude of surface modulation at this frequency will increase. The net result can be growth of periodic structure starting from noise, of both the surface irregularities and the corresponding scattered light components. Just a narrow range of spatial frequency components that diffract light into grazing angle will dominate other components and growth rapidly (these diffracted light along surface should interact longest and strongest with the material surface). Such process leads to the development of highly regular and periodic ripples or surface structures with periods which match one or the other of the above conditions.

The obtained results showed that spontaneously induced grating wave vector is parallel to the polarization direction of input beam and its pitch for normal incidence is $\Lambda \approx \lambda / n_0$. For the off-normal incidence and TM-polarized light, again the waver vector of grating is parallel to the polarization direction and the pitch of grating is:

$$\Lambda \approx \frac{\lambda}{n_0 (1 \pm \sin\theta)} \qquad (3)$$

Where θ, is the incidence angle and λ/n_0 is the wavelength in the medium above the surface (selvedge region). The refractive index of selvedge region with height of $d \langle\langle \lambda$ is between one and refractive index of material (light-induced refractive index). This is corresponding to the Rayleigh wavelength condition for Wood's anomalies to appear at the same incident laser wavelength and angle of incidence (equation 2).

For the off-normal incidence and arbitrarily polarized laser beam, spontaneously formed gratings can have different directions of orientation on the surface especially at large angle of incidence [7]. Also perpendicular grating (with wave vector perpendicular to the polarization of input beam) can be formed at high beam intensities with the pitch of:

$$\Lambda \approx \frac{\lambda}{n_0 \cos\theta} \qquad (4).$$

Circularly polarized beam will create ripples with wave vectors that orient in all directions on the sample surface.

II-4- **Experimental setups and preliminary observations**

The experimental setup used for self-organized SRG formation on the surface of azo polymers is presented in the figure II-3.

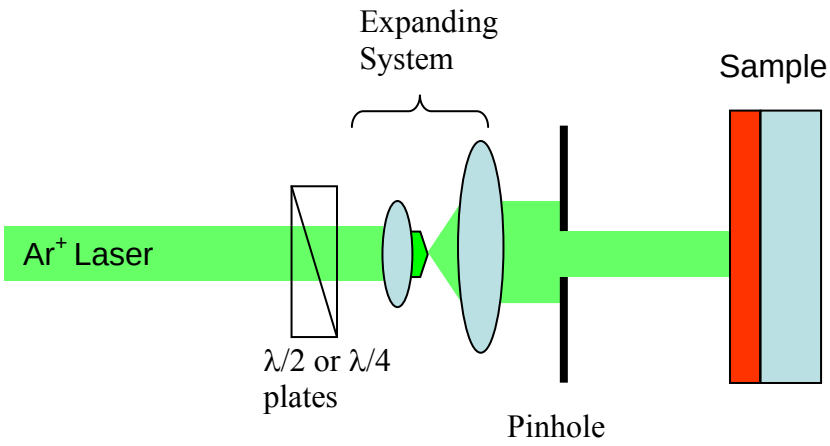

Figure II-3: Experimental setup for self-organized SRG formation

The λ= 476.5 nm laser line of a continuous argon ion laser is used to excite the azo polymer absorption close to its absorption maximum. Absorbance at working wavelength is 1.6 (figure I-14). Incoming light intensity is controlled by the power supply of the laser. Polarization state of the laser beam is controlled using half- and quarter-wave plates. Sample is set perpendicular to the incident laser beam (irradiation under normal incidence). The size of the collimated laser beam impinging onto the polymer sample is controlled with a Kepler-type afocal system and a pinhole. The beam size on the sample surface was 4 mm diameter at $1/e^2$. Our characterization method for self-organized SRG consists in AFM and diffraction studies. The azobenzene-functionalized polymers used in these studies have been presented in section I-5. 50 mg of the azo-polymers are dissolved in 1 mL of THF and spin-coated on clean glass slides to obtain good optical- quality films.

A typical AFM image of self-organized SRG is presented in figure II-4.

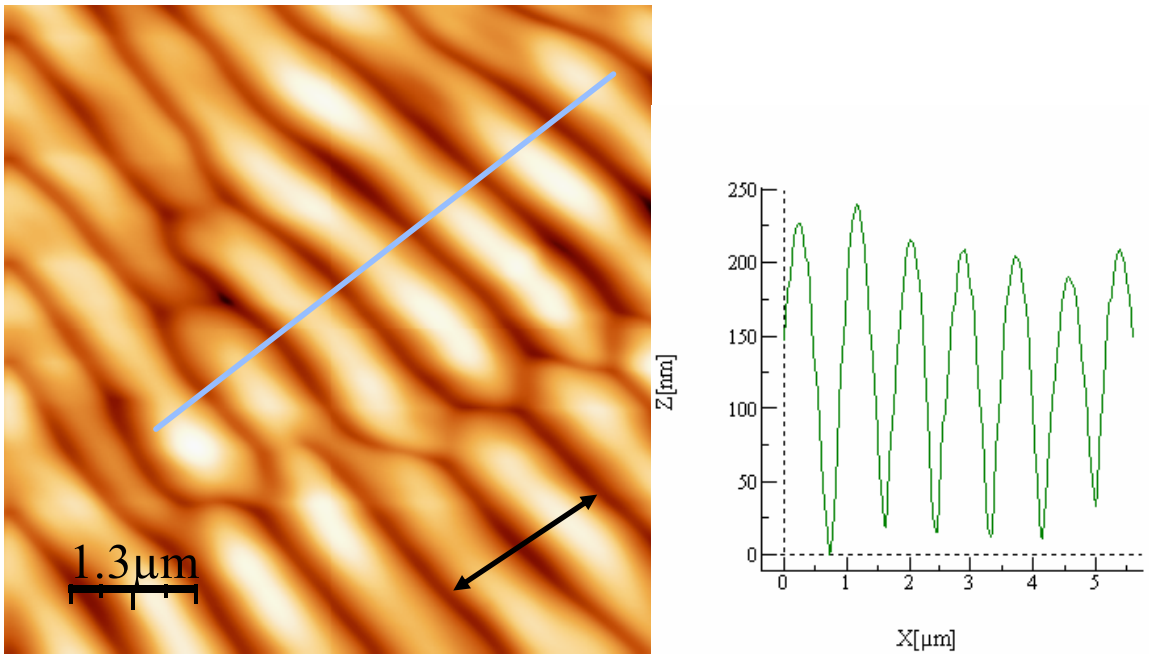

Figure II-4: left) AFM image of self-organized SRG on the surface of an azo-polymer (MB2I). Right) Amplitude profile of the grating taken alonge the bleu line in the SRG pattern shows the regularity of the profile. The arrow shows the polarization direction of the writing beam.

The pitches and amplitudes of periodic structures we have obtained are around 800 nm and several hundreds of nanometers respectively. The wave vector of the grating is parallel to the polarization direction of the writing beam. Rough free surface is necessary for self-organized structure formation. Incidence of laser beam from glass side of the sample did not cause a SRG formation.

When the surface relief starts to form, the writing beam itself is diffracted in several diffraction orders. Self-diffraction occurs in both forward and backward directions. As it is evident from AFM image of formed SRG, the structure has not perfect continuous sinusoidal shape and diffracted beam is diverged. The diverged first-order diffraction beam is collected in the backward direction by a set of lenses and registered as a function of time by a Silicon photodiode (Figure II-5).

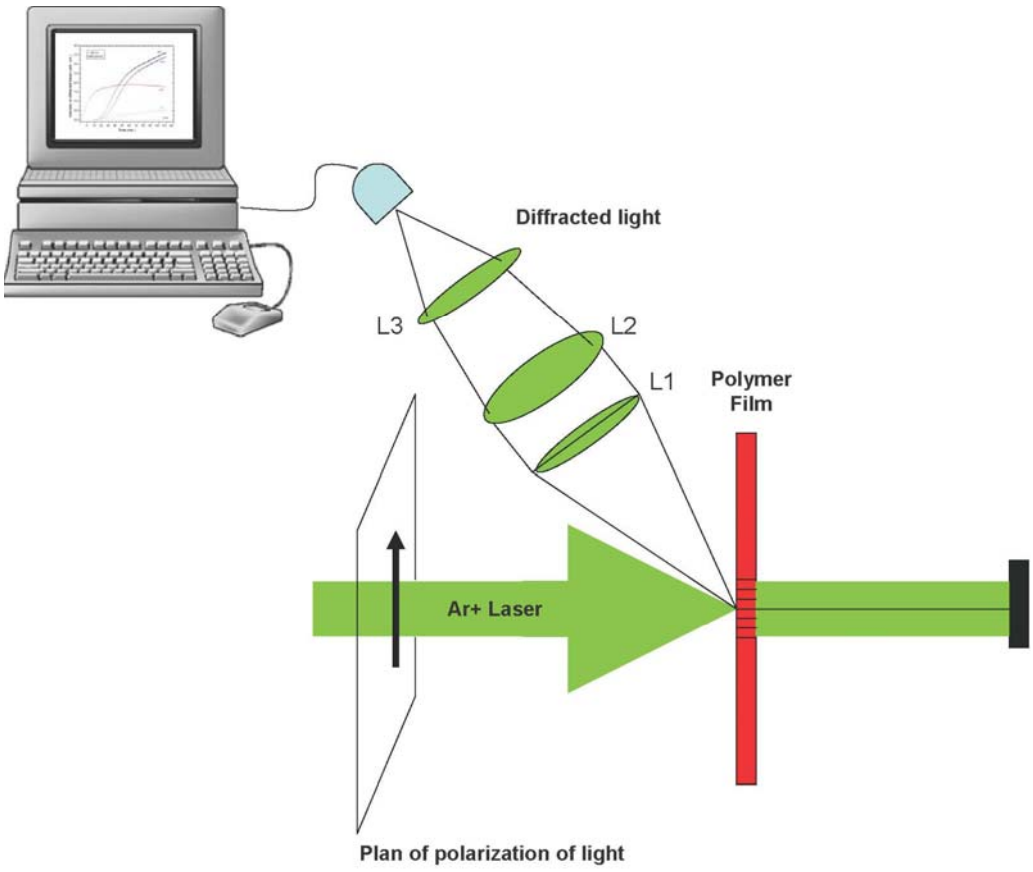

Figure II-5: Experimental setup for the measurement self-diffracted beam intensities. L1, L2 and L3 are the lenses to collect the diverged first order diffraction beam.

The dynamic survey of self-diffracted beam intensity is shown in figure II-6.

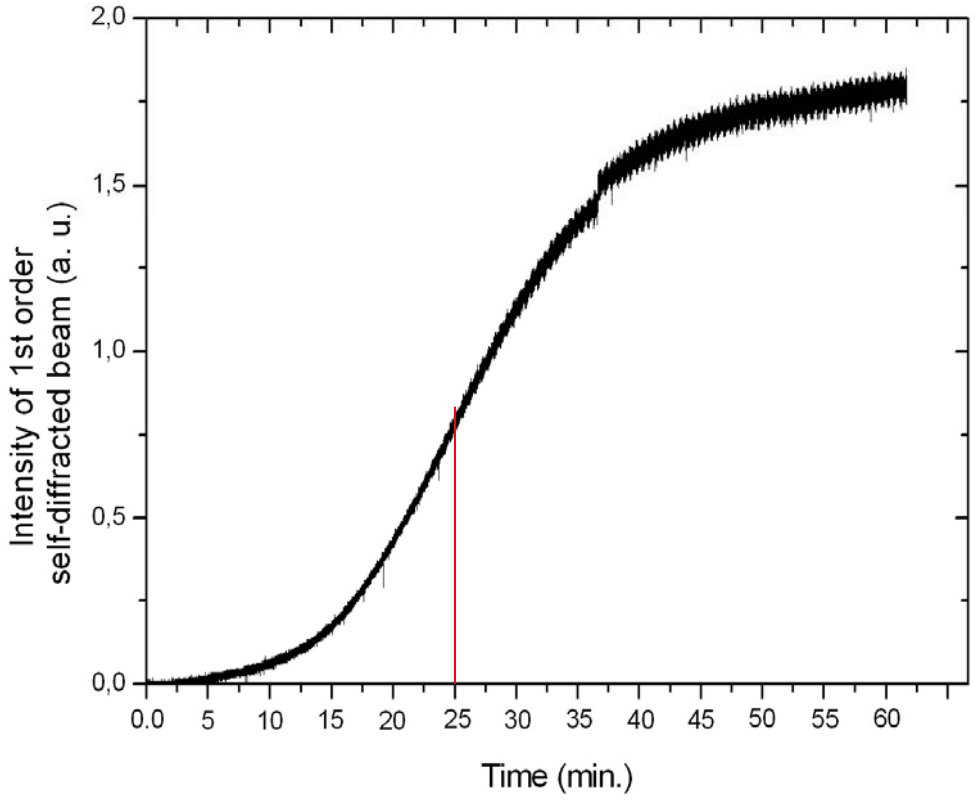

Figure II-6: The self-diffracted beam intensity measured as a function of time. The wavelength and intensity of writing beam are 476.5 nm and 400 mW/cm^2, respectively.

When the writing beam is switched on, the self-organized SRG is generated on the surface of polymer film and the self-diffracted beam intensity increases with time. The growth rate is very small for first few minutes. The signal reaches its highest level after 1 hour and saturates. The diffracted beam intensity shows an inflection around 25 min.

II-5-The influence of material structure

In order to better understand the mechanism of self-organized SRG formation and to design high-performance materials (photo- processability and photo-response behaviour); it is necessary to clarify the relationship between molecular structure and self-organized SRG

patterning. In this aim, we checked the dynamics of spontaneous grating formation in different azo-polymers.

Figure II-7 presents the diffracted beam intensity as a function of time for different materials. The writing beam was the 488 nm line of an Ar+ laser with the intensity of 450 mW/cm^2. For almost all materials (see section I-6), the intensity rises over several tens of minutes and finally saturated for longer illumination times. The rate of growth and maximum value of diffracted beam intensity depend on the material structure.

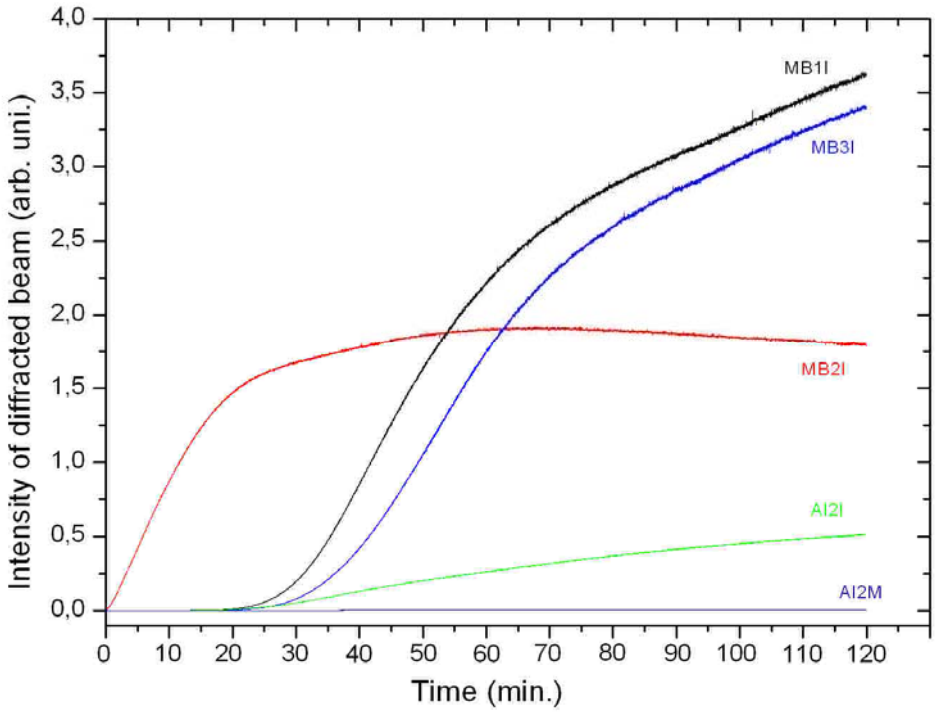

Figure II-7: First order diffracted beam intensity as a function of time for different materials. The intensity of writing beam is 450 mW/cm^2 at 488 nm.

The results suggested that the spontaneous SRG formation process is very slow for low Tg materials (AI2I & AI2M). In the case of AI2M, Tg= 53°C, the diffracted beam intensity is close to zero. The fast growth of spontaneous SRG formation on MB2I, can mainly be attributed to the fact that the dipole moment of 2I chromophore is higher than 1I and 3I. Because of higher Tg, the diffracted beam intensity of MB1I is higher than MB3I. It seems that high Tg azo-polymers with high dipole moment of azo chromophore are more convenient for self-organized SRG formation.

II-6- The influence of writing beam intensity

In order to study the influence of writing beam intensity on the dynamics of self-organized SRG, we irradiated different parts of a sample by the same laser beam with different intensities. We show in figure II-8 the intensity for first order self-diffraction recorded as a function of time for different laser beam intensities.

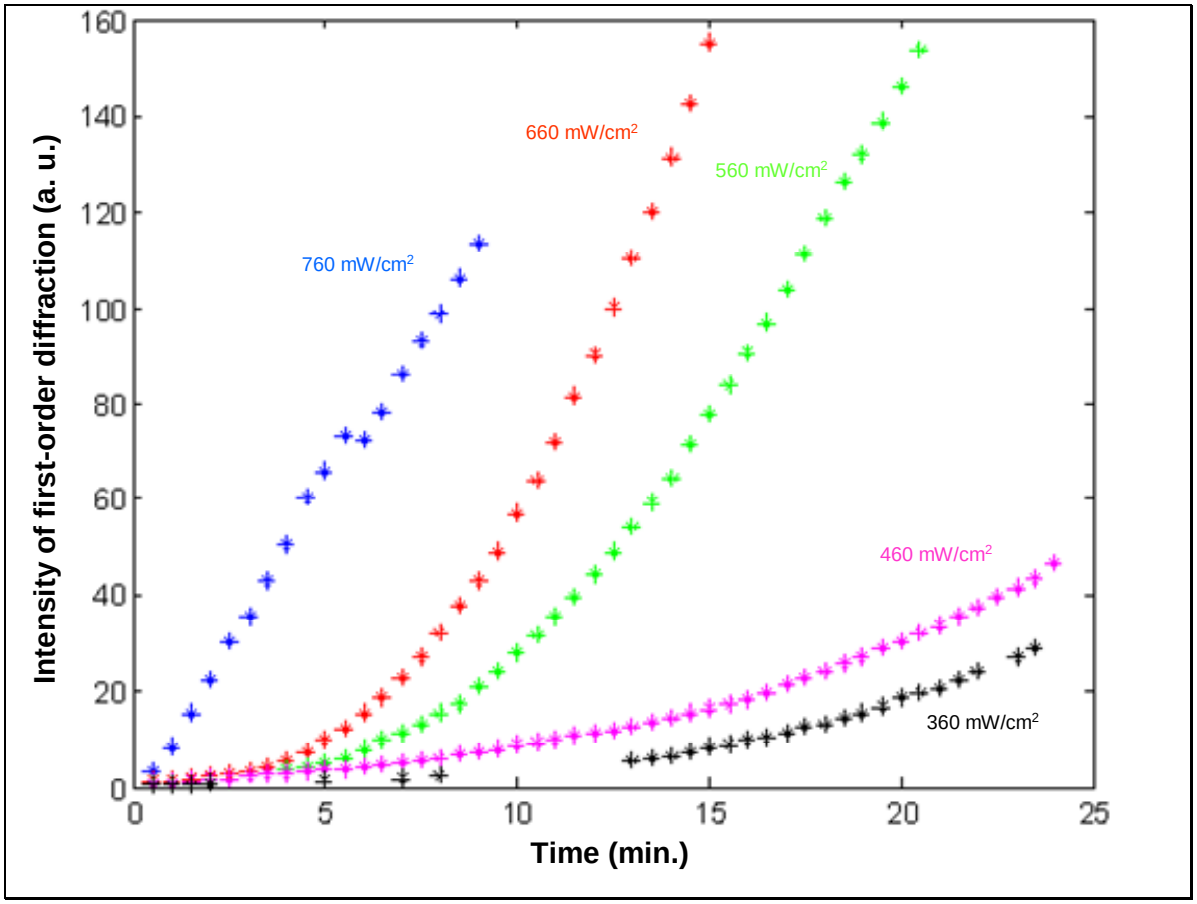

Figure II-8: Intensity of first order diffraction measured as a function of time for different beam intensities. The sample was a MB2I polymer film.

The self-diffraction phenomenon exhibits a threshold depending on the power density. We define a threshold time for the induction of self-diffraction as the inflection point of the curve, where the second derivative changes sign. The threshold is a linear function of the input beam intensity, and its slope is estimated to be ~33 mW.min/cm^2. We checked that this threshold does not depend on polarization. Measurements using different beam sizes of 3–6 mm also confirmed that the threshold time is a function of power density only. In figure II-9 we show

the dynamics of spontaneous SRGs formation for different input beam intensity for longer illumination times (for example MB3I). Except MB2I, the other materials show the same behaviour as MB3I. For different materials, diffracted beam intensity for different input beam intensity increases with different growth rate and reaches a saturation level (formation of permanent grating).

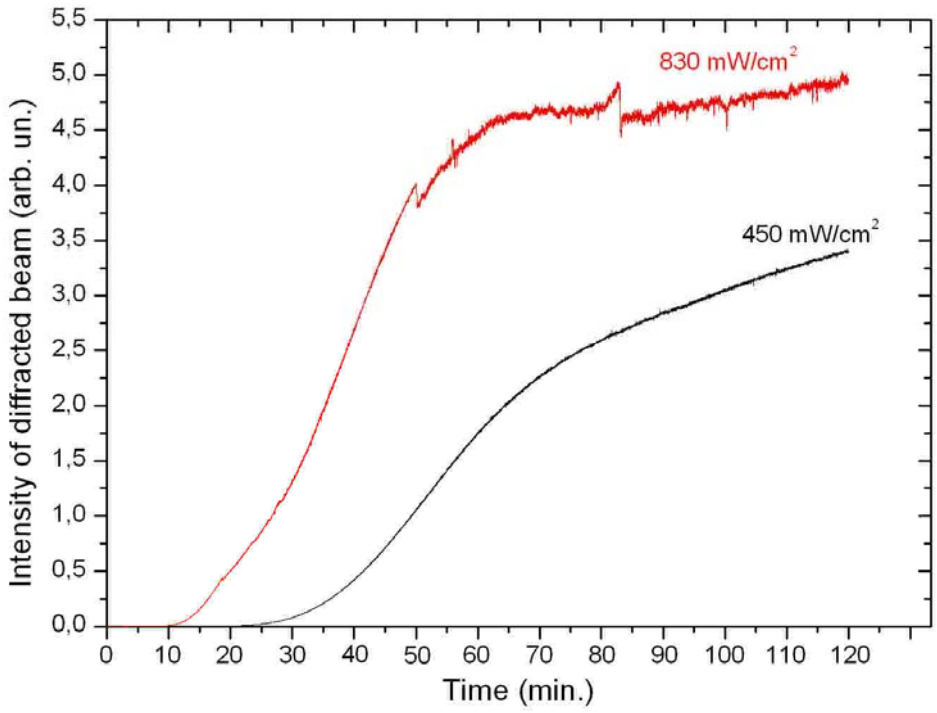

Figure II-9: Intensity of first order diffraction measured as a function of time for different beam intensities up to saturation. The sample is MB3I polymer film.

In the case of MB2I (Figure II-10) for low powers, diffracted beam intensity rises and then saturates like other polymers but for higher intensities it increases, reaching a maximum and then drops to some constant value. The relaxation of diffracted beam intensity can be due to the reorientation of azo group or deformation of inscribed SRG.

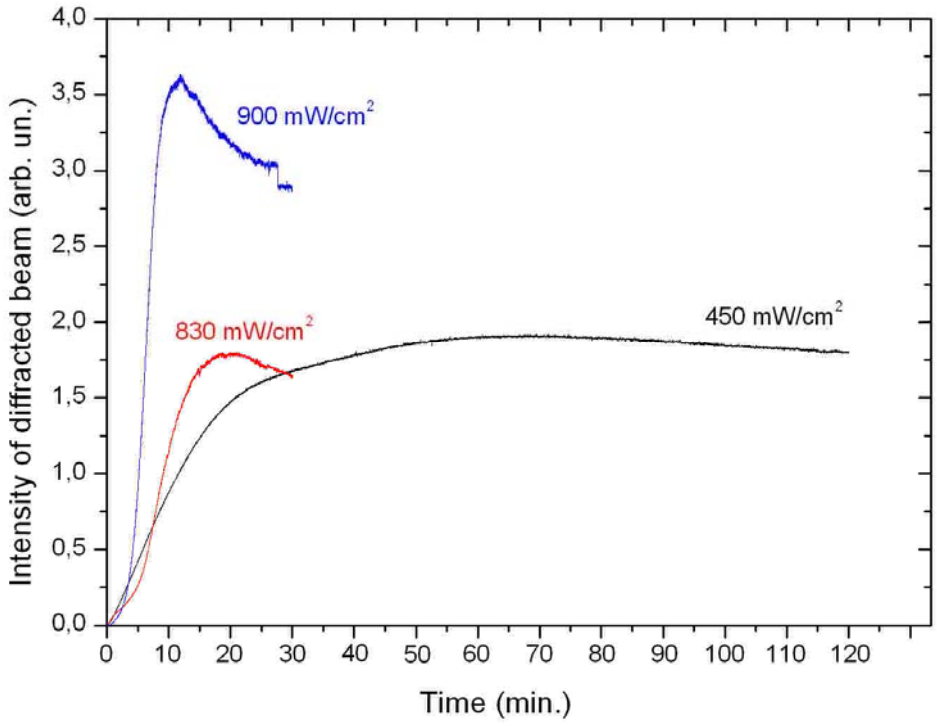

Figure II-10: First-order diffraction beam intensity as a function of time for different writing beam intensities. The polymer is MB2I.

II-7- Time evaluation of spontaneous SRG formation (AFM studies)

We then controlled grating formation at a microscopic level as a function of time (Figure II-11). To get information on the surface relief evolution during the recording period, we printed different gratings on the same sample during different times with a laser intensity of 450 mW/cm2 of 476.5 nm line of Ar+ laser. The laser was s polarized. The azo-polymer was MB2I (because of faster response) with the thickness of 1 □m. Both the height and the pitch of the grating were studied as a function of time by imaging the sample surface with an AFM (Pico SPM from Molecular Imaging, in contact mode).The images were processed using the WSXM software from Nanotec [8]. At the beginning, both the pitch and height of SRG growth slowly, after around 15 minute the rate of growth increases and reaches saturation level (permanent grating formation). All results in Figure II-11, for a 450 mW/cm2 intensity, for either the grating's height or its pitch show a threshold like evolution with inflection around 20 min. For first 20 minutes the pitch of SRG follows the pitch of stimulated Wood

anomalies (□=□/ns). For longer times of illumination the system moves to a more stable state and creates a permanent grating. In this new stable state the pitch of grating is bigger and the corresponding amplitude is also higher.

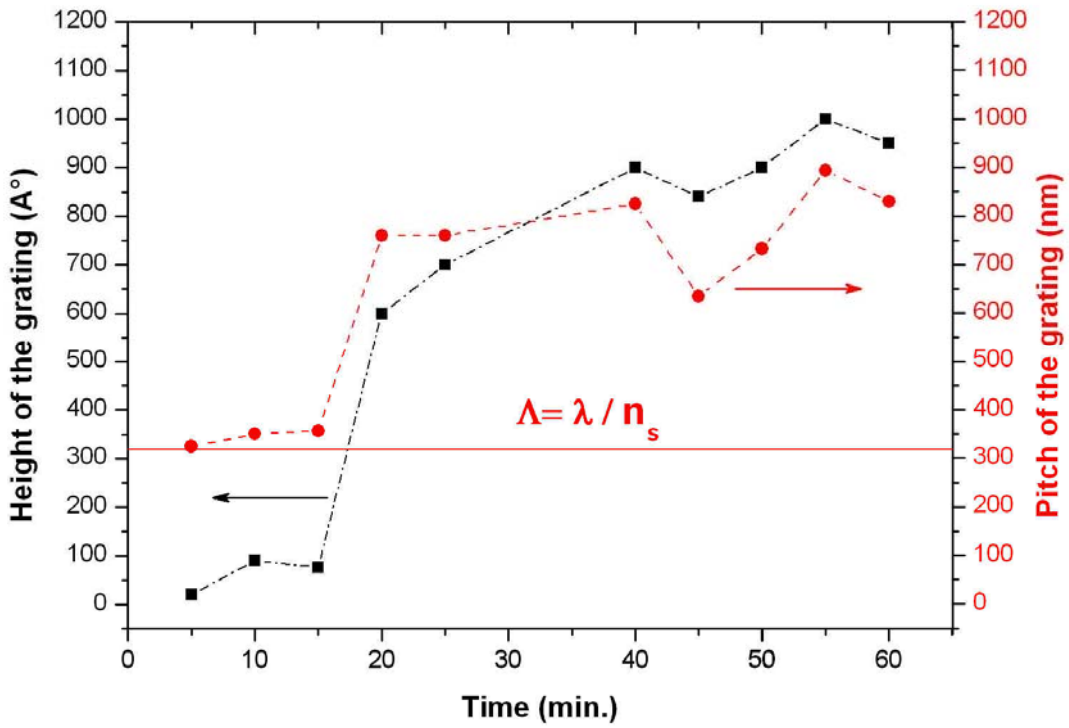

Figure II-11: Evolution of the height and pitch of the grating as a function of time at the beginning of the SRG recording for a beam intensity of 450 mW/cm^2. Theoretical value for pitch of grating has been shown by red solid line.

The red solid line in figure II-11 shows theoretical value for pitch of SRG calculated from $\Lambda = \lambda / n_s$. The refractive index of selvedge region for our system is assumed as n_s=1.5. At the beginning of patterning, the experimentally measured pitch of grating is the same as the calculated one.

II-8- Reversibility

To check the reversibility of spontaneous SRG formed on the azo-polymer films, we used the same experimental setup as figure II-5. The polarization of writing beam was controlled by a half-wave plate. The measurements on backward diffracted beam allow us to keep away influences of input beam. The sample was a film of MB1I on a glass substrate. This polymer showed higher diffraction efficiency. The intensity of writing beam was 400 mW/cm^2.

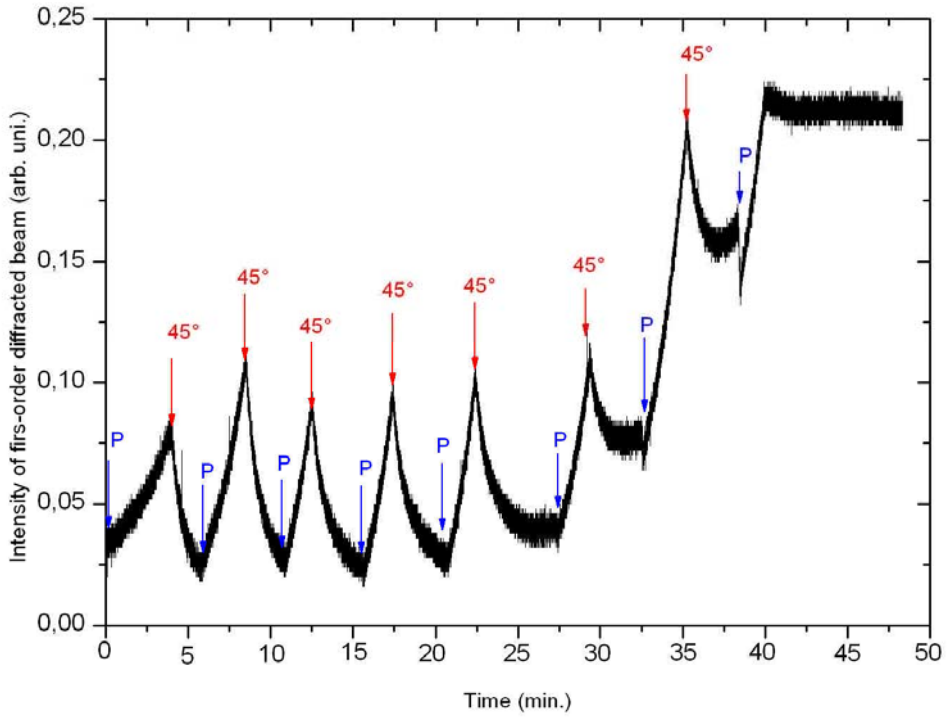

Figure II-12: Intensity of first-order diffraction beam in the direction of P polarization. The arrows show the switching of polarization between P and 45°.

Polarization direction was switched alternatively between 0 (p) to 45° with a period of a few minutes (Figure II-12). For the simplicity of the experimental setup, we set our detection system as to be able to record self-backward first order diffraction beam intensity that is in the direction of beam polarization (parallel to the surface of the optical table) by an optically isolated detector . First we set the polarization of writing beam as p polarized. The diffracted beam intensity increases as a result of grating formation. After 4 minutes of illumination, we switched the polarization of beam to a 45° polarized beam, the diffracted beam intensity decreased back to its initial value (the erasing time is about 2 minutes) since the 45° polarized

beam erased totally the grating induced by p polarized beam and create another grating with a wave-vector parallel to the erasing beam polarization direction (45°). Then by rotating back to the p polarization, again it inscribed a grating in its direction. It takes ~ 2 minutes to reach the same level of diffraction intensity as first grating. The time needed to rotate the polarization of the writing beam is very small compared to the growth rate of grating and it can not affect the phenomena. We see that the phenomenon of grating formation is almost totally reversible during 0.5 hour (first 6 cycles in Figure II-12). After, the structure is not reversible. We see that diffraction direction does not change at all following the last polarization rotation step. This corresponds exactly to the inflection point in figure II-6, which was recorded with about the same laser intensity.

II-9- Influence of writing beam polarization (Polarization multiplexing)

To date, holographic data storage is the best candidate for optical storage devices with potential storage capacities of 1 $TBcm^{-3}$ and transfer rate of 10 GBs^{-1}[9-11]. Different techniques are used to multiplex data pages into the same volume of material. These multiplexing will allow us to achieve high data transfer rate and short access times by parallel recording and readout of data. Usually angular, wavelength, polarization and sometimes combinations of them have been used for multiplexing [12-14].

Owing to the fact that a photon possesses a polarization angular momentum of one, it is well known that a single beam polarization can address only two states in an optical memory device. Indeed, the use of a polarized light can, in principle, only double the storage capacity of digital or holographic optical memory devices [15-17].
The increase of information storage needed in information science and technology has led to significant efforts to increase the capacity of storage media. Holographic memories are promising candidates in this respect because they permit (three dimensional) 3D optical information storage [18]. In this case, coding is done by mixing of two coherent laser beams, an object beam and a reference beam. The angle-selective property of holograms recorded in thick materials makes possible high-density data storage. Two beams are usually necessary to obtain this property. Photorefractive materials are attractive media for hologram recording, but they are weakly sensitive to the intensity distribution of the recording beam and require two beams for multidimensional addressing [19].

In 1985, for the first time, Todorov *et al.* have shown that two holographic recordings can be stored independently inside the same film when one is using different combinations for the polarization states of the reference and the object beams during recording [20]. For the recording of the first image, the reference and object were left and right-hand circularly polarized beams respectively. For the second recording, the reference and object polarizations were interchanged. To reconstruct the first image one should use left-hand circular polarization, whereas using right-hand circular polarization for the reconstruction yields the second image. It is important to mention that to have access to different multiplexed images, this technique needs to change the reconstruction process. Simultaneous readout of these two multiplexed images can also be achieved by using a linear polarized light [21, 22], and these

two orthogonally polarized images can be separated with a polarization beam splitter. However diffraction efficiency of each image is reduced because only half intensity of the reading beam contributes to the reconstruction of each polarization-multiplexed image. Recently Koek *et al.* presented a new technique of simultaneous readout polarization multiplexing for holographic data storage in bacteriorhodopsin films [23]. More recently Su et al. developed a hybrid-multiplexing using angular and polarization multiplexing [24].

We show in the following that peculiar material properties can break this principle. In this study, we demonstrate that multistate storage of a single beam polarization can be achieved and read out in a polymer material simultaneously. Our original technique uses only one beam with controlled polarization to photoinduce a SRG whose wave-vector direction depends on the light polarization. SRGs are produced in a one-step irradiation process in standard laboratory conditions.

Figures II-13(a)–(d) show AFM images of permanent structures induced with four different polarizations of the input laser beam: 0°, 30°, 60°, and 90° with respect to the initial polarization. The laser beam intensity was 450 mW/cm^2. The growth time for the gratings was 1 hour. It corresponds to the first-order diffracted beam intensity's reaching a maximum. AFM measurements retrieve angle values that are in a good agreement with the input polarization direction. Surface gratings have a depth of 50±5 nm, whatever the polarization used. The grating pitch is Λ =800±30 nm, which is in agreement with the value given by first-order diffraction theory in the θ =32.6° direction: $\Lambda=2\lambda/2 \sin\theta$. Figures II-13(e)–(h) show camera pictures of the self-diffracted beam for each polarization angle.

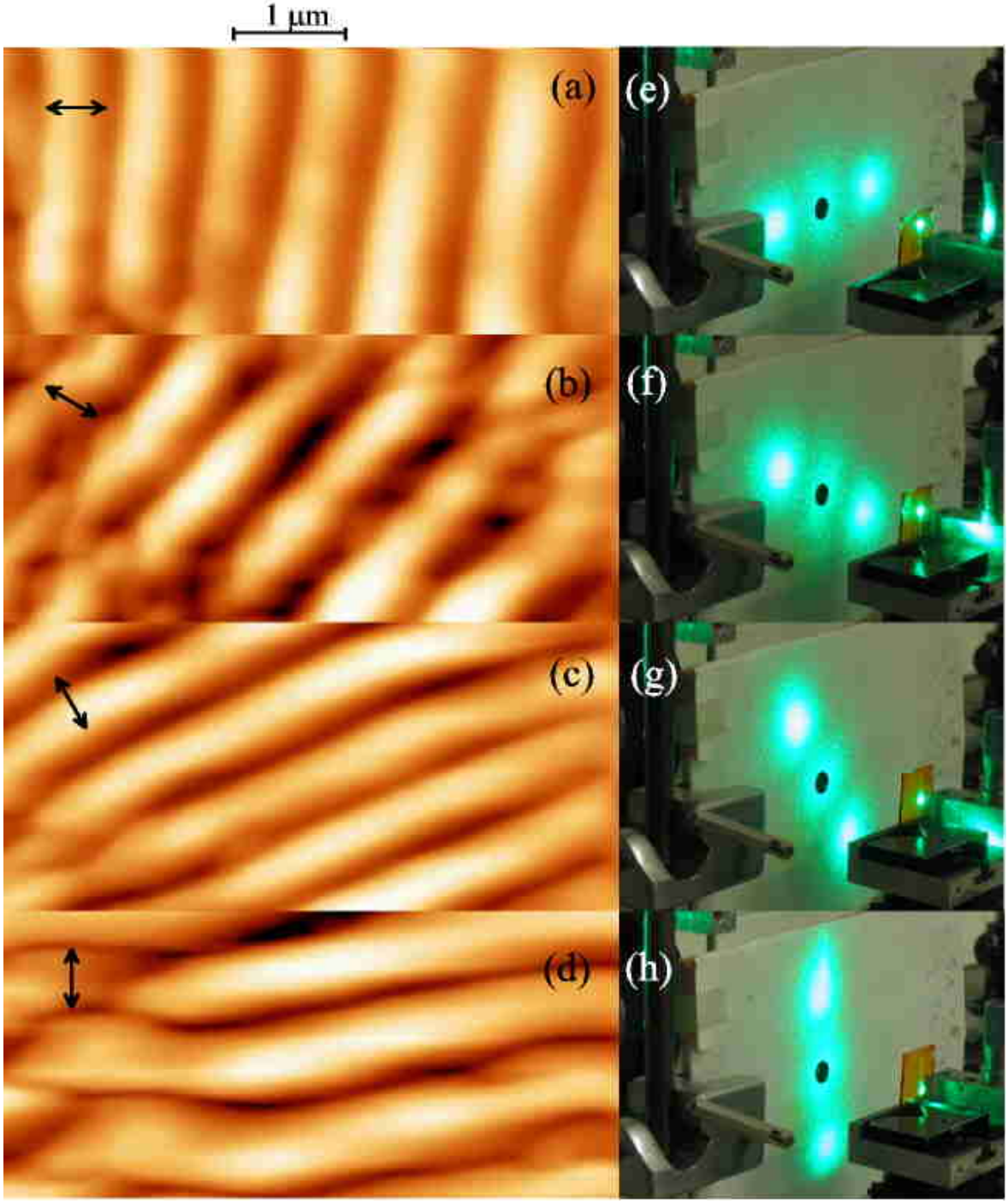

Figure II-13: AFM images of typical surface grating displaying a SRG amplitude of 50 nm and pitch of 800 nm for four different input beam polarizations, (a) $\alpha = 0°$, (b) $\alpha = 30°$, (c) $\alpha = 60°$, (d) $\alpha = 90°$. Polarization direction is indicated by arrows, which size is about 0.5 µm long. Parts (e-h) show the photos of first order backward self-diffraction retrieved with the recording laser.

This result shows that several diffraction directions can be controlled using a single beam polarization direction and more than two independent states can be inscribed using polarization multiplexing on an azo-polymer film. The minimum number of diffraction directions that can be resolved without overlapping is limited by the lateral size of the first-order spots in the Fourier transform of the SRG [Figs. II-13 (a)–(d)]. This Fourier transform is exactly given by the diffraction pattern shown in Figs. II-13(e)-(h). The practical result is a divergence of the diffracted beam: δ=22.6°. If we detect the diffracted beam at a distance D from the polymer film, the spot diameter is d=2D tan δ/2 (figure II-14). So, the maximum number of states N that can be encoded and read out without overlap is N=S/2d= (πsinθ')/(2 tanδ /2), where S is the perimeter of the circle made by the diffraction angle θ' in the detection plane. The factor of 2 in the denominator accounts for negative and positive diffraction orders. We find N=4 in our particular example.

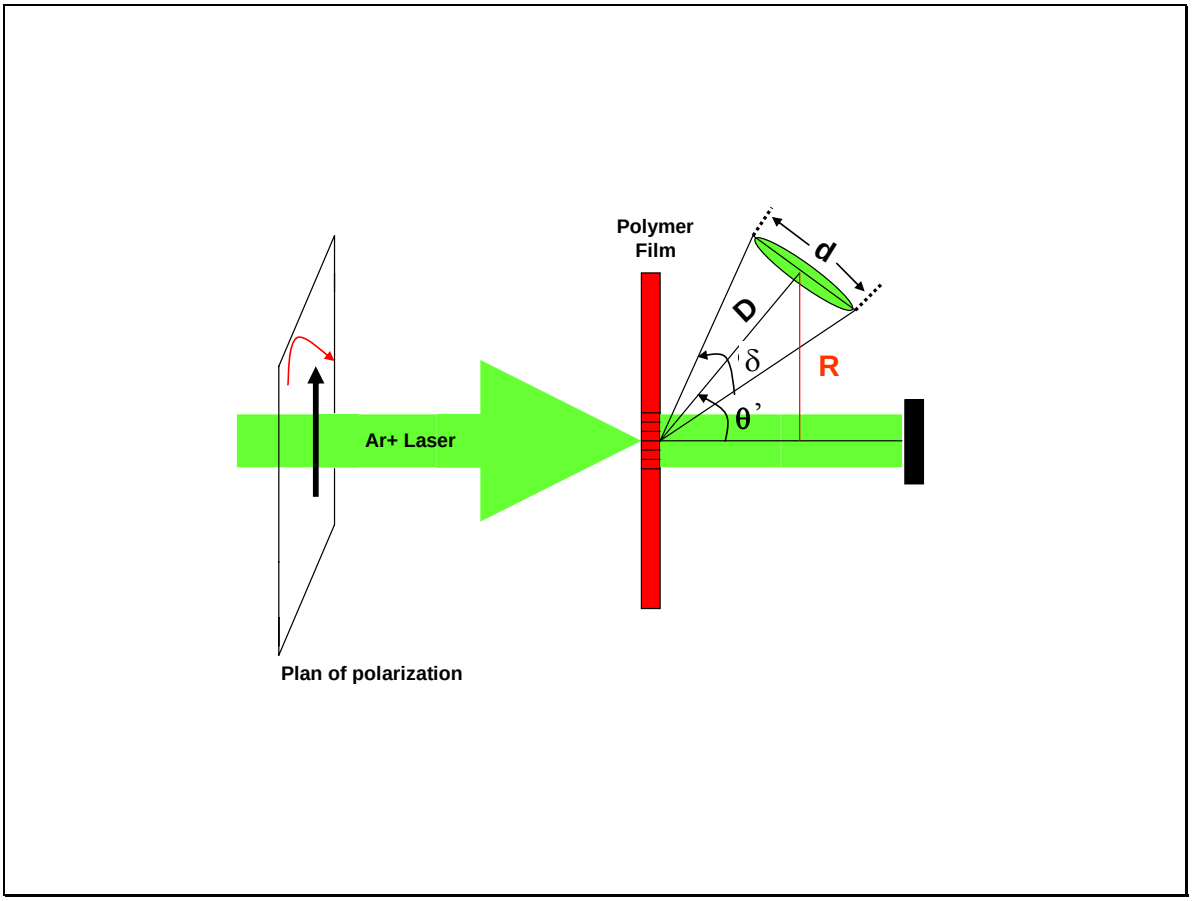

Figure II-14: Schematic representation of diffracted beam divergence. δ and θ' are divergence and diffraction angles, respectively.

It is possible to increase polarization multiplexing number using different beams for writing and readout of gratings (Figure II-15). We used a low power He-Ne laser in the transparency region of azo-polymer as reading beam. This beam can not affect the grating formation process. The multiplexing number will increases by the factor of λ/λ_0, where λ and λ_0 are wavelength of writing and reading beams, respectively.

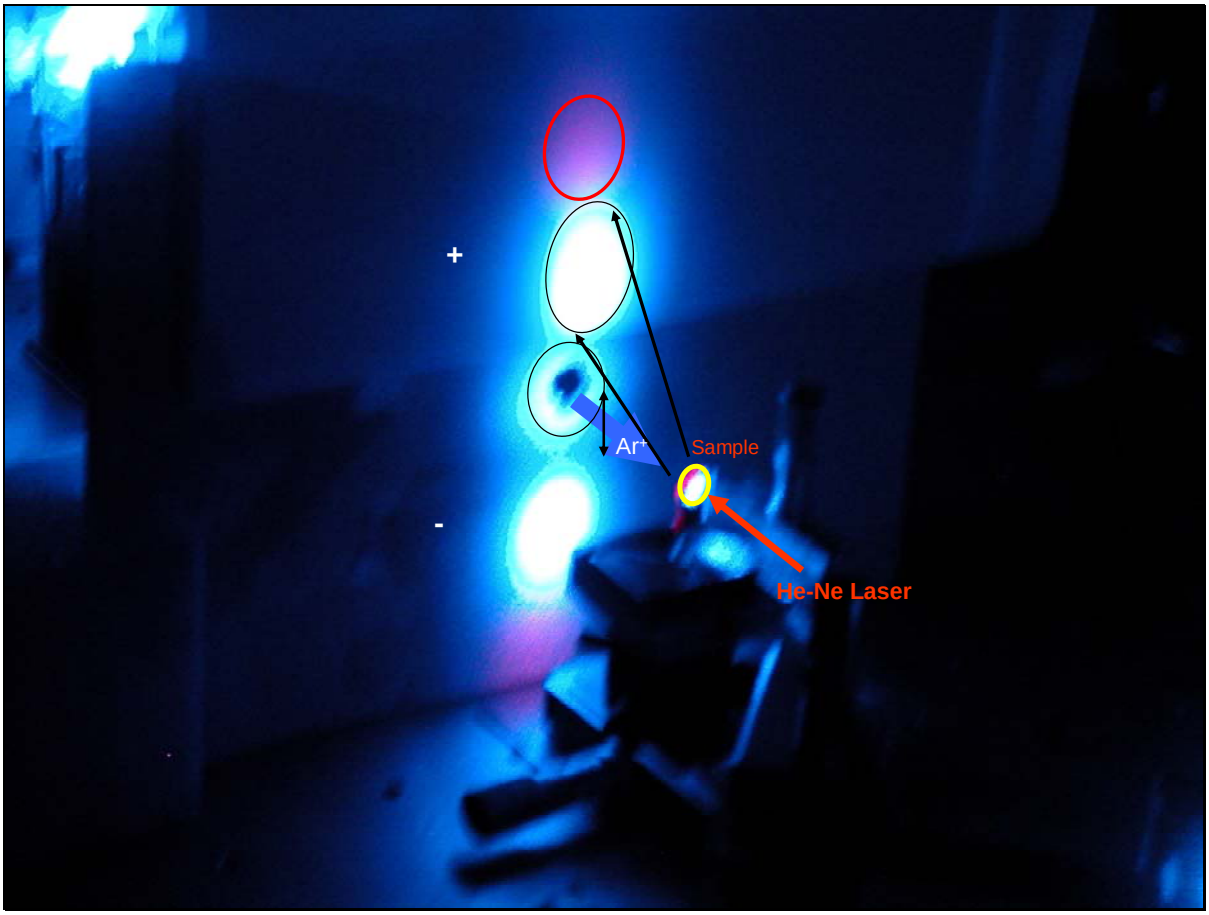

Figure II-15: Simultaneously writing-readout process of SRG on azo-polymer film. 476.5 nm line of Ar+ laser used as writing and readout beam and at the same time a He-Ne laser used as reading beam.+,- signs show positive and negative diffraction orders.

II-10- Influence of incidence angle

We have checked the grating formation for the different writing beam incidence angle. Figure II-16 shows the schematic representation of experimental setup. We have controlled polarization direction of the writing beam using a half-wave plate. This sample has been rotated by a rotating stage. The gratings were inscribed for different angles on the same polymer film and with the same power of laser beam. The power of writing beam was measured on the surface of sample. Because of its faster SRG formation, MB2I has been used for all experiments. These studies will help us to examine the possible influence of interferences generated on the surface of the polymeric film. Interferences occur between the scattered light by random irregularities initially present on the illuminated surface and input laser and produce a sinusoidal component of spatial variation in the light intensity falling on the material surface. As we mentioned before, this sinusoidal intensity variation may cause spontaneous strongly periodic structures at the surface of almost any type of solid materials illuminated by a single pulsed or continuous laser beam with sufficient intensity [6, 25]. The formation of these structures has several properties common with anomalies of Wood present in diffraction patterns (see section II-3).

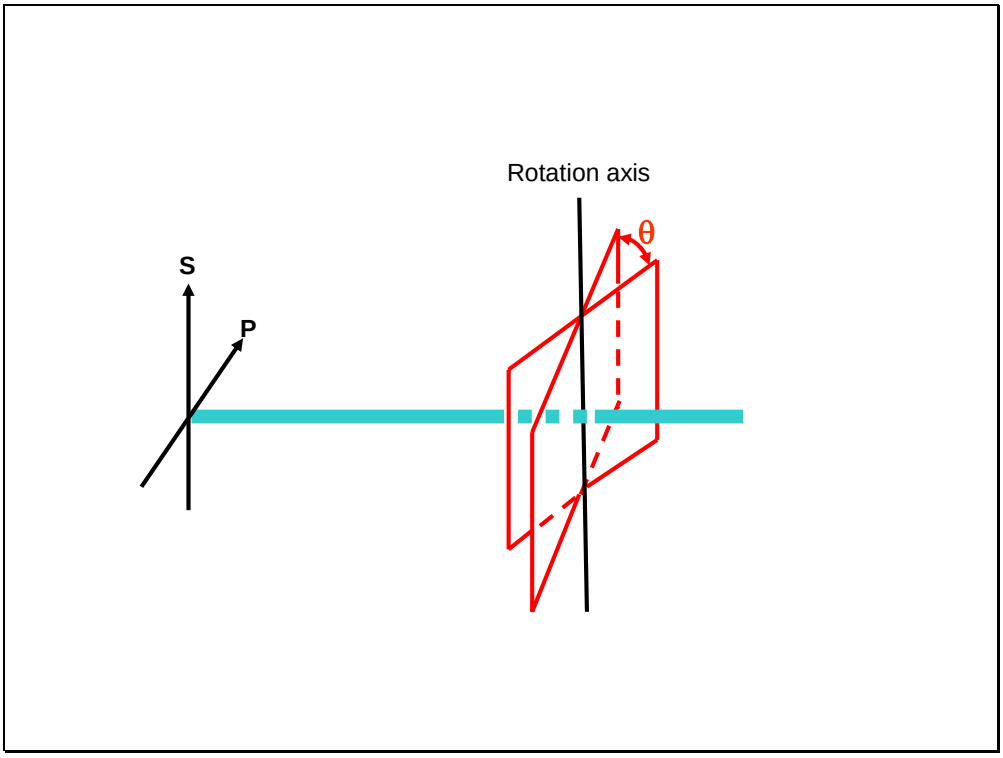

Figure II-16: Experimental setup to check the influence of laser beam incidence angle.

In the following we will study this parameter for p, s and 45° polarized writing beam.

II-10-1- P Polarization

According to stimulated Wood's anomalies, the period of the observed gratings depends on the polarization of the laser beam, and for a TM-polarized beam (p polarization), is defined by the following formula (see previous section):

$$\Lambda \approx \frac{\lambda}{n(1-\sin\theta)} \tag{5}$$

Where θ is the laser beam incidence angle and λ is wavelength of laser beam. n is the refractive index of the medium in which the surface wave is propagated and lies between the index of used polymer and the index of the air (the index of refraction in the selvedge layer). Figure II-17 present the AFM studies on the obtained structures for p polarization.

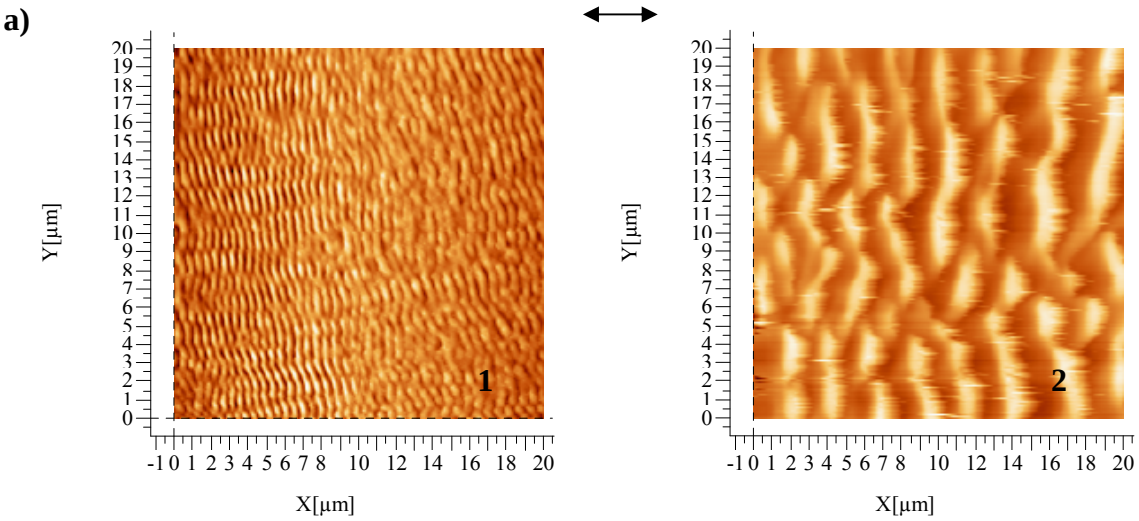

b)

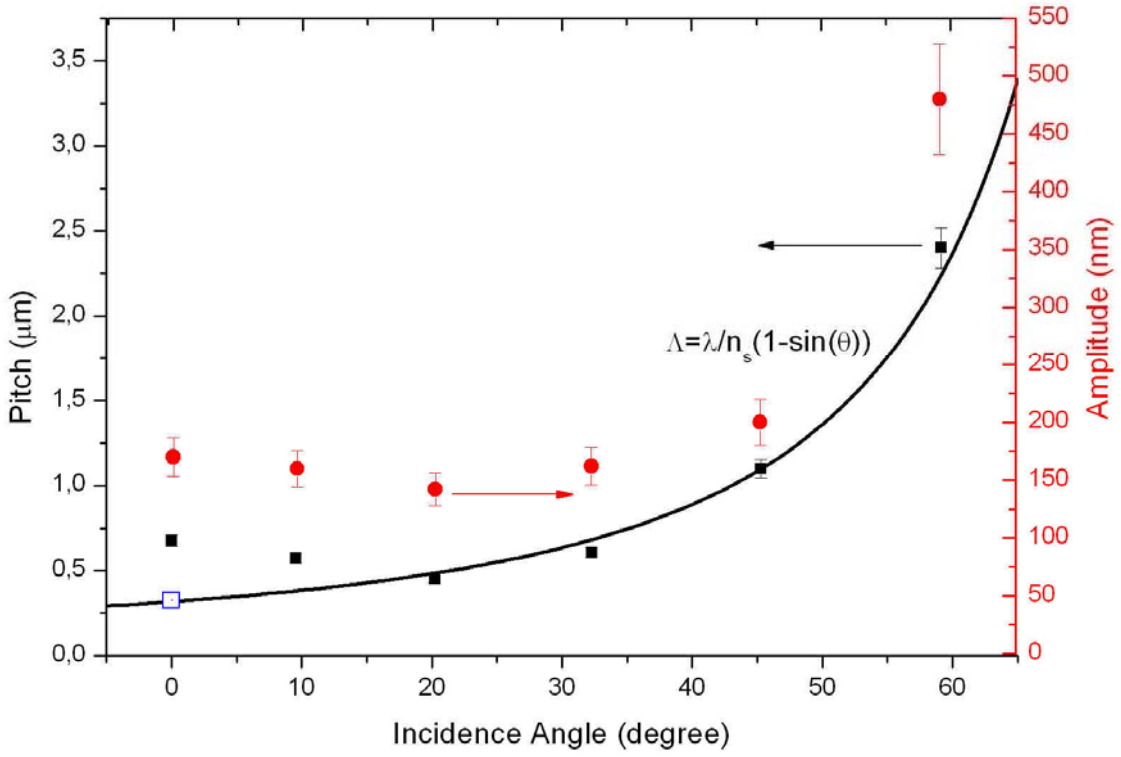

Figure II-17: a) AFM images of SRG for incidence angles of 1)20° and 2) 59° (for example). Polarization direction is indicated by arrow. b) The pitch and amplitude of SRG as a function of angle. The continuous curve shows theoretical results from stimulated wood's anomalies theory. The sample was MB2I azo-polymer. The blue point is the pitch of grating during first 20 minutes of illumination (see figure II-11).

Figure II-17-a) shows the AFM images for two different incidence angles, in both cases the grating wave vector is parallel to the polarization direction of writing beam. In figure II-17-b) the circle and square dots show the experimental result obtained from AFM images for pitch and amplitude of gratings respectively and continues lines indicate the theoretical curve obtained from equation II-5 for different incidence angle. The experimental results consist of two parts: $\theta < 20°$ and $\theta > 20°$.

For $\theta > 20°$ the experimental results are in good agreement with the theoretical calculation from stimulated Wood's anomalies. The laser beam intensity modulation on the surface of the polymer film initiated from interference of scattered beams and input beam. According to asymmetric diffusion model for SRG formation (see section I-7-4-e), azo-polymer migrate

from bright region to dark region of interference pattern. Thus a self-organized SRG will appear on the surface of polymer.

For $\theta < 20°$ experimental results diverge from theoretical curve. As we showed in figure 10, for the first 20 minutes of normal irradiation the pitch of grating satisfies equation II-5 (red line in figure 10). Blue point in figure II-17-b, shows corresponding pitch that is in good agreement with stimulated Wood's anomalies.

The amplitude of gratings shows the same variation as grating pitch (figure II-17-b). The relation between grating pitch and amplitude is presented in figure II-18.

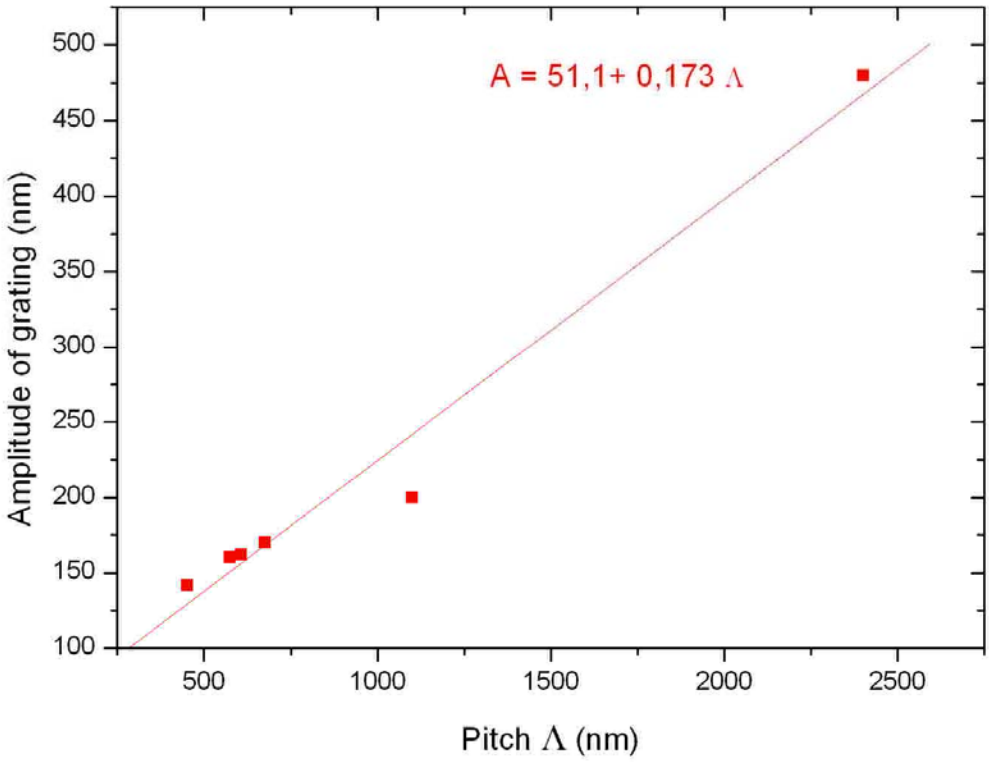

Figure II-18: Relation between pitch and amplitude of gratings.

The gratings amplitude increase almost linearly with their pitch and there is no saturation for longer grating pitch as SRG formation with two beams interference. For larger pitch of spontaneous SRG (2.4 μm), second order diffracted beam also is observed (figure II-19).

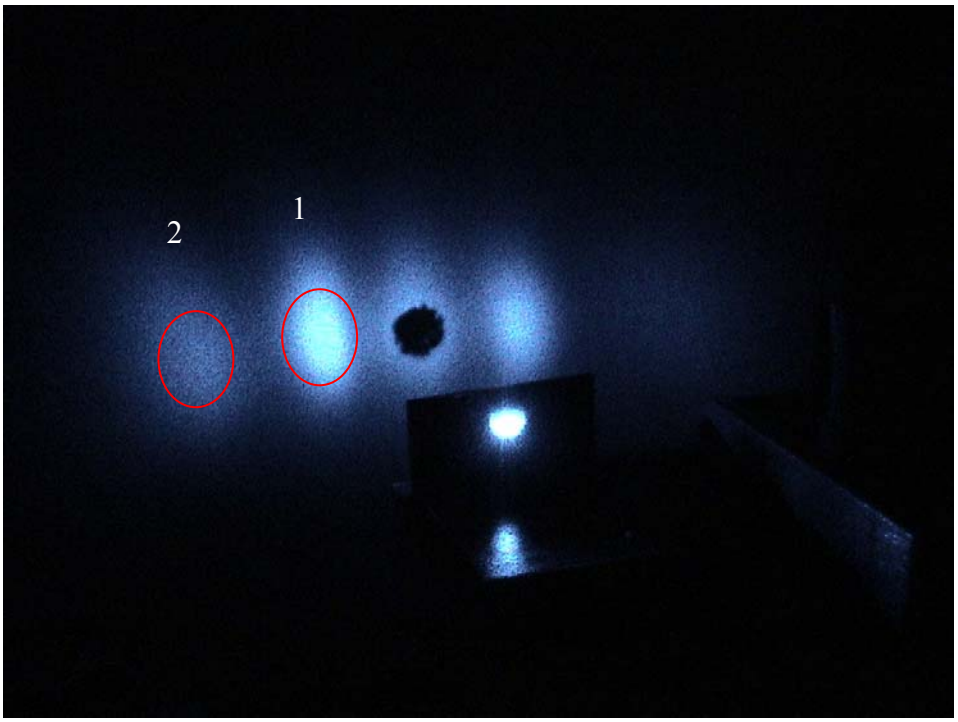

Figure II-19: The photo of first and second order backward self-diffraction retrieved with the recording laser at normal incidence. Incidence angle for inscription of grating was 59°.

II-10-2- S polarization

In the case of s-polarized beam, for the incidence angles less than ~20° the structure was rippled with pitches around 800 nm and amplitude of ~100 nm. But for angles greater than 20°, we obtained complex structures (figure II-20). The pitch and amplitude of such structures were 700 and 90 nm respectively.

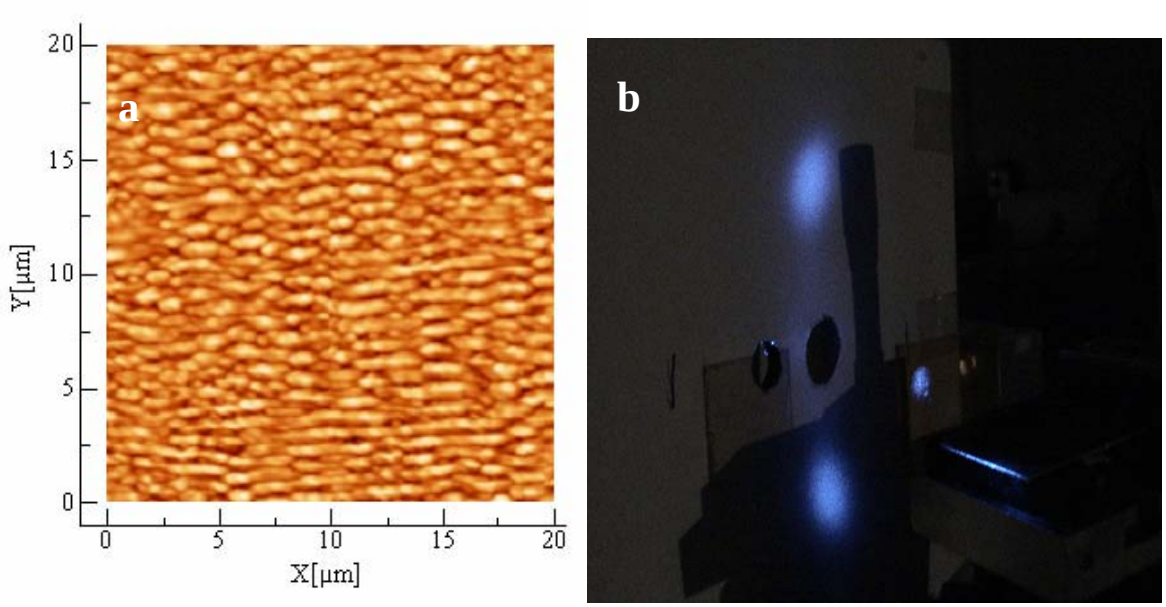

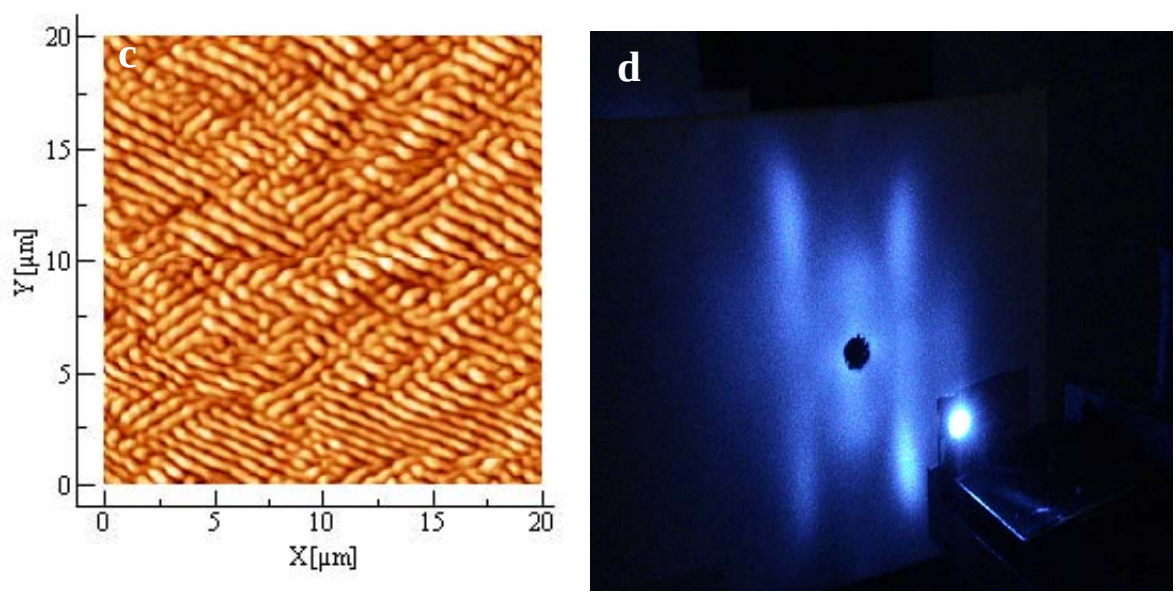

Figure II-20: a and c are AFM images of the structures formed on the surface of polymer for the incidence angles of 20° and 45° respectively. b and d show the photos of backward diffracted beams. The writing beam was s polarized.

According to the stimulated Wood's anomalies, for polarizations other than p(TM) polarization and for larger incidence angle, gratings in other directions can also appear.

II-10-3- 45° polarization

We used a half-wave plate to adjust writing laser beam polarization at 45° with respect to s polarization. Figure II-21 shows the AFM images and their Fourier Transformations for different incidence angles. For angles smaller than ~20°, the direction of grating wave vector rotates by the rotation of sample, but the pitch is almost the same for all of them. Again the angles greater than 20°, the structure becomes more and more complicated. For the first part, by the rotation of sample, the p component of polarization decrease by cosθ (θ is incidence angle) and the resulting polarization on the surface of sample will rotate. The rotated beam will create a SRG with a wave vector parallel to the polarization direction (see Fourier Transformations of AFM images). Around 33° we found a 2D chiral structure that we will discuss in the next chapter.

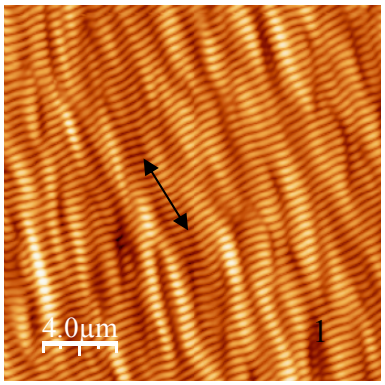
4.0µm
1

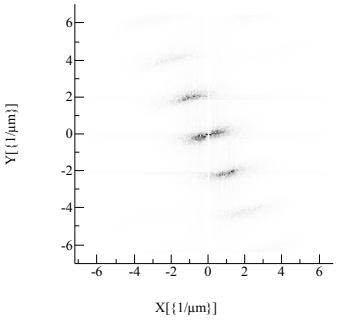
Y[{1/µm}]
X[{1/µm}]

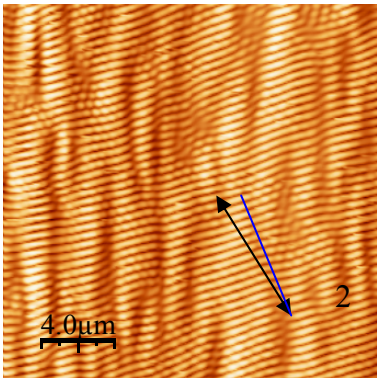
4.0µm
2

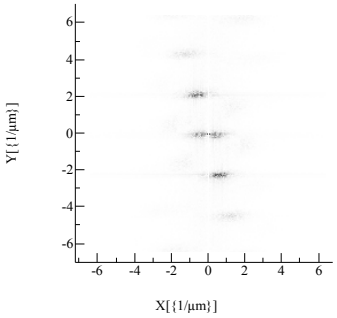
Y[{1/µm}]
X[{1/µm}]

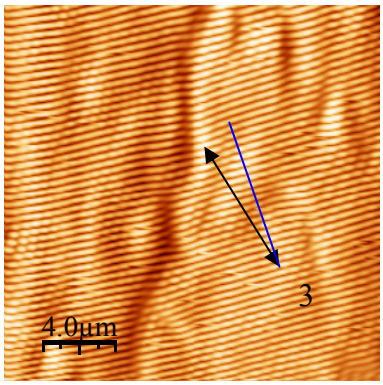
4.0µm
3

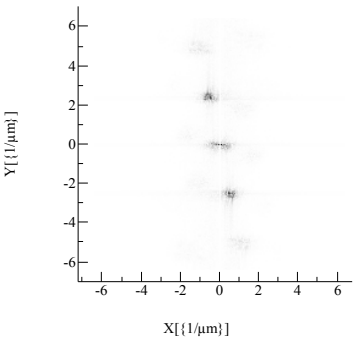
Y[{1/µm}]
X[{1/µm}]

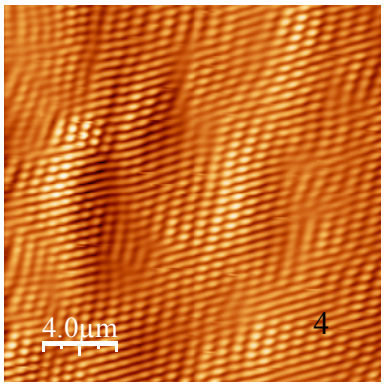
4.0µm
4

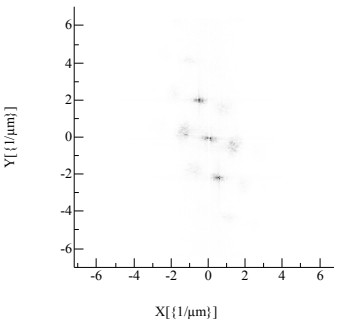
Y[{1/µm}]
X[{1/µm}]

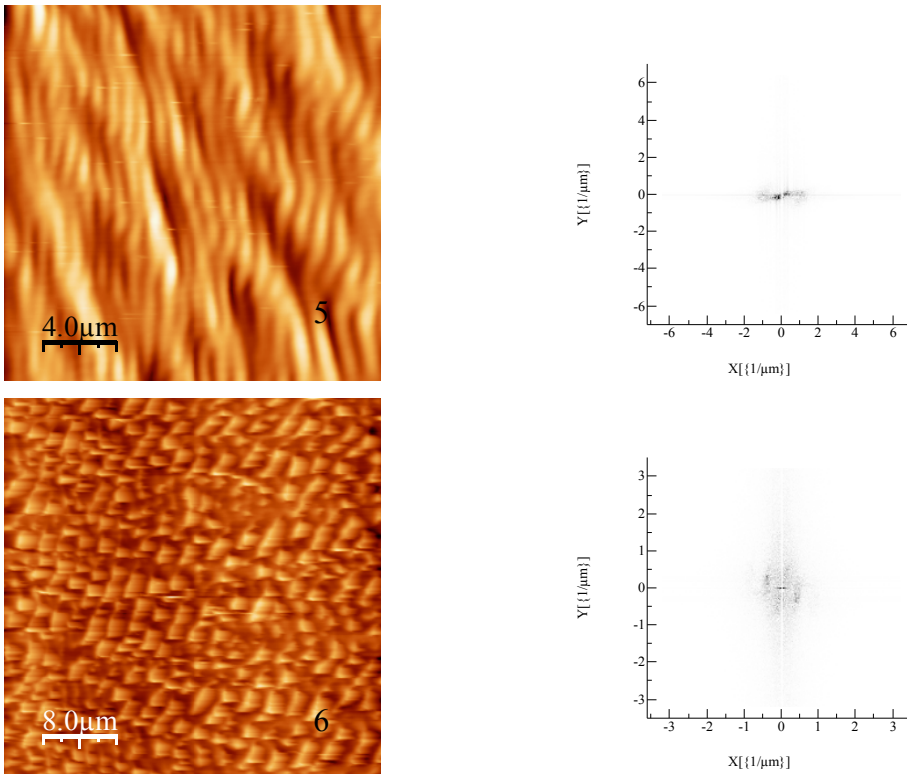

Figure II-21: left) AFM images of spontaneous structures formed on the surface of polymer film. The incidence angles are 1) 5°, 2) 16°, 3) 22°, 4) 33°, 5) 44° and 6) 62°.right) corresponding Fourier transformations.

II-10-4- Circular polarization

We introduced a quarter-wave plate in our experimental setup to obtain circular polarization. At the normal incidence, no privileged orientation can be defined for the structure (figure II-22).

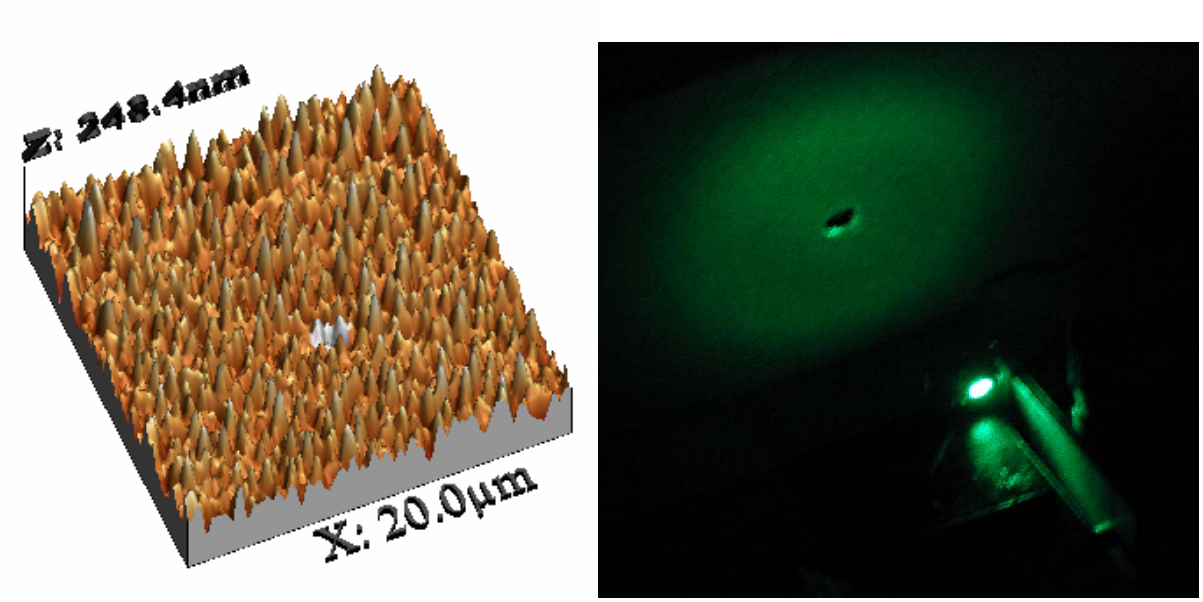

Figure II-22: left) 3D AFM image of polymer surface illuminated with a circular polarized beam. Writing beam was 488 nm line of Ar+ laser. Laser power was 750 mW. Right) backward diffracted beam pattern, readout beam was 514 nm line of Ar+ laser.

The circular form of the backward diffraction pattern (Fourier transform of surface pattern) confirmed the fact that no direction is privileged during the surface structure formation. The self-organized SRGs wave vector is oriented in all directions along the surface of the sample. The structures inscribed by circular polarization confirm also the existence of sub-micron holes. Figure II-23 shows area histogram of holes on the polymer film inscribed by a circular polarized beam. Most of the holes have diameter between 180 nm and 500 nm.

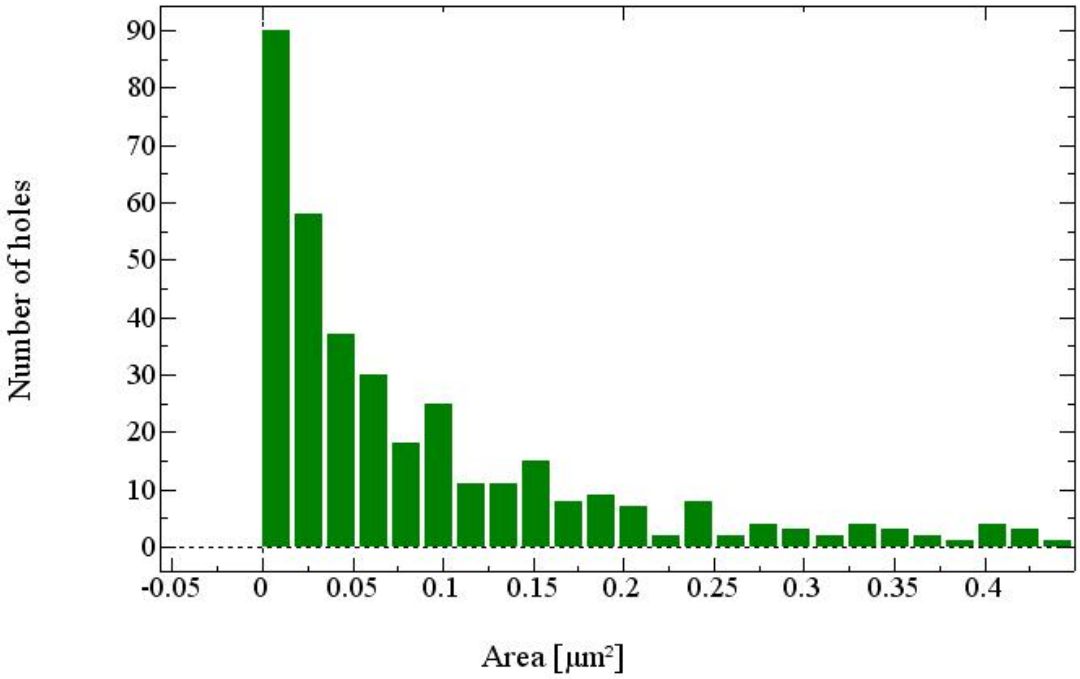

Figure II-23: Area histogram of holes created by circularly polarized laser beam.

We checked the influence of incidence angle for the case of circular polarization. Figure II-24 shows some of AFM images of structures for different incidence angle.

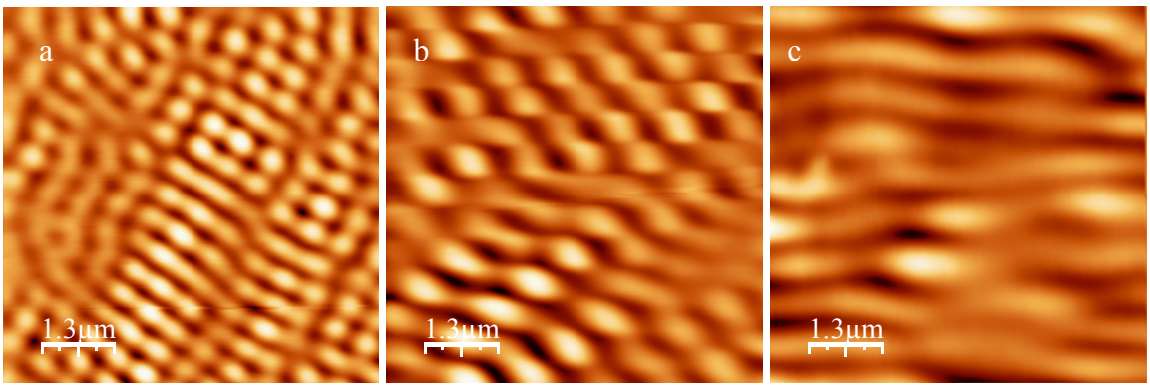

Figure II-24: AFM images of surface structures for circular polarization at incidence angles of a)10° (Λ~450 nm, A ~20 nm) b) 30°(Λ~670 nm, A~ 70 nm) and c) 60°(Λ~700 nm, A~20 nm). L and A are pitch and amplitude of surface gratings.

As we know from basic optics, any state of polarization can be written as superposition of two perpendicular polarizations, let say s and p. When we rotate the sample, the p component changes by cosθ and consequently we will have an elliptical polarization. The azimuth angle

of ellipsoid changes with incidence angle (figure II-24). The corresponding pitch and amplitude of surface grating are presented in the caption of figure.

II-11- Relaxation

The study of relaxation of self-organized SRG can give us more information about its formation mechanism and self-evolution of this phenomenon in dark. To evaluate the relaxation of self-induced SRG, we measured the intensity of diffracted counter-propagating probe (He-Ne laser, 632.8nm, 35mW) beam (figure II-25). We used a red glass filter in front of detector to block up self-diffraction of writing beam and avoid effects of writing beam on the recorded signal.

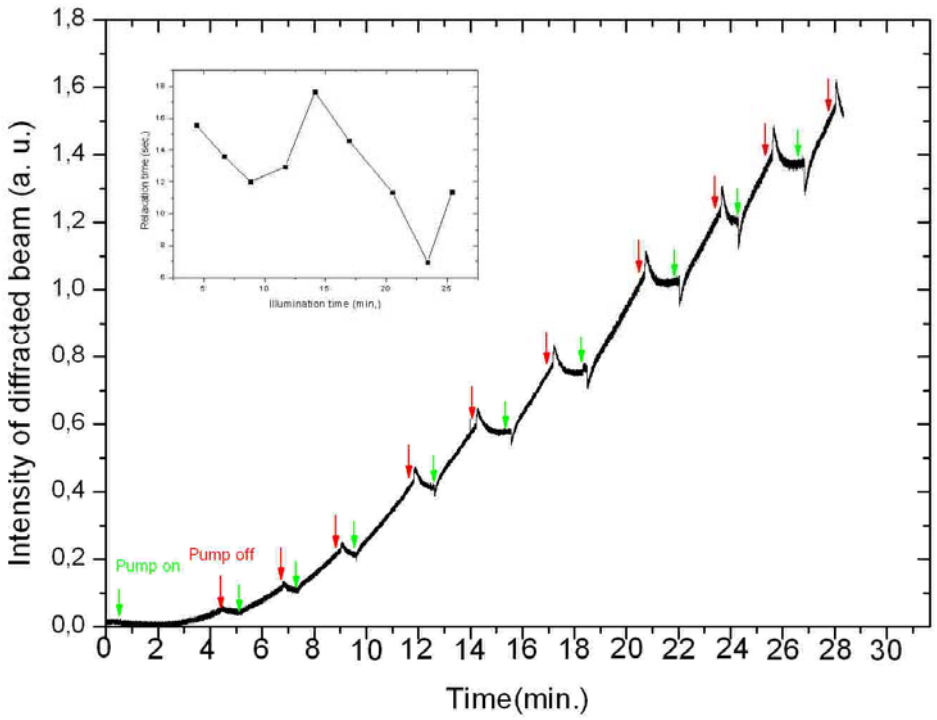

Figure II-25; Irradiation time dependence of diffracted beam intensity. The diffracted beam intensity changes anomalously after switching off the writing beam. The intensity of writing beam is 450 mW/cm^2 at 514 nm. Inset is the relaxation time as function of illumination time.

Just after switching on the writing beam, the photoinduced SRG was formed, and the diffracted beam intensity increased. Two kinds of relaxations can be distinguished from figure

II-25: at the beginning, for the reversible SRG (section II-8), we have a simple exponential relaxation that can be simply due to thermal cis-trans isomerization. The relaxation time decreases with illumination time (figure II-25 inset). For longer illumination, formation of permanent grating, the relaxation behaviour changes. Unlike the case of SRG formed with interference of two beams, after stopping the irradiation of writing beam, the intensity of diffracted beam increased rapidly, decreased slowly, reached to a smaller value and remained at that value [26]. The relaxation time at inflection point increases and decreases by illumination time (figure II-25 inset). Then by switching on the writing beam, after a fast decrease, the intensity of diffracted beam increases again. Matsui et al. related relaxation of SRG to some relaxation mechanisms in azo-containing polymer films such as orientational change of azo-chromophore, cis-trans thermal isomerization and the change of relief height. They concluded that these phenomena are related to the thermal cis-trans isomerization and reorientational relaxation of azobenzene.

The fact that azo polymer migration continued to proceed even in the dark after terminating the light irradiation and again continued to relax even under illumination (spontaneous azo polymer motion),can be related to an asymmetric flow of inelastic fluid induced by light in consideration of the position where it happened and its direction [27]. The clarifying of the role of these mechanisms on the relaxation dynamics of self-photoinduced SRG is under investigation.

II-12- Interpretation

The mechanism proposed to explain the origin of the driving force responsible for SRG formation was partly exposed earlier [28]. It results from photo-isomerization induced translation in which the molecules migrate almost parallel to the polarization direction from high intensity to low intensity of light [29]. In particular, when a collimated laser beam with intensity I impinges onto the sample, light is diffused inside the polymer film in all directions around any micro-roughness (Fig. II-26a) [28].

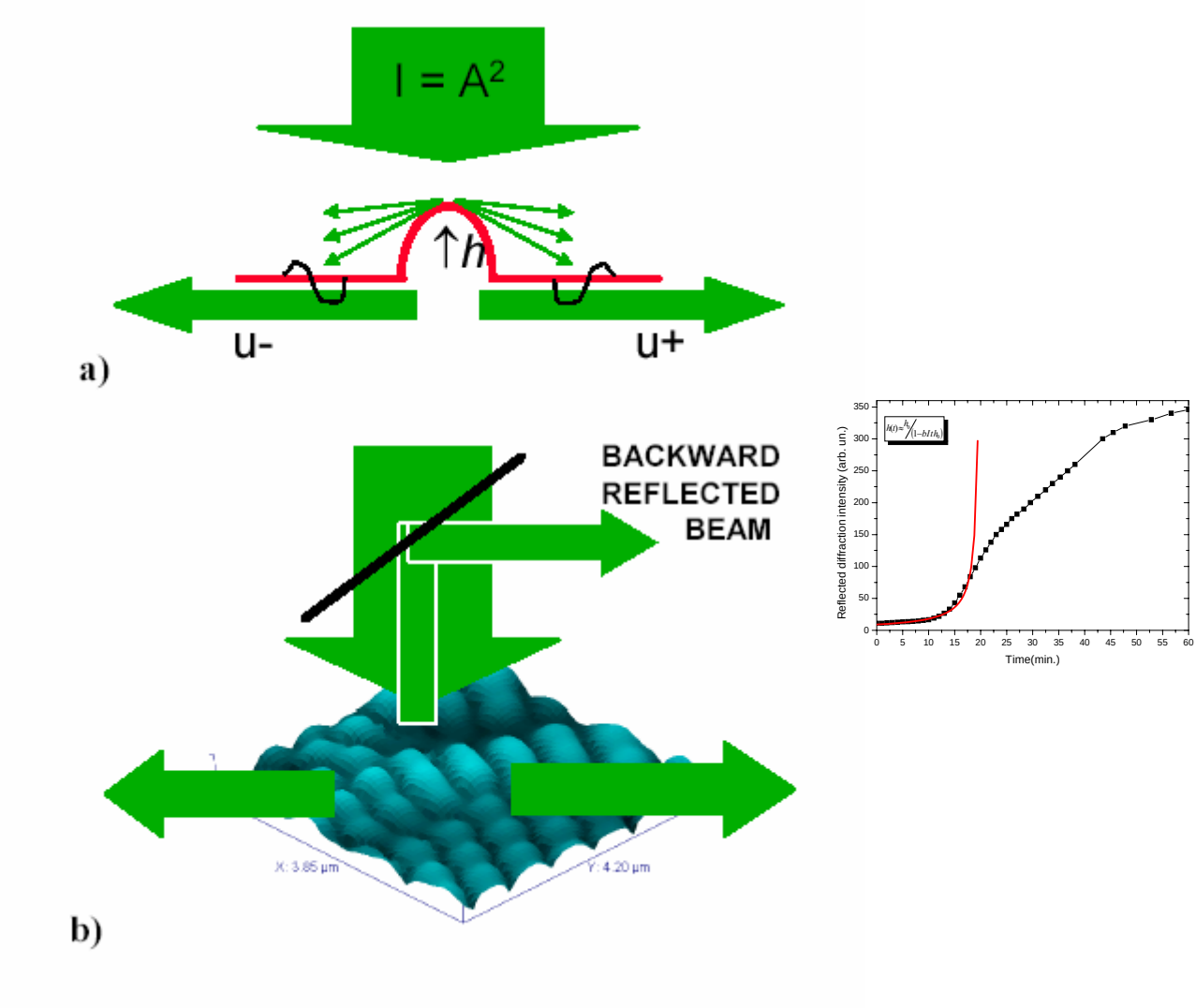

Figure II-26- Scheme of the mechanism of self-structured SRG formation. Left (a) the initiation process which starts from scattered light around nanometer size light induced inhomogeneities and (b) crystallization of the process in a well ordered structure when all scattered amplitudes into the polymer film couple to reemit a backward diffracted beam. Right figure is backward reflected diffraction beam intensity as function of time. Red curve plotted from model.

Let's call h the height of a particular roughness. It will diffract a light amplitude u into the film plane with $u \propto hA$ where $A = I^{1/2}$ is the laser amplitude. According to [29], the rate of growth of the roughness is $\partial h / \partial t \propto u^{+} \bullet u^{-}$ where $u+$ and $u-$ stand for two counter propagating coherent waves interfering into the polymer film plane (Fig. II-26a). So, roughness height h increases with time t from its initial value h_0 as $h(t) \approx h_0 / (1 - b\, I\, t\, h_0)$, up to saturation of the diffraction efficiency.

This explains why the "time threshold" defined above is proportional to the laser light intensity. Coefficient b can be related to the quantum efficiency of the photoinduced translation and surface relief growth process, according to [29]. The process which initially diverges as $b\ I\ t\ h_0$ tends to 1 saturates after time threshold. Indeed, owing to coupled wave theory [30] (Fig. II-26b), SRG amplitude tends to a limit height h_{max} for which more light coupled by diffraction into the polymer film results into more light diffracted out of the polymer film.

A balance is then obtained when incident and diffracted beams reach comparable magnitudes. The measured backward up-diffracted intensity indeed reaches a few percent.

II-13- Conclusion

In this chapter we presented a simple experimental method for self-induced SRG formation on azo-polymer films. We demonstrated for the first time to our knowledge that multistate addressing by polarization can be achieved using a single beam polarization in an azo polymer film. The different polarization states are stored as surface diffraction gratings. The grating orientation follows the direction of the incident beam polarization. The permanent SRG diffracts light into positive and negative diffraction orders in the backward and forward directions along the direction of incident beam polarization. We investigated experimentally the self-SRGs formation on different azo-polymer films. We observed incidence angle dependences of both pitch and amplitude of SRGs for s, p, 45° and circular polarization. The values obtained form p polarized beam for different incidence angles are in good agreement with Stimulated Wood's anomalies for spontaneous grating formation. The results show that these SRGs are optically reversible before inflection time. After this time the structure is permanent. We also experimentally observed the relaxations of formed SRGs.

II-14- References:

1- S. Ahmadi kandjani, R. Barille, S. Dabos-seignon, J. –M. Nunzi, E. Ortyl, S. Kucharski, Multistate polarization addressing using a single beam in an azo polymer film, Opt. Lett., 2005, **30**, 1986-1988.

2- R. W. Wood, On a remarkable case of uneven distribution of light in a diffraction grating spectrum, Proc. Phys. Soc. (London), 1902, **18**, 269-275.

3- R. W. Wood, On a remarkable case of uneven distribution of light in diffraction grating problems, Phil. Mag., 6th ser., 1902, **4**, 396-402.

4- Lord Rayleigh, On the dynamical theory of gratings, Proc. Roy. Soc. (London)**,** 1907, **A79**, 399-416.

5- Lord Rayleigh, Note on the remarkable case of diffraction spectra described by Prof. Wood, Phil. Mag.*,* 6th ser., 1907, **14**, 60-65.

6- A. E. Siegman, P. M. Fauchet, Stimulated Wood's anomalies on laser-illuminated surfaces, IEEE J. Quantum Electron., 1986, **QE-22**, 1384-1403.

7- J. E. Sipe, Jeff F. Young, J. S. Preston, H. M. Driel, Laser-induced periodic surface structure: I- Theory, Phys. Rev. B, 1983, **27**,1141-1154.

8- I. Horcas, R. Fernandez, J.M. Gomez-Rodriguez, J. Colchero, J. Gomez-Herrero and A.M. Baro, WSXM: A software for scanning probe microscopy and a tool for nanotechnology, Rev. sci. Instrum., 2007, **78**,013705.

9- G. Berger, C. Denz, S. S. Orlov, B. Phillips, L. Hesselink, Associative recall in a volume holographic storage system based on phase-code multiplexing, Appl. Phys. B, 2001, **73,** 839–845.

10- S. S. Orlov, W. Phillips, E. Bjornson, Y. Takashima, P. Sundaram, L. Hesselink, R. Okas, D. Kwan, R. Snyder, High-transfer-rate high-capacity holographic disk data-storage system, Appl. Opt., 2004, **43,** 4902–4914.

11- G. W. Burr, J. Ashley, H. Coufal, R. K. Grygier, J. A. Hoffnagle, C. M. Jefferson, B. Marcus,Modulation coding for pixel-matched holographic data storage, Opt. Lett., 1997, **22,** 639–641.

12- F. Heanue, M. C. Bashaw, L. Hesselink, Volume holographic storage and retrival of digital data, Science, 1994, **265**, 749-752.

13- S. Campbell, X. Yi, P. Yeh, Hybrid sparse-wavelength angle-multiplexed optical data storage system, Opt. Lett., 1993, **19**, 2161-2163.

14- D. Lande, J. F. Heanue, M. C. Bashaw, L. Hesselink, Digital wavelength-multiplexed holographic data storage system, Opt. Lett.,1996, **21**, 1780-1782.

15- J. M. Brom, F. Rioux, Polarized light and quantum mechanics: an optical analogue of the Stern–Gerlach experiment, Chem. Educator, 2002, **7**, 200-204.

16- K. Kawano, J. Minabe, T. Ishii, Digital data storage and computing by a vector holographic memory system, Jpn. J. Appl. Phys., 2001, **40**, 1841-1845.

17- B. Yao, M. Lei, L. Ren, N. Menke, Y. Wang, T. Fischer, N. Hampp, Polarization multiplexed write-once-read-many optical data storage in bacteriorhodopsin films, Opt. Lett., 2005, **30**, 3060-3062.

18- S. Orlic, S. Ulm, H. J. Eichler, 3D bit-oriented optical storage in photopolymers, J. Opt. A Pure Appl. Opt., 2001, **3**, 72-81.

19- P. M. Lundquist, C. Poga, R. G. DeVoe, Y. Jia, W. E. Moerner, M.-P. Bernal, H. Coufal, R. K. Grygier, J. A. Hoffnagle, C. M. Jefferson, R. M. Macfarlane, R. M. Shelby, G. T. Sincerbox, Holographic digital data storage in a photorefractive polymer, Opt. Lett., 1996, **21**, 890-892.

20- T. Todorov, L. Nikolova, K. Stoyanova, N. Tomova, Polarization holography. 3: Some applications of polarization holographic recording, Appl. Opt., 1985, **24**, 785-788.

21- W. C. Su, C. C. Sun, N. Kukhtarev, A. E. T. Chiou**,** Polarization-multiplexed volume holograms in $LiNbO_3$ with 90-deg geometry, Opt. Eng., 2003, **42**, 9-10.

22- W. C. Su, S. H. Ma, C. C. Sun, A. E. T. Chiou, N. Kukhtarev, Volume holographic storage using polarization multiplexing, Proc. SPIE, 2003, **5206**, 118-124.

23- W. D. Koek, N. Bhattacharya, J. J. M. Braat, V. S. S. Chan, J. Westerweel, Holographic simultaneous readout polarization multiplexing based on photoinduced anisotropy in bacteriorhodopsin, Opt. Lett., 2004, **29**, 101-103.

24- W. C. Su, C. –M. Chen, Y. Ouyang, Orthogonal polarization simultaneous readout for volume holograms with hybrid angle and polarization multiplexing in LiNbO3, To be published in Applied Optics, Accepted: 26 January 2007.

25- D. Bäuerle, Instabilities and structure formation, *Laser processing and chemistry*, Springer, 2000, 571.

26- T. Matsui, S. Yamamoto, M. Ozaki, K. Yoshino, F. Kajzar, Relaxation kinetics of photoinduced surface relief grating on azopolymer films, J. Appl. Phys., 2002, **92,** 6959-69-65.

27- T. Ubukata, T. Higuchi, N. Zettsu, T. Seki, M. Hara, Spontaneous motion observed in highly sensitive surface relief formation system, Colloids and Surfaces A: Physicochem. Eng. Aspects, 2005, **257–258**, 123–126.

28- P. Lefin, C. Fiorini, J.-M. Nunzi, Anisotropy of the photoinduced translation diffusion of azobenzene-dyes in polymer matrices, Pure Appl. Opt., 1998, **7**, 71-82.

29- C. Hubert, C. Fiorini-Debuisschert, P. Raimond, J.-M. Nunzi, J.-J. Simon, L. Escoubas, Spontaneous photo-induced structuration of the surface of azo-benzene polymer films by the molecular migration effect, Nonlin. Opt, Quant. Opt., 2004, **31**, 221-230.

30- H. Kogelnik, Coupled wave theory for thick hologram gratings, Bell Sys. Technol. J., 1969, **48**, 2909-2947.

Chapter III

Incoherent light induced self-organization of molecules

III-1- Introduction

In this chapter, we will show that a well-defined SRG is induced in an azo-polymer film by the combination of a low-power coherent laser beam with another high-power partially or totally incoherent and unpolarized beam. It appears that the low-power beam carries information about pitch and orientation of the diffraction grating that is transferred to the high-power beam. The low power coherent beam creates the structure. The spatial coherence of the large-power assistance beam is varied from low to high coherency and the diffraction efficiency of the self-induced SRG is monitored. Information in our experiment is given as diffraction characteristics by the coherent signal beam. We show that, without coherence, no well defined diffraction pattern is induced. With some degree of coherence, a self-induced diffraction pattern is formed more or less rapidly. We thus get a measurement of the information exchange duration in terms of coherence of laser beam. We also give quantitative insight into the cooperativity of the process.

Practically, information given by the signal beam is related to the orientation and pitch of the grating. Our experiments show that photoactive molecular films come into a unique cooperative organization although most of the individual molecules have a random light-

assisted movement. We find in this way a simple system allowing us to figure out the minimal requirements to organize disordered materials into well-organized structures. We verify experimentally that random motion plus information exchange lead to self-organization. The information is exchanged locally by the relief of the polymer surface.

S. Ahmadi Kandjani, R. Barille, S. Dabos-Seignon, J.-M. Nunzi, E. Ortyl, S. Kucharski, Incoherent light-induced self-organization of molecules, Opt. Lett., 2005, **30**, 3177-3179.
R. Barille, S. Ahmadi Kandjani, , E. Ortyl, S. Kucharski, J.-M. Nunzi, Cognitive ability experiment with photosensitive organic molecular thin films, Phys. Rev. Lett., 2006, **97**, 048701.

III-2- Introduction to self-organization of molecules with incoherent light

Usually in holographic gratings (volume or surface relief) coherent beams interference are necessary for grating formation and incoherent light has been used as a uniform background light or post-exposure [1,2]. In polarization gratings, the applied incoherent beam modifies the field distribution and consequently resulting grating [1]. An incoherent UV-blue light causes trans-cis photoisomerization in azobenzene systems. Yan et al. used an incoherent assisting light with respect to interfering beams to increase the rate of SRG formation in an azo-polymer [3], the SRG was formed by two coherent laser beams. Ubukata et al. have formed SRG on a liquid-crystalline azo-polymer film by unpolarized incoherent light using a photomask [4]. Again a well known pattern of light has been produced using a photomask on azo-polymer film.

We have reviewed optical self-organized structures in section I-3. Incoherent light has bean used for self-organized pattern formation in nonlinear optical materials.

We contradict the general opinion about SRGs that patterning of photoactive systems requires coherent light [5]. It relies on the common sense that interferences and therefore coherency of the interacting waves are mandatory for long-range ordering [6]. Some molecules move under light excitation [7]. Motion is not an organized process, but if the molecules exchange position information, they can organize into well-defined structures. Spontaneous pattern formation arises from the interplay between self-action (e.g., photoisomerization) [8] and long-range interaction (e.g., diffraction) [9]. The phenomenon is initiated by noisy random fluctuations. The perturbations bearing a particular periodicity are enhanced, forming regular patterns, [10] according to the “winner takes all” theory [11]. Self-organized photoinduced structures find applications in optoelectronic devices [12]. It was previously recognized that self-organization can occur directly from the short range interaction between molecules [13]. Self-organized optical patterns are also induced from incoherent light beams in photorefractive crystals [14, 15]. More generally, feedback effects induce self-organization into well-ordered patterns in all kinds of dynamic systems [16]. Spatial patterns may also arise spontaneously as a consequence of nonlinear wave mixing processes in the transverse cross section of coherent optical beams [17]. As a universal feature, these effects require a coherent excitation which simultaneously carries the information and excites the degrees of freedom of the system: excitation, rotation, and translation in the case of photochromic molecules.

In the standard model of SRG formation in azo-dye-based photoactive polymers, the photoactive molecules are excited by the illumination pattern. The highly reactive molecules move in a nonuniform way, inducing a mass transport from the bright to the neighbouring dark regions [5]. The maximum heights of the light-induced SRG correspond to light intensity minima.

III-3- Experimental details

The experimental setup is shown in figure III-1.

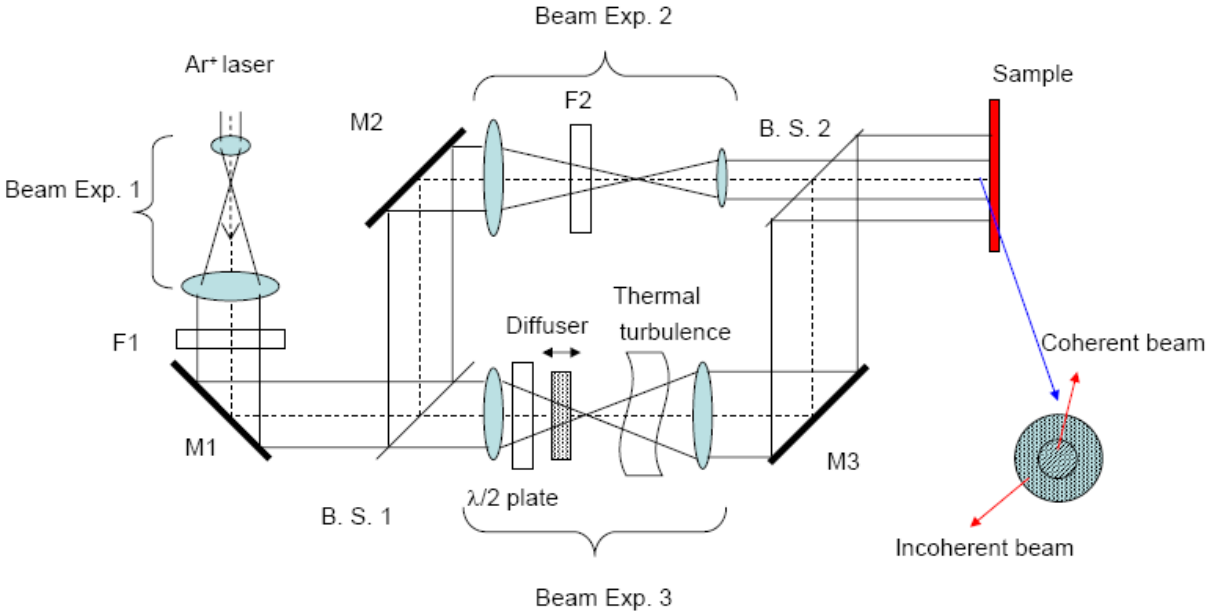

Figure III-1: Experimental scheme for surface relief grating formation on azo-polymer films using the combination of a narrow low power coherent beam and a large high power incoherent beam. M1, M2 and M3 are mirrors.

Our samples are 1µm-thick MB2I azo-polymer films. The λ=476.5 nm laser line of a continuous argon-ion laser excites the azo-polymer close to its absorption maximum. The laser power is 500 mW .The beam width is increased to 5.8 mm by an afocal system made of two lenses. Experimentally, the laser beam is divided into two arms of a Mach–Zehnder interferometer. The first arm carries the seed and is reduced to a width of 2.1 mm by another afocal. This first coherent beam acts as a signal beam. The second arm carries the totally incoherent and unpolarized pump beam. A wave plate is inserted in the main path of the beam to control the polarisation of the incoherent beam. Incoherent pump beam is provided by focusing the laser beam through a diffuser made of a piece of tarnished plexiglass or frosted glass produced by acid etching of a clear sheet of glass and recollimating the scattered beam. A hot-air gun used as a turbulent layer generator is inserted along its path to ensure total incoherency and depolarization [18]. The air motion indeed produces random temperature variations which in turn produce fluctuations of the index of refraction and optical turbulence. Signal and pump beams overlap spatially at the exit of the interferometer, with the thinner

signal aligned in the center of the pump. Both beams illuminate the polymer film from the polymer side.

III-4- Results and discussion

To check the SRG formation with incoherent pump light, we performed the following experiments. In these experiments, the signal beam has 0.7 mW power, 2.1 mm diameter, and linear polarization. The pump beam is totally incoherent and unpolarized (hot-gun is on) has 87 mW power and 5.8 mm diameter. The peak-to-peak height of all the gratings is 100±5 nm. Their mean pitch is Λ=890±30 nm. The pitch is close to the theoretical value given by first order diffraction theory in the backward direction θ =32.6°:$\Lambda=2\lambda/2 \sin\theta$.

In the first series of experiments, we verified that the surface grating stored cannot be the result of one beam alone: the signal beam is first sent alone onto the sample without the incoherent beam. The laser intensity is chosen in order to excite the polymer below the threshold for inducing a SRG on the film. We have evidence that a SRG is induced by measuring the first-order diffraction in reflection with an appropriate combination of lenses and photodiode. By a careful control of the diffraction intensity, we have checked that no effect was produced on the polymer surface after more than 1 h of illumination with coherent signal beam powers less than 0.7 mW. Second, the unpolarized incoherent pump beam is sent alone onto the film. No SRG is induced and no diffraction detected, even with a longer exposure time. Third, when the two beams are sent together and overlap onto the polymer film, a SRG is induced after 0.5 h exposure. We performed following experiments in order to precise the point that: which beam brings on information about the orientation of the periodic structure? The hot-air gun is not used and only the diffuser decreases the pump beam coherency. The polarization directions of signal and incoherent beams were controlled by a half-wave plate in each arm. The detector is set to measure first-order self backward diffraction intensity at θ = 32.6° in the horizontal plane, which would correspond to the diffraction direction of self-organized SRG by p-polarized writing beam. Figure III-2 presents the results of diffraction from different polarisation combinations. When the signal beam is s-polarised and the pump beam is p-polarised (curve A in figure III-2), no signal is detected, which means that the SRG has no wave-vector component in the p-direction. The SRG inscribed by signal beam has wave vector and diffraction in vertical direction that is not detectable. When the signal beam is p-polarised (horizontal) and the pump beam s-polarised (vertical), diffraction is detected (curve B in figure III-2). When the signal beam is p-polarised

and the pump beam p-polarised, a strong diffraction is detected (curve C in figure III-2). This shows that the coherent signal beam carries all the information about the structure formation and its polarization direction determines the direction of grating wave-vector. The incoherent pump beam which is almost three times more powerful and larger in size activates molecular motion, by accelerating the trans-cis-trans photo-isomerization, into a pattern which reflects the information carried by the weaker signal beam. When both of beams have p-polarization, the incoherent pump beam enhanced SRG formation rate and contributed in the diffracted beam intensity.

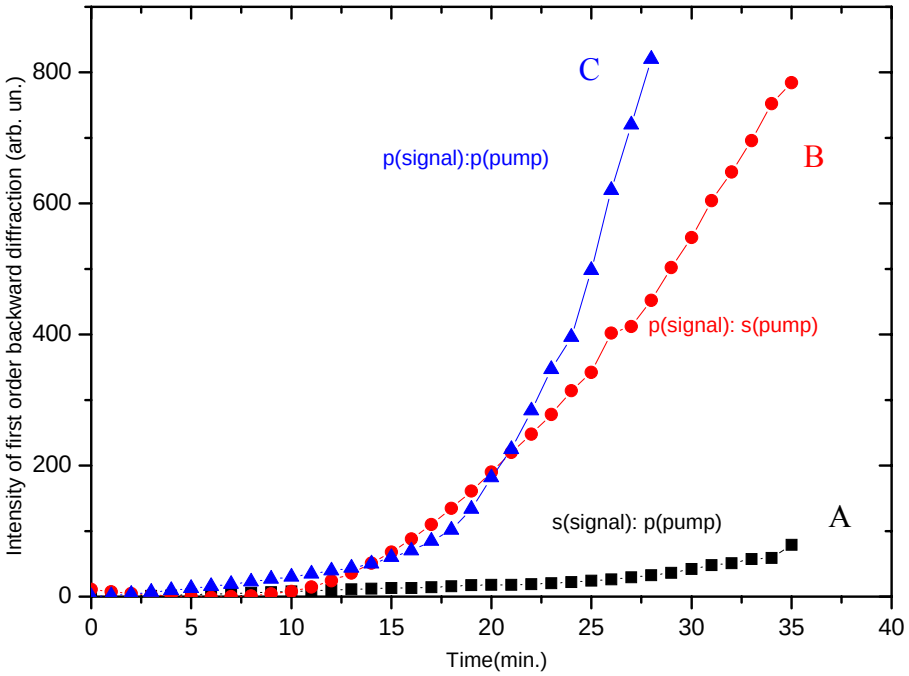

Figure III-2: The intensity of the first order diffracted beam as a function of time for different polarisation configurations of the signal and incoherent beams. The detector is set to measure the diffraction intensity in the horizontal plane (p-polarization direction).

To verify topology of surface, both the height and the pitch of the grating were retrieved using a contact-mode atomic force microscope (see section II-7). A well-defined SRG is induced in the overlapping region of the coherent signal beam [Fig. III-3(a)]. The structures observed in the nonoverlapping region [Fig. III-3(b)] reflect amplified fluctuations due to the random photoinduced molecular movements by the incoherent beam. The grating wave vector is parallel to the linear polarization of the signal, which is in the p-plane. Far outside of the coherent beam region, no grating is induced after 0.5 h illumination.

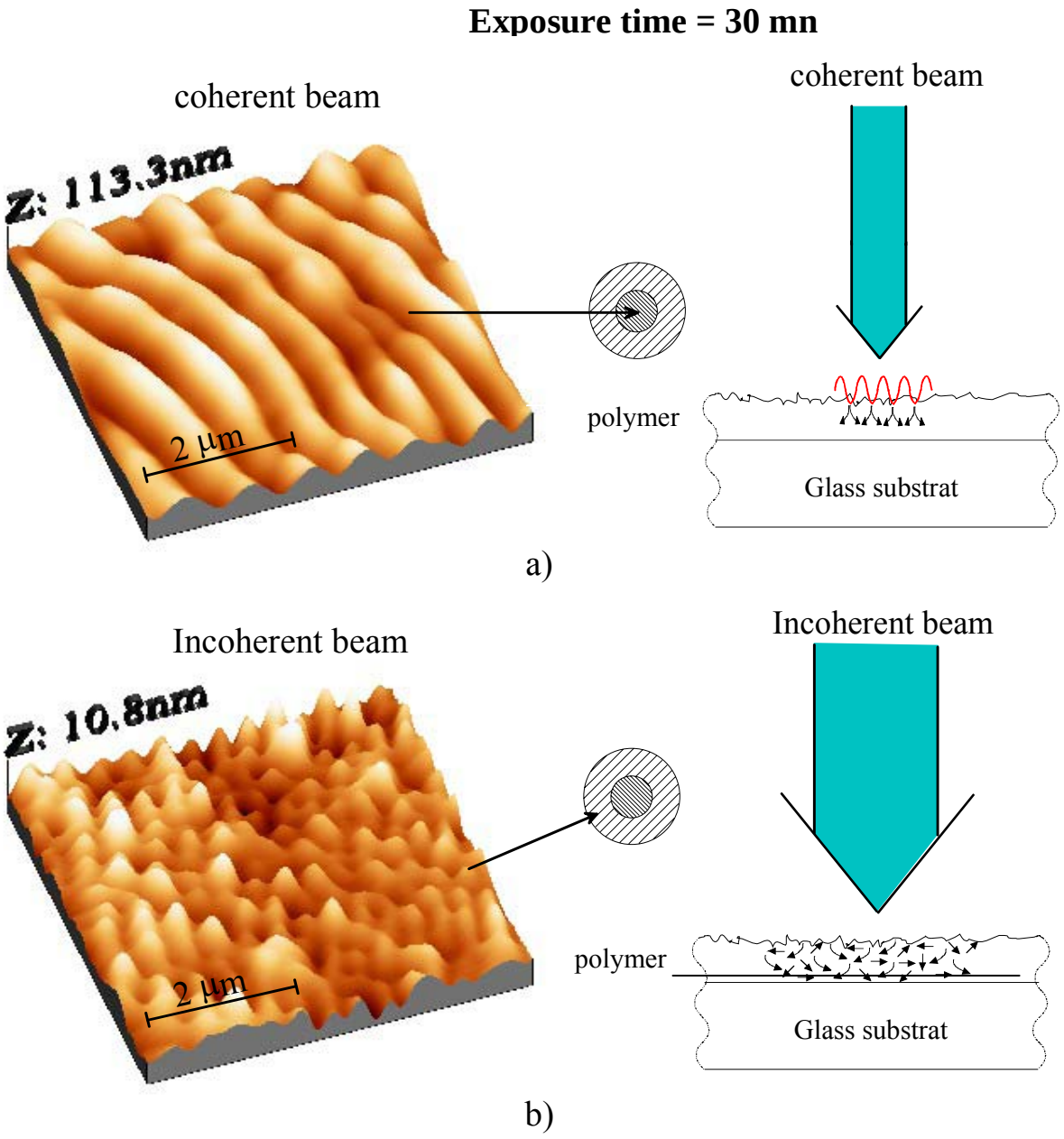

Figure III-3: AFM images of self-patterned SRG structures obtained after 30 min exposure with a low-power coherent beam and a large power incoherent beam. (a) We scan the SRG in the central part of the coherent beam region. Isomerization induces a molecular migration almost parallel to the polarization direction. In particular, when a collimated laser beam impinges onto the polymer surface, light is diffused inside the polymer film in all directions around any microroughness. It will diffract a light amplitude into the film plane. The roughness amplitude is increased. This creates a surface modulation that organizes coherently to diffract the incident laser light out of the polymer film. The modulation amplitude increases with time from its initial value, up to saturation of the diffraction efficiency. Saturation corresponds to the balance between incident and diffracted intensities: more light coupled by diffraction into the polymer film resulting into more light diffracted out of the polymer film. Backward diffracted intensity experimentally reaches about 1%. (b) Within the outer incoherent laser beam region, light induces a random motion of the molecules. No well-defined pattern can be produced. Within short exposures, roughness amplitude is increased, without any coherent coupling.

In another series of experiments, the coherent signal is first sent alone onto the polymer with a large power of 125 mW for 1 h. A well-defined SRG is stored. Its spatial frequency profile [normalized Power Spectral Density (PSD)] is shown as a continuous curve in Fig. III-4(d). One dimensional PSD function is obtained from the Fourier image. The position and width of PSD peaks give us the wavelengths and lateral ordering of SRGs. Second, the coherent beam power is decreased to 0.7 mW. The coherent beam overlaps partially with the totally incoherent beam [scheme in Fig. III-4 (b)]. After 2 h of exposure, a well defined SRG is also stored [Fig. III-4 (a)]. Importantly, the amplitude profile of the SRG taken in all places inside the incoherent beam region has the same characteristics in height, pitch, and orientation as the one induced by the high-power coherent beam alone. This is confirmed by the Fourier transform given in Fig. III-3 (d). It shows that the two patterns have the same spatial frequency within experimental uncertainties. So the SRG has expanded from the central coherent beam region to the whole region exposed to the incoherent beam. In this way we see that a totally incoherent beam can provide the movement that is necessary to induce a well-defined SRG. The information brought by the coherent signal has been transmitted to the peripheral incoherent region by the molecular self-assembling process: i.e., the organized molecules communicate nonlocal information about photoinduced structural organization to the nonorganized neighboring ones. In another word, the molecules which respond to the coherent beam create a diffraction pattern and then transmit the pattern step by step to all of their neighbors. Information is exchanged locally via the relief: pits sending more light to the neighboring and dips sending less light, thus replicating the pattern [19-21].

We also checked that before reaching saturation, the self-structuring process that occurs under incoherent illumination continues up to saturation after removal of the signal. Moreover, if the incoherent beam is polarized, the polarization of the signal still governs the orientation of the structure. No structure appears out of the incoherently illuminated region.

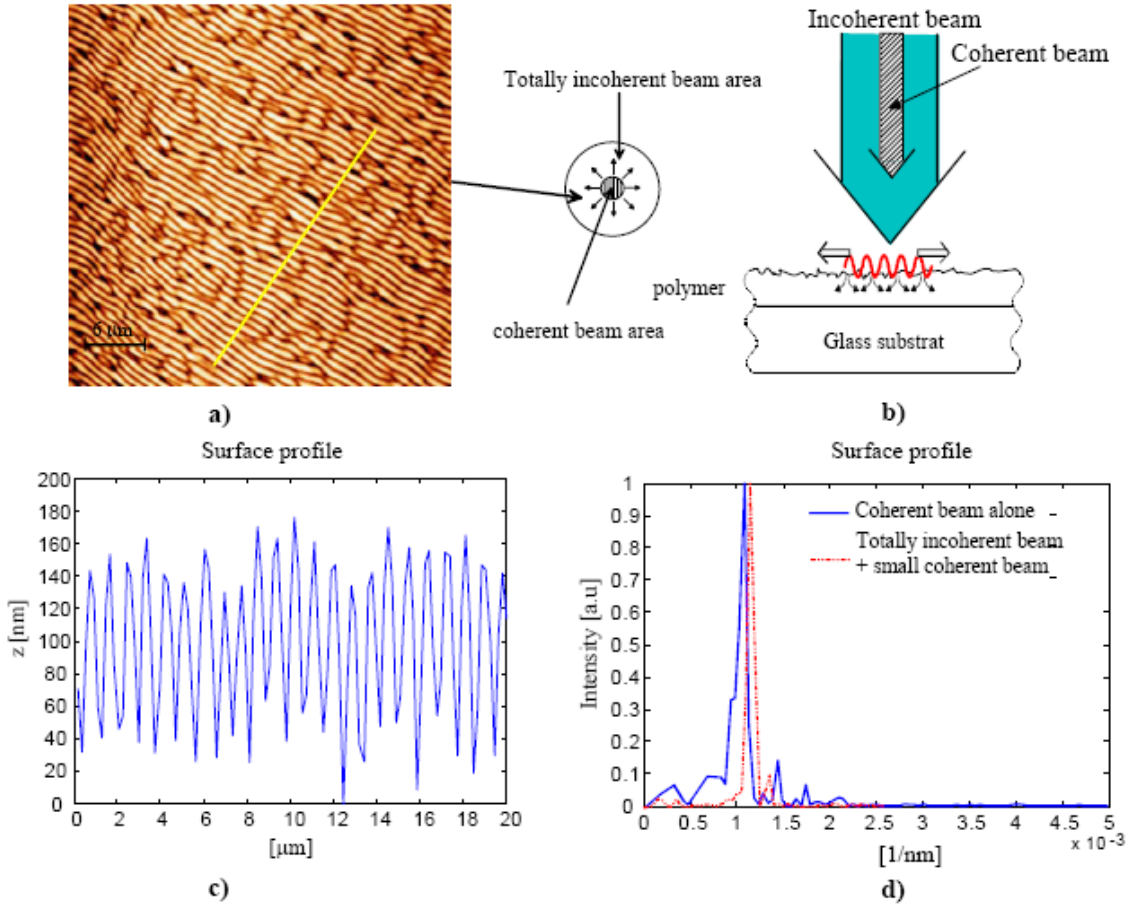

Figure III-4: Self-patterned SRGs obtained with a totally incoherent beam after 2 h of exposure. (a) AFM image of the self-patterned SRG induced by the incoherent beam, outside of the coherent beam region. This pattern shows that the information about the structure was transmitted from the coherent to the incoherent regions. (b) Sketch of the expansion mechanism showing propagation of the structure from the coherent to the incoherent region, up to the whole illuminated area. (c) Amplitude profile of the grating taken along the yellow line in the SRG pattern shows the regularity of the profile. Grating amplitude is 100 nm; pitch is 890 nm. (d) Plot of the spatial frequency pattern allows comparison of the SRGs formed using a strong coherent beam alone and in the region outside of the coherent beam in the dual beam experiment of part (b).

We have characterized the remaining coherency of the pump beam by moving the diffuser in front of the first lens of the beam expander. In figure III-5 from 1 to 3 the diffuser moves from focal point to first lens. When the diffuser is close to the focal point, the rate of SRG formation is high and it decreases moving the diffuser toward the first lens. This demonstrates that when the diffuser is close to the first lens is gives a maximum of incoherency. We

checked also that interferences from a Young's slit (450 µm wide and 10 mm long) setup with an incoherent beam had zero visibility (appendix 1).

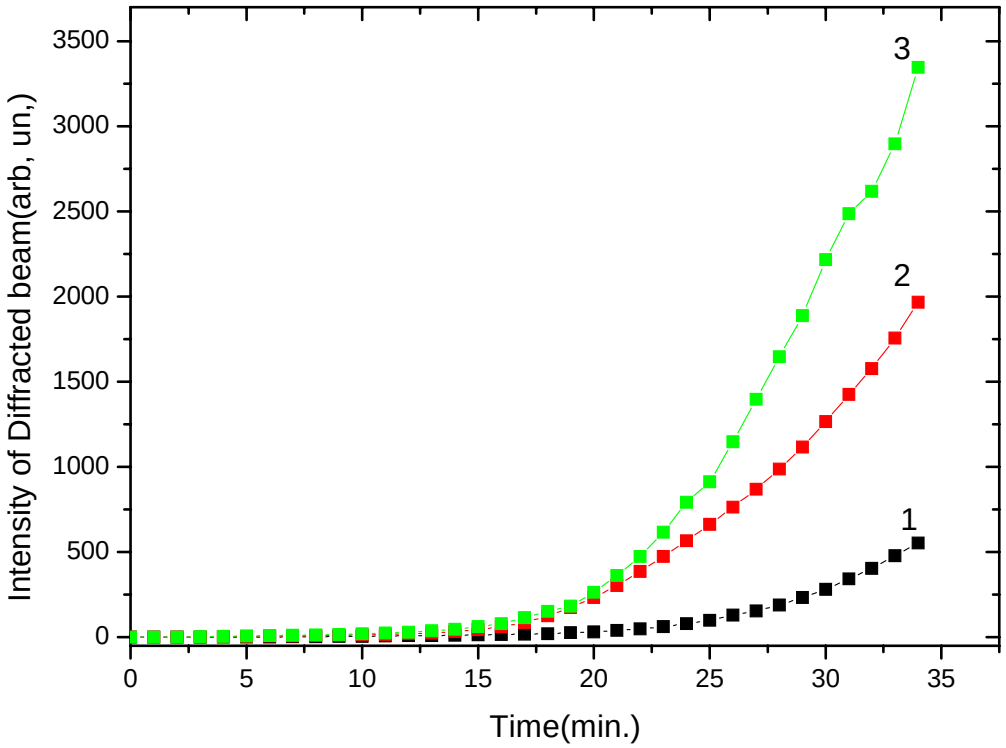

Figure III-5: Diffracted beam intensity as a function of time for different positions of diffuser. From 1 to 3, the diffuser is closer to focal point of the first lens of third beam expander.

We have measured the growth of diffraction intensity for different pump beam coherence lengths σ_μ (figure III-6). Coherence length is measured as the speckle size $\sqrt{S/N}$ [22], in which S is the illuminated surface and N the number of speckle spots. Spatial coherence length varies practically from 0 to 1500 λ. Almost complete incoherence and depolarization ($\sigma_\mu/\lambda \approx 0$) are obtained using the hot-air gun. In this condition, the grating growth rate is the slowest. For all gratings stored for different pump coherent lengths, the height and pitch of the gratings were retrieved using a contact-mode atomic force microscope. Again, in all cases and in every region of the illuminated polymer area, the peak to peak height of the grating is 100

± 5 nm; its mean pitch is Λ= 888 ± 30 nm; the grating wave vector is parallel to the polarization of the signal beam.

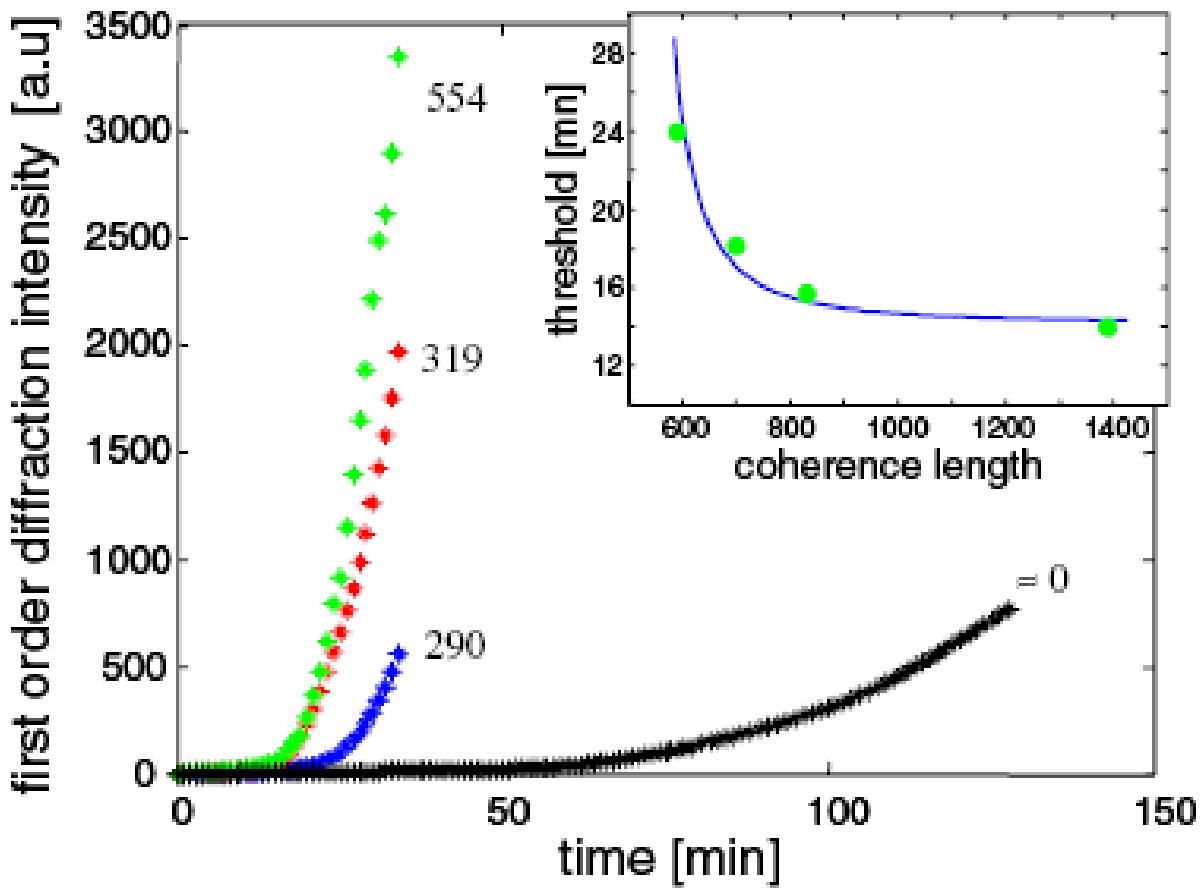

Figure III-6: First order self-diffraction intensity as a function of time for different values of the beam coherence σ_μ/λ given as an index to the curves. Coherence of the pump is modified by moving the diffuser between the two lenses. $\sigma_\mu/\lambda \to 0$ corresponds to complete incoherence. The inset shows the time threshold for first order self-diffraction as a function of the transverse coherence length. The curve is fitted with $A/(\sigma_\mu/\lambda)^B$.

The results in figure III-6 show that partial coherence of the pump beam accelerates the transfer of information from the signal to all of the illuminated area in which self-organization takes place. It is illustrated by plotting the time threshold for self-diffraction of the pump beam as a function of pump coherence length (inset in figure III-6). This one yields duration of the information exchange as a function of coherence. Time threshold is taken as the point

at which a straight-line fit to the linear portion of the diffraction intensity curve intercepts the *X* axis (figure III-6). The result is fitted with the test function $I_t = A/\left(\sigma_\mu/\lambda\right)^B$, in which *A* and *B* are constants; the limit $\sigma_\mu \to \infty$ represents a spatially coherent source and $\sigma_\mu \to 0$ an incoherent one.

Then, we measured the time evolution of the diffraction intensity when polarization of one of the beams is rotated. The hot-air gun is not used and pump polarization is maintained; the pump is then partially coherent. Initially we set the polarization of both coherent and incoherent beams as p polarized (maximum growth rate in figure III-2). In figure III-7, the signal beam polarization is rotated after 1 h of interaction (circles). Diffraction which follows the signal beam polarization [23] then changes its direction. When the pump polarization is rotated, also after 1 h of interaction while keeping the signal beam polarization unchanged (stars in figure III-5), diffraction continues to increase after about 10 minutes of time lag. This shows that leadership is acquired by the low-power coherent signal beam, whatever its direction of polarization. The pump permits collective SRG growth but does not participate in the decision on the grating characteristics. The time lag after pump polarization rotation corresponds to the time needed for leadership to take place. Practically, it corresponds to the time taken by the molecules moving under the partially coherent pump action outside of the signal region to receive the information on the grating characteristics from the signal.

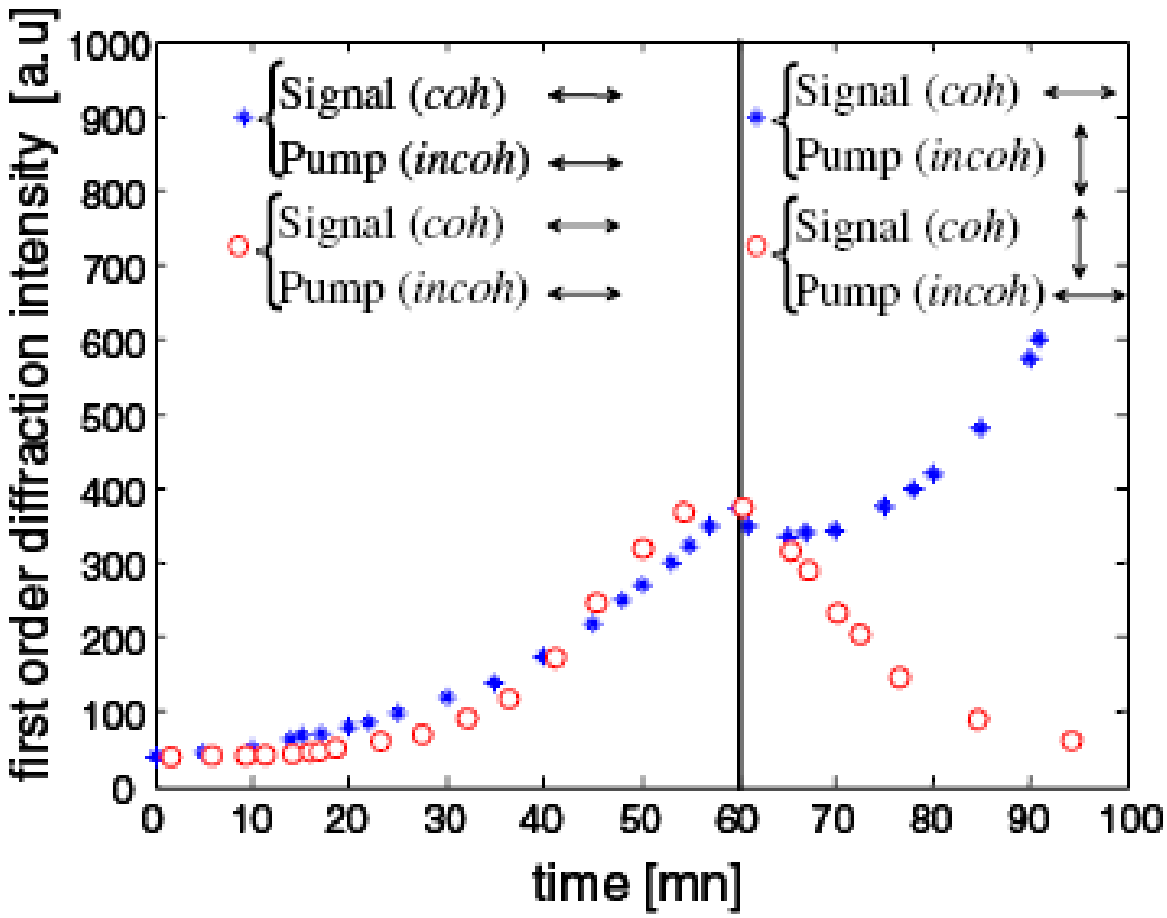

Figure III-7: First order self-diffraction intensity as a function of time for the case of a partially coherent pump without the hot-air gun. When the signal beam polarization is rotated, the SRG changes direction and diffraction which is emitted in a perpendicular direction is no more recorded by the photodiode (circles). When the pump beam polarization is rotated, the surface-induced grating continues to grow (stars).

This lag may be considered as the minimum learning time in our cognitive process. This experiment gives further information on the leadership process within azopolymers: a cooperative decision on the grating characteristics is driven by a few informed molecules differing in behaviour from the majority which undergoes almost random molecular migration under the incoherent light exposure.

In last experiment, we again illuminated our sample with two beams. The coherent signal beam is stopped after about 1 h of SRG self-organization, and only the incoherent beam is left to irradiate the polymer. Figure III-8 shows that the diffraction intensity continues to increase, proving that the SRG continues to self-organize. The SRG expands laterally, covering finally the entire illuminated surface. It expands step by step due to the short range interference of the diffracted waves with the incident beam.

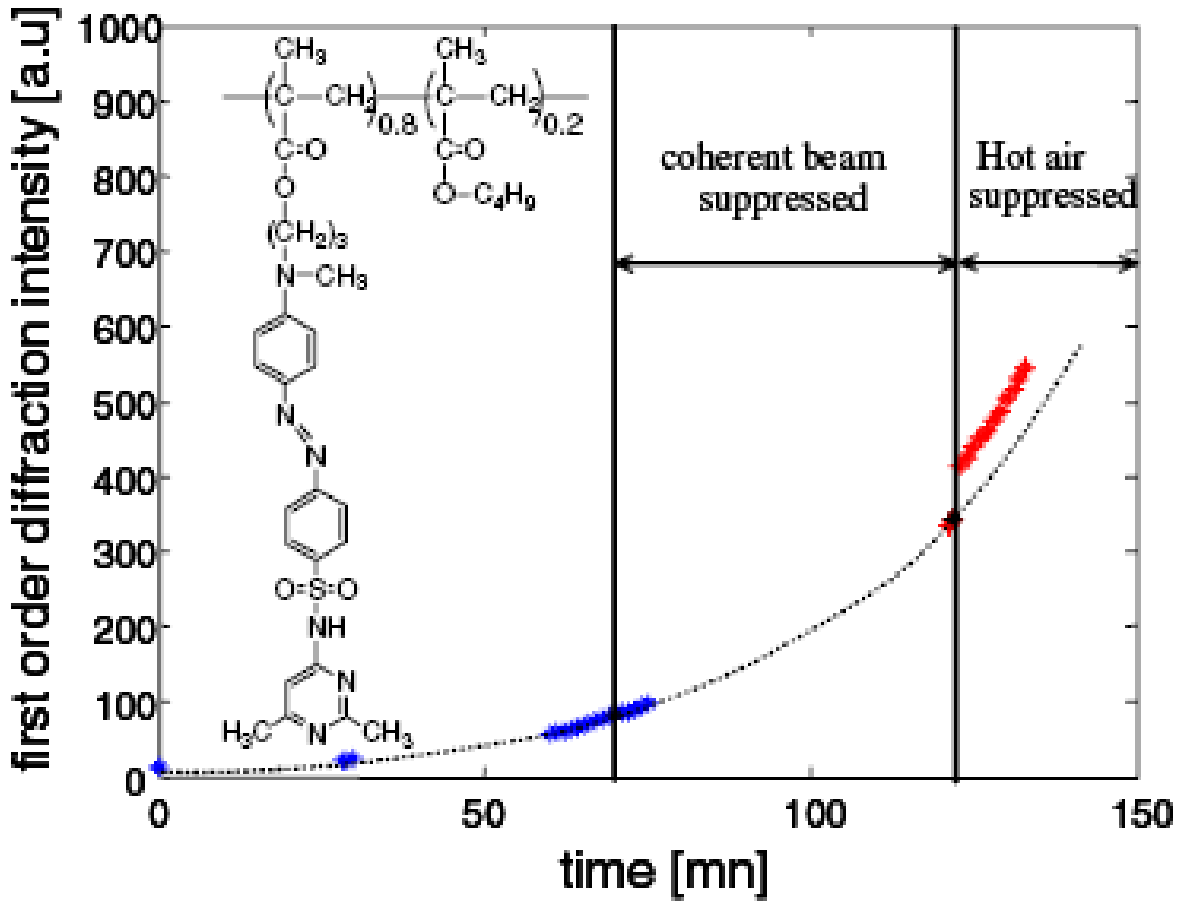

Figure III-8: Intensity of first order self-diffraction as a function of time under incoherent pumping. When the signal beam is turned off, the SRG continues to grow under the incoherent light excitation. When the hot air is suppressed, the pump beam becomes partially coherent and the SRG grows faster. The dashed line is a parabolic guide to visualize evolution with time. The inset shows the chemical formula of the polymer.

After two hours, the hot-air gun is stopped, increasing spatial coherence of the pump. We see that the diffracted intensity increases about 15% in a 2 minute time lag, without modification

of the evolution law. This shows that learning is accelerated by coherence (information exchange) without modification of the information content: namely, the SRG characteristics.

III-5- Mechanism of self-organized SRG formation

The origin of the driving force responsible for SRG formation is summarized in the following. As a result of photoinduced trans-cis-trans isomerization of azobenzene moieties, the molecules migrate along their main axis, almost parallel to the polarization direction [20]. They diffuse from illuminated to dark regions and get trapped in the dark regions. In particular, when a collimated laser beam impinges onto the sample, light is diffused by the polymer film according to Huygens principle, as a spherical wave in all directions around microroughnesses. This creates light intensity fluctuations: there is less light below the roughness peaks and more light in the near vicinity around the peaks. Molecule migration amplifies the roughness into surface profile fluctuations. Some diffracted light will interfere constructively in the diffraction direction [9]. This will order the surface profile fluctuations into a periodic pattern. The process will self-saturate when a balance between incident and diffracted light is reached, following coupled-wave theory [24]. The process that starts from random fluctuations will converge into a well-organized SRG initialized by the information contained in the coherent signal beam. We illuminated the molecules with totally incoherent light and added a coherent signal beam. The molecules that respond to the coherent signal beam create a diffraction pattern and then transmit the pattern step by step to all their neighbours. Information is exchanged locally by the relief: pits sending more light to the neighbours and dips sending less light, thus replicating the pattern. As a consequence, temporal coherence between pump and signal should not be necessary, but little spatial coherence of the incoherent beam is necessary within a few micrometer length scales.

In order to find a quantitative vision of the cooperativity of the process, we assume that molecules undergo molecular migration when they are brought into the cis state [20]. The coherent signal intensity represents about 0.08% of the incoherent pump power and 13% of the total surface. Let us consider a simplified trans-cis isomery model [25]. When the polymer is illuminated by a depolarized background light superimposed to a linearly polarized signal

beam with respective intensities I_b and I_S, the *cis* population in the steady state is given by (Appendix 2):

$$N_C = N_{to}\frac{q_T\sigma_T\left(I_S\cos^2\theta + I_b\right)}{q_T\sigma_T\left(I_S\cos^2\theta + I_b\right) + q_C\sigma_C\left(I_S + I_b\right) + K} \qquad (1)$$

where N_C is the concentration of molecules in the cis state under illumination and N_{to} the total number of molecules in the dark; θ is the average angle between the molecular orientation of the *trans* molecules and the signal beam polarization; q_T and q_C are the quantum yields for trans-to-cis and cis-to-trans isomery, respectively; σ_T and σ_C are the absorption cross sections of the trans and cis forms, respectively; K is the thermal relaxation rate from cis to *trans*. This equation assumes implicitly that molecules in the cis state do not have polarized absorption. We have $N_{to} = 7.18\times10^{20}\,cm^{-3}$. We use the following set of parameters: q_T = 0.1; q_C = 0.4 [26], and $\sigma_T = 0.75\times10^{-16}\,cm^{-2}$; $\sigma_C = 0.11\times10^{-16}\,cm^{-2}$; $K = 0.094\ s^{-1}$ [27]. We assume θ=0 for simplicity. The photon flux is $7.8\times10^{15}\,cm^{-2}s^{-1}$. We get $N_C = 2.25\times10^{20}\,cm^{-3}$ molecules for the steady-state cis concentration under illumination. Derivation of equation (1) with respect to I_s gives the ratio r of molecules which move under the signal influence. We call them the informed ones:

$$r = \left(I_S/N_C\right)\left(\partial N_C/\partial I\right) \approx 0.003$$

This result illustrates the cooperativity of the process: 0.3% of the molecules possessing decisive information drive gradually the other molecules into a collective decision. Although the detailed process is different, this high level of cooperativity can be confronted in other experiments borrowed from solid-state physics. For example, a photoinduced phase transition from the neutral to ionic (ferroelectric) form in an organic charge-transfer crystal was triggered by a tiny femtosecond laser pulse [28]. The phenomenon is triggered by less than 1 excited molecule for about 100 molecules in the crystal. In another example, cooperative chiral order was induced in a copolymer containing a minority of chiral units (so-called sergeants) among achiral units (so-called soldiers) [29]. The same optical activity as using a pure chiral homopolymer is induced with only 15% of chiral units, and substantial activity appears with as low as 0.5% of chiral units. In our experiments, we chose a surface ratio of 7.6 between pump and signal beams for demonstration purposes. Changing this ratio changes

the speed of growth but not the final cognitive effect. We expect a threshold when the signal beam size becomes commensurate with the speckle size.

III-6- Conclusion

In conclusion we have shown that a well-defined pattern can be printed in an azo-polymer film illuminated by a large power incoherent beam, starting from the information brought by a weak confined laser beam. Information about the SRG characteristics (pitch and orientation) is given by coherent signal beam, and molecular migration is powered by a strong incoherent or partially coherent pump beam. The rate of information exchange is directly related to the coherence of the pump beam. Cooperative organization outside of the coherent beam area between the informed molecules and the other photoactivated ones is the result of molecular migration, which optimizes light scattering away from the polymer film. Learning is achieved step by step with less than 1% of molecules initially informed. Our experiments should find applications in optoelectronics in which a low-power compact laser source can be used to code information which will be transferred to a polymer film assisted by a strong incoherent light source. More importantly our experiment shows that complex behaviour can be experimented using simple systems: weak coherent light can serve as a carrier to exchange information into a polymer film in such a way that molecules powered by incoherent light will build and propagate well defined complex structures. We propose our experiment as a paradigm for studies on cognitive ability: Various grating parameters can indeed be accessed by tuning the coherent beam characteristics [22]; this is the initial information from which the system finds optimal light scattering efficiency conditions like as the behaviour of colonies of insects or other living assemblies which exchange information locally using signs or pheromones and end up building complex structures or network in a smart way, perfectly adapted to the external constrains [30]. A practical interest of surface structuring using incoherent light could be that a powerful incoherent light is easier and cheaper to obtain than coherent light.

III-7- References:

1- M. Helgert, B. Fleck, L. Wenke, Incoherent modification of polarization gratings in photoanisotropic media, Opt. Comm., 2000, **177**, 95-104.

2- K. Pavani, I. Naydenova, S. Martin, V. Toal, Photoinduced surface relief studies in an acrylamide-based photopolymer, J. Opt. A: Pure Appl. Opt., 2007, **9**, 43–48.

3- K. Yang, S. Yang, X. Wang, J. Kumar, Enhancing the inscription rate of surface relief gratings with an incoherent assisting light beam, Appl. Phys. Lett., 2004, **84**, 4517-4519.

4- T. Ubukata, T. Higuchi, N. Zettsu, T. Seki, M. Hara, Spontaneous motion observed in highly sensitive surface relief formation system, Colloid Surf. A, 2005, **257-258**, 123-126.

5- C. Cojocariu and P. Rochon Tribute to Almeria Nathanson: Light-induced motions in azobenzene-containing polymer, Pure Appl. Chem., 2004, **76**, 1479-1497.

6- M.C. Cross, P.C. Hohenberg, Pattern formation outside of equilibrium', Review of modern physics, 1993, **65**, 851-1123.

7- Y. Tabe, T.Yamamoto, H. Yokoyama, Photo-induced travelling waves in condensed Langmuir monolayers, New J. Phys., 2003, **5**, 65.1-65.11.

8- C Jones and S. Day, Shedding light on alignment, Nature (London), 1991, **351**, 15.

9- A. E. Siegman, P. M. Fauchet, Stimulated Wood's anomalies on laser-illuminated surfaces, IEEE J. Quant. Electr., 1986, **22**, 1384-1403.

10- C. Hubert, C. Fiorini-Debuisschert, I. Maurin, J. M. Nunzi, P. Raimond, Spontaneous patterning of hexagonal structures in an azo-polymer using light-controlled mass transport, Adv. Mat., 2002, **14**, 729-732.

11- W. J. Firth, Pattern formation in passive nonlinear optical systems, in Self-Organization in optical systems and applications to information technology, M. A. Vorontsov, W. B. Miller, eds. (Springer, Berlin), 1995, 69-96.

12- A. Natansohn and P. Rochon, Photoinduced motions in Azobenzene-based amorphous polymers: Possible photonic devices, Adv. Mater., 1999, **11**, 1387-1391.

13- W. Lu, D. Salac, Patterning multilayers of molecules via self-organization, Phys. Rev. Lett., 2005, **94**, 146103.

14- D. Kip, M. Soljacic, M. Segev, E. Eugenieva, D. N. Christodoulides, Modulation Instability and Pattern Formation in Spatially Incoherent Light Beams, Science, 2000, **290**, 495-498.

15- T. Schwartz, T. Carmon, H. Buljan, M. Segev, Spontaneous Pattern Formation with Incoherent White Light, Phys. Rev. Lett., 2004, **93**, 223901.

16- A. S. Mikhailov, V. Calenbuhr, 'From Cells to Societies: Models of Complex Coherent Action', Springer, Berlin, (2002).

17- J.Y. Courtois and G. Grynberg, Spatial pattern formation for counterpropagating beams in a Kerr medium: a simple model, Opt. Commun., 1992, **87**, 186-192.

18- A. Consortini, Y. Y. Sun, C. Innocenti, Z. P. Li, Measuring inner scale of atmospheric turbulence by angle of arrival and scintillation, Opt. Comm., 2003, **216**, 19-23.

19- P. Lefin, C. Fiorini, J. –M. Nunzi, Anisotropy of the photo-induced translation diffusion of azobenzene dyes in polymer matrices , Pure and applied optics, 1998, **7**, 71-82.

20- S. Ahmadi Kandjani, R. Barille, S. Dabos-Seignon, J.-M. Nunzi, E. Ortyl, S. Kucharski, Incoherent light-induced self-organization of molecules, Opt. Lett., 2005, **30**, 3177-3179.

21- R. Barille, S. Dabos-Seignon, J.-M. Nunzi, S. Ahmadi-Kandjani, E. Ortyl, S. Kucharski, Nonlocal communication with photoinduced structures at the surface of a polymer film, Opt. express, 2005, **13**, 10697-10702.

22- Y. Piederrière, J. Cariou, Y. Guern, B. Le Jeune, G. Le Brun, and J. Lortrian, Scattering through fluids: speckle size measurement and Monte Carlo simulations close to and into the multiple scattering, Opt. Express, 2004, **12**, 176-188.

23- S. Ahmadi kandjani, R. Barille, S. Dabos-seignon, J. -M. Nunzi, E. Ortyl, S. Kucharski, Multistate polarization addressing using a single beam in an azo polymer film, Opt. Lett., 2005, **30**, 1986-1988.

24- H. Kogelnik, Coupled wave theory for thick hologram gratings, Bell Sys. Technol. J., 1969, **48**, 2909-2947.

25- X. S. Wang, W. L. She, W. K. Lee, Optical spatial solitons supported by photoisomerization nonlinearity in a polymer, 2004, Opt. Lett., 29, 277-279.

26- S. Sajti, A. Kerekes, M. Barabas, E. Lorincz, S. Hvilsted,and P. S. Ramanujam, Simulation of erasure of photoinduced anisotropy by circularly polarized light, Opt. Commun., 2001, **194**, 435-442.

27- E. Ortyl, R. Janik, S. Kucharski, Methylacrylate polymers with photochromic side chains containing heterocyclic sulfonamide substitued azobenzene, Eur. Poly. J., 2002, **38**, 1871–1879.

28- E. Collet, M. H. Leme´e-Cailleau, M. Buron-Le Cointe, H. Cailleau, M. Wulff, T. Luty, S. Koshihara, M. Meyer, L. Toupet, P. Rabiller, S. Techert, Laser-induced ferroelectric structural order in an organic charge-transfer crystal, Science,2003, **300**, 612-615.

29- J.V. Selinger and R. L. B. Selinger, Cooperative chiral order in copolymers of chiral and achiral units, Phys. Rev. E, 1997, **55**, 1728-1731.

30- G. Theraulaz, J. Gautrais, S. Camazine, J- L. Deneubourg, The formation of spatial patterns in social insects: from simple behaviours to complex structures, Phil. Trans. R. Soc. Lond. A, 2003, **361**, 1263-1282.

Chapter IV

Applications of Self-organized SRGs

IV-1- Introduction

Surface relief structures have many potential applications. In the first chapter we have reviewed some important applications of surface relief gratings. All those applications were based on SRGs inscribed by the interference of two coherent beams. This chapter is dedicated to describe some of the possible applications of self-organized SRGs on the azo-polymer films. First we will present our experimental results of optical processing and logic gates operation with self-organized SRG formation. In the last chapter we explained that how cooperative organization between photoactive molecules in a system consist of one low power coherent and another high power incoherent beam, results a self-organized SRG under incoherent beam illumination. In a system of two spatially separated coherent beams surrounded with a large high power incoherent beam, nonlocal communication between molecules under coherent beams can be use as a neuronal network. AND and OR logic gates will implement in this system. The control of biological cell growth direction is very important from biophysical and engineering point of view. The second application that we will present here is the control of cell growth direction by self organized SRG.
Finally we will discuses the application of self-organized SRG in waveguide couplers, optical diffusers and 2D chirality.

IV-2- Optical processing

IV-2-1-Introduction

Electronic devices play an increasing role in our daily lives. Furthermore, we need to follow higher technologies regularly. Therefore development of new systems to copy the operation of electronic logic gates and circuits is very important. Besides their integration in the heart of digital computers, electronic logic circuits control the operation of a variety of devices around us, from calculators and store automation to video games and music equipment.

Cutrona, *et al.* and VanderLugt., introduced the coherent optical processors as first optical signal processors [1, 2]. The main advantage of these coherent processors is the use of optics features. Consequently, intensive research efforts were started and they continued for about two decades. In spite of the characteristics of optics, technical difficulties, like lack of proper devices and their inflexibility, oblige researchers to turn toward digital computing. They tried to replace electrons by photons, an approach which was doomed due to the fundamental differences between the behaviour of light and electrons.

The photons can solve the wave equation with any boundary conditions. This wave equation is solved almost instantaneously, in parallel, and with no expenditure of energy. In optical systems, only detection of final results dissipates energy. In contrast, digital computers dissipate energy for each intermediary step of a calculation even if those intermediary calculation results are not interesting. As pointed out by Caulfield and Shamir in 1990[3], this attribute alone is an adequate incentive to pursue optical signal processing. Optical Fredkin gates and gate-arrays [4–7] were also introduced within the effort to exploit the non-dissipative nature of processing with light.

Binary logic operations need the systems that are able to produce only two output states: zero and one. In physical systems the values of both zero and one states should be nonzero but distinguishable. The current electronic binary logic systems use a low voltage as zero, and a higher voltage as one.

Two perpendicular polarization state of light (s-p or right-left circular) can be used to implement binary logic gates. The two states of polarization were used to represent logic one and logic zero. Recently, Y. A. Zaghloul and A. R. M. Zaghloul proposed an all optical binary logic system that is able to implement any logic gate [8]. They divided a laser beam into two paths with different polarizations. Each path allows a certain polarization to pass and block

other polarization. Different processes applied independently to logic 1 and to logic zero beams with a single control module for each. Because of special design of system, at the output point just one of the beams is active. In this system the intensity of the beam carries no information. The produced all-optical-processing polarization-based binary-logic system implemented any logic gate or processor.

Again technological difficulties and relative inflexibility are the main disadvantages of optical signal processing and computing in comparison with their electronic counterparts.

We show that it is possible to implement an optical network and to transfer information from one point to another point without overlapping of the light beams. Logical operations between the beams can also be performed. The optical-network model of computation consists in many elementary processing nodes (neurons), communicating each other with interconnection weights [9, 10]. Associated with each node is an activation level which is transformed into a weighted sum of the activity levels of all the other nodes [11]. The node in our experiment is a surface induced relief grating (SRG) whose input is both the pitch and the orientation coded when the network is operated in the static mode. The grating which results from a photodynamic polymer transport process is recorded in photoactive polymer thin films with one single laser beam and shows regularly spaced surface relief structures [12–14]. The grating spacing and orientation can be controlled by the incidence angle and polarization of the incident laser beam, respectively, as discussed in Ref. [15]. All the networking nodes can be activated simultaneously or sequentially by a laser beam with sufficient exposure time per node. The neuron output is then the acquisition of a polarization state and grating pitch, and subsequent light diffraction. The network in our system is a set of multiple SRG. We implement and test such system using the nonlocal self organization aspect of SRG under incoherent light power. Indeed, we reported previously in chapter III that when we send a low intensity coherent seed beam simultaneously with a large intensity incoherent pump beam on the photopolymer surface, a SRG is induced and propagates all over the incoherent beam area, outside of the coherent beam: it bears all the features of the SRG induced by a large intensity coherent beam. We believe that our simple experimental optical processor could be useful to implement and test new ideas relevant to neuronal photonics.

IV-2-2- Experimental details

The λ = 476.5 nm laser line of a continuous argon ion laser is used to excite the MB2I azo-polymer close to its 438 nm-absorption maximum. Polarization direction of the laser beam 2 is varied using a half-wave plate. Our experimental set-up is sketched in Fig. IV-1.

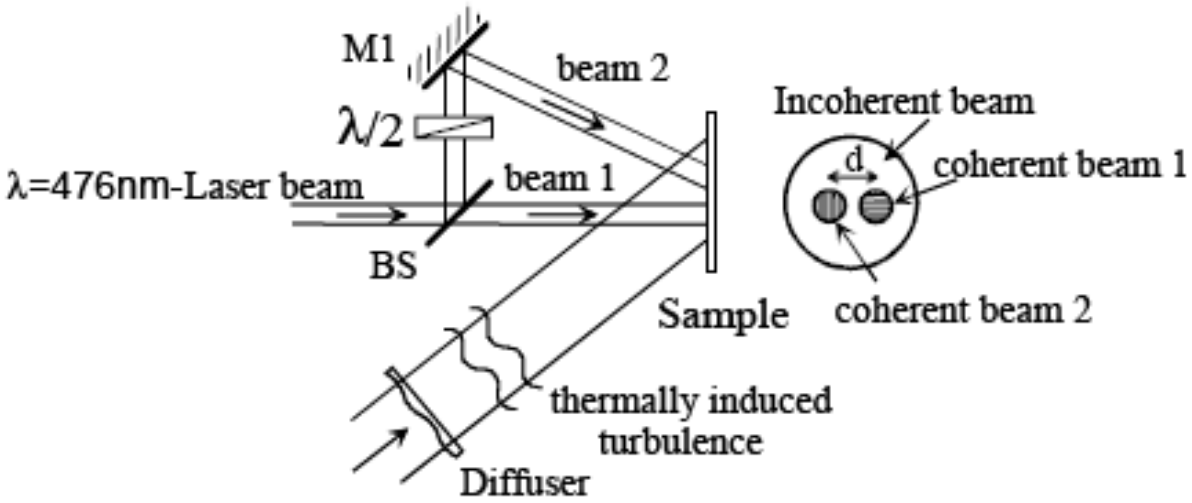

Figure IV-1: Experimental set-up. Beam 1 is at normal incidence on the sample. Beam 2 is at a 32°-incidence angle. The beam 1 is vertical (s) polarized and polarization of beam 2 rotated by 45° with respect to input beam polarization(s). BS: beam splitter; M1: mirror; λ/2: half wave plate.

Laser power is 500 mW. The beam width is increased to 5.8 mm by a two lenses afocal system. The beam is then divided in the two equal arms of a Mach-Zehnder. In the first arm, the beam is reduced to a width w_0 = 750 μm by another afocal and is divided into two equal power spots. Power of each beam is attenuated down to 0.07 mW. These two narrow beams are the signal beams. The second one is the pump beam. The pump beam is made spatially incoherent by focusing the laser beam through a diffuser. It can also be made temporally incoherent with the signal beams using an additional delay line with retardation path larger than the 5.7 cm-coherence length of our laser. An additional hot-air gun is used as a turbulent layer generator and is inserted along the beam path in order to insure total incoherence and depolarization. The diffuser and the turbulence generator introduce a random phase which

varies much faster than the time constant for grating formation in the sample. The signal and pump beams are spatially overlapped at the exit of the Mach-Zehnder, with the thinner signal beams fixed in the pump beam central region. They illuminate the polymer sample. Pump beam power is 87 mW.

IV-2-3- Results and discussion

We first checked the material response for the coherent signal beams alone, without incoherent pump beam. In this test, the signal beams are not attenuated, their power is 0.6 mW. The two beams are sent on the sample (Fig. IV-1) and the SRG is recorded after one hour illumination. The distance between the edges of the two w_0 = 750 μm spots is fixed to d = 920 μm.

One of the beams (beam 2) has 32°-incidence angle and the other (beam 1) is normal to the sample surface. The beam 1 is vertical (s) polarized and polarization of beam 2 rotated by 45° with respect to input beam polarization(s). Both the height and pitch of the grating were retrieved after illumination with a contact-mode AFM (see section II-7). For beam 1, the grating pitch is Λ_1 = 880 nm and for beam 2, Λ_2 =590 nm, both with a grating amplitude of 150 nm ± 20 nm. These pitches are in agreement with the values calculated by first order diffraction at an angle θ. In both cases the pitch is uniform in one direction and the two dimensional Fourier transforms in Fig. IV-2(A) show only one single spatial frequency component ν_x or ν_y. This proves that the two beams do not interact. They do not interact as long as they do not overlap spatially.

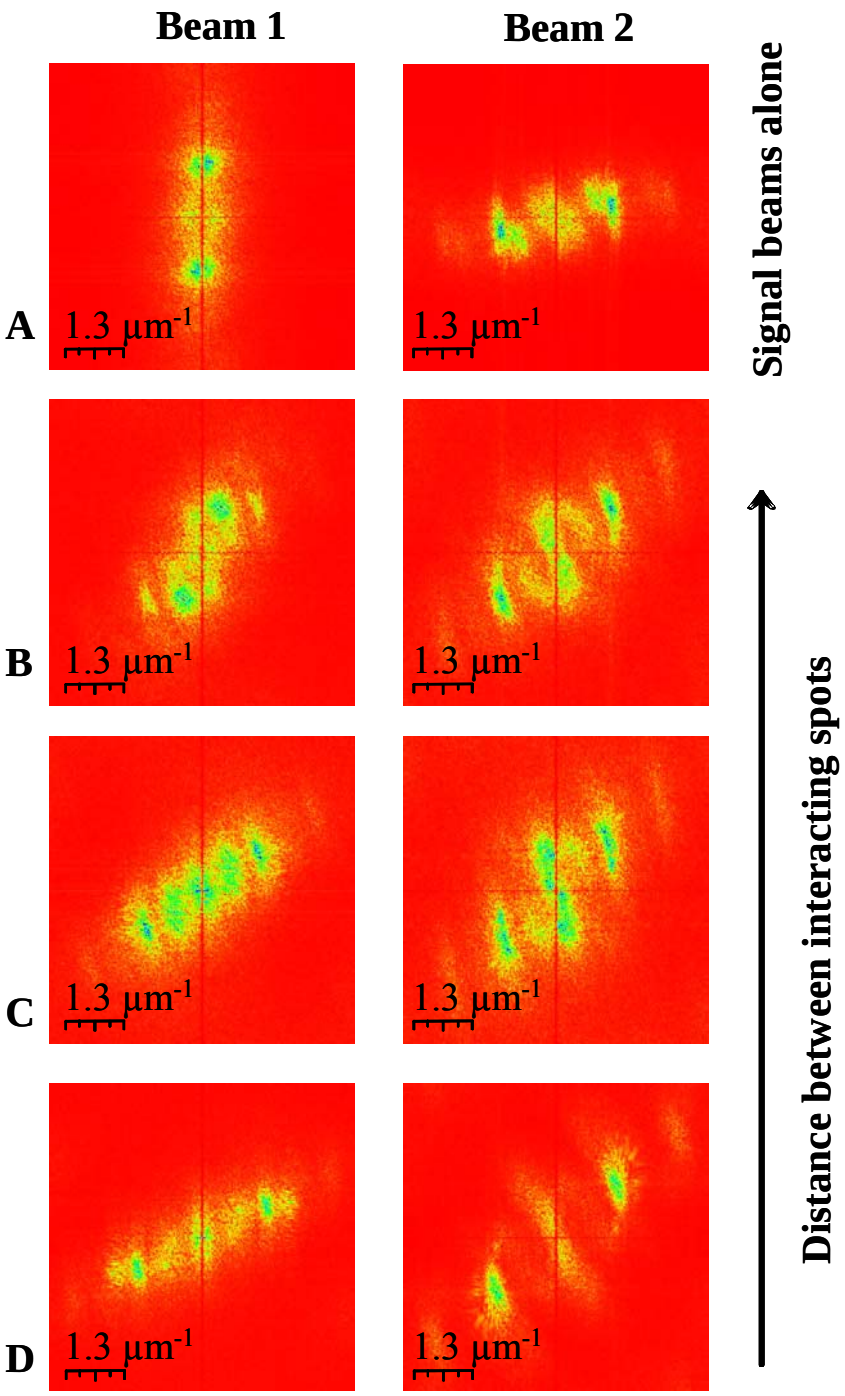

Figure IV-2: Two dimensional Fourier transform of the two SRG spots (A) under the two signal beams without the incoherent pump. The same with the incoherent pump overlapping with the signal beams separated by a distance d = 920 µm (B), d = 650 µm (C) and d = 450 µm (D). The SRGs under beams 1 and 2 have a pitch Λ_1 = 880 nm and Λ_2 = 590 nm, respectively. The Fourier transform reflects the far field diffraction pattern of the SRG.

In a second step the 87 mW incoherent pump beam overlaps with the two 0.07 mW coherent signal beams. We check SRG construction for three different horizontal separations between the edges of the spots: 450, 650, and 920 μm, corresponding to a ratio w_0/d of 1.6, 1.15, and 0.8 respectively. Figure IV-2 shows the two dimensional Fourier transforms of the SRG below beams 1 and 2. When the two spots get closer, we see that the spatial frequency spectrum is enlarged. For the SRG below beam 1, the rotation of its frequency spectrum corresponds to the mutual interaction with beam 2. We see the same rotation in a reverse direction for beam 2, the two grating orientations becoming almost the same. When the two spots become closer (Fig. IV-2(D)), the two spatial frequency spectra become very similar. This shows that the two beams interact, the information on polarization is exchanged first at large distance and the information about the pitch is mixed, with appearance of new frequencies at shorter distance. Surface profile and power spectral densities (PSD) of these images are represented in Fig. IV-3 for two cross-sections in the vertical (blue lines) and horizontal (red lines) directions and for ratios w_0/d of 1.7 and 0.8. For each beam, the spatial frequency corresponding to the original pitch is conserved, with additional frequencies appearing when the separation distance is reduced. For the spot under beam 1 the horizontal frequency $\nu_x = 1/\Lambda_2$ appears in the power spectrum for the shortest separation. In the same way, for the spot under beam 2 the vertical frequency $\nu_y = 1/\Lambda_1$ appears in the power spectrum for the shortest separation. The numerical criterion for appearance of a new spatial frequency is chosen arbitrarily in our experiment as being a peak emerging above 50% in the normalized PSD spectrum. That is the way the mutual influence between the two beams takes place.

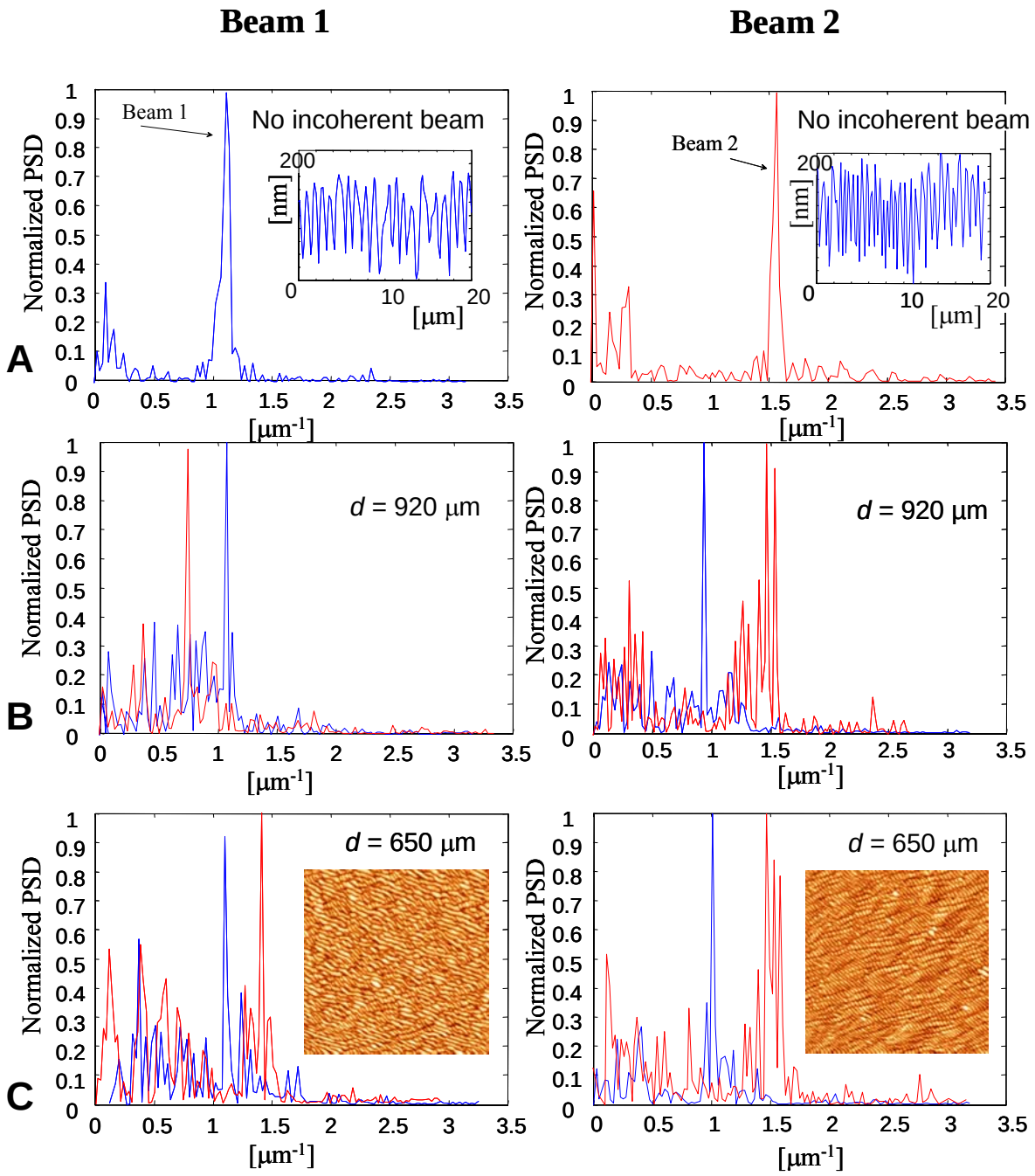

Figure IV-3: Power spectral density for different distances between the spots. PSD is measured for the vertical (blue lines) and horizontal (red lines) cross-sections of the SRG patterns under beam 1 (left) and 2 (right). Without coupling by the incoherent beam (A), coupled with 920 μm distance (B) and coupled with 650 μm distance (C). Inset in (A) shows the surface profile. Inset in (C) shows the AFM scan of a 20×20 μm^2 region below the signal beams.

A last experiment was performed with the half-wave plate in Figure IV-1 placed on the path of beam 2 and its polarization fixed at 45°. Beam 1 polarization is vertical as given by the laser. The lateral distance between the spots is reduced to d = 180 µm. A photodiode is set to measure the first order which would be diffracted from the self-induced SRG by a beam 2 with horizontal polarization. We must recall that the direction of diffraction follows the polarization direction [16], as shown in figure. IV-2(A). This signal shown in figure IV-4 is thus the transfer of polarization from beam 2 to beam 1, associated with the new horizontal spatial frequency created beam 2 in figure IV-3(C). This new spatial frequency induces the horizontal diffraction which is detected by the photodiode. Obviously, polarization of the diffracted beam is the one of beam 1: vertical. The signal in figure IV-4 saturates after 100 minutes of illumination, when the information transfer is completed. This experiment proves that information transfer between two non-overlapping beams is effectively achieved: it is mediated by the incoherent beam.

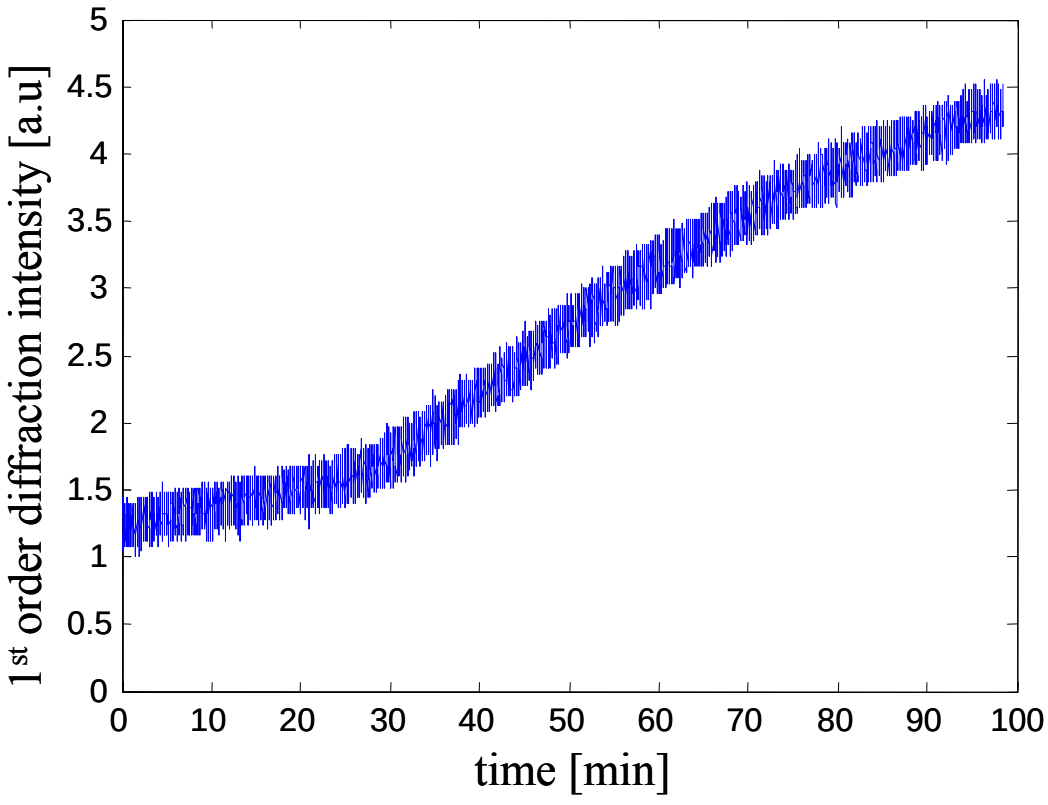

Figure IV-4: First order diffraction intensity as a function of time for the coherent beam 1. Beam 2 polarization is fixed at 45° and beam 1 polarization is vertical. The photodiode is set to measure the first order of diffraction from beam 1 in the horizontal direction. The signal detected is a signature of the polarization transfer from beam 2 to beam 1.

Different nodes can be lighted up on the surface below the incoherent beam. Associated with each SRG node i is its spatial Fourier spectrum described by a function $y_i^{(n)} = f(x_i^{(n)})$, where x_i is the activation level created by the weighted sum of the activity parameters of the other nodes: $x_i^{(n)} = \sum_i \omega_{ij} y_j^{(n-1)}$. As shown in figure 3, the weights ω_{ij} are function of the distance w_0/d between the nodes. The number of iterations n is 1 in our experiment. We implemented two basic logic operations in our simple network using this neuronal principle. The results of the two Boolean operations OR and AND are given in tables IV-1 and IV-2, respectively. In table IV-1, we consider the pitch of the SRG under beam 1 as a test parameter y_1. We assign the value 1 to the pitch of the SRG under the beam 1 which arrives alone at normal incidence. Any other SRG pitch will be assigned the value 0. The pitch $y_i^{(0)}$ of the SRG is addressed by the beam incidence. The results in table 1 show that we implement an OR gate in this way.

Table IV-1: Implementation of an OR logic gate with pitch Λ_i as test parameter.

$y_1^{(0)} = \Lambda_1$	$y_2^{(0)} = \Lambda_2$	$y_1^{(1)}$
1	1	1
0	0	0
1	0	1
0	1	1

In table IV-2, we consider the orientation of the SRG under beam 1 as a test parameter y_1. We assign the value 1 to a vertical orientation of the SRG under the beam 1 which arrives alone with vertical polarization. Any other orientation will be assigned the value 0. The orientation $y_i^{(0)}$ of the SRG is addressed by the beam polarization. The results in table IV-2 show that we implement an AND gate in this way. We see that our simple network can perform simple logic operations. More complicated operations can be achieved if more signal beams interact within the incoherent beam at the polymer surface.

Table IV-2: Implementation of an AND logic gate with polarization P_i as test parameter.

$y_1^{(0)} = P_1$	$y_2^{(0)} = P_2$	$y_1^{(1)}$
1	1	1
0	0	0
1	0	0
0	1	0

IV-2-4- Conclusion

We have implemented a very simple neurocomputer where the individual neuron is the self-induced SRG below a coherent signal beam. In this experiment, the network is configured in the static mode and each neuron is configured by the photoinduced polymer transport process. The neurons interact through the self-induced SRG which dissipate the strong incoherent pump beam. The learning process of each neuron consists in the acquisition of the pitch and polarization parameters. The result of the activation is processed from the weighted sum of the activity levels of the individual neurons. This basic implementation can be extended to a more complex network structure. For instance, a large number of nodes can be implemented in a single polymer film under incoherent illumination. The neurons can also interact between several cascaded planes as each individual neuron bears an underlying SRG which diffracts efficiently in privileged directions [7]. The process is partly reversible: work is now in progress to exploit the dynamic reconfiguration of the network (more than $n = 1$ iteration) which is permitted as long as saturated growth of the SRG is not achieved [7]. Work is also in progress to improve the time response of the system using faster responsive polymers. We see that our simple experiment on optical processing is relevant to the implementation and evaluation of new concepts related to neuronal photonics.

IV-3- Neuron growth engineering

IV-3-1- Introduction

Biological engineering for the development of cellular patterning has attracted much attention due to huge potentialities for medicine or electronic applications. Cells respond to the topography of their surroundings. Then an understanding of conditions that influence cell positioning and alignment are important not only in development of biology but also in tissue engineering.

Most of the studies are focused on the role of the molecular basis for the contact guidance. However, the response of cells to topographical features of a substratum surface is far from misunderstanding [17, 18]. The use of photolithography and non-lithographic methods has allowed more detailed and systematic investigation on the effects of various grooves and ridge dimensions but these technologies don't allow facilities in the study. The modification of topographical structures for additional purpose, for example forming a new groove to change the cell orientation is impossible.

On the other hand the combination of microelectronics and circuits with nerve cells was pure science fiction 20 years ago but now a hybrid circuit of a semiconductor chip and synaptically connected neurons was recently implemented [19]. This new technology needs networks of nerve cells.

In Section I-10-7 we have described cell growth mechanism on the surface of a hologhraphically made SRG. The SRG inscribed on the surface of an azo-polymer by interference of two coherent laser beams. In this section we propose single beam self-organized SRGs for cell growth. As we discussed in previous chapters, self-organized SRG fabricated by one single beam illumination and its orientation controlled by polarization of writing beam. This one beam experiment allows submicron-scale topological control scheme during cell growing. The pitch and depth of structure is controlled by incidence angle. Different polarization states for different incidence angles arise different (sometimes complex) structures. Further implementations of defined cell network can be reconfigured easily and extended on the polymer surface. These characteristics make self-organized SRGs as a good candidate for cell culturing and cell network engineering.

IV-3-2- Experimental details

IV-3-2-a- Self-organized SRG

The experimental details of self-organized SRG formation have been explained in the chapter IV. Figure IV-5 shows a typical AFM image and surface profile of self-organized SRG formed on the surface of an azo-polymer film (MB2I).

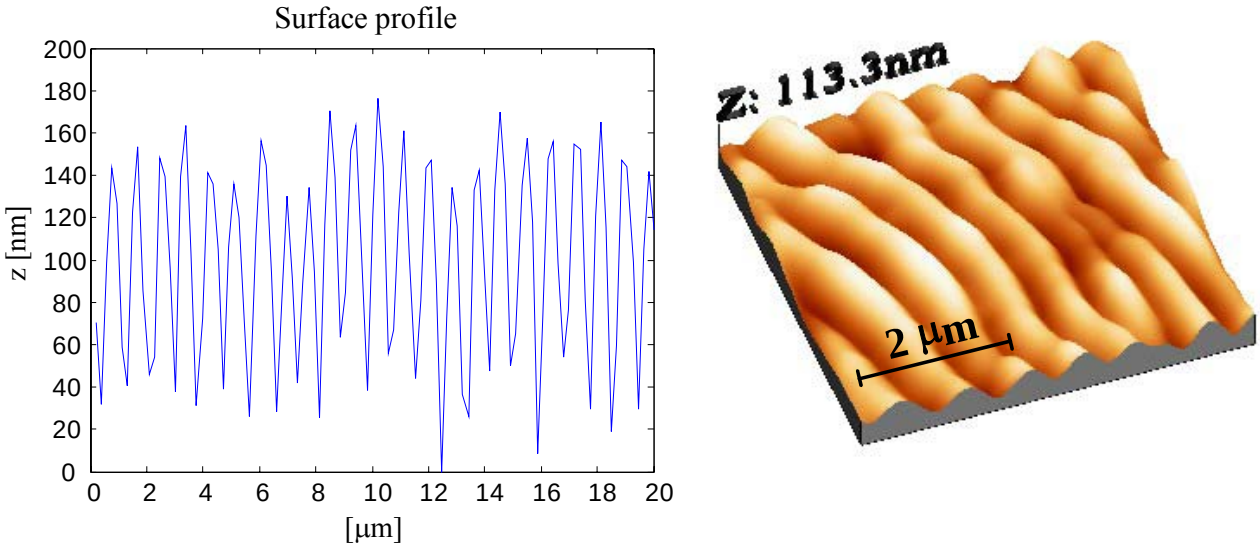

Figure IV-5: AFM image and surface profile of self-organized SRG on the surface of an azo-polymer thin film. The typical grating depth is about 100 nm and the pitch is Λ = 800 nm ± 30 nm.

IV-3-2-b- Cell culture

Neuron cells were NIH3T3 and PC12 grown in DMEM media (Eurobio, France), containing 10 % fetal calf serum (Biomedia, France), 1 % L-Glutamin (Invitrogen, France), 1 % antibiotic (Invitrogen, France). At 80 % confluence, cells were transfected with the pDsRed2-mito or pGFP-Tub plasmids (Clonetech, France) using Fugene reagent (Roche, France). The following day, cells were trypsinized, collected in two 100 mm dishes, and the selection with G418 (350 μg/ml; Invitrogen, France) started 24 hours latter. G-418 is used to select and

maintain stable cell lines that have been transfected. When transfected cells (cells with an antibiotic-resistance gene) and untransfected cells are exposed to an antibiotic, such as G-418, only the transfected cells survive and grow. Clones were expanded and stored in liquid nitrogen. They were then analyzed by fluorescent microscopy [20].
At 80 % confluence, cells were trypsinized and harvested on coverslips (10 000 cells per ml) that were previously coated with the polymer. PC12 cells were differentiated with Nerve Growth Factor (NGF 7S, 150ng/ml, Promega, France) for 48 hours. Coverslips were collected and cells were washed in PBST (PBS, 0.2 % Triton-X100), and fixed in PFA (4 %). Azo-polymer grating samples were mounted using glycerol in PBS (90 %) and assessed for the presence of fluorescence using a Leica DMR microscope (with a IM500 software).

IV-3-3- Results and discussion

The NIH3T3 and PC12 were tested for growing on the SRG. The cells were first let during one week on the polymer surface in Petri dishes and immersed in liquid PBS.
The neuritis of neurons grow parallel to the direction of the grooves and in the perpendicular direction of the pitch with a relatively higher rate in the parallel orientation while outside the SRG the neurites expand in random directions. The contact guidance can be obtained with grooves as shallow as one hundred of nanometers where the effect is less available. The circularity which relates cell's shape has been evaluated to be close to 0.2 giving a linear shape. Moreover, cells can survive where there is no spatially chemistry comprising protein absorbing and non-absorbing areas that allow control over the absorption of cell-adhesive glycoproteins. Figure IV-6 shows cultured cells on the patterned surface. We see that on the SRG, the cell proliferation is still toward the groove direction.

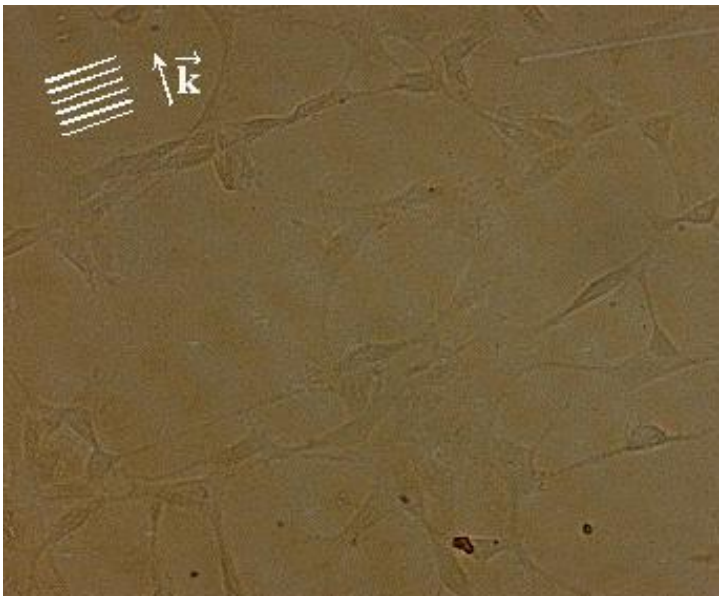

Figure IV-6: Controlled cell orientation toward the groove direction after one week of inoculation in PBS liquid. Most of the cells are in a preferred direction normal to the grating vector and elongated along the groove lines.

A detail of the preference for the cell attachment on the SRG is presented on the figure IV-7. These results show that the cells can be attached on gratings with a depth as shallow as 100 nm where the topological effects are the less available.

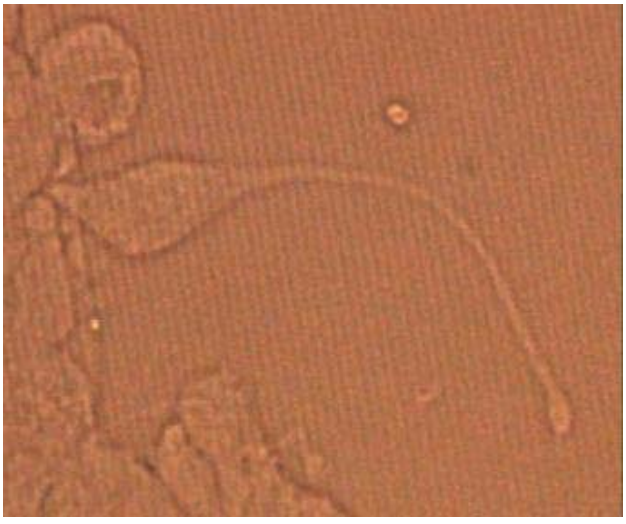

Figure IV-7: Detail for the direction of growing. The cell begins to grow randomly and then is attracted by the groove direction.

This confirms precedent studies of contact guidance on grooved quartz [21] where the maximum of orientation response for rat hippocampal neuritis is done with groove depth of

130 nm. Deeper grooves don't lead to better results. Moreover for Xenopus spinal neuritis, the direction of neurite growth reaches 100% at the threshold of 130 nm with the same results with larger values of groove deep. Then it seems that 100 nm is the greatest perpendicular threshold response.

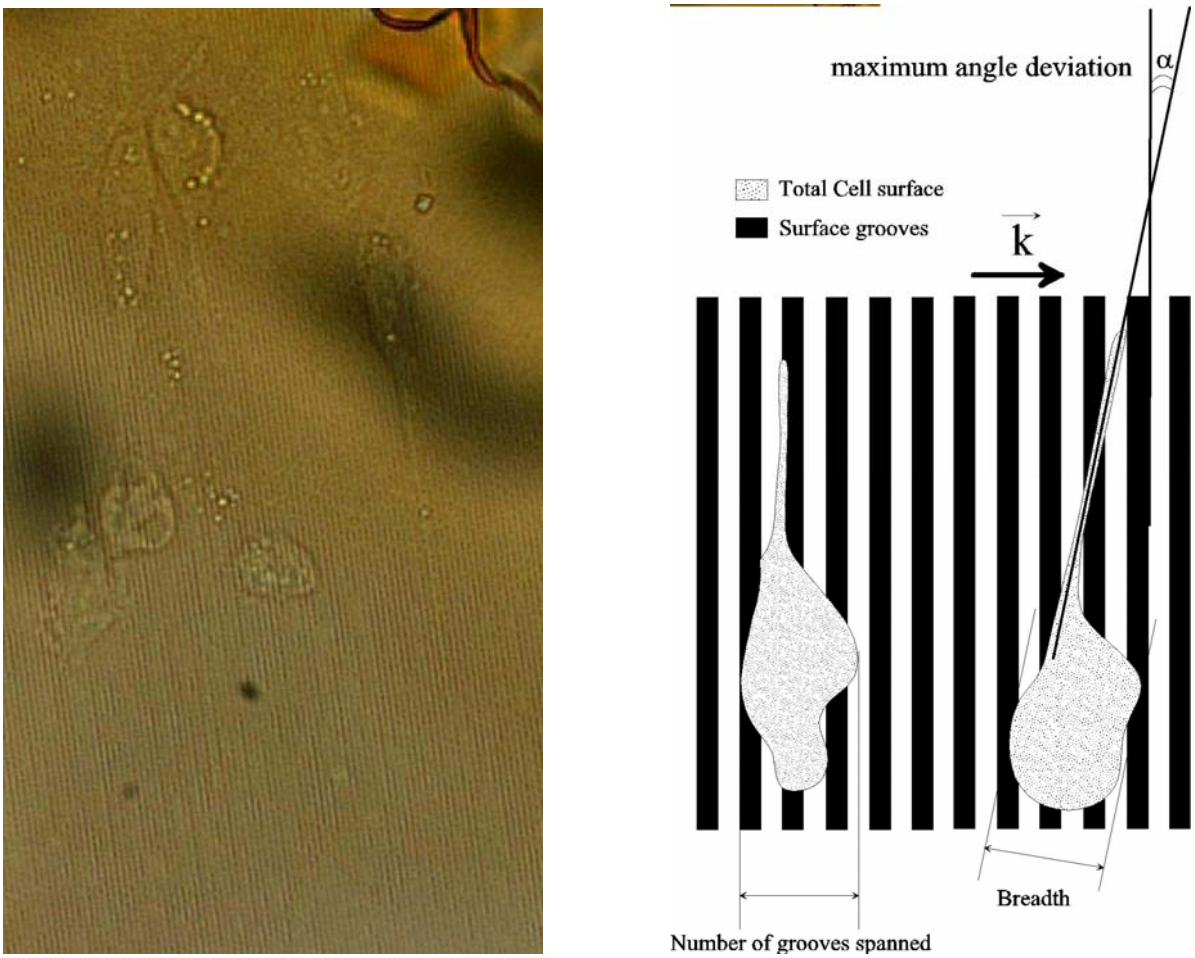

Figure IV-8: Left: optical microscope image of cells on the self-organized SRG. Right: schematic representation of the parameters of statistical calculation of cellular orientation. α represents the angle of cellular orientation relative to the SRG.

We have controlled the percentages of parallel or perpendicular neurites in an oriented population of neurons. The procedure is done by counting the number of cells in the direction of grooves as in the figure IV-8. We use an image processing in order to calculate the cell's edge detection, and then the number of object inside each image is calculated.

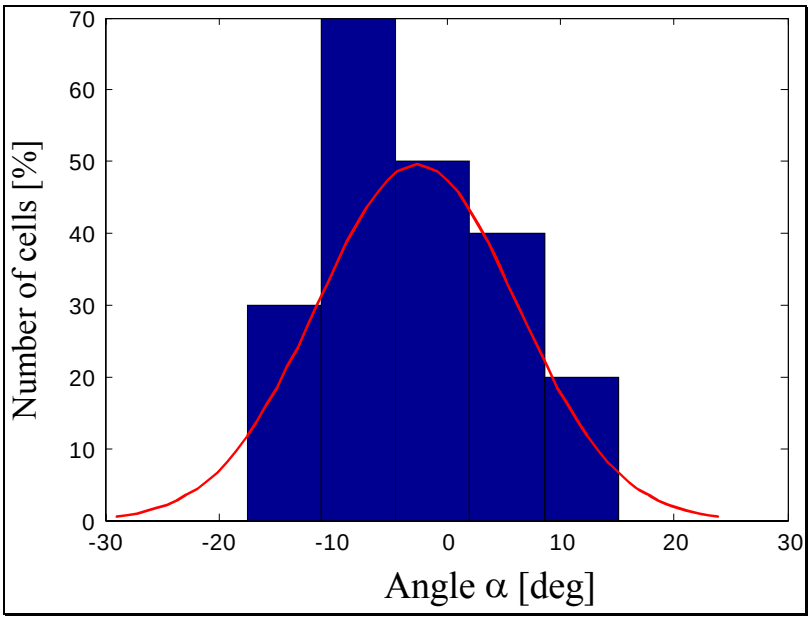

Figure IV-9: Statistics of the cellular orientation relative to the surface submicron grooves of the SRG

The parameter used in the calculation is the angle between the cellular neuritis and the groove direction (figure IV-8). The results are given in the figure IV-9. The maximum percentages of cells have an angle of orientation in the groove direction. This statistics for angles is the same for both cells (NIH3T3 and PC12). We didn't calculate the statistics of cell direction with respect to the grooves as a function of time during the cell growth.

IV-3-4- Conclusion

The self-organized pattern leading to SRG formation is an efficient method for controlling the cell growth direction. The cells attached and oriented on the self organized SRG. The surface structure is created by mass transport of azo-polymers under single laser beam illumination. The shape and orientation of this surface structure can be control by beam polarization characters (direction and state) and incidence angle. These advantages give us opportunity to control cell growth architecture in one and two dimensions to create cell network. In spite of the shallowness in SRG depth relative to other structures realized on quartz typically about 100 nm the neuronal cells are highly oriented along the groove direction.
The results are particularly useful and promising in plastic neuroelectronics engineering [22].

IV-4- Other applications

IV-4-1- Waveguide coupler

In section I-10-1 we have explained how SRGs is used to introduce light into a waveguide. Here we show that self organized SRGs can be used as a coupler to coupling light into and out of waveguides. We inscribed several SRG on the same azo-polymer (MB2I) film with p polarized laser beam. For inscribing each grating, the film was under illumination for 1 hour. It has been shown that for self-organized hexagonal structures, at normal incidence, the light can couple into the polymer film. But in the case of a self-organized SRG, we couldn't observe any coupling of light inside polymer film or glass substrate for normal incidence. By rotating polymer film in front of a He-Ne laser at 633 nm, at certain angle of incidence, we observed the coupling of light inside polymer film (Figure IV-10).

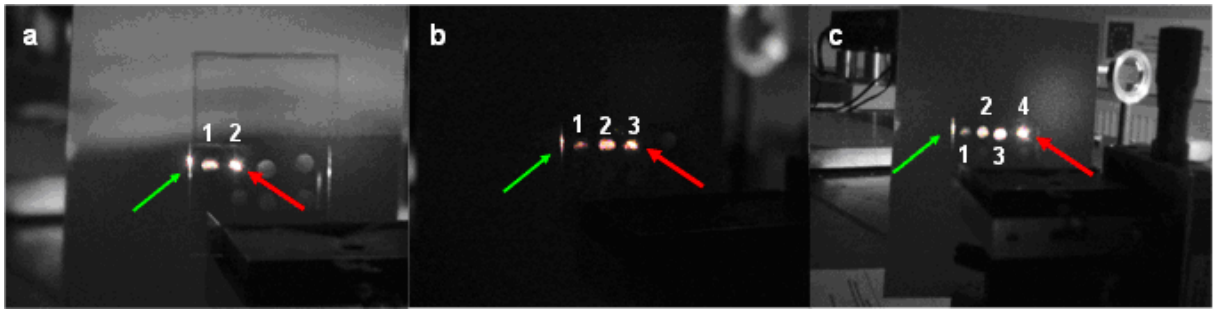

Figure IV-10: Coupling of a He-Ne laser at 633 nm inside polymer film. The red and green arrows show input and output, from edge of film, beams respectively. The self-organized SRGs are numbered from left edge. a) The light couples into the polymer film from SRG-2 and couples out from SRG-1 and the edge of the film. b) The light couples into polymer film from SRG-3 and couples out from SRG-2, SRG-1 and the edge of the film. c) The light couples into polymer film from SRG-4 and couples out from SRG-3, SRG-2, SRG1 and the edge of the film.

In figure IV-1(a) laser beam has been sent into polymer film through grating number 2. A portion of coupled beam couples out from SRG-1 and another part from the edge of film. Figures IV-1(b) and 1(c) show the same effects for the coupling of light through SRG-3 and SRG-4 respectively. These observations are explained by the formula of gratings:

$$K_d\, n_2 \sin\theta_d = K_{in}\, n_1 \sin\theta_{in} \pm m\frac{2\pi}{\Lambda}\ , \qquad K_d = \frac{2\pi}{\lambda_d}, K_{in} = \frac{2\pi}{\lambda_{in}}$$

Where n_1, θ_{in} and λ_{in} are refractive index of incident medium, angle of incidence and wavelength of input beam respectively. n_2, θ_d and λ_d are refractive index of medium that light diffracted into, diffraction angle and diffracted beam wavelength respectively (figure 2). Λ is the pitch of grating and m is the diffraction order.

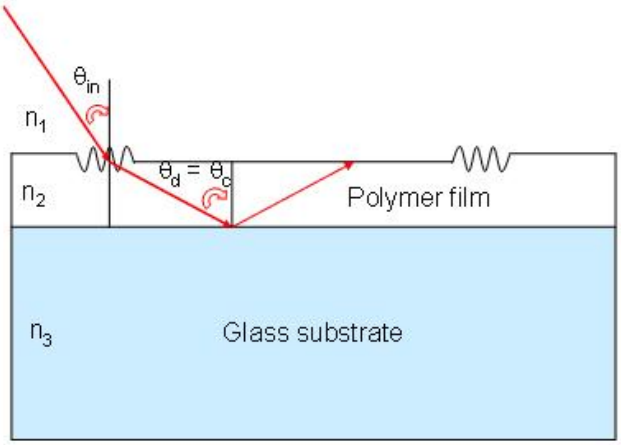

Figure IV-11: Schematic representation of light coupling into polymer film. θ_c is the angle at which total reflection takes place.

This relation shows that for a grating with given pitch Λ, light with certain wavelength can diffract at angle θ_c to guide in polymer film. In like manner, the light can couple out from another grating.

IV-4-2- Light diffuser

As soon as liquid-crystal displays (LCDs) have been presented as a non emissive display, its market has been increasing extremely. One of the important elements of LCDs is optical diffuser. Optical diffusers are required to achieve large viewing and high brightness. Usually display manufactures are using, ground glass, opal glass, white plastic, polycarbonate and polyethylene diffuser. Several methods have been developed for manufacturing diffusers [23-26]. Because of suitable scattering pattern, holographically made diffusers are useful for LCDs applications [27]. In this technique diffusion angle is controllable by choosing convenient parameters for holographic material and experimental setup. More or less all

holographic materials are suitable for diffuser fabrication. To fabricate holographic diffusers, there is no need for pre or post-treatment, but for certain materials like photopolymers, process should be done in darkroom. Recently Sakai et al reported surface relief holographic diffusers in azo-polymer films [28]. They used a source diffuser to create a speckle pattern on an azo-polymer film. They inscribed this pattern on the polymer surface as relief.

During self-organized SRGs formation we observed divergence in first order diffracted beams (figure IV-12). Self-organized SRGs have not regular sinusoid shape and they present several discontinuities in their structure. Also the pitch of such SRGs is not exactly same over whole illuminated surface (see for example figure IV-5). These lead to diffusion of light when it diffract from self-organized SRGs. The total diffusion angle is around 23°.

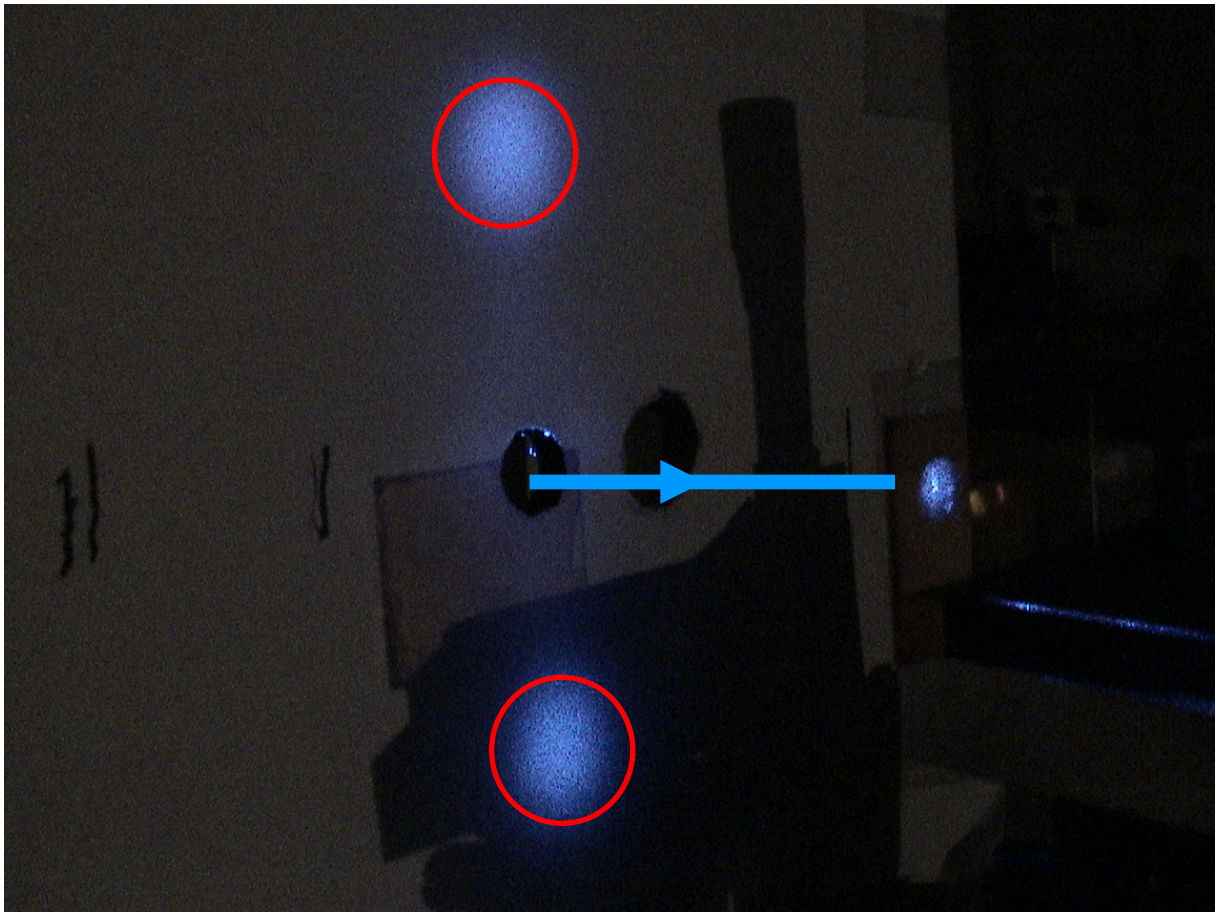

Figure IV-12: Diffusion of first order diffracted beam from self-organized SRG.

Obtained diffusion angle is around half of commercialized diffusers [42].As we have discussed in section II-10-4, self organized structure inscribed with circularly polarized writing beam consists of gratings oriented in all the directions on the surface of film.

The pitch of all this grating should be same as gratings created with linearly polarized beam. So, diffraction pattern of this structure is a uniformly filled disc. Figure IV-13 shows 2D Fourier transformation of image II-22.

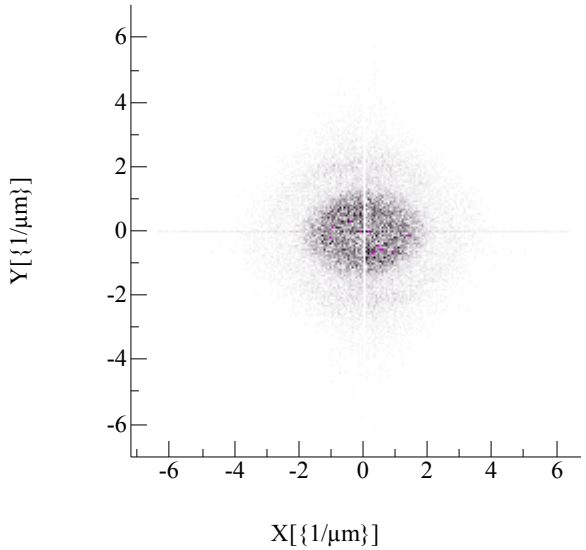

Figure IV-13: 2D Fourier transformation of image II-22.

The diffraction angle of self-organized SRG with linearly polarized beam is 32.6°. Thus diffusion angle for this structure is around 65° that is even bigger than diffusion angle of usual diffusers [28].

Our method is very simple in comparison to all other methods. Our sample diffuse light to diffracted beams in transmission and reflection. Reflected diffraction beam allows us to use it in broad band of wavelengths; while for holographic materials it is restricted to transmission band of materials. The main disadvantage of this method is low diffraction efficiency of self-organized SRGs.

IV-4-3- 2D chirality

Existing theories of the origin of life accepted that chirality of prebiotic molecules leads to appearance of life [29, 30]. Lord Kelvin introduced and defined chirality as: “I call any geometrical figure, or group of points, chiral, and say it has chirality, if its image in a plane mirror, ideally realized, cannot be brought to coincide with itself” [31].

Chiral molecules play key role in our life. All key biologically active molecules and macromolecules like amino acids, peptides, enzymes, proteins as well as DNA, RNA and sugars, polysugars, terpenes and biologically active heterocyclic molecules are chiral. These molecules and macromolecules exist and are biologically active under only one of the two possible mirror images. For instance essentially only the L-amino acids and only the D-sugars like ribose and deoxyribose (the key constituents of RNA and DNA macromolecules and the chiral sites of their monomeric units) are biologically active.

These chiral molecules and macromolecules are able to rotate and change the polarization state of light. So a chiral system is optically active. Chiral expression at surface (2D) has attracted increasing attention in recent years. In 2D systems, the chirality is restricted to the asymmetry of objects lying in a plane. Papakostats et al. fabricated 2D chiral media using direct-write electron beam lithography in metallic and dielectric films and experimentally showed that such 2D chiral systems also able to affect polarization state of light [32].

In this section we will present a simple method for fabrication of 2D chiral system. In section II-10 we showed that the self-organized structure formation is very sensitive to the angle of incidence. For different state of polarization different structures has been obtained. Let us consider the case of 45° polarization. In this case at incidence angle of ~33°, formed structure is asymmetric and it does not have a symmetry axis in 2D plane (figure IV-14). Figure IV-14(a) shows AFM image of self-organized structure and its mirror image, the AFM image is not superimposable with its mirror image if we rotate the image in its plane. On the other hand the mirror image of Fourier Transform of AFM image also is not coinciding with Fourier Transform of AFM image [figure IV-14(b)]. The images were processed using the WSXM software from Nanotec [see section II-7]. Consequently this structure is a 2D chiral structure.

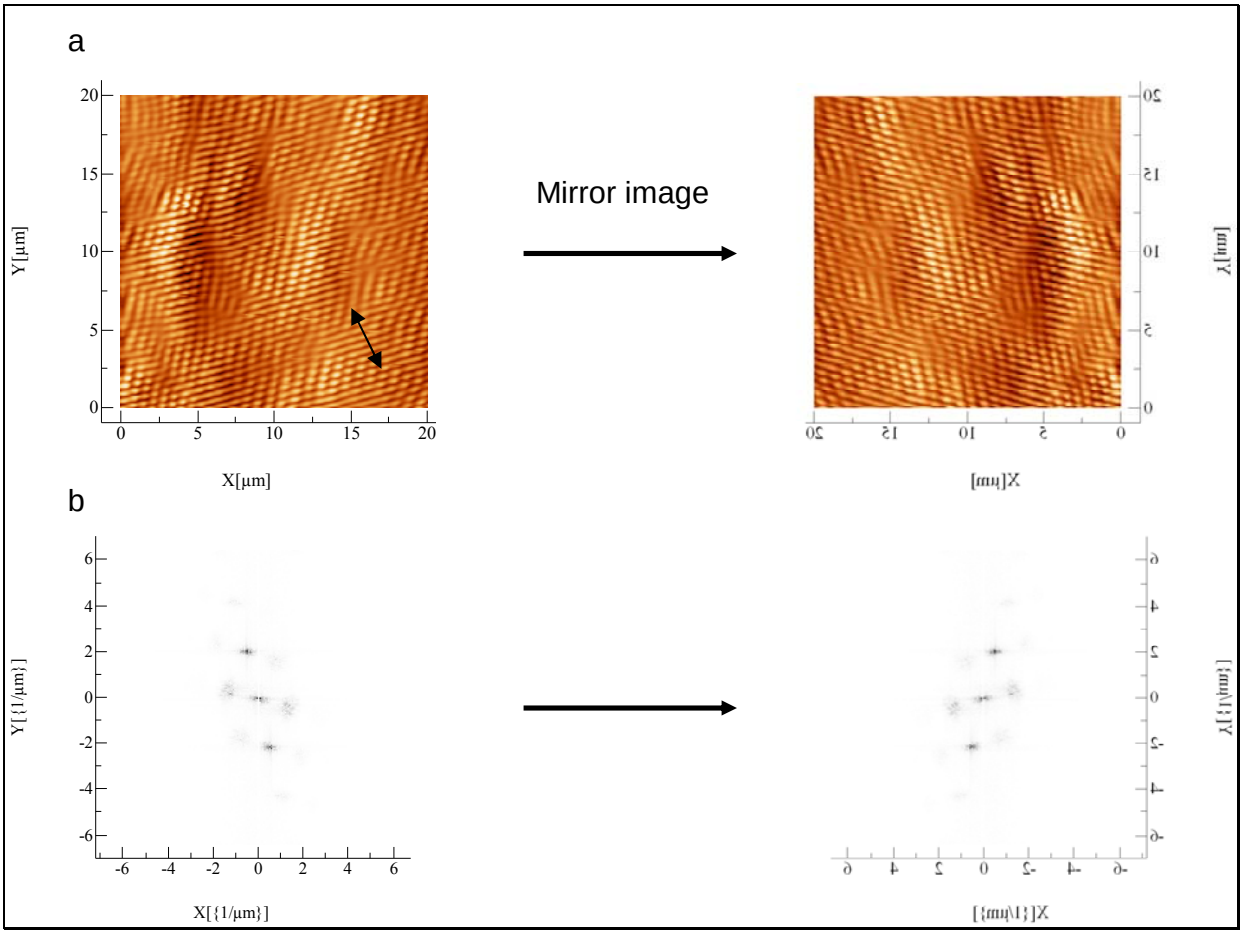

Figure IV-14: a) AFM image of self-organized structure on the surface of an azo-polymer film and its mirror image. b) 2D Fourier Transform of this structure and its mirror image. The azo-polymer is MB2I. The arrow indicates writing beam polarization direction.

Experimental setup for measuring optical activity of the polymeric chiral structure is presented is figure IV-15.

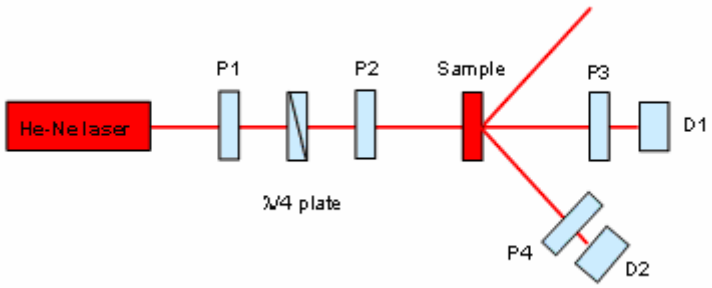

Figure IV-15: Experimental setup for measuring optical activity of self-organized structure. P1, P2, P3 and P4 are polarizer. D1 and D2 are detectors.

A He-Ne laser of 633 nm is input normal to the pattern face of sample. The laser beam passes trough a linear polarizer, quarter – wave plate and another linear polarizer to obtain a controllable linear polarization. Polarization direction of input beam was defined with respect to the polarization direction of writing beam (Figure IV-14). We measured difference between the polarization azimuth of incident beam and that of zero and first order diffracted beams in transmission. Figure IV-16-a(1) shows diffracted beam azimuth rotation versus input polarization azimuth.

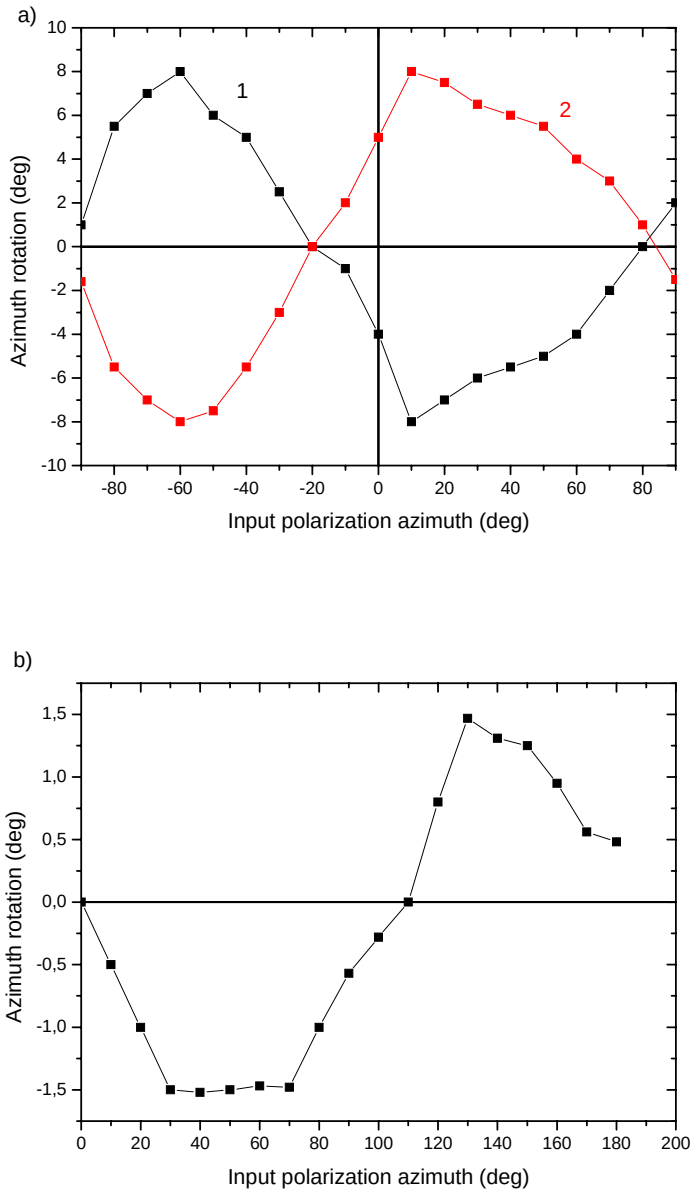

Figure IV-16: a) and b) show azimuth rotation of diffracted (from polymer side 1 and glass side 2) and transmitted beams polarization respectively.

The azimuth rotation is not symmetric related to the writing beam polarization direction. When laser beam input normal to the sample from opposite side of pattern (i.e. from glass side), azimuth rotation changes its sign [figure IV-16-a (2)]. The zero-order transmission beam azimuth rotation is presented in figure IV-16-b. The results show that azimuth rotation of zero-order transmitted beam is very small and its maximum value is around 1.5° (comparable with the previous result 2° in [33, 34]).These patterns show the capability to rotate the polarization state of diffracted light in the transmission regime. The changes in the polarization state of light associate with the chirality of sample. This is a one-step very simple and reversible method to fabricate 2D chiral systems.

IV-5-Conclusion

In this chapter we described some interesting applications of self-organized SRGs. We presented a simple experimental method to implement optical processors and logic gates. The photoactive azo molecules self-organized to a well defined structure under coherent light irradiation. The study of self-organization SRG characteristics (orientation and pitch) in the zones of two spatially separated coherent beams inside a large incoherent beam zone shows that it is possible to modify features of zones by changing the polarization of coherent beam in one of them. That means the molecules in two separated zones communicate with each other.

We have showed that self-organized SRG is convenient for the controlling of cell growth direction. Cells orient in the direction of SRG grooves. The shape and the direction of self-organized SRGs wave-vector are controllable with polarization of writing beam. Therefore it allows us to create cell networks.

We also presented three other applications for self-organized SRG. The resulting SRG allows coupling light into and out of slab waveguides. The diffusion of diffracted beam also gives us opportunity to propose it as optical diffuser. We found that self-organized structure for 45°-polarized beam with incidence angle of ~33° shows 2D chirality. The results show that rotation of output polarization azimuth for diffracted beam is bigger than transmitted one.

IV-6- References:

1- L. J. Cutrona, E. N. Leith, C. J. Palermo, L. J. Porcello, Optical data processing and filtering systems, IRE Trans. Inform. Theory, 1960, **IT-6**, 386-400.

2- A. B. VanderLugt, Optical data processing and filtering systems, IRE Trans. Inform. Theory, 1964, **IT-10**, 139-145.

3- H. J. Caulfield, J. Shamir, Wave-particle duality processors - characteristics, requirements and applications, J. Opt. Soc. Am. A, 1990, **7**, 1314-1323.

4- J. Shamir, H. J. Caulfield, W. Micelli, R. J. Seymour, Optical Computing and the Fredkin Gates, Appl. Opt., 1986, **25**(10), 1604-1607.

5- J. Shamir, Three-dimensional optical interconnection gate array, Appl. Opt., 1987, **26**, 3455-3457.

6- M. M. Mirsalehi, J. Shamir, H. J. Caulfield, Residue arithmetic processing utilizing optical Fredkin gate arrays, Appl. Opt., 1987, **26,**3940-3946.

7- K. M. Johnson, M. Surette, J. Shamir, Optical interconnection network using polarization-based ferroelectric liquid crystal gates, Appl. Opt., 1988, **27**, 1727-1733.

8- Y. A. Zaghloul, A. R. M. Zaghloul, Complete all-optical processing polarizationbased binary logic gates and optical processors, Opt. Express, 2006,**14**, 9879-9895.

9- Y. Owechko, Cascaded-grating holography for artificial neural networks, Appl. Opt., 1993, **32**, 1380-1385.

10- P. E. Keller, A. F. G. Gmitro, Design and analysis of fixed planar holographic interconnects for optical neural networks, Appl. Opt., 1992, **32**, 5517-5523.

11- G. D. Boyd, Optically excited synapse for neural networks, Appl. Opt., 1987, **26**, 2712–2720.

12- A. Natansohn, P. Rochon, Photoinduced motions in Azobenzene-based amorphous polymers: Possible photonic devices, Adv. Mater., 1999, **11**, 1387-1391.

13- C. Cojocariu, P. Rochon, Tribute to Almeria Nathanson: Light-induced motions in azobenzene-containing polymer, Pure Appl. Chem., 2004, **76**, 1479-1497.

14- C. Hubert, C. Fiorini-Debuisschert, I. Maurin, J.-M. Nunzi, P. Raimond, Spontaneous patterning of hexagonal structures in an azo-polymer using light-controlled mass transport, Adv. Mater.,2002, **14**, 729-32.

15- S. Ahmadi Kandjani, R. Barille, S. Dabos-Seignon, J.-M. Nunzi, E. Ortyl, S. Kucharski, Multistate polarization addressing using one single beam in an azo polymer film, Opt. Lett.,2005, **30**, 1986-1988.

16- S. Ahmadi Kandjani, R. Barille, S. Dabos-Seignon, J.-M. Nunzi, E. Ortyl, S. Kucharski, Incoherent light-induced self-organization of molecules, Opt. Lett., 2005, 30, 3177-3179.

17- R. G. Harrison, On the stereotropism of embryonic cells, Science, 1911, **34**, 279.

18- Y. A. Rovensky, I. L. Slavnaya, Spreading of fibroblast-like cells on grooved surfaces, Exp. Cell. Res., 1973, **84**, 199-206.

19- G. Zeck, P. Fromherz, Noninvasive neuroelectronic interfacing with synaptically connected snail neurons immobilized on a semiconductor chip, PNAS, 2001, **98**(18), 10457-10462.

20- F. Letournel, A. Bocquet, R. Perrot, A. Dechaume, F. Guinut, J. Eyer, A. Barthelaix, Neurofilament high molecular weight–green fluorescent protein fusion is normally expressed in neurons and transported in axons: A neuronal marker to investigate the biology of neurofilaments, Neuroscience, 2006, **137**(1), 103-111.

21- I. Nagata, A. Kawana, N. Nakatsuji, Perpendicular contact guidance of CNS neuroblasts on artificial microstructures, Development, 1993, **117**, 401-408.

22- J. C. Chang, G. J. Brewer, B. C. Wheeler, Modulation of neural network activity by patterning, Biosensors & Bioelectronics, 2001, **16**, 527-533.

23- R. L. Longini, Optical Characteristics of Sheets of Scattering Materials, J. Opt. Soc. Am., 1949, **39**, 551-553.

24- W. E. Knowles Middleton, Diffusion of ultraviolet and visible light by ground surfaces of fused quartz, J. Opt. Soc.Am., 1960, **50**, 747–749.

25- S. Wadle, D. Wuest, J. Cantalupo, Holographic diffusers, Opt. Eng., 1994, **33**, 213–218 .

26- C. Gu, J.-R. Lien, F. Dai, J. Hong, Diffraction properties of volume holographic diffusers, J. Opt. Soc. Am. A, 1996, **13**, 1704-1711.

27- S. I. Kim, Y. S. Choi, Y. N. Ham, C. Y. Park , J. M. Kim, Holographic diffuser by use of a silver halide sensitized gelatin process, Appl. Opt., 2003, **42**, 2482-2491.

28- D. Sakai, K. Harada, S. Kamemaru, M. A. El-Morsy, M. Itoh, T. Yatagai, Direct Fabrication of Surface Relief Holographic Diffusers in Azobenzene Polymer Films, Opt. Rev., 2005, **12**, 383-386.

29- W. A. Bonner, Origin and amplification of biomolecular chirality, Origin of Life and Evolution of Biosphere, 1991, **21,** 59-111.

30- G. A. Goodfriend, M. J. Collins, M. L. Fogel, S. A. Macko, J. F. Wehmiller (editors) Perspectives in Amino Acid and Protein Geochemistry (New York: Oxford University Press), 2000.

31- W.T. Kelvin, Baltimore Lectures on Molecular Dynamics and the Wave Theory of Light (C.J. Clay, London, 1904), 619.

32- A. Papakostas, A. Potts, D.M. Bagnall, S.L. Prosvirnin, H.J. Coles, N.I. Zheludev, Optical Manifestations of Planar Chirality, Phys. Rev. Lett.,2003, **90**, 107404-4.

33- A. Potts, A. Papakostas, D.M. Bagnall , N.I. Zheludev, Planar chiral meta-materials for optical applications, Microelec. Eng., 2004, **73–74**, 367–371.

34- W. Zhang, A. Potts, A. Papakostas, D. M. Bagnall, Intensity modulation and polarization rotation of visible light by dielectric planar chiral metamaterials, Appl. Phys. Lett., 2005, **86**, 231905-3.

CONCLUSIONS AND PERSPECTIVES

We have presented self-organized SRG formation in a new series of azo-polymers. The first part of study dealt with characterization of these new azo-polymers for their light induced birefringence and SRG formation measurements. Birefringence has been induced by a linearly polarized Ar+ laser and measured with a probe He-Ne laser. SRG inscribed on the azo-polymer film using Lloyd mirror setup.

In the second part we demonstrated a simple experimental setup based on stimulated Wood's anomalies to induce spontaneous SRG formation on azo-polymers. The direction of grating wave vector is parallel to the polarization of writing beam. It was shown that polarization multiplexing only can double the capacity of digital optical data storage. Our results showed that it is possible to have more than two state polarization multiplexing using a single laser beam (multistate polarization addressing). The self-diffraction from this grating showed a threshold depending on the power density. The threshold was a linear function of the input beam intensity with a slope of ~33 mW.min/cm^2. A good agreement was obtained between measurements of SRG pitch vs. incidence angle and stimulated Wood's anomalies. Different kinds of patterns were obtained by varying the polarization of laser beam and the incidence angle.

In the third part we investigated cooperative organization of azo-molecules under incoherent light illumination. Overlap of one small low power coherent beam and a large high power incoherent beam on the surface of the polymer film has been used for this purpose. Incoherent beam is not able to create a regular pattern. SRG formed in coherent beam region and propagate via cooperative organization of azo-molecules and covers whole incoherent beam region.

Finally we have presented some possible applications of self-organized SRG in this thesis. As we mentioned before azo-molecules could communicate through cooperative self-organization. Using two separate coherent beams surrounded with a large high power incoherent beam, we have realized nonlocal communication between molecules in coherent beams zones. We have controlled characteristics of self-organized SRGs in both coherent

beam zones by varying polarization direction of one of them that can be used for neural network and logic gate purposes.

Neural network organization is possible by controlling of the cell growth and orientation direction. For this aim we have presented self-organized structures. The main advantages include easy fabrication, single beam required, variety of patterns ect..

We also suggest that by using self-organized SRG, it is possible to fabricate waveguide coupler, optical diffuser and 2D chiral structure.

Future perspectives

One can not hope to participate in all parts of the endeavor sketched above, especially when taking into account the origin of self-organization in such systems.

In the following, we will focus on future works that are related to the current research:

- Materials structures can be optimized to have fast self-organization.
- From some experimental results, not presented in this study, it is evident that self-organized patterns have different shapes for high Tg and low Tg polymers. So the study of polymers with different Tg should be interesting.
- Computer simulation of the phenomena can help its better understanding.
- The research presented here can be extended to the other self-organized systems.

Appendix 1:

Coherency

Coherency is defined by the correlation properties between quantities of an optical field. Usual interference is the simplest phenomenon revealing correlations between light waves. Michelson introduced a technique for measuring the temporal coherence (Michelson interferometer). Spatial coherence is best illustrated by Young's double-slit experiment. When considering temporal coherence we compare a light wave with itself at different times. When considering spatial coherence we compare two light waves at different points in space. To describe these two cases the self coherence function and spatial coherence function can be used. Both concepts, however, do not cover the interference properties of a light field in their entirety. To deal with this more general case, we introduce spatiotemporal coherence. For that, the mutual coherence function is defined:

$$\Gamma(r_1, r_2; t_1, t_2) = \Gamma_{12}(t_1, t_2) = \Gamma_{12}(\tau) = \left\langle E(r_1, t+\tau) E^*(r_2, t) \right\rangle$$

where $\left\langle E(r_1, t+\tau) E^*(r_2, t) \right\rangle$ is interference term of two optical fields originated from points r_1 and r_2 at point P(figure A1-1).

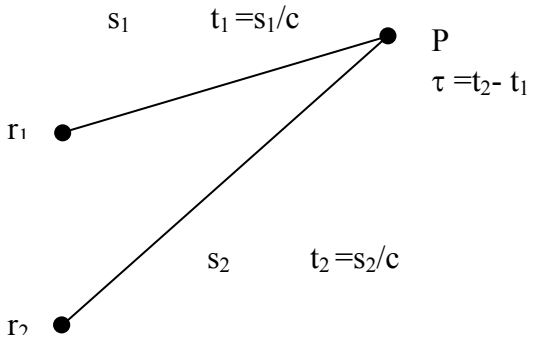

Figure A1-1: Notation used in the derivation of equations. r_1 and r_2 are two light sources. P is a point on the interference screen. s_1 and s_2 are optical pathways of two interfering beams, and τ is time delay between two beams at point P.

For $r_1=r_2$ purely temporal coherence is obtained; for $\tau=0$, it is purely spatial. The mutual coherence function includes the following notations:

$\Gamma_{11}(\tau)$ = self coherence function at r_1

$\Gamma_{22}(\tau)$ = self coherence function at r_2

$\Gamma_{12}(0)$ = spatial coherence function

$\Gamma_{11}(0)$ = intensity at r_1

$\Gamma_{22}(0)$ = intensity at r_2.

As with the self coherence function the mutual coherence function can be normalized. The quantity;

$$\gamma_{12}(\tau) = \frac{\Gamma_{12}(\tau)}{\sqrt{\Gamma_{11}(0)\Gamma_{22}(0)}}$$

is called the degree of mutual coherence. The intensity I_P at a point P can be written as:

$$I_P = I_P^{(1)} + I_P^{(2)} + 2\sqrt{I_P^{(1)} I_P^{(2)}}\ \mathrm{Re}\{\gamma_{12}(\tau)\}.$$

The visibility (contrast) of interference fringes can be determined from the degree of mutual coherence:

$$K = \frac{I_{\max} - I_{\min}}{I_{\max} + I_{\min}} = 2\frac{\sqrt{\Gamma_{11}(0)\Gamma_{22}(0)}}{\Gamma_{11}(0) + \Gamma_{22}(0)}\left|\gamma_{12}(\tau)\right| .$$

When the two interfering waves are of equal intensity, we have $K = \left|\gamma_{12}(\tau)\right|$. The following cases may be distinguished:

$\left|\gamma_{12}(\tau)\right| \equiv 1$ Complete coherence

$0 \le \left|\gamma_{12}(\tau)\right| \le 1$ Partial coherence

$\left|\gamma_{12}(\tau)\right| \equiv 0$ Complete incoherence.

So when the visibility of interference pattern has disappeared, the field is incoherent.

Appendix 2:

A simple photo-process model

As we explained in first chapter of this thesis, azo-dye molecules have two isomers: trans and cis. Only trans isomer is stable in darkness. Under illumination with suitable light, i.e. in the absorption band of trans isomer, a trans-cis photo-isomerization takes place and a photo-stationary equilibrium is reached. So, some molecules are in cis form.

Let us to consider a simplified model of trans ↔ cis isomerization. We assumed that under illumination there are three processes taking place in the azo-polymer:

1- Optically induced trans-cis transition.
2- Optically induced cis-trans transition.
3- Thermally activated cis-trans transition.

The rate constant K_1 of first process is proportional to the exciting beam intensity ***I***, to the absorption cross section σ_T of the trans isomer and quantum yield of process q_1, that is $K_1 = q_T I \sigma_T$. Because of molecular shape of trans isomer, its absorption is strongly anisotropic and if incidence light beam is linearly polarized, for each molecule, σ_T depends to the angle between direction of light beam polarization and molecular orientation θ.

$$\sigma_T = \sigma_T^{\parallel} \cos^2\theta + \sigma_T^{\perp} \sin^2\theta ,$$

where $\sigma_T^{\parallel}$, $\sigma_T^{\perp}$ are absorption cross section of exciting light in the trans-cis photoisomerization for the molecules parallel and perpendicular to the electric field of light, respectively. From the experimental results it is evidence that $\sigma_T^{\perp} \approx 0$ [1]. The rate constant for cis-trans photoisomerization is $K_2 = q_C I \sigma_C$ .The absorption cross section for cis to trans photo-isomerization σ_C is independent of light beam polarization direction. The absorption cross sections for both photo-induced transitions are strongly wavelength dependent. For this simple model we neglect the diffusion or molecular rotations during trans-cis-trans isomerization. The thermal cis-trans relaxation rate constant depends only on the dye chemical structure and its surroundings (independent of light intensity).

In this simple model, the change in the concentration of molecules in trans state N_T is given by:

$$\frac{dN_T}{dt} = -q_T \sigma_T^{\parallel} N_T I \cos^2\theta + q_C \sigma_C I (N_{to} - N_T) + K(N_{to} - N_T),$$

Where N_{to}, is the total number of molecules. The steady-state concentration is expressed by;

$$N_T = N_{to} \frac{q_C \sigma_C I + K}{q_T \sigma_T^{\parallel} I \cos^2\theta + q_C \sigma_C I + K} .$$

At the same time, the steady-state concentration of cis isomers is described by:

$$N_{to} = N_T + N_C \quad \rightarrow \quad N_C = N_{to} \frac{q_T \sigma_T^{\parallel} I \cos^2\theta}{q_T \sigma_T^{\parallel} I \cos^2\theta + q_C \sigma_C I + K} .$$

Let us consider a two beam case. Along one coherent laser beam with the intensity of I_S, the polymer thin film illuminated with another incoherent and unpolarized background beam with the intensity of I_b. The wavelength of both beams is the same and lies in the absorption bound of azo-polymer. Change in the concentration of cis isomer is given by,

$$N_C = N_{to} \frac{q_T \sigma_T \left(I_S \cos^2\theta + I_b\right)}{q_T \sigma_T \left(I_S \cos^2\theta + I_b\right) + q_C \sigma_C \left(I_S + I_b\right) + K} .$$

Transitions induced with background beam are uniform in all directions.